

Chemical Transformations of the Pyrene K-Region for Functional Materials

Dissertation zur Erlangung des Grades

„Doktor der Naturwissenschaften“

am Fachbereich Chemie, Pharmazie und Geowissenschaften

der Johannes Gutenberg-Universität Mainz

Lukas Julian Zöphel

geboren in Kirchheimbolanden

Mainz im Jahr 2012

Dekan: [REDACTED]

1. Berichterstatter: [REDACTED]

2. Berichterstatter: [REDACTED]

Tag der mündlichen Prüfung: 13.09.2012

Die vorliegende Arbeit wurde in der Zeit von Dezember 2008 bis Dezember 2011 am Max-Planck-Institut für Polymerforschung in Mainz unter Betreuung von [REDACTED] durchgeführt.

Ich danke [REDACTED] für seine unterstützende und unermüdliche Diskussionsbereitschaft zur wissenschaftlichen Bearbeitung dieses interessanten Themas.

Meinen Eltern

Table of Contents

| | | |
|----------|--|-----------|
| 1 | Introduction | 11 |
| 1.1 | Pyrene Chemistry | 12 |
| 1.1.1 | Positions 1, 3, 6 and 8 | 13 |
| 1.1.2 | Positions 2 and 7 | 15 |
| 1.1.3 | Positions 4, 5, 9 and 10 | 17 |
| 1.1.4 | Pyrene as Building Block for Large π -Conjugated Systems | 20 |
| 1.2 | Characterization Methods | 22 |
| 1.2.1 | X-Ray Crystallography | 22 |
| 1.2.2 | 2D Wide Angle X-Ray Scattering | 23 |
| 1.2.3 | Scanning Tunneling Microscopy | 24 |
| 1.2.4 | Organic Field-Effect Transistors | 26 |
| 1.3 | Bibliography | 27 |
| | | |
| 2 | Objectives and Motivation | 31 |
| 2.1 | Bibliography | 35 |

| | | |
|----------|---|------------|
| 3 | Donor/Acceptor Pyrenes | 39 |
| 3.1 | Introduction | 39 |
| 3.2 | Synthesis of 4,5- versus 9,10-Donor/Acceptor Pyrene | 42 |
| 3.3 | Optical and Electronic Properties | 47 |
| 3.4 | Crystal Structure Analysis | 54 |
| 3.5 | Charge-Transfer Complex | 56 |
| 3.6 | Summary | 60 |
| 3.7 | Bibliography | 62 |
| | | |
| 4 | Pyrenocyanines | 65 |
| 4.1 | Introduction | 65 |
| 4.2 | Synthesis | 69 |
| 4.3 | NMR Investigations | 71 |
| 4.4 | Optical Properties | 76 |
| 4.5 | Self-Assembly at the Liquid/Solid Interface (STM) | 80 |
| 4.6 | Self-Assembly in the Bulk (2D WAXS) | 87 |
| 4.7 | Pyrenopyrazinocyanines | 93 |
| 4.7.1 | Synthesis | 94 |
| 4.7.2 | Optical Properties | 96 |
| 4.8 | Summary | 98 |
| 4.9 | Bibliography | 100 |
| | | |
| 5 | Dithienobenzo[e]pyrenes | 105 |
| 5.1 | Introduction | 105 |
| 5.2 | Synthesis | 107 |
| 5.3 | Optical and Electronic Properties | 110 |
| 5.4 | OFET Performance | 118 |

| | | |
|----------|--|------------|
| 5.5 | Summary | 127 |
| 5.6 | Bibliography | 129 |
| 6 | Hexaaryl[<i>a,c,fg,j,l,op</i>]tetracenes | 133 |
| 6.1 | Introduction | 133 |
| 6.2 | Synthesis | 135 |
| 6.2.1 | Dibenzo[<i>fg,op</i>]tetrathieno[<i>a,c,j,l</i>]tetracenes | 139 |
| 6.2.1.1 | Optical and Electronic Properties | 141 |
| 6.2.2 | Hexabenz[<i>a,c,fg,j,l,op</i>]tetracenes | 144 |
| 6.2.2.1 | Optical and Electronic Properties | 149 |
| 6.3 | Crystal Structure Analysis | 152 |
| 6.5 | Summary | 158 |
| 6.6 | Bibliography | 160 |
| 7 | <i>Peri</i>-Pentacene | 163 |
| 7.1 | Introduction | 163 |
| 7.2 | Synthesis | 167 |
| 7.3 | Conformational Investigations of 7-5 | 176 |
| 7.4 | Optical and Electronic Properties | 182 |
| 7.5 | Transformation of the Tetraketone Structure | 189 |
| 7.6 | Summary | 197 |
| 7.7 | Bibliography | 199 |
| 8 | Conclusion and Outlook | 203 |
| 9 | Experimental Part | 209 |
| 9.1 | General Methods | 209 |

| | | |
|-----------|--|------------|
| 9.2 | Analytical Techniques | 210 |
| 9.3 | Donor/Acceptor Pyrenes | 216 |
| 9.4 | 4,5-Pyrenocyanines | 224 |
| 9.5 | Dithienobenzo[<i>e</i>]pyrenes | 237 |
| 9.6 | Hexaaryl[<i>a,c,fg,j,l,op</i>]tetracenes | 246 |
| 9.7 | <i>Peri</i> -Pentacene | 258 |
| 9.8 | Crystal Data | 262 |
| 10 | List of Publications | 283 |
| 11 | Acknowledgements | 285 |
| 12 | Curriculum Vitae | 289 |

Index of Abbreviations

| | |
|---------|---|
| 2D WAXS | two-dimensional wide angle X-ray scattering |
| AcOH | acetic acid |
| AIBN | azo-bis-(isobutyronitrile) |
| COSY | correlation spectroscopy |
| CV | cyclic voltammetry |
| d | doublet (NMR) |
| d | days |
| D | Debye |
| DBTTT | dibenzo[<i>fg,op</i>]tetrathieno[<i>a,c,j,l</i>]tetracene |
| DBU | 1,8-diazabicyclo[5,4,0]undec-7-en |
| DCM | dichloromethane |
| DCTB | <i>trans</i> -2-[3-(4- <i>tert</i> -butylphenyl)-2-methyl-2-propenylidene]malononitrile |
| DDQ | 2,3-dichlor-5,6-dicyano-1,4-benzoquinone |
| DFT | density functional theory |
| DMSO | dimethyl sulfoxide |
| DPV | differential pulse voltammetry |

| | |
|-----------|--|
| ESI MS | electrospray ionization mass spectrometry |
| ESR | electron spin resonance |
| FD | field desorption |
| GPC | gel permeation chromatography |
| h | hours |
| H,H COSY | two-dimensional correlated proton NMR spectroscopy |
| HAT | hexaaryl[<i>a,c,fg,j,l,op</i>]tetracene |
| HBT | hexabenz[<i>a,c,fg,j,l,op</i>]tetracene |
| HBC | hexa- <i>peri</i> -hexabenzocoronene |
| HOMO | highest occupied molecular orbital |
| HOPG | highly ordered pyrolytic graphite |
| HPLC | high performance liquid chromatography |
| HSQC | heteronuclear single quantum coherence |
| ITO | indium tin oxide |
| LUMO | lowest unoccupied molecular orbital |
| m | multiplet (NMR) |
| MALDI-TOF | matrix-assisted laser desorption/ionization time-of flight |
| Mes | mesityl |
| min | minutes |
| MS | mass spectrometry |
| NMP | <i>N</i> -methylpyrrolidinone |
| NMR | nuclear magnetic resonance |
| NOESY | nuclear OVERHAUSER enhancement spectroscopy |
| OFET | organic field-effect transistor |
| OLED | organic light emitting diode |
| OPV | organic photovoltaics |
| PAH | polycyclic aromatic hydrocarbon |
| Pc | phthalocyanine |

| | |
|--------------------|--|
| PCBM | [6,6]-phenyl-C61-butyric acid methyl ester |
| PDI | perylene diimide |
| PIFA | phenyliod(III)bis(trifluoroacetate) |
| ppm | parts per million |
| Pyc | pyrenocyanine |
| q | quartet (NMR) |
| RFID | radio frequency identification tag |
| RT | room temperature |
| s | singlet (NMR) |
| STM | scanning tunneling microscopy |
| t | triplet (NMR) |
| TAP | tetraazaporphyrin |
| TBABH ₄ | tetrabutylammonium borohydride |
| ^t Bu | <i>tert</i> -butyl |
| TCNQ | tetracyanoquinodimethane |
| TFA | trifluoroacetic acid |
| Tf ₂ O | trifluoromethanesulfonic anhydride |
| THF | tetrahydrofuran |
| TIPS | triisopropylsilyl |
| TLC | thin layer chromatography |
| UV/vis | ultraviolet/visible |

Preface

“Laurent hat 1837 ein Gemenge verschiedener, der Theerdestillation entstammender Kohlenwasserstoffe unter Händen gehabt, dessen wesentlicher Bestandteil der später von Gräbe mit dem Namen Pyren bezeichneten Körper war; daßs Laurent's Untersuchungsmaterial keine einheitliche Substanz darstellte, ergibt sich schon aus dem Intervall von 10 Graden, innerhalb dessen der von ihm beobachtete Schmelzpunkt lag; seiner Formel $C_{15}H_{12}$ ist – wie schon von anderer Seite hervorgehoben wurde – um so weniger Werth beizulegen, als die Analyse unter Zugrundelegung des richtigen Atomgewichts vom Kohlenstoff ein Deficit von 2 pC. aufweist. Gräbe (1870) isolierte das Pyren zuerst in nahezu reinem Zustand aus den höher wie Anthracen siedenden Fraktionen eines braunschweigischen Steinkohlentheers, charakterisierte es als chemisches Individuum, stellte die richtige Formel $C_{16}H_{10}$ fest und begründete sie außer durch zahlreiche Analysen durch eine Reihe von Derivaten, unter welchen als Wichtigstes das Pyrenchinon $C_{16}H_8O_2$ hervorzuheben ist, das bei der Oxydation des Kohlenwasserstoffs mittelst Chromsäure auf normale Weise erzeugt wird, indem zwei Sauerstoffatome die Stelle zweier Wasserstoffatome einnehmen.

Hintz nimmt im Jahre 1878 die Untersuchung über das Pyren, die nach Gräbe's grundlegender Arbeit 8 Jahre ruht, wieder auf, lehrt den Kohlenstoff selbst sowie einige Derivate zuerst in absolut reinem Zustand

darstellen und bestätigt die Angaben G r ä b e ' s. Nur in Bezug auf den Verlauf des mit Chromsäure ausgeführten Oxydationsprocesses gelangt er zu völlig widersprechenden Resultaten : Er verwirft die für das Chinon geltende Formel $C_{16}H_8O_2$, ersetzt dieselbe durch die sehr befremdlich erscheinende $C_{12}H_6O_2$ und findet als Produkt der Oxydation neben dem rothen Chinon eine zweite, in kohlsaurem Natrium lösliche, gelbe Substanz, für welche er auf Grund mehrerer, annähernd unter einander übereinstimmender Analysen die Formel $C_{15}H_6O_4$ ableitet. Das rothe Chinon $C_{12}H_6O_2$ geht nach seiner Beobachtung durch andauernde Oxydation allmählich in das gelbe Product $C_{15}H_6O_4$ über.

Die Widersprüche zwischen den Angaben von G r ä b e und H i n t z finden ihre Lösung in einer 6 Jahre später veröffentlichten Arbeit von G u i d o G o l d s c h m i e d t, welche sich durch peinlichste Sorgfalt des experimentellen Details auszeichnet. Auf Grund zahlreicher Analysen und verschiedenartiger Reactionen setzt G o l d s c h m i e d t die alte Formel von G r ä b e $C_{16}H_8O_2$, in welcher die Beziehungen des Chinons zum Pyren $C_{16}H_{10}$ einen so einfachen Ausdruck finden, wieder in ihr Recht ein und führt das Irrthümliche der H i n t z ' schen Resultate mit überzeugender Schärfe auf mangelhafte Reinigung der analysirten Substanz zurück. [...] “[1]

Eugen Bamberger 1887

Mittheilung aus dem chem. Laboratorium der
königlichen Academie der Wissenschaften zu München

1 Introduction

Pyrene has firstly been discovered by the french chemist Auguste Laurent in 1837 by extraction from coal tar but the correct chemical formula has been determined later by Gräbe 1871 and the structure by Bamberger and Philip in 1887.^[1-3] Those basic studies were written in German language and date from the period before the daily use of sophisticated analytical methods like NMR spectroscopy or high-resolution mass spectrometry. Nevertheless, the found molecular formula remains still valid whereupon pyrene consists of 16 carbon atoms within four rings forming the polycyclic aromatic hydrocarbon (PAH). Using Clar's sextet rule, pyrene can be drawn with two circles and two double bonds (Figure 1.1 c). Arising from this description, pyrene appears as a biphenyl annulated with two further rings in the *armchairs*. Indeed, these double bonds exhibit increased reactivity towards oxidation due to less stabilization although still being aromatic. The positions 4, 5, 9 and 10 are referred to as K-region and are discussed to be mainly involved into the carcinogenic effect of pyrene upon its oxidation.^[4-6]

Since its discovery pyrene has predominantly attracted attention for its outstanding photophysical properties, which is why pyrene is called “the fruit fly of photochemists”.^[7] Pyrene is well known for its long lifetime of the excited state of the monomer in solution of 68 ns, high fluorescence quantum yields and the concentration dependent shift of the emission spectrum upon

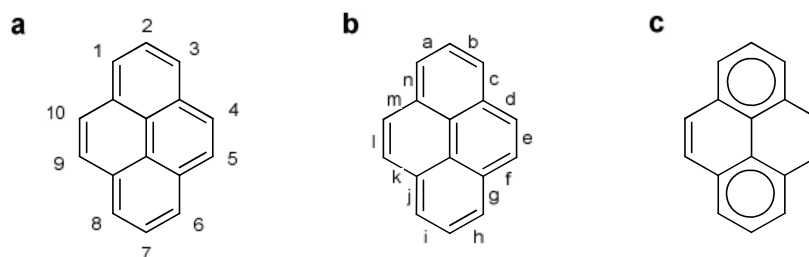


Figure 1.1: Nomenclature of positions (a) and edges (b) of pyrene; (c) depiction according to Clar's sextet rule.

excimer formation.^[8] Monomeric pyrene emits between 370 nm and 400 nm whereas emission of the excimer appears red-shifted.^[9-10] These properties make pyrene one of the most frequently applied fluorescence markers by using the excimer signal to monitor dynamics of polymer chains and protein structures.^[11-14] After selective cysteine labeling of proteins with *N*-(1-pyrenyl)maleimide the appearance or absence of the excimer signal provides information about the spatial distance of labeled residues.

The latter example shows that no sophisticated chemistry is required for this application and the introduction of functional groups at position 1 is already known for more than 70 years. Nevertheless, pyrene chemists have greatly extended the variety of available protocols in the meantime to variously functionalize pyrene for respective applications. Especially in the last decade a large number of path breaking methods have been reported making new classes of pyrene based materials accessible for material scientists.

In the following an overview of pyrene chemistry sorted by the site-specificity shall be given.

1.1 Pyrene Chemistry

Pyrene has three mirror planes (one lies in the plane of the molecule) which divide the molecule into four quarters with three types of positions which

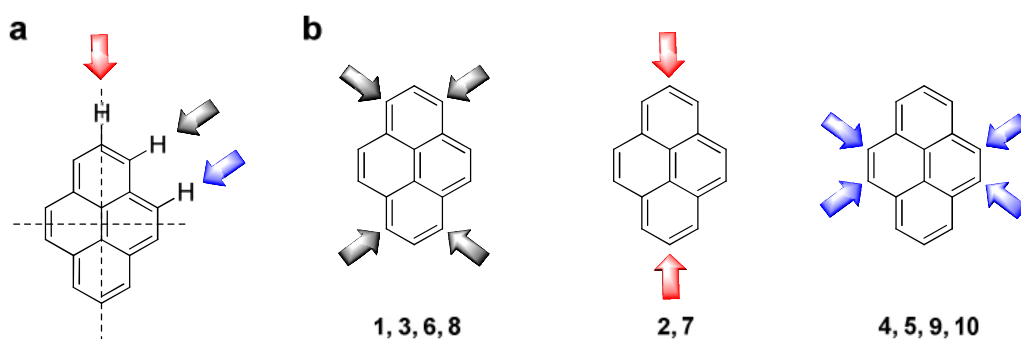
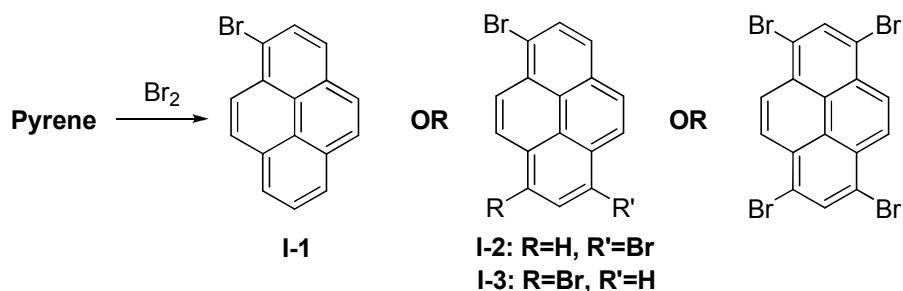


Figure 1.2: (a) Mirror plane showing three chemically distinguishable sites; (b) Three main groups of chemically identical sites.

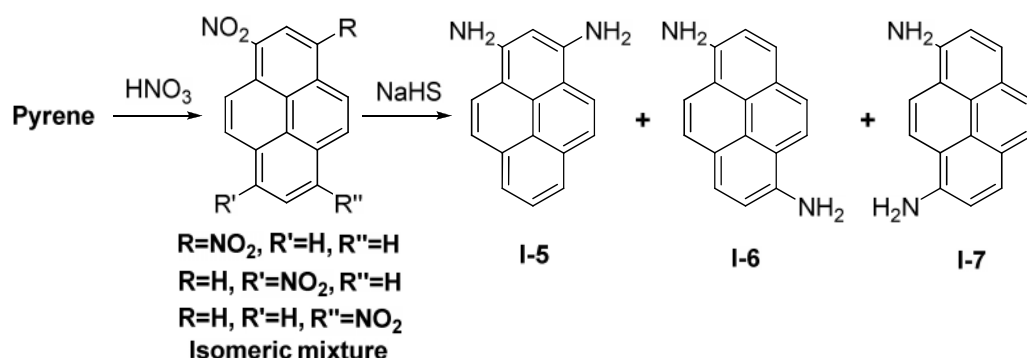
exhibit strong difference in chemical reactivity. Therefore, the overview about reported chemical methods to substitute pyrene is grouped into “1,3,6,8”, “2,7” and “4,5,9,10” in the following. Additionally, chemists have invented multi-step syntheses starting from benzene derivatives to achieve otherwise impossible substitution of pyrene. Those ones and methods utilizing combinations of the substitution patterns of the three main groups are included according to the synthetic order of reactions.

1.1.1 Positions 1, 3, 6 and 8

Reactivity of pyrene at positions 1, 3, 6 and 8 towards electrophiles arises from the large orbital coefficients at these carbon atoms. First protocols are reported 1937 by Vollmann et al. in his paper on the synthesis of mono-, double-, tri or tetra-substituted pyrene derivatives.^[15] By the appropriate amount of Br₂ the degree of bromination is controlled effectively (Scheme 1.1). An isomeric mixture of 1,6- and 1,8-dibromopyrene always results upon double bromination which cannot be separated by chromatography. Due to different solubility fractional crystallization can be used to separate the isomers **I-2** and **I-3**.^[16] By analogy to bromine mono- and tetrachloropyrene have also been reported.^[15]



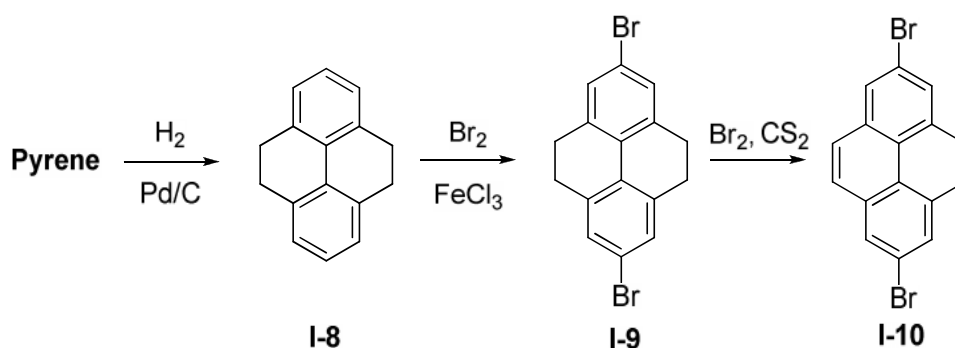
Scheme 1.1: Products of pyrene bromination.



Scheme 1.2: Nitration followed by reduction to the diaminopyrene isomers **I-5**, **I-6** and **I-7**.

An alternative to the troublesome fractional crystallization of dibromopyrene isomers might be given by the nitration of pyrene. The treatment of pyrene in concentrated nitric acid gives the tetra-nitrated pyrene derivative.^[15] Reaction in acetic acid and addition of the respective amount of nitric acid yields 1-nitropyrene or the isomeric mixture containing the 1,3-, 1,6- and 1,8-dinitro isomers in the ratio of 1:2:2 (Scheme 1.2).^[17] It is reported that after reduction to the diaminopyrene the separation by silica column chromatography makes all three isomers accessible. In contrast to halogenation and nitration the Friedel-Crafts acylation with benzoyl chloride and aluminum chloride is described to proceed only twice giving the expected 1,6- and 1,8-dibenzoylpyrene.^[15]

It can roughly be estimated from the pyrene derivatives shown in the review on pyrene-based materials for organic electronics^[7] that the derivatization at positions 1, 3, 6 and 8 has been used most frequently for substitution. Particularly bromopyrene derivatives are highly valuable because of the



Scheme 1.3: Synthesis of 2,7-dibromopyrene **I-10** in three steps.^[18]

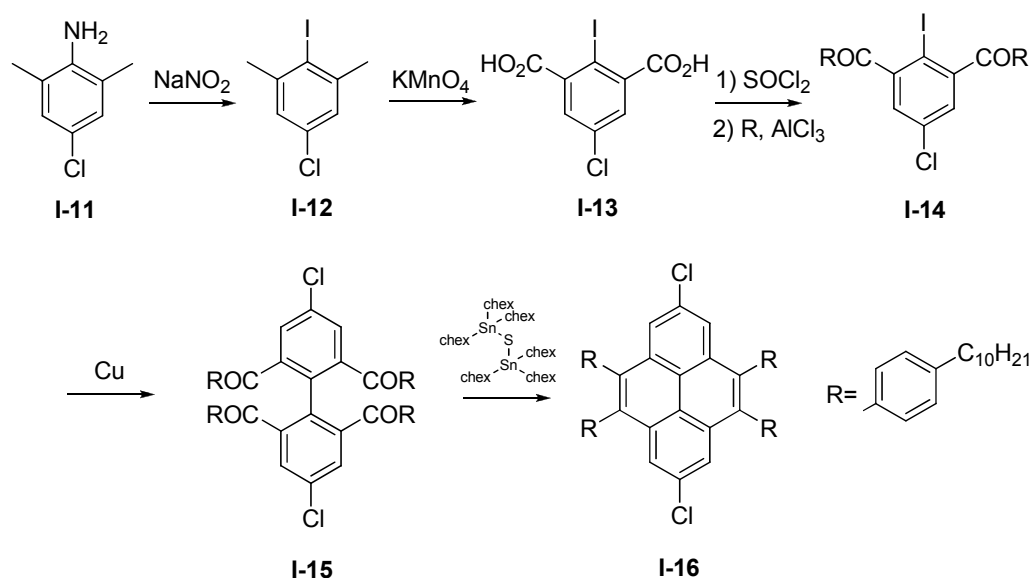
versatile use in palladium-catalyzed cross-coupling reactions like Suzuki, Stille, Sonogashira, and Buchwald-Hartwig.^[19]

1.1.2 Positions 2 and 7

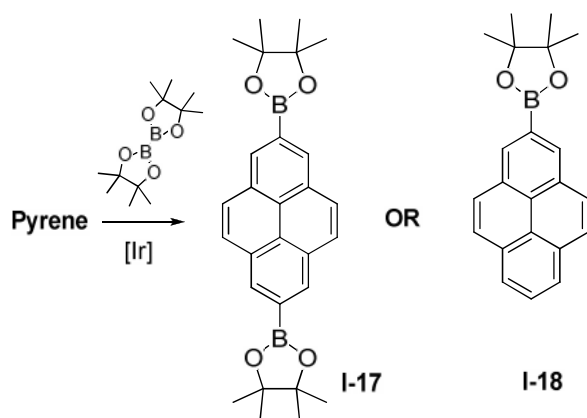
For a long time positions 2 and 7 could not be functionalized with reactive groups in one step. As no direct access has been available, chemists pursued multi-step routes to build 2,7-dihalopyrenes. Reduction of pyrene using palladium on carbon under hydrogen atmosphere at elevated pressure gives a mixture of reduced pyrene species. 4,5,9,10-Tetrahydropyrene **I-8** can be isolated by column chromatography (Scheme 1.3).^[20] Like biphenyl the tetrahydropyrene brominates in the 2,7 positions. Treatment with bromine in carbon disulfide gives **I-10** quantitatively.^[21]

Starting the synthesis from benzene derivative **I-11** Kawano et al. used a sophisticated route of five steps for the synthesis of 2,7-dichloro-4,5,9,10-tetraphenylpyrene as precursors for Yamamoto polymerization of poly(2,7-pyrenylene) (Scheme 1.4).^[18] Moreover, this route enabled the introduction of phenylalkyl substituents at positions 4, 5, 9 and 10, which will be discussed in more detail in the next section.

A breakthrough has been published in 2005 when Coventry et al. reported the iridium catalyzed direct conversion of pyrene with bis(pinacolato)diboron to



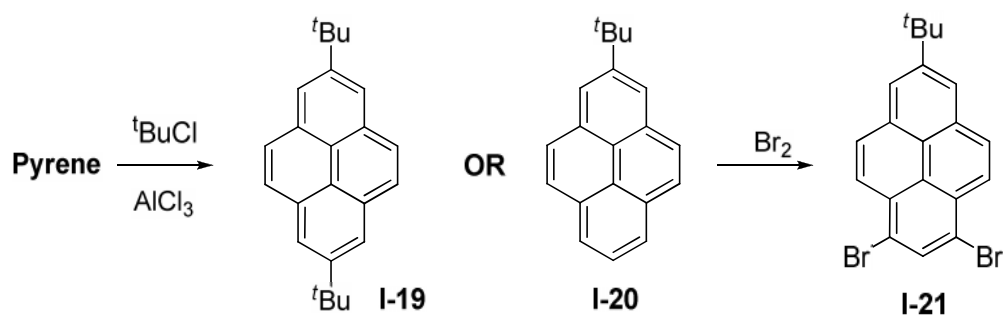
Scheme 1.4: Synthesis of 2,7-dichloro-4,5,9,10-tetraphenylpyrene **I-16**.



Scheme 1.5: Iridium catalyzed mono- and diborylation of pyrene.

give pyrene-2,7-bis(boronate) (Scheme 1.5).^[22] The authors ascribe the success of the reaction to the proposed key intermediate complex $[\text{Ir}(\text{bpy})(\text{Bpin})_3]$ of iridium, bipyridyl ligand and Bpin and its crowded nature, preferably activating the exposed C-H bonds at 2 and 7.

Although no reactive group is introduced, the treatment of pyrene with the Lewis acid aluminum chloride (AlCl_3) and *tert*-butyl chloride gives 2,7-di-*tert*-butyl pyrene **I-19** (Scheme 1.6).^[23-24] Equimolar ratio of pyrene and *tert*-butyl chloride enables mono-substituted species **I-20**.^[25-26] The site-selectivity most probably is determined by spatial effects.

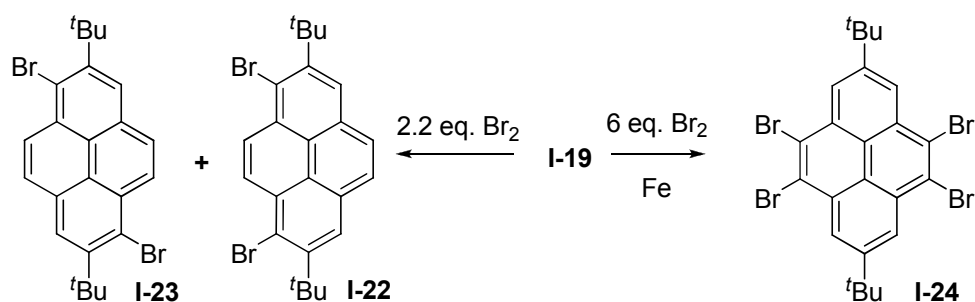


Scheme 1.6: *Tert*-butylation of pyrene at positions 2 and 7.

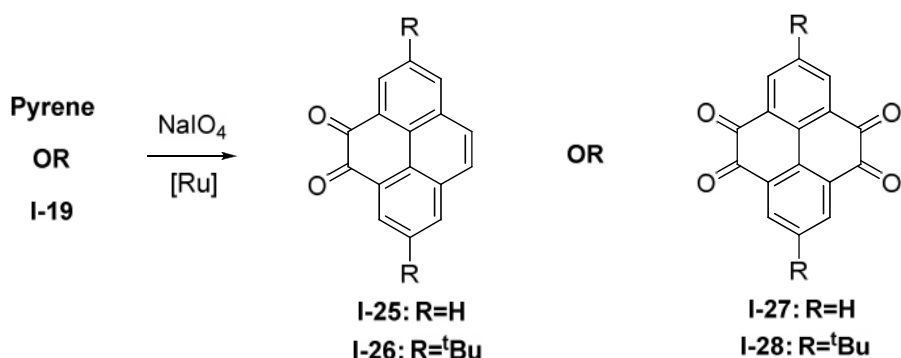
Even though *tert*-butyl groups cannot further be modified easily the importance of pyrene derivative **I-19** and **I-20** is not solely referred to the increased solubility. Teresa Figueira-Duarte from our research group used 2-(*tert*-butyl)pyrene **I-20** to block adjacent positions and further brominate exclusively positions 1 and 3.^[26] Compound **I-21** was used as monomer for the blue emitting poly(1,3-pyrene. In contrast to **I-20**, molecule **I-19** with two *tert*-butyl groups is used to direct bromination from 1, 3, 6 and 8 to difficultly accessible pyrene positions 4, 5, 9 and 10.

1.1.3 Positions 4, 5, 9 and 10

The four positions in the K-region of pyrene are neither accessible by the treatment with bromine as described above nor can bromination simply be redirected by spatial blocking of the positions 1, 3, 6 and 8 using bulky *tert*-butyl groups at positions 2,7 as one might expect. Instead, treatment of **I-19** with 2.2 equivalents of bromine gives a mixture of dibromo isomers **I-22** and **I-23** (Scheme 1.7). Tashiro et al. found out that under addition of iron powder and 6.0 equivalents Br_2 **I-24** is obtained exclusively and in 90 % yield.^[23, 27] The authors ascribe the formation of **I-24** to an in-situ generated FeBr_3 catalyzed isomerization which was confirmed by the isomerization of 1-bromo-2,7-di-*tert*-butylpyrene to 4-bromo-2,7-di-*tert*-butylpyrene after the addition of



Scheme 1.7: K-region directed bromination of **I-19**.

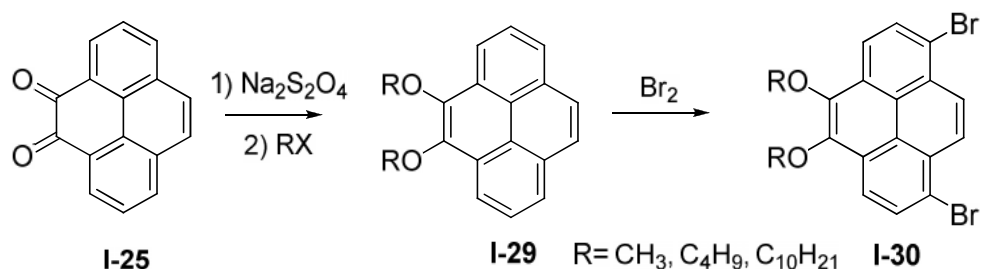


Scheme 1.8: Ruthenium-catalyzed oxidation of pyrene and 2,7-di-*tert*-butylpyrene to the respective 4,5-di- and 4,5,9,10-tetraketones.

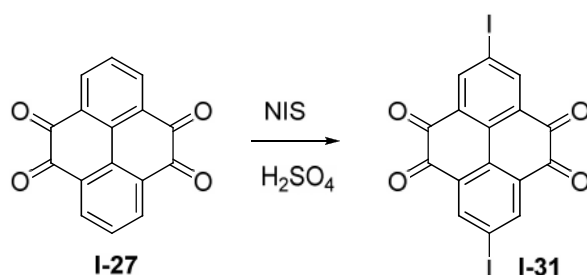
FeBr₃. Up to now, no other method is reported to direct halogens to these positions without *tert*-butyl groups.

As alternative to the bromination chemists have been working on OsO₄- and RuO₄-catalyzed oxidation at the K-region of pyrene using H₂O₂ and NaIO₄ but beside a number of byproducts **I-25** or **I-27** could only be obtained in very low yield.^[28] Another approach started from oxidation of pyrene to 4,5-phenanthrenedicarboxylic acid (H₂WO₄/H₂O₂) and subsequent esterification with MeI and intramolecular acyloin condensation with sodium in three steps to give **I-25**.^[29]

One-step and gram scale availability of di- and tetraketopyrenes **I-25** to **I-28** has finally been achieved by Hu et al. describing the oxidation of pyrenes and the *tert*-butylated derivative using RuCl₃ and NaIO₄ (Scheme 1.8).^[30] By the excess of oxidizing agent and the reaction temperature it can be



Scheme 1.9: Unexpected region selectivity of bromination of **I-29**.



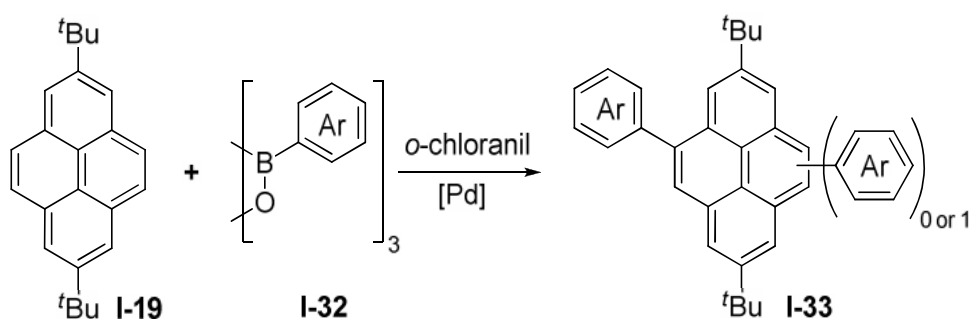
Scheme 1.10: Halogenation at positions 2 and 7 of pyrene-4,5,9,10-tetraone **I-27**.

controlled whether the di- or the tetraone is formed. Although yields between 36 % and 47 % are reported, these conditions are superior to the old routes and the article has nearly been cited 40 times so far, emphasizing the popularity of this method and the respective ketopyrenes **I-25** to **I-28**.

In parallel to this work, three groups published new methods for pyrene substitutions in 2010 and 2011. At first, Bodwell et al. reported the bromination at positions 1 and 8 of 4,5-dimethoxypyrene **I-29** (Scheme 1.9).^[31] The selectivity versus positions 3 and 6 is ascribed to spatial blocking of the alkoxy groups. The unique 1,8-substitution allowed 1,8-pyrenylene-ethynylene macrocycles with solubilizing alkoxy chains at positions 4 and 5 and is a current example for a new substitution pattern at the pyrene core.

Secondly, the introduction of iodine in 2,7 positions on pyrene-4,5,9,10-tetraone **I-27** was patented and published shortly after by two independent groups (Scheme 1.10).^[32-34]

Thirdly, novel C-H activated arylation in the K-region of pyrene, phenanthrene and benzo[*a*]anthracene has been described by Itami et al.



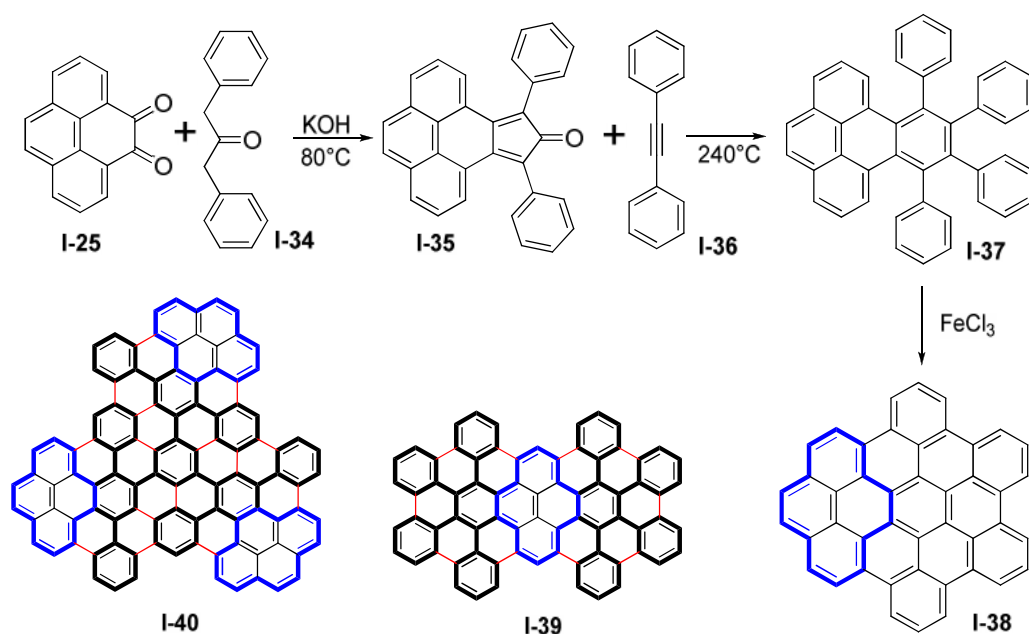
Scheme 1.11: C-H activated arylation of pyrene in the K-region.

(Scheme 1.11).^[35] Dependent on the excess of the boron compound, single or double arylation can be achieved, whereas an isomeric mixture of 4,9- and 4,10-diarylmethylpyrene **I-33** is obtained. This C-H activated arylation is applicable to bare pyrene and aryl compounds **I-32** being substituted with sterically demanding groups in *ortho* position.

To achieve an isomerically pure 4,10-substitution multi step synthesis as reported by Walker et al. must be used to obtain a 4,10-diiodopyrene derivatives.^[36]

1.1.4 Pyrene as Building Block for Large π -Conjugated Systems

K-region chemistry has been utilized for the syntheses of large aromatic discs **I-38**, **I-39** and **I-40** in Scheme 1.12. The sequence of three steps is exemplarily shown with the pyrene-4,5-dione **I-25** but the *tert*-butylated form **I-26** or the tetraone **I-28** for the synthesis of **I-39** could also be used. *Knoevenagel* condensation yields the cyclopentadienon derivative **I-35** applying potassium hydroxide as base to abstract a proton from **I-34**. *Diels-Alder* reaction with tolane **I-36** in diphenyl ether at 240°C gives **I-37** which is planarized to **I-38** via cyclodehydrogenation so-called *Scholl* reaction.^[37-39] Solubilizing peripheral substituents can easily be introduced by the choice of a respective ketone **I-34** or tolane **I-36**.



Scheme 1.12: Usage of pyrene as building block for the synthesis of large π -conjugated discs **I-38**,^[37, 40] **I-39**^[39] and **I-40**^[37] in the three subsequent steps of *Knoevenagel* condensation, *Diels-Alder* reaction and oxidative cyclodehydrogenation; blue: pyrene moiety, black bold: introduced phenyl rings, red: bonds formed by FeCl_3 ; peripheral alkyl substituents are omitted for simplicity.

Structures **I-38**, **I-39** and **I-40** are examples for the value of pyrene as building block which loses its inherent properties to be converted into a new class of carbon materials. The principle of the introduction of aryl substituents followed by oxidative cyclodehydrogenation shall be used later in this work.

1.2 Characterization Methods

The so far described synthetic methods in Chapter 1.1 lay the groundwork for the synthesis of novel pyrene-derived materials. Besides the investigation of the molecular properties of the new compounds is an important part of this work and common methods like UV/vis absorptions spectroscopy and cyclic voltammetry provide the possibility to study the electronic properties.

For the use of organic molecules in many applications like organic field-effect transistors (OFETs), organic photovoltaic cells (OPVCs) and organic light emitting diodes (OLEDs) the properties are closely related to the molecular order which points towards the need of the careful investigation of the non-covalent assembly. For instance, the performance of OFETs is strongly dependent on the interactions between the organic molecules which are responsible for the formation of a conduction path.^[41] Due to the importance of OFETs for this work, their working principle is briefly explained in subchapter 1.2.4.

In the following, characterization methods and techniques are briefly described which allow insights into the molecular ordering in the solid state and the liquid-solid interface.

1.2.1 X-Ray Crystallography

Irradiation of solid samples with X-ray beams causes scattering at the electron surface of atoms and diffraction patterns can be recorded. The investigation of single crystals of organic molecules with X-ray has firstly been reported in 1923^[42] and has grown to a mostly standardized method nowadays.

Scattering by crystals from good quality and a dimension of at least 0.1 mm^3 gives sharp reflection patterns which are recorded upon irradiation from gradually changed angles. The whole set of patterns can be combined into a three-dimensional reflection pattern which enables mathematically complex

calculation of the mean chemical bond lengths, angles and the intermolecular distances. X-Ray crystallography is the most valuable tool for the unambiguous determination of molecular structure and the molecular packing in high resolution. Thus, distortion phenomena, packing parameters and close contacts can be revealed. Unfortunately, this method is limited by crystal size as well as crystal quality, and hence, restricted to rather small molecules.

1.2.2 2D Wide Angle X-Ray Scattering

Larger and non-crystalline molecules like polymers or highly alkylated discotic molecules do not form perfect and highly packed crystals but can still exhibit a supramolecular order arising from π - π -interactions, van der Waals forces, dipole-dipole interactions or electrostatic interactions. Two-dimensional wide-angle X-ray scattering (2D WAXS) can be utilized for the exploration of those materials and to determine their order.^[43-45]

Therefore, the material is extruded into a fiber at elevated temperature with an inner diameter of 0.7 mm (Figure 1.3). During this process an orientation of the molecules along the extrusion can occur. The fiber is orientated perpendicularly to the incident X-ray beam and the reflection pattern is recorded.^[44] For the interpretation of results from 2D WAX scattering it has to be taken into account that sheer forces during the extrusion process significantly affect the orientation of the molecules.

From this pattern, information about the intra- and intercolumnar supramolecular organization can be obtained. The meridional reflections provide information about the disc stacking and the equatorial reflections distribution gives insight into the intercolumnar order. A heating unit enables the measurement at various temperatures, and thus, parameters like π -stacking distances and intercolumnar distances can be determined in dependence of the temperature.

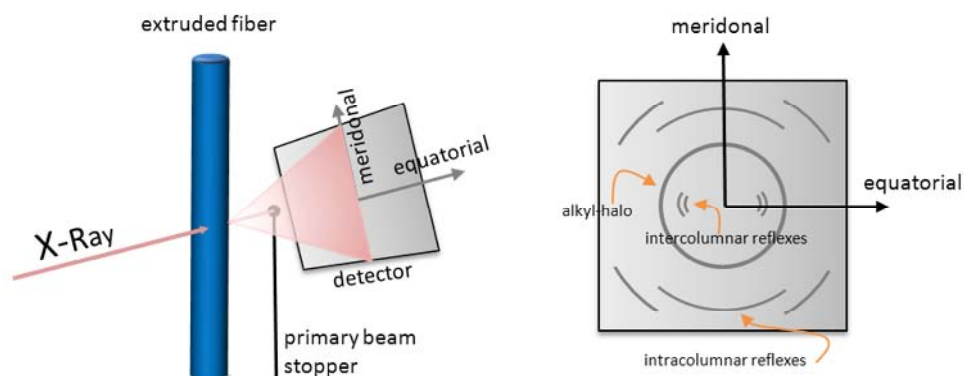


Figure 1.3: Experimental 2D WAXS setup for the investigation of extruded fibers and typical reflexes from discotic liquid crystals.

1.2.3 Scanning Tunneling Microscopy

STM was invented by scientists at the IBM Zürich Research Centre in 1981 based on the electrons tunneling through vacuum between a metal tip and a platinum sample.^[46] In contrast to electron microscopes which utilize electrons of high energy, the electrons involved in STM have low energy allowing non-destructive atomic resolution imaging. A great advantage of STM is the working ability in air, in liquid and in vacuum because there are no free electrons involved. This nowadays widespread method enables the visualization of atomic scale structures and processes and to image atomic structures directly in real space. Like in this study, STM can be applied for the investigation of self-assembling molecules on the liquid/solid interface.^[47-48]

The STM working principle is rather simple.^[46, 49] The precondition and likewise limitation of STM is the need of a conducting tip and sample. A bias voltage is applied and the tip is brought close to the sample surface (~ 1 nm). The space can be vacuum, air, liquid, adsorbate or liquid/adsorbate. Due to the applied bias voltage and the short distance between the tip and the sample surface, electrons are able to tunnel between the two electrodes. This tunneling current is used to probe the physical properties locally at the sample surface as well as to control the distance between the tip and sample.

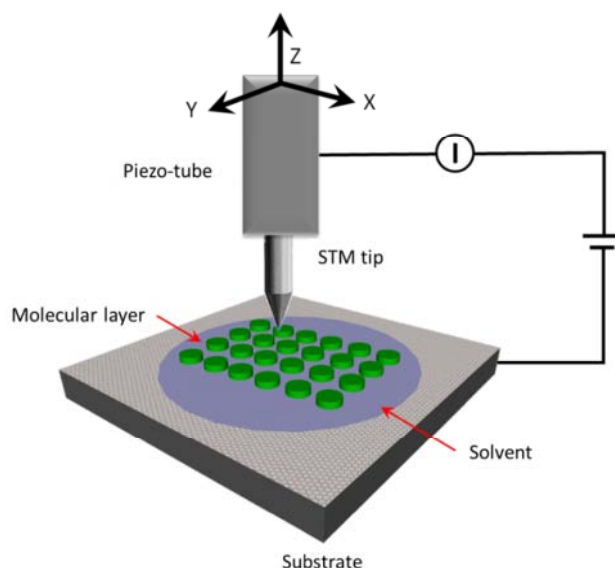


Figure 1.4: Schematic setup of a Scanning Tunneling Microscope (STM).

The tip is mounted on a piezoelectric element and can be raster scanned across the sample surface (Figure 1.4). STM can be operated in *constant height* or *constant current* mode, whereas the latter one is used for investigations in this work and most widely operated. In *constant current* mode, a feedback circuit regulates the tip sample distance to keep the detected tunneling current at a preset value. The tip is scanned along x and y co-ordinates over the surface, while it follows the contours of the surface. Whenever the tip detects higher (lower) topography and/or larger tunneling current, the tip accordingly moves up (down) in the z-direction. Although such an image shows a quasi topography, its interpretation is complicated by the contribution of electronic features of the surface in the image. A more proper way to interpret this type of image is to regard it as a contour of constant charge density, containing properties of both, tip and sample.

In *constant height* mode the voltage and height are both held constant while scanning, whereas the current changes in order to keep the height constant. Variations in the tunneling current are recorded and mapped to produce an image. A precondition for this method is that the sample surface must be nearly atomically flat.

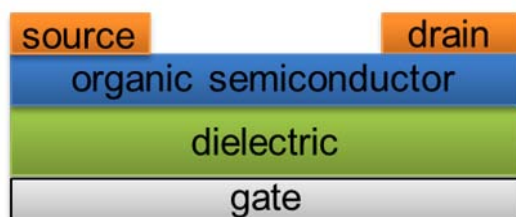


Figure 1.5: Popular geometry of simplified OFET: bottom gate, top contact configuration.

1.2.4 Organic Field-Effect Transistors

In order to test organic materials for their semiconductive properties it is incorporated into a field-effect transistor. A common setup depicted in Figure 1.5 schematically. The organic semiconductor is deposited onto a dielectric which separates the source and drain electrodes from the gate electrode. Application of a gate voltage (V_{SG}) between gate and source electrode creates an electric field which induces the accumulation of charges in the semiconductive layer also referred to as field-effect. The current between source and drain (I_{SD}) passing through the organic material is modulated by V_{SG} .^[41]

To evaluate the transistor performance, output (I_{SD} against V_{SD} ; at fixed V_{SG}) and transfer curves (I_{SD} against V_{SG} ; at fixed V_{SD}) are recorded and thereof threshold voltage (V_T), on/off ratio and charge carrier mobility (μ) are determined, three characteristic parameters to evaluate the transistor performance. The on/off ratio is the current ratio of the “on”- and “off”-state of the transistor and the threshold voltage describes the gate voltage (V_{SG}) at which conductivity through the organic material can be measured. The charge carrier mobility given in $\text{cm}^2\text{V}^{-1}\text{s}^{-1}$ characterizes the quickness of charges moving through the semiconductor and is an important criterion for organic material applied in the FETs.

1.3 Bibliography

- [1] E. Bamberger, M. Philip, *Justus Liebigs Annalen der Chemie* **1887**, 240, 147-192.
- [2] C. Gräbe, *Justus Liebigs Annalen der Chemie* **1871**, 158, 285-299.
- [3] G. Goldschmiedt, *Justus Liebigs Annalen der Chemie* **1907**, 351, 218-232.
- [4] J. P. Lowe, B. D. Silverman, *Accounts of Chemical Research* **1984**, 17, 332-338.
- [5] S. H. Goh, R. G. Harvey, *Journal of the American Chemical Society* **1973**, 95, 242-243.
- [6] R. M. Moriarty, P. Dansette, D. M. Jerina, *Tetrahedron Letters* **1975**, 2557-2560.
- [7] T. M. Figueira-Duarte, K. Müllen, *Chemical Reviews* **2011**, 111, 7260-7314.
- [8] J. B. Birks, I. H. Munro, D. J. Dyson, *Proceedings of the Royal Society of London Series a-Mathematical and Physical Sciences* **1963**, 275, 575-+.
- [9] C. Bohne, E. B. Abuin, J. C. Scaiano, *Journal of the American Chemical Society* **1990**, 112, 4226-4231.
- [10] F. Hauke, A. Hirsch, S. Atalick, D. Guldi, *European Journal of Organic Chemistry* **2005**, 1741-1751.
- [11] J. Duhamel, *Accounts of Chemical Research* **2006**, 39, 953-960.
- [12] A. K. Mathew, H. Siu, J. Duhamel, *Macromolecules* **1999**, 32, 7100-7108.
- [13] G. S. Jackson, R. A. Staniforth, D. J. Halsall, T. Atkinson, J. J. Holbrook, A. R. Clarke, S. G. Burston, *Biochemistry* **1993**, 32, 2554-2563.
- [14] K. Jung, H. Jung, J. H. Wu, G. G. Prive, H. R. Kaback, *Biochemistry* **1993**, 32, 12273-12278.
- [15] H. Vollmann, H. Becker, M. Corell, H. Streeck, *Justus Liebigs Annalen der Chemie* **1937**, 531, 1-159.
- [16] J. Grimshaw, Trochagr.J, *Journal of the Chemical Society-Perkin Transactions I* **1972**, 1622-&.
- [17] Y. Hashimoto, K. Shudo, *Chemical & Pharmaceutical Bulletin* **1984**, 32, 1992-1994.
- [18] S. I. Kawano, C. Yang, M. Ribas, S. Balushev, M. Baumgarten, K. Müllen, *Macromolecules* **2008**, 41, 7933-7937.
- [19] X.-F. Wu, P. Anbarasan, H. Neumann, M. Beller, *Angewandte Chemie International Edition* **2010**, 49, 9047-9050.
- [20] P. P. Fu, H. M. Lee, R. G. Harvey, *Journal of Organic Chemistry* **1980**, 45, 2797-2803.
- [21] H. Lee, R. G. Harvey, *Journal of Organic Chemistry* **1986**, 51, 2847-2848.

- [22] D. N. Coventry, A. S. Batsanov, A. E. Goeta, J. A. K. Howard, T. B. Marder, R. N. Perutz, *Chemical Communications* **2005**, 2172-2174.
- [23] T. Yamato, M. Fujimoto, A. Miyazawa, K. Matsuo, *Journal of the Chemical Society-Perkin Transactions I* **1997**, 1201-1207.
- [24] J. Pataki, M. Konieczny, R. G. Harvey, *Journal of Organic Chemistry* **1982**, 47, 1133-1136.
- [25] Y. Miura, E. Yamano, A. Tanaka, J. Yamauchi, *Journal of Organic Chemistry* **1994**, 59, 3294-3300.
- [26] T. M. Figueira-Duarte, P. G. Del Rosso, R. Trattnig, S. Sax, E. J. W. List, K. Müllen, *Advanced Materials* **2010**, 22, 990-993.
- [27] M. Tashiro, T. Yamato, *Journal of the American Chemical Society* **1982**, 104, 3701-3707.
- [28] F. G. Oberender, J. A. Dixon, *Journal of Organic Chemistry* **1959**, 24, 1226-1229.
- [29] E. R. R. Young, R. L. Funk, *Journal of Organic Chemistry* **1998**, 63, 9995-9996.
- [30] J. Hu, D. Zhang, F. W. Harris, *Journal of Organic Chemistry* **2005**, 70, 707-708.
- [31] G. Venkataramana, P. Dongare, L. N. Dawe, D. W. Thompson, Y. M. Zhao, G. J. Bodwell, *Organic Letters* **2011**, 13, 2240-2243.
- [32] S. I. Kawano, M. Baumgarten, K. Müllen, T. Murer, T. Schaefer, M. Saleh, in *WO2010006852*, **2010**.
- [33] J. A. Letizia, S. Cronin, R. P. Ortiz, A. Facchetti, M. A. Ratner, T. J. Marks, *Chemistry-a European Journal* **2010**, 16, 1911-1928.
- [34] S. I. Kawano, M. Baumgarten, D. Chercka, V. Enkelmann, K. Müllen, *to be submitted*.
- [35] K. Mochida, K. Kawasumi, Y. Segawa, K. Itami, *Journal of the American Chemical Society* **2011**, 133, 10716-10719.
- [36] D. B. Walker, J. Howgogo, A. P. Davis, *Synthesis-Stuttgart* **2010**, 3686-3692.
- [37] Z. H. Wang, E. Tomovic, M. Kastler, R. Pretsch, F. Negri, V. Enkelmann, K. Müllen, *Journal of the American Chemical Society* **2004**, 126, 7794-7795.
- [38] M. Kastler, J. Schmidt, W. Pisula, D. Sebastiani, K. Müllen, *Journal of the American Chemical Society* **2006**, 128, 9526-9534.
- [39] D. Wasserfallen, M. Kastler, W. Pisula, W. A. Hofer, Y. Fogel, Z. H. Wang, K. Müllen, *Journal of the American Chemical Society* **2006**, 128, 1334-1339.
- [40] K. Müllen, Y. Fogel, M. Kastler, Z. H. Wang, D. Andrienko, G. J. Bodwell, *Journal of the American Chemical Society* **2007**, 129, 11743-11749.
- [41] M. Mas-Torrent, C. Rovira, *Chemical Reviews* **2011**, 111, 4833-4856.
- [42] R. G. Dickinson, A. L. Raymond, *Journal of the American Chemical Society* **1923**, 45, 22-29.
- [43] K. Tashiro, S. Sasaki, *Progress in Polymer Science* **2003**, 28, 451-519.

-
- [44] W. Pisula, Z. Tomovic, C. Simpson, M. Kastler, T. Pakula, K. Müllen, *Chemistry of Materials* **2005**, *17*, 4296-4303.
- [45] I. Fischbach, T. Pakula, P. Minkin, A. Fechtenkotter, K. Müllen, H. W. Spiess, K. Saalwachter, *Journal of Physical Chemistry B* **2002**, *106*, 6408-6418.
- [46] D. A. Bonnell, *Scanning Tunneling Microscopy and Spectroscopy*, VCH Publishers, Inc., New York, **1993**.
- [47] P. Samori, J. P. Rabe, *Journal of Physics-Condensed Matter* **2002**, *14*, 9955-9973.
- [48] S. B. Lei, K. Tahara, X. L. Feng, S. H. Furukawa, F. C. De Schryver, K. Müllen, Y. Tobe, S. De Feyter, *Journal of the American Chemical Society* **2008**, *130*, 7119-7129.
- [49] G. Binnig, H. Rohrer, *Helvetica Physica Acta* **1982**, *55*, 726-735.

2 Objectives and Motivation

Pyrene is a well-studied and fascinating organic molecule because of its unique optical properties. More precisely, because of its emission of light and the application as fluorescence probe and light-emitting material pyrene has been termed as the “fruit fly of photochemists”.^[1-12] In respect to its chemistry the polycyclic aromatic hydrocarbon (PAH) skeleton of pyrene bears 10 C-H positions which have been relentlessly treated by chemists for the purpose of site selectivity and functional diversity. Within the last 80 years a considerable number of protocols has been reported and recent progress towards new methods militates for the current interest in new pyrene derivatives.^[13-18]

In this work, pyrene has been chosen as structural core motif with the focus on the two K-regions and the development of new synthetic accessibilities. The K-regions of pyrene have often been addressed for the extension of the conjugate system.^[19-22] Similar to phenanthrene and other PAHs containing one or more K-regions, pyrene can be oxidized to the respective α -diketone.^[15, 23-25] This step strongly alters the electronic properties and the reactivity and might enable novel substitution patterns on the pyrene core.

The approach presented here aims at the asymmetric substitution of pyrene's positions 4,5 versus 9,10 (Figure 2.1) for the purpose of bifunctional substitution of the aromatic core. The implementation of asymmetric

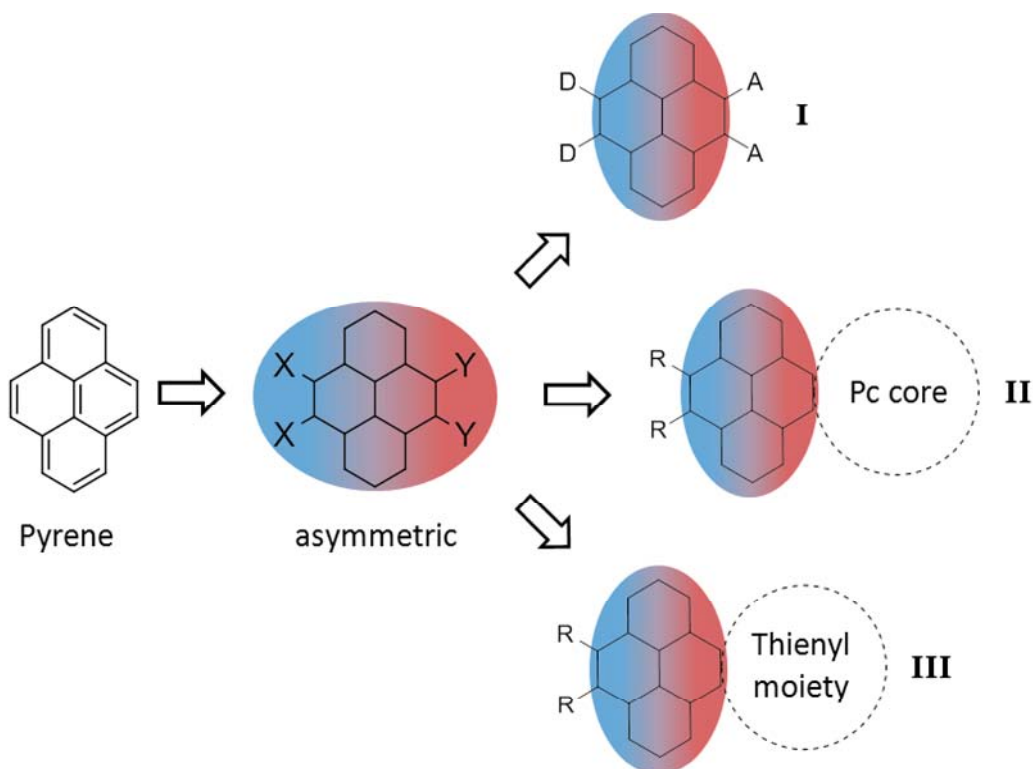


Figure 2.1: Schematic illustration of asymmetric substitution pattern of pyrene opening into concepts I, II and III.

substitution patterns on PAHs has always been a great challenge for organic chemists. Consequently, the development of such a protocol for the K-regions of pyrene plays a key role in this work and shall be based on the α -diketone at one side of pyrene. Concerning the second function, orthogonal reactivity to the α -diketone is required in order to ensure selective addressability.

Halogen functionalization oppositely to the α -diketone meets these requirements and represents a flexible and broadly applicable synthetic concept. Among others, highly versatile palladium-catalyzed cross-coupling reactions shall be enabled by this approach.^[26-27]

In the next step, the choice and especially the combination of substituents shall open the way to novel pyrene derived materials. Arising from the asymmetric pyrene building block (Figure 2.1 and Figure 2.2), four conceptional substitution patterns shall be targeted:

- I. **Donor versus acceptor** substitution is a widespread approach to narrow the energy gap between the frontier orbitals.^[28-29] In the case of oppositely located K-regions a permanent dipole shall be induced in order to direct molecular orientation.
- II. Phthalocyanines (Pcs) constitute an important class of organic dyes. Extension of Pcs aromatic residues strongly alters their optical properties.^[30] **One-sided fusion** of pyrene at 4, 5 to the Pc core for π -extension and **flexible chains** in the opposite at 9, 10 are supposed to render three targets possible: tuning the absorption, providing solubility, rigid core/flexible shell motif for self-assembly.^[31-33]
- III. Combination of **thiophene, alkyl chains** and the flat pyrene π -spacer in between for solution processable semiconductive materials. Plain pyrene exhibits a pronounced order in the solid state as a consequence of π -stacking and its tendency to crystallize.^[34-36] Such features like close π - π -distances and highly ordered packing are believed to be an important characteristic for active materials in organic field-effect transistors (OFETs).^[37-38] Pyrene derived materials have already been applied in OFETs successfully.^[39-42]
- IV. Conversion of pyrene **from an asymmetric to a symmetric** K-region building block for palladium-catalyzed cross-coupling reactions shall be applied to construct uniquely shaped PAHs (Figure 2.2).

The last stated concept focuses on the symmetric K-region arylation and the modular use of the aromatic pyrene scaffold. Synthetically, the reductive conversion of ketones to triflates shall be realized because triflates are known to undergo palladium-catalyzed cross-coupling reactions as halide analogons.^[27, 43-44] As illustrated in Figure 2.2 the shape of the pyrene core (bold black) provides the possibility for the syntheses of differently rimmed PAHs. *Armchair*^[45-48] and *zig-zag* edges,^[46, 49] *cove*^[50] and *fford*^[51] regions crucially influence molecular characteristics like electronic properties, reactivity, stability, three-dimensional shape, solubility or chirality, which strongly motivates the build-up of such structures using the pyrene core.

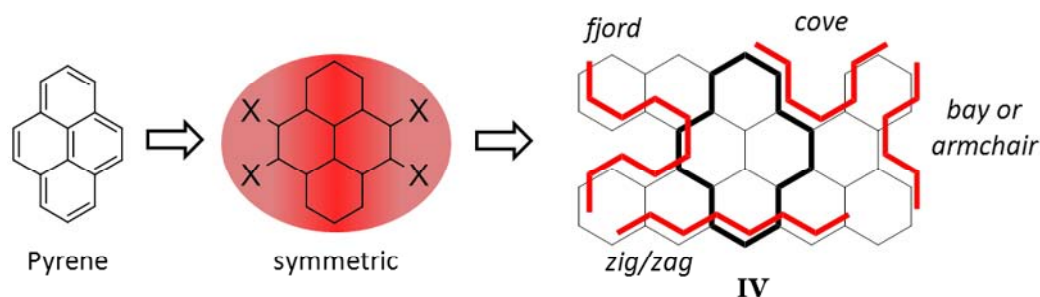


Figure 2.2: Symmetric substitution for concept **IV**; *bay* or *armchair*, *cove*, *fjord* and *zig/zag* motifs on pyrene related PAH.

Peri-pentacene exhibits a rectangular shape with *zig-zag* edges at the long sides (10 bonds long) and one *armchair* motif at the short sides (compare **IV**, Figure 2.2). It belongs to the PAH subclass of *peri*-acenes and the synthesis shall be targeted in this work using a pyrene-based approach. *Peri*-acenes are of high interest as structurally well-defined graphene fragments in order to study and understand the electronic and magnetic characteristics of graphene.^[52-53] So far, higher *peri*-acenes from *peri*-tetracene onwards have not been realized synthetically mostly likely due to missing methods and expected instability.^[52, 54]

Generally spoken, this work aims for a chemically and structurally driven approach towards new pyrene derived materials. Beside standard analytical techniques, X-ray scattering of crystalline and waxy materials and Scanning Tunneling Microscopy will be utilized to reveal molecular packing and self-assembly properties. Such investigations hold promise for a detailed understanding of the intermolecular interactions determining the arrangement in bulk and at the liquid-solid interface. These findings on the molecular level will be correlated to the molecular structure and the material properties.

2.1 Bibliography

- [1] R. Rieger, K. Müllen, *Journal of Physical Organic Chemistry* **2010**, 23, 315-325.
- [2] T. M. Figueira-Duarte, K. Müllen, *Chemical Reviews* **2011**, 111, 7260-7314.
- [3] J. Duhamel, *Accounts of Chemical Research* **2006**, 39, 953-960.
- [4] H. Maeda, T. Maeda, K. Mizuno, K. Fujimoto, H. Shimizu, M. Inouye, *Chemistry-a European Journal* **2006**, 12, 824-831.
- [5] B. Geffroy, P. Le Roy, C. Prat, *Polymer International* **2006**, 55, 572-582.
- [6] C. Tang, F. Liu, Y. J. Xia, J. Lin, L. H. Xie, G. Y. Zhong, Q. L. Fan, W. Huang, *Organic Electronics* **2006**, 7, 155-162.
- [7] K. C. Wu, P. J. Ku, C. S. Lin, H. T. Shih, F. I. Wu, M. J. Huang, J. J. Lin, I. C. Chen, C. H. Cheng, *Advanced Functional Materials* **2008**, 18, 67-75.
- [8] H. Oh, C. Lee, S. Lee, *Organic Electronics* **2009**, 10, 163-169.
- [9] C. Bohne, E. B. Abuin, J. C. Scaiano, *Journal of the American Chemical Society* **1990**, 112, 4226-4231.
- [10] G. S. Jackson, R. A. Staniforth, D. J. Halsall, T. Atkinson, J. J. Holbrook, A. R. Clarke, S. G. Burston, *Biochemistry* **1993**, 32, 2554-2563.
- [11] K. Jung, H. Jung, J. H. Wu, G. G. Prive, H. R. Kaback, *Biochemistry* **1993**, 32, 12273-12278.
- [12] J. B. Birks, I. H. Munro, D. J. Dyson, *Proceedings of the Royal Society of London Series a-Mathematical and Physical Sciences* **1963**, 275, 575-+.
- [13] H. Vollmann, H. Becker, M. Corell, H. Streeck, *Justus Liebigs Annalen Der Chemie* **1937**, 531, 1-159.
- [14] M. Tashiro, T. Yamato, *Journal of the American Chemical Society* **1982**, 104, 3701-3707.
- [15] J. Hu, D. Zhang, F. W. Harris, *Journal of Organic Chemistry* **2005**, 70, 707-708.
- [16] D. N. Coventry, A. S. Batsanov, A. E. Goeta, J. A. K. Howard, T. B. Marder, R. N. Perutz, *Chemical Communications* **2005**, 2172-2174.
- [17] G. Venkataramana, P. Dongare, L. N. Dawe, D. W. Thompson, Y. M. Zhao, G. J. Bodwell, *Organic Letters* **2011**, 13, 2240-2243.
- [18] K. Mochida, K. Kawasumi, Y. Segawa, K. Itami, *Journal of the American Chemical Society* **2011**, 133, 10716-10719.
- [19] K. Müllen, Y. Fogel, M. Kastler, Z. H. Wang, D. Andrienko, G. J. Bodwell, *Journal of the American Chemical Society* **2007**, 129, 11743-11749.
- [20] L. X. Wang, B. X. Gao, M. Wang, Y. X. Cheng, X. B. Jing, F. S. Wang, *Journal of the American Chemical Society* **2008**, 130, 8297-8306.

- [21] N. Kulisic, S. More, A. Mateo-Alonso, *Chemical Communications* **2011**, 47, 514-516.
- [22] D. Wasserfallen, M. Kastler, W. Pisula, W. A. Hofer, Y. Fogel, Z. H. Wang, K. Müllen, *Journal of the American Chemical Society* **2006**, 128, 1334-1339.
- [23] R. Wendland, J. Lalonde, *Organic Syntheses* **1954**, 34, 76-78.
- [24] R. Rieger, M. Kastler, V. Enkelmann, K. Müllen, *Chemistry-a European Journal* **2008**, 14, 6322-6325.
- [25] Z. H. Wang, E. Tomovic, M. Kastler, R. Pretsch, F. Negri, V. Enkelmann, K. Müllen, *Journal of the American Chemical Society* **2004**, 126, 7794-7795.
- [26] X.-F. Wu, P. Anbarasan, H. Neumann, M. Beller, *Angewandte Chemie International Edition* **2010**, 49, 9047-9050.
- [27] N. Miyaura, A. Suzuki, *Chemical Reviews* **1995**, 95, 2457-2483.
- [28] J. Roncali, *Chemical Reviews* **1997**, 97, 173-205.
- [29] Y. Yamashita, M. Tomura, *Journal of Materials Chemistry* **1998**, 8, 1933-1944.
- [30] E. Orti, M. C. Piqueras, R. Crespo, J. L. Bredas, *Chemistry of Materials* **1990**, 2, 110-116.
- [31] B. Tylleman, G. Gbabode, C. Amato, C. Buess-Herman, V. Lemaure, J. Cornil, R. G. Aspe, Y. H. Geerts, S. Sergeyev, *Chemistry of Materials* **2009**, 21, 2789-2797.
- [32] M. Kastler, W. Pisula, D. Wasserfallen, T. Pakula, K. Müllen, *Journal of the American Chemical Society* **2005**, 127, 4286-4296.
- [33] W. Pisula, Z. Tomovic, C. Simpson, M. Kastler, T. Pakula, K. Müllen, *Chemistry of Materials* **2005**, 17, 4296-4303.
- [34] S. Ohmori, S. Ito, M. Yamamoto, *Macromolecules* **1990**, 23, 4047-4053.
- [35] T. M. Figueira-Duarte, P. G. Del Rosso, R. Trattnig, S. Sax, E. J. W. List, K. Müllen, *Advanced Materials* **2010**, 22, 990-993.
- [36] Z. Q. Wang, C. Xu, W. Z. Wang, X. M. Dong, B. T. Zhao, B. M. Ji, *Dyes and Pigments* **2012**, 92, 732-736.
- [37] M. Mas-Torrent, C. Rovira, *Chemical Reviews* **2011**, 111, 4833-4856.
- [38] J. E. Anthony, B. Purushothaman, *Organic Field-Effect Transistors Vi* **2007**, 6658, L6580-L6580.
- [39] H. J. Zhang, Y. Wang, K. Z. Shao, Y. Q. Liu, S. Y. Chen, W. F. Qiu, X. B. Sun, T. Qi, Y. Q. Ma, G. Yu, Z. M. Su, D. B. Zhu, *Chemical Communications* **2006**, 755-757.
- [40] M. Ashizawa, K. Yamada, A. Fukaya, R. Kato, K. Hara, J. Takeya, *Chemistry of Materials* **2008**, 20, 4883-4890.
- [41] F. Moggia, C. Videlot-Ackermann, J. Ackermann, P. Raynal, H. Brisset, F. Fages, *Journal of Materials Chemistry* **2006**, 16, 2380-2386.
- [42] Y. Wang, H. M. Wang, Y. Q. Liu, C. A. Di, Y. M. Sun, W. P. Wu, G. Yu, D. Q. Zhang, D. B. Zhu, *Journal of the American Chemical Society* **2006**, 128, 13058-13059.

- [43] P. Espinet, A. M. Echavarren, *Angewandte Chemie-International Edition* **2004**, *43*, 4704-4734.
- [44] V. Farina, V. Krishnamurthy, W. J. Scott, in *Organic Reactions*, John Wiley & Sons, Inc., **2004**.
- [45] J. M. Cai, P. Ruffieux, R. Jaafar, M. Bieri, T. Braun, S. Blankenburg, M. Muoth, A. P. Seitsonen, M. Saleh, X. L. Feng, K. Müllen, R. Fasel, *Nature* **2010**, *466*, 470-473.
- [46] D. E. Jiang, S. Dai, *Chemical Physics Letters* **2008**, *466*, 72-75.
- [47] E. H. Fort, P. M. Donovan, L. T. Scott, *Journal of the American Chemical Society* **2009**, *131*, 16006-16007.
- [48] J. L. Li, C. J. Jiao, K. W. Huang, J. S. Wu, *Chemistry-a European Journal* **2011**, *17*, 14672-14680.
- [49] B. Purushothaman, M. Bruzek, S. R. Parkin, A. F. Miller, J. E. Anthony, *Angewandte Chemie-International Edition* **2011**, *50*, 7013-7017.
- [50] A. Mukherjee, K. Pati, R. S. Liu, *Journal of Organic Chemistry* **2009**, *74*, 6311-6314.
- [51] Y. Shen, C.-F. Chen, *Chemical Reviews* **2011**.
- [52] Z. Sun, J. S. Wu, *Journal of Materials Chemistry* **2012**, *22*, 4151-4160.
- [53] D. E. Jiang, B. G. Sumpter, S. Dai, *Journal of Chemical Physics* **2007**, *127*.
- [54] J. Aihara, *Physical Chemistry Chemical Physics* **1999**, *1*, 3193-3197.

3 Donor/Acceptor Pyrenes

3.1 Introduction

Aromatic molecules being substituted with electron-withdrawing and -donating groups have been in the focus of research for long time.^[1-2] Commonly, π -systems bridge donor and acceptor moiety and the resulting push-pull effect comes along with a decrease of the energy gap.^[3-4] This class of materials has been discussed for potential application in optoelectronic devices due to long-wavelength absorption (near-IR dyes) and their electroluminescence properties.^[5-6] Small donor/acceptor substituted π -systems are further known to interact non-linearly with light. Being referred to as nonlinear optics (NLOs), this field of research is of high interest among physicists.^[4, 7-8] Beaded alternately in a chain, donor- and acceptor-moieties in polymers are often used in OFETs and OPVCs.^[9-10] The low band gap of those polymers makes them especially valuable for the absorption of sun light and the conversion into electric current.^[11]

Synthetically, quite a few donor OR acceptor substituted pyrenes are reported. Just to mention some, the acceptors 4,5,9,10-tetraketo-,^[12] 4,5,9,10-tetracyano-,^[13] 1,3,6,8-tetranitro-^[14] and 1,3,6,8-tetracyanopyrene^[14] derivatives are easily accessible molecules. Enumerating donors, a whole series of

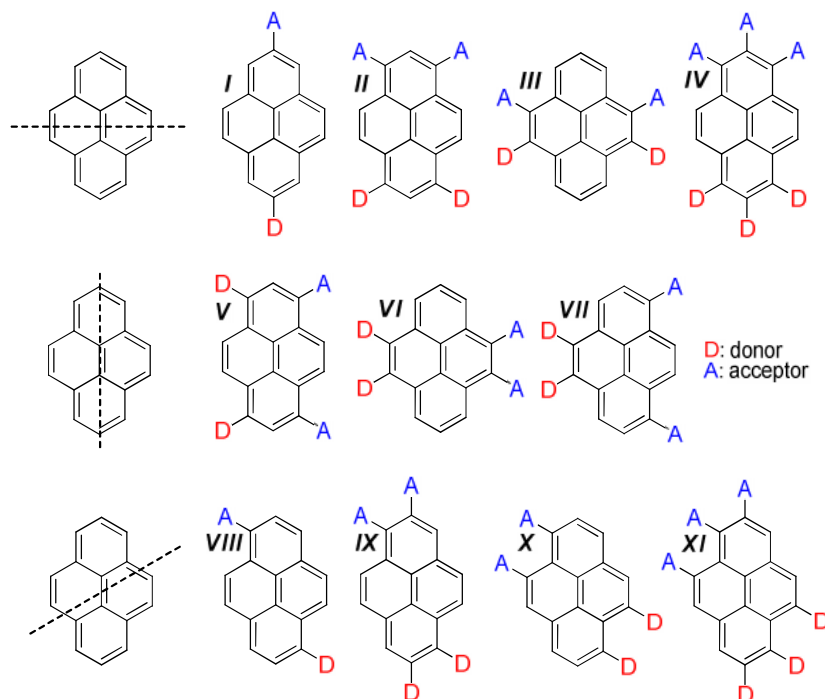


Figure 3.1: Examples for possible donor/acceptor patterns on pyrene.

1,3,6,8-tetrasubstituted derivatives is known: tetrakis(dimethylamino)pyrene,^[15] tetrakis(methylthio)pyrene,^[16] tetrathienylpyrene,^[17] tetrakis(ethynyl-*para*-aminophenyl)pyrene.^[18] Reported examples of K-region donor substituted are 4,5-dimethoxypyrene^[19] and 2,7-di-*tert*-butyl-4,5,9,10-tetrakis[(4-methoxyphenyl)ethynyl]pyrene.^[20]

In contrast, mixed donor and acceptor substitution patterns are rare, which is most probably due to the lack of protocols for asymmetric functionalization. Some imaginable patterns of donor/acceptor pyrenes are depicted in Figure 3.1. A classification of three groups was made by an imaginary cut through pyrene. Beside the strong influence, and thus, the possibility to tune the molecular frontier orbitals, the introduction of oppositely arranged electron-withdrawing and -donating groups introduces a dipole in the molecule. Rigid organic molecules with a permanent dipole are known to exhibit strong solvatochromic shifts of their fluorescence. Furthermore, the introduction of dipoles might orientate the molecules during the crystallization process which is useful in terms of crystal engineering.^[4] The donor/acceptor pattern **VI** has already been

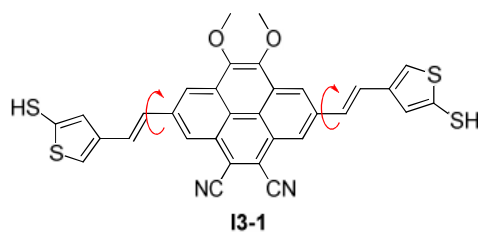
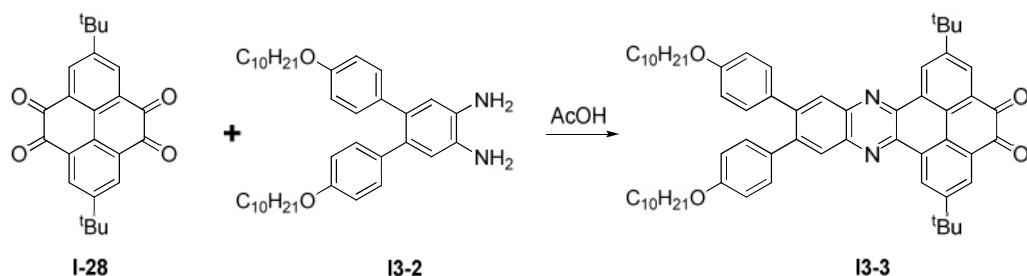


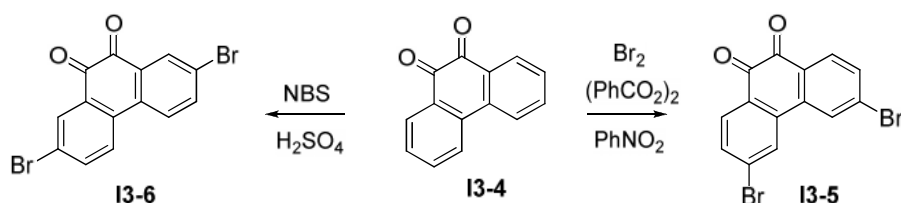
Figure 3.2: Pyrene rotor with a calculated dipole moment of 9.8 D.^[21]

mentioned within the theoretical investigation of all-electric single-molecule motors. Therein, the pyrene derivative **13-1** depicted in Figure 3.2 was proposed as molecular dipole motor with a calculated dipole moment of 9.8 D.^[21]

In view of so far reported chemistry on pyrene and the high value of novel K-region functionalization, it was aimed for the synthesis of pyrene donor/acceptor substitution pattern **VI**.



Scheme 3.1: One-sided condensation of **I-28** with 1 eq. **I3-2** to give **I3-3** in 52 % yield.^[22]



Scheme 3.2: Bromination of phenanthrene-9,10-dione using bromine^[23] and NBS^[24].

3.2 Synthesis of 4,5- versus 9,10-Donor/Acceptor Pyrenes

The asymmetric substitution of positions 4,5 versus 9,10 has so far only been achieved by one-sided condensation reaction of pyrene-4,5,9,10-tetraone with an *ortho*-diaminobenzene (Scheme 3.1)^[22] or by the reaction sequence of 4,5-oxidation followed by condensation and a second oxidation at the opposite pyrene side.^[25] Beside the low yield of the statistic condensation reaction or the oxidation in two steps, these protocols are limited to reactions of the α -diketone. Instead, the importance and versatility of halogenated PAHs have greatly increased by the availability of modern palladium-catalyzed cross-coupling reactions such as Suzuki, Heck, Negishi, Buchwald or Stille.^[26]

Looking at the structurally related phenanthrene-9,10-dione **I3-4**, side-selectivity of the bromination is controlled by the conditions: bromine^[23] with a radical initiator addresses positions 3,6 (**I3-5**) whereas *N*-bromosuccinimide^[24] (NBS) in concentrated sulfuric acids gives 2,7-dibromophenanthrene-9,10-

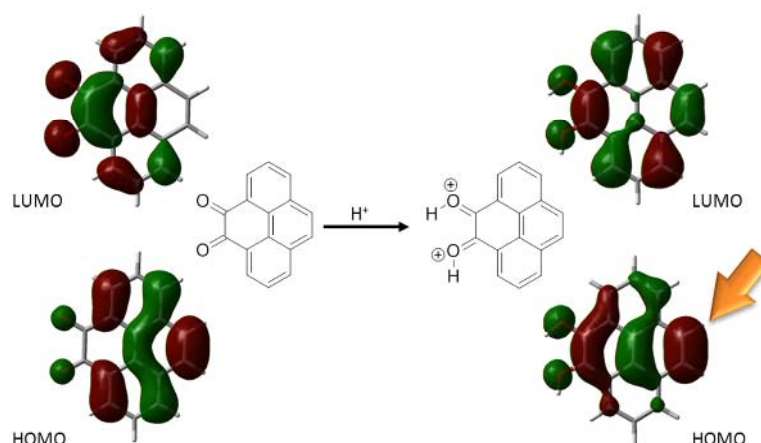
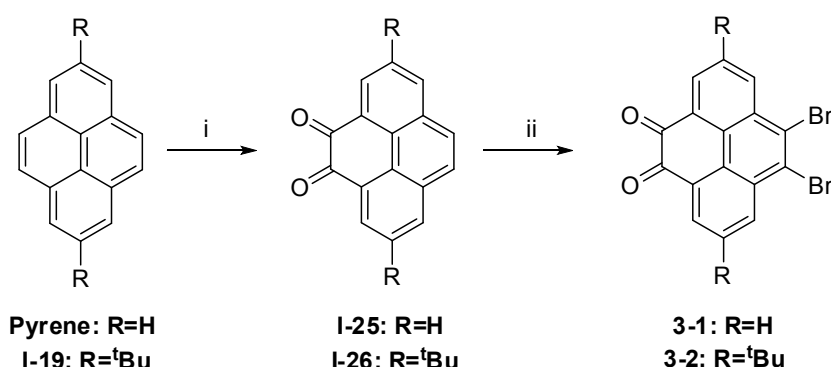


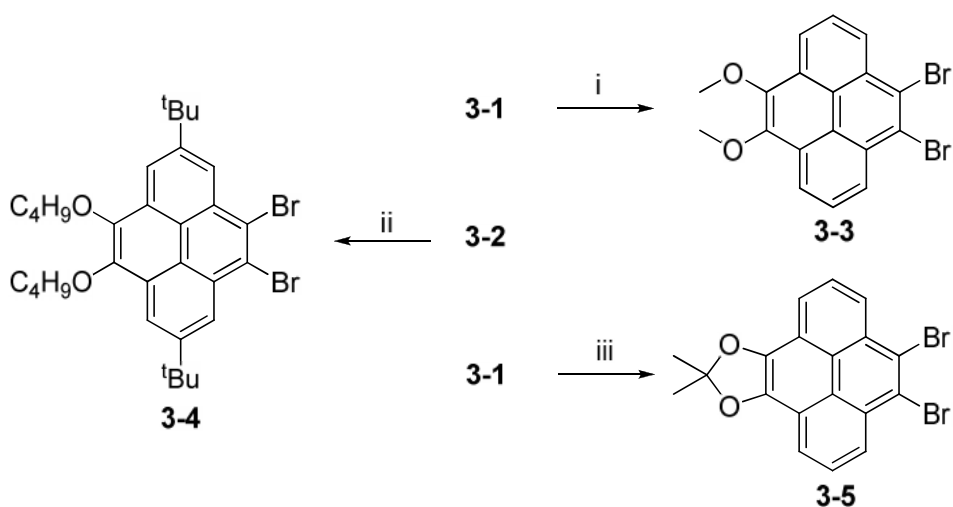
Figure 3.3: DFT/B3LYP/6-31G(d) calculations of the frontier orbitals (HOMO: below; LUMO: above) pyrene-4,5-dione **I-25** (left) and its protonated species (right); positive charges are not drawn mesomerically distributed over the molecule for simplicity.



Scheme 3.3: Synthesis of 9,10-dibromopyrene-4,5-dione **3-1** and **3-2**. Conditions: *i* RuCl₃, NaIO₄, 45 % for **I-25** and 46 % for **I-26**,^[12] *ii* NBS, H₂SO₄, RT, 4 h, quantitative for **3-1** and 80 % for **3-2**.^[27]

dione (**I3-6**) (Scheme 3.2). The combination of NBS and H₂SO₄ was reported to be a strong method for the bromination of deactivated aromatics.^[28]

Therefore, DFT calculations were performed of pyrene-4,5-dione **I-25** and in the protonated form which was presumed under reaction conditions (Figure 3.3). The HOMO of **I-25** exhibits similar coefficients at positions 1, 3, 6, 8, 9 and 10. Upon protonation the coefficients in the HOMO oppositely to the ketones at positions 9 and 10 (indicated by the orange arrow in Figure 3.3) greatly increase and shrink at 1, 3, 6 and 8. Thus, the calculation predicted increased reactivity at positions 9 and 10 for **I-25** in strong acidic media for HOMO controlled reactions.



Scheme 3.4: Synthesis of 4,5-alkoxy pyrenes **3-3**, **3-4** and **3-5**. Conditions: *i* Na₂S₂O₄, Me₂SO₄, KOH, Bu₄NBr, H₂O/THF, 40°C, overnight, 65%; *ii* Na₂S₂O₄, 1-bromobutane, KOH, Bu₄NBr, H₂O/THF, 40°C, overnight 41 %; *iii* 2-nitropropane, Na₂CO₃, acetonitrile/THF/H₂O, 55°C, overnight, 61 %.

According to the calculations the diketone **I-25** was quantitatively converted to **3-1** by treatment with NBS in conc. H₂SO₄ (Scheme 3.3). The respective *tert*-butylated derivative **3-2** was obtained under the same conditions. Both compounds show the required ¹H NMR signals whereas **3-1** exhibits low solubility at room temperature, and thus, NMR spectroscopy had to be carried out at elevated temperatures.

For the introduction of donor substituents at one pyrene side, reductive alkylation was performed with sodium dithionite and subsequent addition of an alkylation reagent (Scheme 3.4). In case of **3-1**, dimethyl sulfate gave the methylated species **3-3**. By the addition of 1-bromobutane **3-4** was obtained and proved the versatility of this method towards alkyl chains of different length.

Treatment of **3-1** with 1-nitropropane gave 9,10-dibromopyrene-4,5-diolacetonide **3-5** in 61 % yield. The acetonide is of high interest in two different ways. First, the usage as protecting group for α -diketones is superior to methoxy group because the deprotection followed by oxidation proceeds smoother than the cleavage of MeO. Second, the acetale structure is a stronger donor, and thus, holds promise for a decreased energy gap and an increased dipole moment of the respective donor/acceptor pyrene derivative.

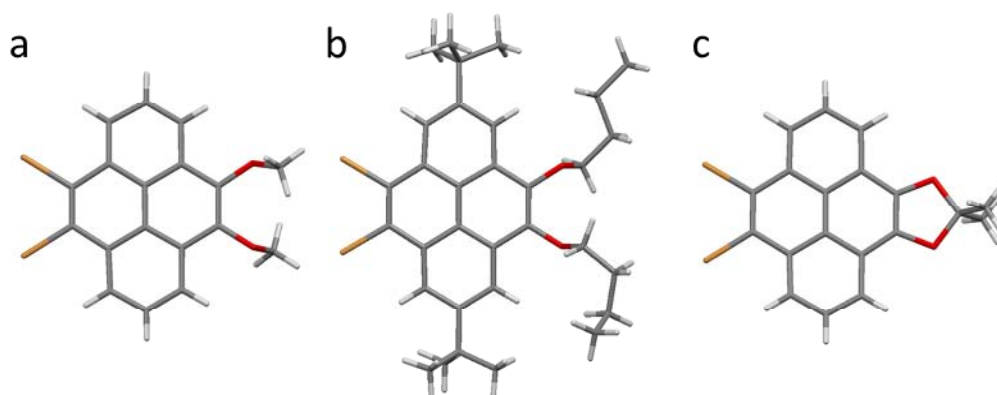
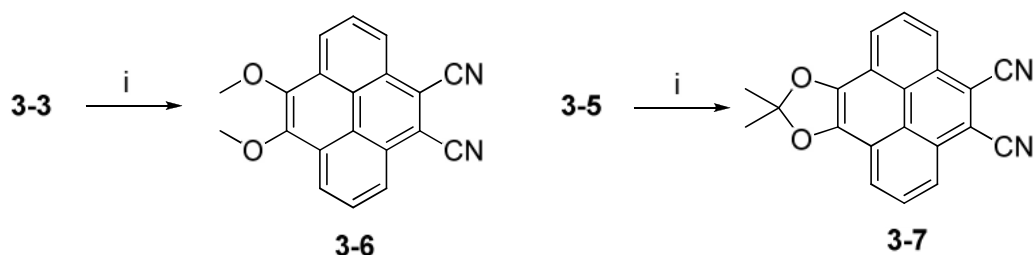


Figure 3.4: Front view of the crystal structure of pyrene derivatives **3-3** (a), **3-4** (b) and **3-5** (c).

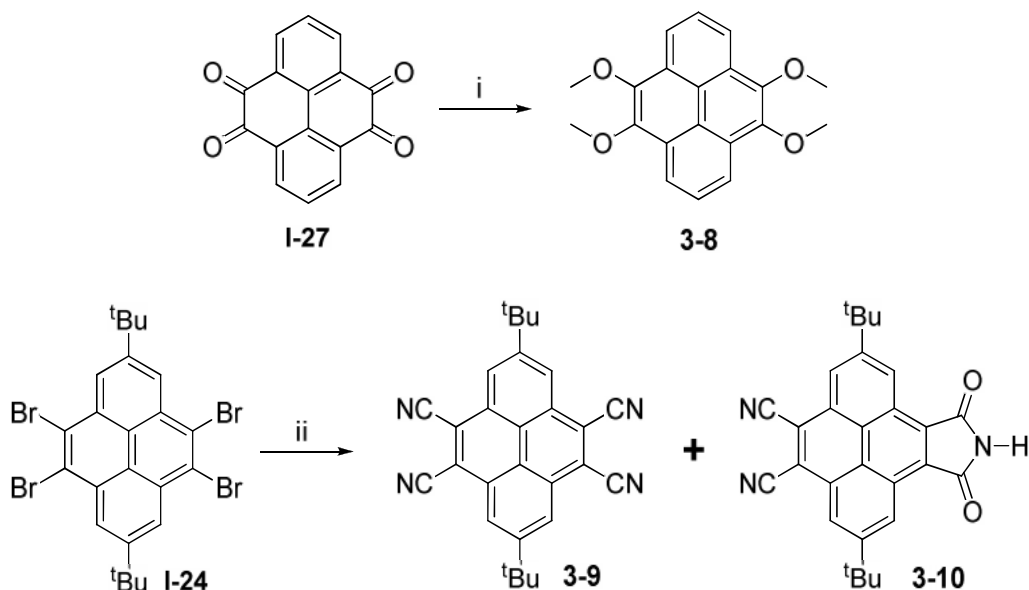
Slow evaporation of the solvent from DCM solutions gives colorless crystals for pyrene derivatives **3-3** and **3-4**. Yellow crystals suitable for X-ray analysis of **3-5** were obtained by crystallization from ethanol. The solved structures are depicted in Figure 3.4 and unambiguously confirm the selectivity of the bromination reaction. All three exhibit a planar pyrene plane but the oxygen binding angle of the acetonide ($\sim 105^\circ$) is decreased by $\sim 10^\circ$ compared to **3-3** and **3-4** ($\sim 115^\circ$) due to the five-membered ring.

As described above the asymmetric functionalization of positions 4,5 versus 9,10 works selectively and in good to excellent yields with and without *tert*-butyl groups. Having proved applicability, and thus, versatility of the protocol on both pyrene molecules, it was exclusively focused on pyrene derivatives with hydrogen at position 2 and 7 in the following. *tert*-Butyl groups exhibit a strong space-filling character and undisputedly interfere with π - π -interaction, which is unwanted for the investigations described herein. Nevertheless, **3-4** seems to be a promising candidate as monomer for soluble and non-aggregating poly(4,5-pyrenylenes)s for potential use in OLEDs.

In order to change bromines on 4 and 5 to a stronger electron-withdrawing group, the halogen-cyano exchanged under Rosenmund-von Braun conditions using copper(I)cyanide in dry *N*-methylpyrrolidone (NMP) at 190°C was carried out (Scheme 3.5). Compounds **3-6** and **3-7** were obtained in similar yields as orange and red solid, respectively. The colors already give a hint towards a narrowed energy gap of the donor/acceptor molecules.



Scheme 3.5: Rosenmund-von Braun reaction of *ortho*-dibromo derivatives **3-3** and **3-5**.
 Conditions: *i* CuCN, dry NMP, 190°C, 3 d, 45 % for **3-6**, 48 % for **3-7**.



Scheme 3.6: Synthesis of donor **3-8** and acceptor **3-9**. Conditions: *i* Na₂S₂O₄, Me₂SO₄, KOH, Bu₄NBr, H₂O/THF, 40°C, 1 h, 74%; *ii* CuCN, NMP, 190°C, 3 d, 8 % of **3-9**, 19 % of **3-10**.

To compare optical and electronic properties of the donor/acceptor pyrenes the respective exclusively donor- and acceptor-substituted pyrene derivatives are needed. 4,5,9,10-Tetramethoxypyrene **3-8** was received from Dr. Ralph Rieger from this research group. The synthesis has been accomplished by the reduction of tetraone **I-27** and dimethyl sulfate analog to the reductive methylation of **3-1** (Scheme 3.6).^[29]

For the bromine-cyano exchange **I-24** was treated with CuCN over three days at 190°C and subsequently stirred at 60°C for two hours after the addition of aqueous Fe(NH₄)₂(SO₄)₂·6H₂O (Mohr's salt) for the coordination of

remaining cyanide. From the reaction mixture two compounds could be isolated by column chromatography which turned out to be the product **3-9** and the byproduct **3-10**, whose structure was additionally confirmed by single crystal X-ray crystallography (see Experimental Part). Owing to the identification of the formed byproduct, the low yield of 8 % for **3-9** can be explained by the intramolecular imide formation. This reaction is known to proceed for aromatic *ortho*-dinitriles in the presence of an alkoxide followed by hydrolysis.^[30] The presence of water during the reaction time might be an explanation. Nevertheless, no efforts have been made to further increase the yield because sufficient material was obtained.

Shortly afterwards, Kobayashi et al. published 2011 the synthesis of **3-9** in 29 % yield with a reaction time of 2 hours at 220°C but without the crystal structure proof.^[13]

3.3 Optical and Electronic Properties

UV/Vis Spectroscopy

Having donor **3-8**, acceptor **3-9** as well as donor/acceptor pyrenes **3-6** and **3-7** in hand, UV/vis absorption and emission properties were investigated in THF solutions. All spectra are depicted in Figure 3.5 and the values are listed in Table 3.1 on page 49.

Large optical energy gaps ($E_{g(opt)}$) of 2.95 eV and 3.25 eV were found for **3-8** and **3-9** (Figure 3.5 **c** and **d**). Both spectra exhibit the vibrational structure of the absorption bands. The UV/vis absorption and emission spectra of **3-6** and **3-7** are of similar shape (Figure 3.5 **a** and **b**). The absorption maximum at the longest wavelength is red-shifted by 65 nm in case of the acetone **3-7** which corresponds to a decrease of the $E_{g(opt)}$ by 0.43 eV. It is assumed that fixing the

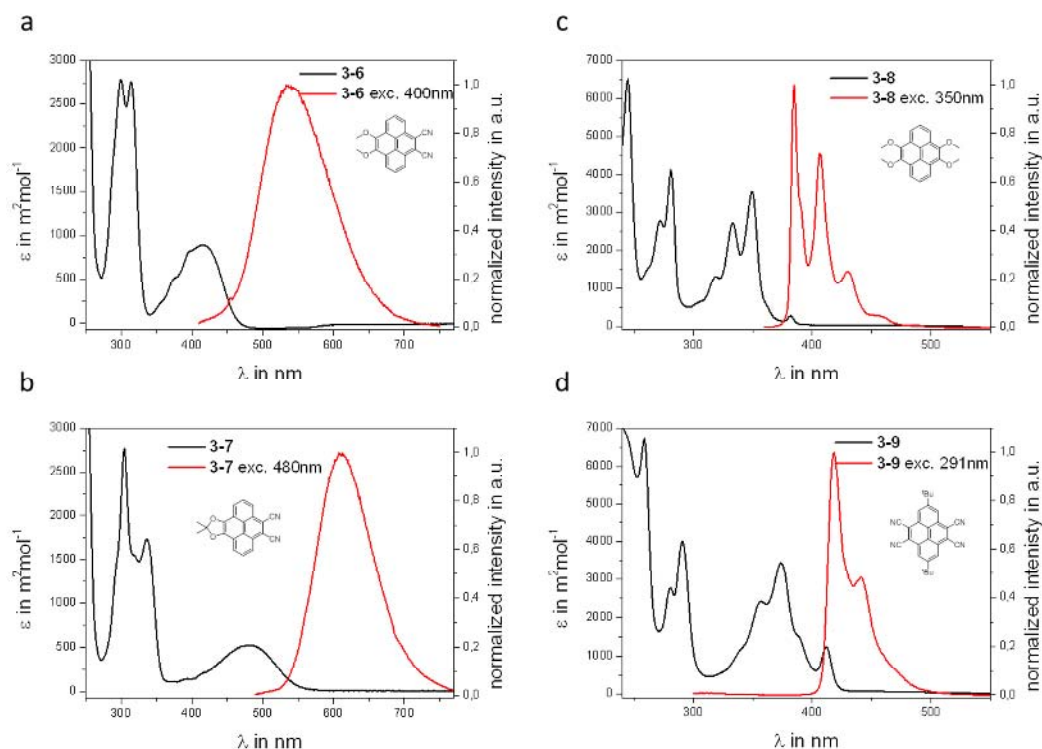


Figure 3.5: UV/vis absorption and emission spectra of donor/acceptor pyrenes **3-6** (a) and **3-7** (b) and donor **3-8** (c) and acceptor **3-9** (d) in THF at 10^{-5} M concentration.

oxygen atoms in a five-membered ring enhances electron-donating character of the oxygen lone-pairs, and thus, raises the HOMO level to a bigger extent. Calculations using Gaussian^[31] confirmed the decrease of the energy gap (Table 3.1).

Furthermore, the absorption band of the longest wavelength appears broadened for the donor/acceptor pyrenes as well as their emission spectrum. Related work on 2,7-donor/acceptor-substituted 4,5,9,10-tetrahydropyrenes shows similar long wavelength bands which were assigned to arise from intramolecular charge-transfer (ICT).^[32-33] Those donor/acceptor molecules bear dimethylamine as donor and nitro, cyano or acetyl groups as acceptor moiety. By addition of TFA the dimethylamino groups are protonated, and thus, the ICT is inhibited by the disappearance of the initial ICT band and an arising new band at shorter wavelength.

Unfortunately, protonation cannot be used to probe the origin of this band in

Table 3.1: Optical and electronic properties of compounds **3-6**, **3-7**, **3-8** and **3-9**.^[a]

| | $\lambda_{\text{abs}}^{[b]}$ | $\lambda_{\text{em}}^{[c]} (\lambda_{\text{ex}})^{[d]}$ | λ_{edge} | $E_{\text{g(opt)}}^{[e]}$ | $E_{\text{g(cal)}}^{[f]}$ | $\mu^{[f]}$ |
|------------|------------------------------|---|-------------------------|---------------------------|---------------------------|-------------|
| 3-6 | 415 nm | 536 nm (400 nm) | 461 nm | 2.69 eV | 3.18 eV | 8.8 D |
| 3-7 | 480 nm | 613 nm (480 nm) | 549 nm | 2.26 eV | 2.72 eV | 9.2 D |
| 3-8 | 388 nm | 385 nm (350 nm) | 382 nm | 3.25 eV | 3.73 eV | 0.0 D |
| 3-9 | 412 nm | 418 nm (291 nm) | 421 nm | 2.95 eV | 3.34 eV | 0.1 D |

[a] All absorption and emission spectra were measured in THF. [b] λ_{abs} is the absorption band appearing at the longest wavelength. [c] λ_{em} is the fluorescence band appearing at the shortest wavelength. [d] λ_{ex} wavelength of excitation. [e] Calculated from λ_{edge} [f] Calculated DFT/B3LYP/6-31G(d) using Gaussian.

case of **3-6** and **3-7** because treatment with acid results in cleavage of the acetonide group and the methoxy groups are uneasy to protonate compared to amines. But still, it is assumed that the lowest energy transition has ICT character.^[4, 6, 34]

Solvatochromic Effect

Quantum mechanical calculations (DFT/B3LYP/6-31G(d)) on structures **3-6** to **3-9** in vacuum give strongly different values for the molecular dipole moment μ in the ground state and are listed in Table 3.1. The donor/acceptor substitution induces dipoles of 8.8 D and 9.2 D, respectively, which is in line with the calculated value (9.8 D) for structurally related compound **I3-1**.

Calculations (AM1) on afore mentioned 2,7-donor/acceptor-substituted 4,5,9,10-tetrahydropyrenes predict dipole moments from 4.6 D to 8.3 D in the ground state and values of 21.6 D to 23.7 D are reported for the excited state.^[32-33] A pronounced dependency on the solvent polarity of the emission wavelength is described for these molecules. Due to structural and electronic similarities such behavior can be expected for **3-6** and **3-7** as well, which is referred to as solvatochromic effect.

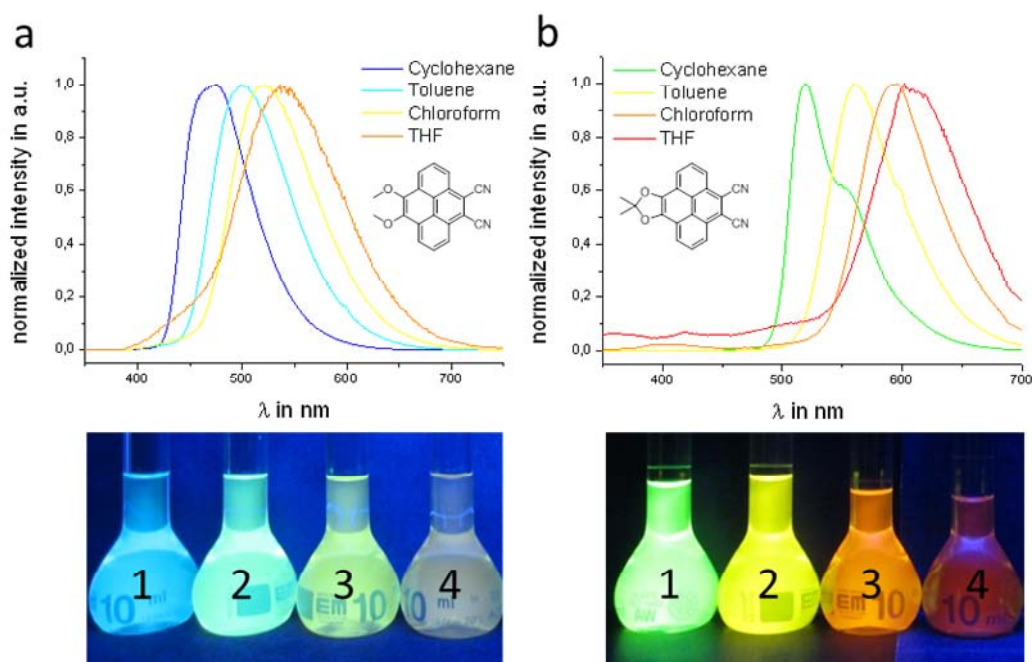


Figure 3.6: Solvatochromism of **3-6** and **3-7**. Emission spectra in solvents of different polarity at 10^{-5} M concentration upon excitation at 300 nm. Below: photographs of donor/acceptor pyrenes ($\lambda_{\text{ex}}=366$ nm) in different solvents **1**: cyclohexane, **2**: toluene, **3**: chloroform, **4**: tetrahydrofurane.

Solvatochromism describes the dependency of absorption and fluorescence of molecules from solvent polarity.^[35-36] Since polarities of the ground state and the excited state differ, the stabilizing effect of the solvent is dependent on its respective polarity. The solute/solvent interaction can strongly influence shape, intensity and energy of the absorption and emission bands. Positive solvatochromism terms a red-shift with increasing solvent polarity whereas a blue-shift is called negative solvatochromism. Molecules that show strong solvatochromism can be used as solvent polarity indicators.^[36]

3-6 and **3-7** show almost no change in the absorption behavior in different solvents. Solely in cyclohexane the vibronic fine structure of the long wavelength band is better resolved. In contrast, the emission is strongly influenced by the solvent polarity (Figure 3.6 and Table 3.2). The emission maxima are bathochromically shifted by increasing polarity from cyclohexane to THF by 62 nm and 92 nm for **3-6** and **3-7**, respectively: the higher the

Table 3.2: Solvatochromism of **3-6** and **3-7** in different solvents excited at 300 nm.

| Solvent | | $\lambda_{em}^{[a]}$ |
|------------|-------------|----------------------|
| 3-6 | Cyclohexane | 474 nm |
| | Toluene | 498 nm |
| | Chloroform | 520 nm |
| | THF | 536 nm |
| 3-7 | Cyclohexane | 519 nm |
| | Toluene | 559 nm |
| | Chloroform | 594 nm |
| | THF | 611 nm |

[a] λ_{em} is the fluorescence band appearing at the shortest wavelength.

polarity of the solvent, the better the stabilization of the excited state. This observed behavior indicates positive solvatochromism. It can be concluded that **3-7** undergoes a larger change of the dipole moment upon excitation than **3-6** indicated by the larger red-shift. The emission shifts are in the same order of other aromatic donor/acceptor molecules.^[6, 32, 34, 37]

As expected, negligible solvatochromism of the emission was observed for compounds **3-8** and **3-9**.

Cyclic Voltammetry

Further investigation of the electronic properties was performed by cyclic voltammetry (CV) together with DFT calculations.^[31] All CV experiments in this work were performed under identical conditions (1 mM solution of the analyte, dry DCM, Argon atmosphere, Bu₄NPF₆ as conductive salt) to ensure comparability of the results. Ferrocene (1 mM) has always been added as internal standard to normalize all cyclovoltograms to the ferrocene half-wave potential of 0.600 V versus SCE according to the literature.^[38] While the current flow was measured, the voltage was ramped with the speed denoted in the

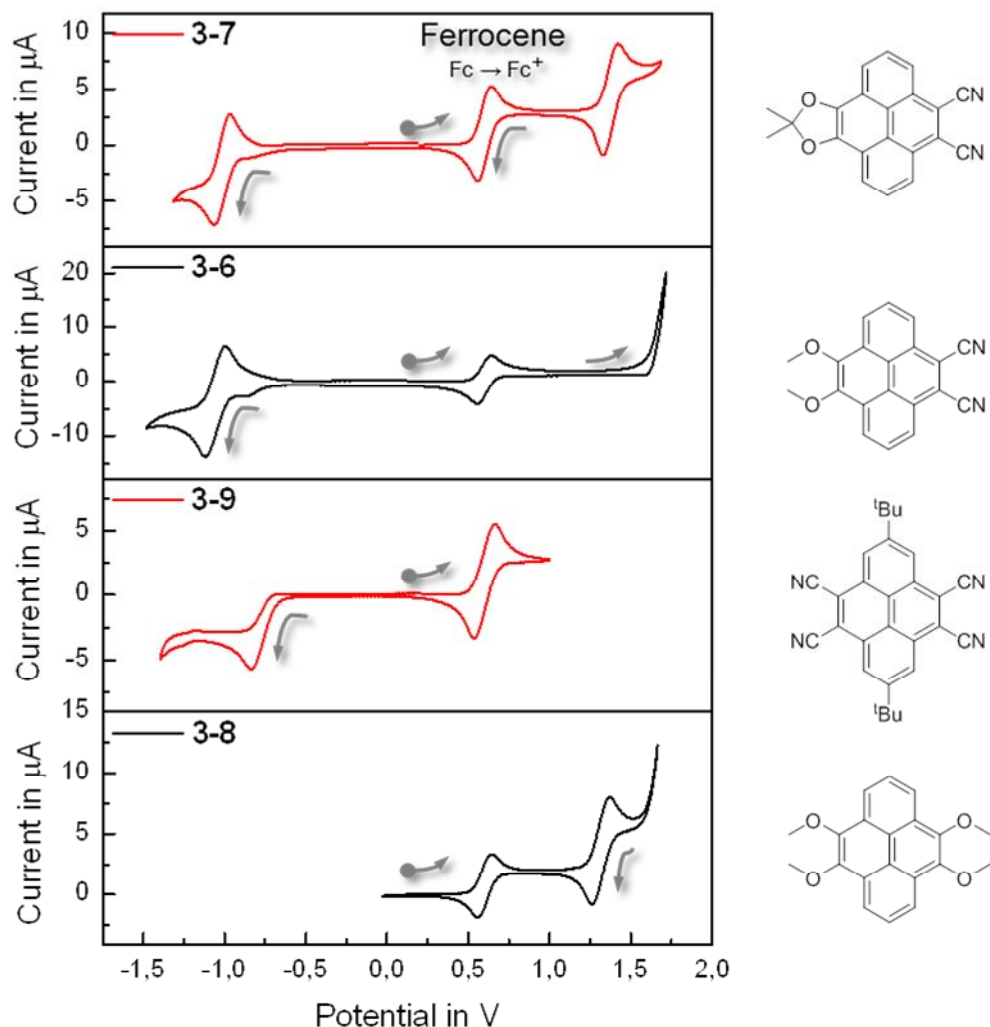


Figure 3.7: Cyclovoltograms of **3-6** (100 mV/s), **3-7**, **3-8** and **3-9** are recorded at scan rate of 50 mV/s. Ferrocene half-wave potential is set to of 0.600 V versus SCE.

figure caption. For the analysis, the onset of the respective oxidation or reduction wave was used uniformly regardless whether a reversible or irreversible process occurred.

The cyclovoltograms of compounds **3-6** to **3-9** are shown in Figure 3.7 and the extracted values are listed in Table 3.3 on page 54. Under measurement conditions for donor **3-8** only a reversible oxidation wave and for acceptor **3-9** an irreversible reduction wave could be observed, corresponding to a HOMO level at -5.43 eV (**3-8**) and LUMO level at -3.52 eV (**3-9**).

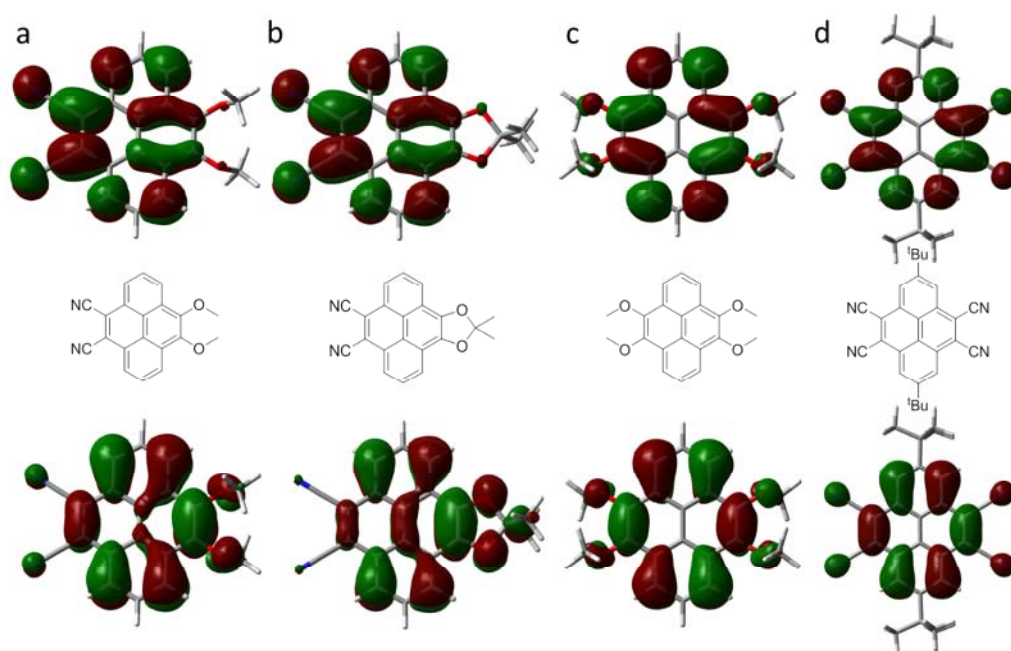


Figure 3.8: Orbital surfaces of the HOMO (below the formulae) and LUMO (above the formulae) of **3-6**, **3-7**, **3-8** and **3-9** (from left to right) determined by DFT calculations on 6-31G(d) basis.

In case of the donor/acceptor substituted pyrenes **3-6** and **3-7** both processes (oxidation and reduction) could be measured due to a narrowed energy gap.^[4] **3-6** exhibits a reversible reduction and irreversible oxidation process giving an energy gap ($E_{g(CV)}$) of 2.60 eV. Oxidation and reduction of **3-7** proceeds reversibly and $E_{g(CV)}$ was determined as 2.24 eV. The energy gaps obtained from CV measurements are almost identical to the optical energy gaps of 2.69 eV and 2.26 eV, respectively. CV further revealed that the LUMO levels of **3-6** and **3-7** are nearly identical (same acceptor moiety) but the HOMO level of **3-7** is raised by 0.32 eV because of the stronger donor moiety.

The pure donor **3-8** and acceptor **3-9** bear the double number of the respective electron-donating or -withdrawing substituents compared to donor/acceptor pyrene **3-6**. Thus **3-8** exhibits the highest HOMO and **3-9** the lowest LUMO level.

Table 3.3: Electronic properties of compounds **3-6** to **3-9** experimentally (CV) and calculated.

| | $E_{\text{HOMO(CV)}}^{[a]}$ | $E_{\text{LUMO(CV)}}^{[a]}$ | $E_{\text{g(CV)}}^{[b]}$ | $E_{\text{HOMO(cal)}}^{[c]}$ | $E_{\text{LUMO(cal)}}^{[c]}$ | $E_{\text{g(cal)}}^{[d]}$ |
|------------|-----------------------------|-----------------------------|--------------------------|------------------------------|------------------------------|---------------------------|
| 3-6 | -5.82 eV | -3.22 eV | 2.60 eV | -5.90 eV | -2.72 eV | 3.18 eV |
| 3-7 | -5.50 eV | -3.26 eV | 2.24 eV | -5.44 eV | -2.72 eV | 2.72 eV |
| 3-8 | -5.43 eV | * | * | -5.06 eV | -1.33 eV | 3.73 eV |
| 3-9 | * | -3.52 eV | * | -6.69 eV | -3.35 eV | 3.34 eV |

[a] CV measured in 0.1 M n-Bu₄NPF₆/DCM with scan rates between 50 mV/s and 100 mV/s; values calculated using the ferrocene HOMO level: $E_{\text{HOMO(CV)}} = -(E_{\text{ox,onset}} - E_{\text{Fc/Fc}^+}^{(1/2)} + 4.8)$ eV [b] calculated from $E_{\text{HOMO(CV)}}$ and $E_{\text{LUMO(CV)}}$ [c] Calculated DFT/B3LYP/6-31G(d) using Gaussian; [d] calculated from $E_{\text{HOMO(cal)}}$ and $E_{\text{LUMO(cal)}}$; * could not be determined under measurement conditions.

The influence of the donor and acceptor substituents on the frontier orbitals is visually supported by the calculated orbital surfaces. Biggest orbital coefficients were found at the donor side in the HOMO and at the acceptor side in the LUMO in Figure 3.8 **a** and **b**. It is important to note that the usual nodal plane in the 2-7 direction of the substituted pyrenes is lost for the asymmetric 4,5 and 9,10 substitution. This supports the assumption of an intramolecular charge transfer taking place between the donor and acceptor side.

3.4 Crystal Structure Analysis

Suitable crystals of **3-6**, **3-8** and **3-9** for X-ray analysis were obtained by slow evaporation from a dichloromethane solution. It shall be noted that **3-6** showed high tendency to form large and three-dimensional crystals. In case of **3-7** fine needles could only be grown by gas diffusion method using chloroform as good and cyclohexane as bad solvent.

Figure 3.9 shows the crystal structures of donor **3-8** (**c**), acceptor **3-9** (**d**) and the donor/acceptor pyrenes **3-6** (**a**) and **3-7** (**b**). For all four molecules the pyrene core was found to be planar. *ortho*-Methoxy groups are twisted out of the pyrene plane oppositely.

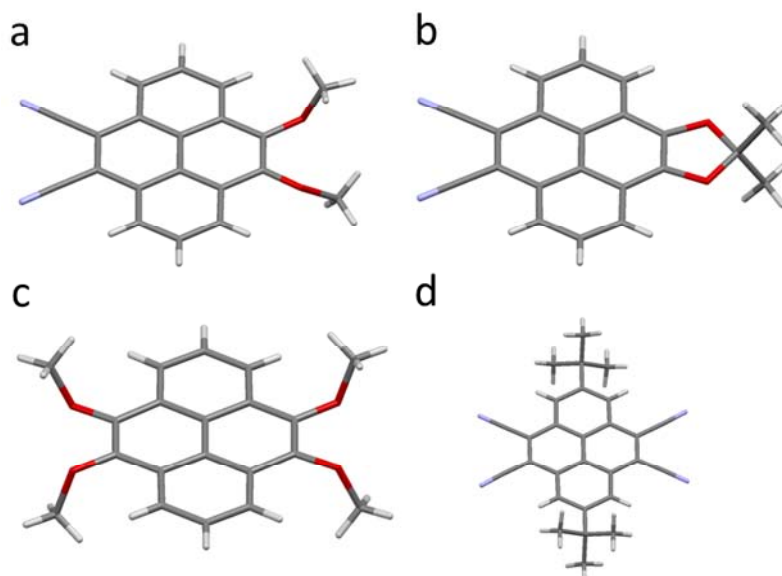


Figure 3.9. Crystal structures of pyrene derivatives **3-6** (a), **3-7** (b), **3-8** (c) and **3-9** (d).

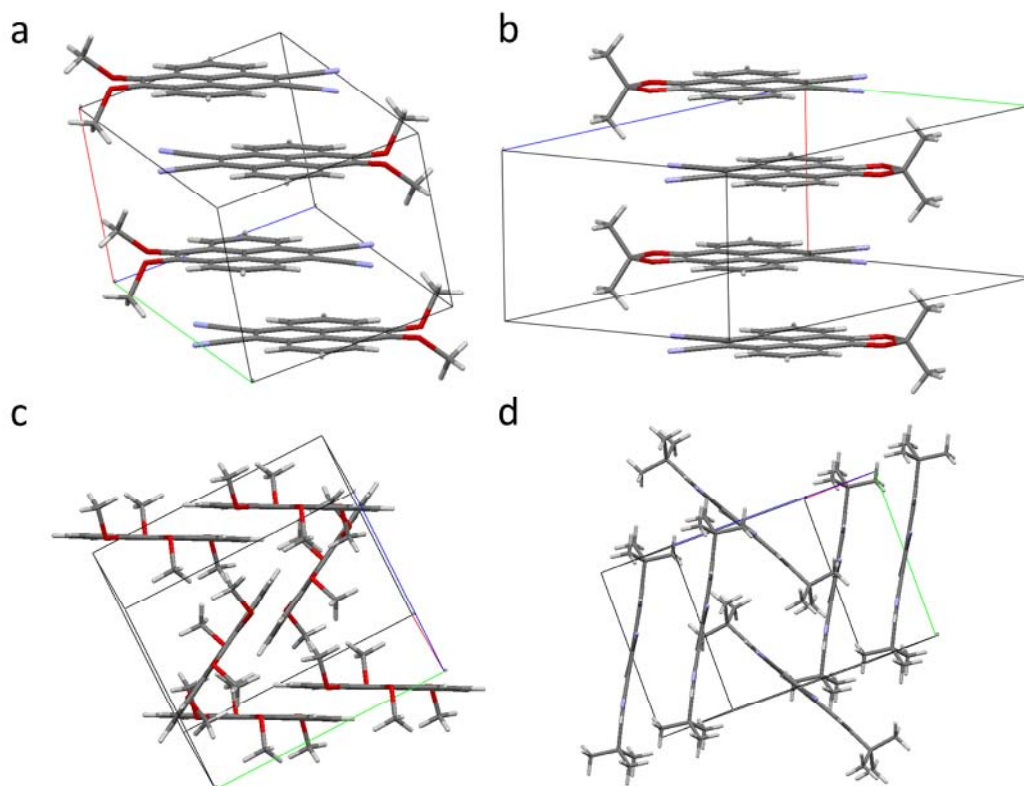


Figure 3.10: Crystal packing of donor/acceptor pyrenes **3-6** (a) and **3-7** (b) and donor **3-8** (c) and acceptor **3-9** (d).

The crystal packing of compounds **3-6** to **3-9** is depicted in Figure 3.10. The packing of **3-9** is strongly influenced by the bulky *tert*-butyl groups. Thus, no π - π -stacking was observed. A similar arrangement was found for **3-8** without any parallel overlap of the pyrene planes. The found order can be best described as herringbone motif without π - π -interaction due to an offset of the molecules.

The packing of donor/acceptor pyrene derivatives **3-6** and **3-7** (Figure 3.10 **a** and **b**) exhibits stacks of the molecules with an alternating rotation of 180°. In this way the donor side is located on top of the acceptor side and vice versa. Distances of 3.38 Å (**3-6**) and 3.41 Å (**3-7**) were determined for the π - π -stacking between the planar molecules. Although crystallization is a complex process and is determined by a large number of parameters, it is generally believed that the tendency for antiparallel molecular arrangements increases with the dipolar characteristics of a molecule.^[39] Accordingly, it seems in case of donor/acceptor pyrenes that besides other factors like the spatial influence of the bulky methoxy groups and π - π -interactions, the donor/acceptor substitution has an impact on the orientation of the molecules *via* intermolecular electrostatic forces. Furthermore, **3-6** and **3-7** were found to crystallize in centrosymmetric space groups. A detailed study by Desiraju et al. showed a strong tendency towards centrosymmetry for conjugated or aromatic molecules with large dipole moments.^[39] It is thus concluded that the observed orientation of the donor/acceptor pyrenes proves the motivation of a dipole supported crystal arrangement.^[40]

3.5 Charge-Transfer Complex

As described above the dipole induced by donor/acceptor substitution shows an impact on the molecular orientation in the solid state. Having donor **3-8** and acceptor **3-9** at hand, the next step of studying the influence of symmetric substitution on the intermolecular interaction in respect to possible charge-transfer (CT) is obvious.

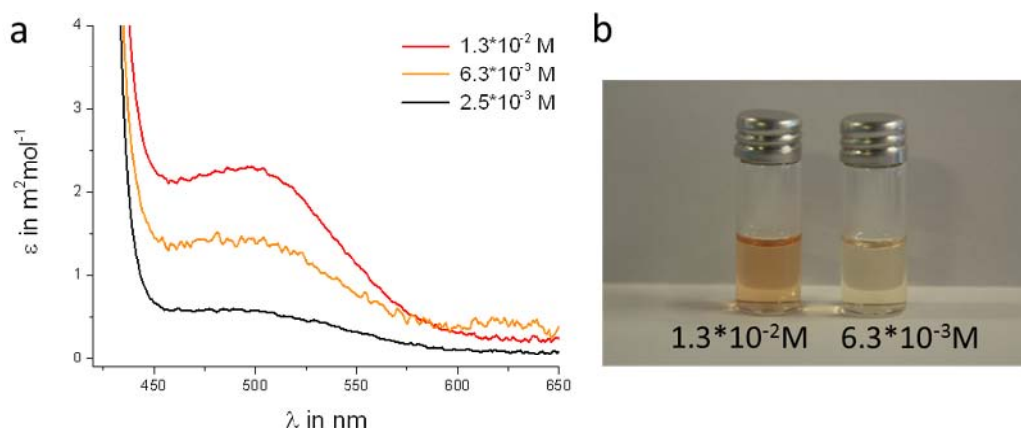


Figure 3.11: Charge-transfer complex of pyrene donor **3-8** and acceptor **3-9** in THF at various concentrations; (a) UV/vis spectrum, (b) photograph of the solutions.

CT complexes have been deeply investigated in the past due to found conductivity or even superconductivity.^[41-44] The principle of charge-transfer complexes lies in the partial transfer of charge from an electron-donor to an electron-acceptor. Therefore, some electron density from the donor HOMO is transferred to the acceptor-LUMO which is indicated by the occurrence of CT absorption bands. Consequently, generated electrostatic forces cohere the paired molecules. The formation of CT complexes in solution strongly depends on the concentration as the association of donor and acceptor molecule is crucial and an equilibrium controlled process.

Pyrene and its derivatives have already been applied successfully as the donor moiety in CT complexes. For instance, Melby et al. found a weak complex between pyrene and TCNQ.^[45] Later, complexes of TCNQ with 1,6-diaminopyrene and 1,3,6,8-tetrakis(dimethylamino)pyrene, respectively, were investigated.^[15, 46] Medjanik and co-workers studied the partial transfer of charge in complexes of 4,5,9,10-tetramethoxypyrene and 2,4,5,7,9,10-hexamethoxypyrene with TCNQ.^[47]

Solutions of donor **3-8** and acceptor **3-9** were in a 1:1 ratio were prepared at different concentrations and the UV/vis spectra are depicted in Figure 3.11. Only a very weak charge-transfer band could be observed with a maximum at

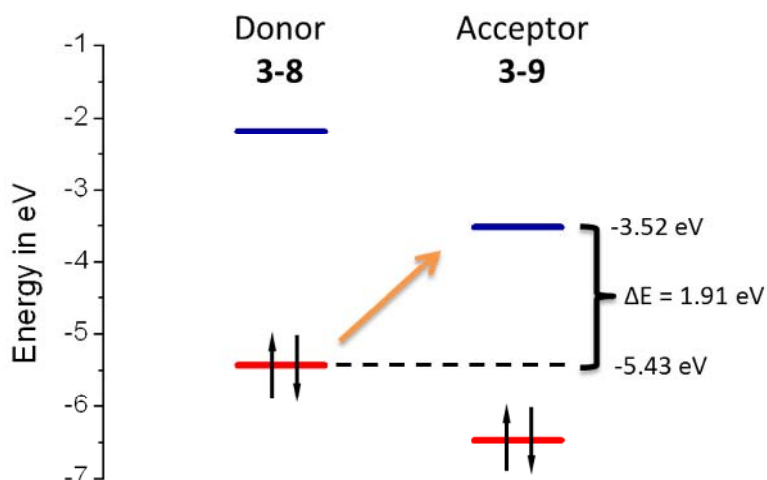


Figure 3.12: Energy diagram of the frontier orbitals of **3-8** and **3-9** and illustration of the intermolecular CT process. Values from CV measurements are used for HOMO₃₋₈ and LUMO₃₋₉; LUMO₃₋₈ and HOMO₃₋₉ are calculated from the $E_{g(opt)}$.

around 500 nm, and thus, very high concentration of 10^{-2} M of both molecules was required to visualize the CT band. In contrast, strong CT complexes showed CT band at one order of magnitude lower concentrated solutions.^[47-48] As the formation of a charge-transfer complex is dependent on an association equilibrium it is assumed that either the electronic levels of the pyrene derivatives do not match well and/or the *tert*-butyl groups strongly hinder the association of the donor and acceptor for efficient charge-transfer.^[48-49] Referring to CV measurements, the gap between the HOMO of the donor **3-8** and the LUMO of the acceptor **3-9** is 1.91 eV, and thus in the range of the intermolecular CT band onset (Figure 3.12). This rather high energy difference supports the assumption of a weak complex.

For a better understanding of the intermolecular interaction between the donor and acceptor, crystals of the CT complex were grown by the slow evaporation of the solvent from a highly concentrated and equimolar solution of **3-8** and **3-9**. The resulting crystals show a bright orange color and the crystal structure is depicted in Figure 3.13. Mixed stacks of donor and acceptor are formed with a staggered conformation which has often been found for CT complexes.^[50] The inlay illustrates the herringbone motif in which a donor of

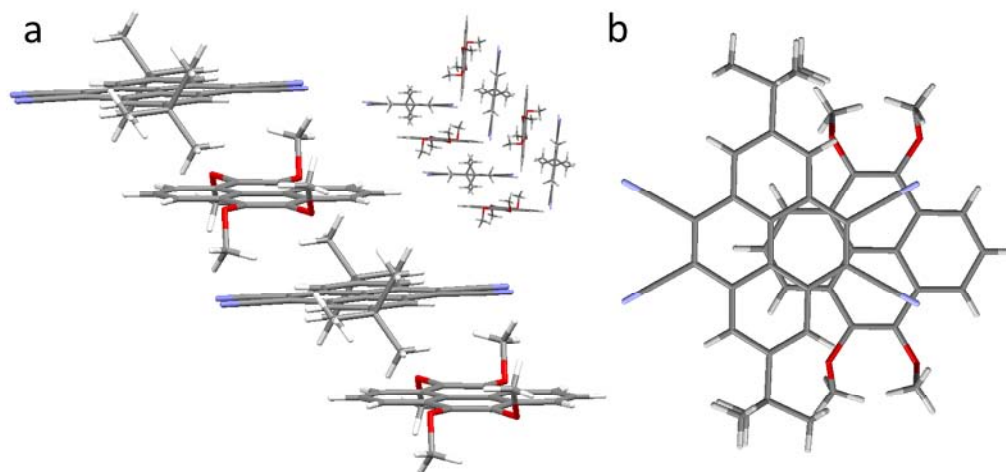


Figure 3.13: Crystal packing of the charge-transfer complex of donor **3-8** and acceptor **3-9**. Side (a) and front view (b) of the stacks.

one stack is bordered by an acceptor of an adjacent stack and vice versa. The determined space group exhibits centrosymmetry which is mainly found for CT complexes.^[50] The packing of pure **3-8** and **3-9** does not reveal stacks (compare Figure 3.10), and thus, emphasizes the influence of the CT between the donor and acceptor pyrene.

Figure 3.13 **b** shows the front view on one pair of donor and acceptor. The acceptor is rotated by an angle of 90° and is centered above the 2 position of the donor. It seems that the shift and the rotation within a pair of **3-8** and **3-9** are caused by the steric demand of the *tert*-butyl and methoxy groups. Unfortunately, the *tert*-butyl groups could not be avoided due to synthetic reasons.^[51-52] Determination of distance between pyrene planes gave an average value of 3.51 Å because the planes are slightly non-parallel. Compared to so far reported π -stacking distances of pyrene-based CT complexes of 3.32 Å^[47] for **3-8**/TCNQ and 3.32 Å to 3.50 Å^[50, 53] for unsubstituted pyrene with other small acceptors, the here found value is high but still in the range of reported CT complexes.

3.6 Summary

The successful bromination of pyrene-4,5-dione at positions 9 and 10 provided the basis for novel 4,5 versus 9,10 asymmetric substituted pyrene derivatives. The described protocol proved versatility by the successful application on 2,7-di-*tert*-butylpyrene.

Based on the new pyrene building block, two intramolecular donor/acceptor substituted pyrenes were synthesized utilizing pyrene as flat and π -conjugated space in between the electron withdrawing and donating moiety. Keeping the identical cyano moiety as acceptor, the donor was varied from methoxy to the five-membered acetonide. The latter one exhibits stronger electron-donating character which leads to a smaller optical energy gap by 0.43eV revealed by UV/vis spectroscopy. Cyclic voltammetry provided information about the position of the molecular frontier orbitals, and thus, confirmed a higher HOMO level of the acetonide.

The two donor/acceptor molecules show a pronounced solvatochromic effect of the fluorescence in solvents of different polarity. It could be shown that the emission is shifted to longer wavelength with increasing polarity by up to 92 nm from cyclohexane to THF.

Crystals could be grown from asymmetrically substituted pyrenes and the structures have been solved. It was found that both compounds arrange in stacks in which each molecule is rotated by 180°, and thus, the donor moiety packs on top of the acceptor moiety and vice versa. The formation of this antiparallel arrangement is supported by the dipole moments of the molecules caused by the asymmetric substitution. This observation confirms the initial motivation to manipulate the solid state molecular order by appropriate substitution.

Switching from asymmetrically to symmetrically substituted pyrene derivatives, an exclusively donor- and acceptor-substituted pyrene derivative, respectively, were synthesized in order to investigate their intermolecular

interaction as an effect of charge-transfer. Mixing donor-substituted and acceptor-substituted pyrene in a 1:1 ratio showed a weak intermolecular CT band and highly concentrated solutions (10^{-2} M) were necessary for visualization. Co-crystallization was applied and yielded bright orange crystals. X-ray analysis revealed shifted stacks of alternating donor- and acceptor-pyrenes with a rotation angle of 90° between the molecules. The spatial demand of *tert*-butyl and methoxy substituents seems to cause that shift and to prevent closer π - π -distances than the observed 3.51 Å. Nevertheless, it could be shown that the CT interaction between the different pyrene derivatives strongly altered the molecular arrangement.

The herein described synthetic route on asymmetric pyrene chemistry shall be the basis for the synthesis of new, pyrene-based materials in the next chapters.

3.7 Bibliography

- [1] H. Meier, *Angewandte Chemie-International Edition* **2005**, *44*, 2482-2506.
- [2] A. E. Reed, L. A. Curtiss, F. Weinhold, *Chemical Reviews* **1988**, *88*, 899-926.
- [3] J. Roncali, *Chemical Reviews* **1997**, *97*, 173-205.
- [4] Y. Yamashita, M. Tomura, *Journal of Materials Chemistry* **1998**, *8*, 1933-1944.
- [5] A. Mishra, R. K. Behera, P. K. Behera, B. K. Mishra, G. B. Behera, *Chemical Reviews* **2000**, *100*, 1973-2011.
- [6] S. Sahasithiwat, T. Mophuang, L. Menbangpung, S. Kamtonwong, T. Sooksimuang, *Synthetic Metals* **2010**, *160*, 1148-1152.
- [7] A. S. Batsanov, M. R. Bryce, M. A. Coffin, A. Green, R. E. Hester, J. A. K. Howard, I. K. Lednev, N. Martin, A. J. Moore, J. N. Moore, E. Orti, L. Sanchez, M. Saviron, P. M. Viruela, R. Viruela, T. Q. Ye, *Chemistry-a European Journal* **1998**, *4*, 2580-2592.
- [8] A. J. Moore, M. R. Bryce, A. S. Batsanov, A. Green, J. A. K. Howard, M. A. McKervey, P. McGuigan, I. Ledoux, E. Orti, R. Viruela, P. M. Viruela, B. Tarbit, *Journal of Materials Chemistry* **1998**, *8*, 1173-1184.
- [9] M. Zhang, H. N. Tsao, W. Pisula, C. D. Yang, A. K. Mishra, K. Mullen, *Journal of the American Chemical Society* **2007**, *129*, 3472-+.
- [10] Y. J. Cheng, S. H. Yang, C. S. Hsu, *Chemical Reviews* **2009**, *109*, 5868-5923.
- [11] R. Kroon, M. Lenes, J. C. Hummelen, P. W. M. Blom, B. De Boer, *Polymer Reviews* **2008**, *48*, 531-582.
- [12] J. Hu, D. Zhang, F. W. Harris, *Journal of Organic Chemistry* **2005**, *70*, 707-708.
- [13] S. Shimizu, S. Nakano, T. Hosoya, N. Kobayashi, *Chemical Communications* **2011**, *47*, 316-318.
- [14] H. Vollmann, H. Becker, M. Corell, H. Streeck, *Justus Liebigs Annalen der Chemie* **1937**, *531*, 1-159.
- [15] G. Saito, S. Hirate, K. Nishimura, H. Yamochi, *Journal of Materials Chemistry* **2001**, *11*, 723-735.
- [16] G. Heywang, S. Roth, *Angewandte Chemie-International Edition in English* **1991**, *30*, 176-177.
- [17] H. J. Zhang, Y. Wang, K. Z. Shao, Y. Q. Liu, S. Y. Chen, W. F. Qiu, X. B. Sun, T. Qi, Y. Q. Ma, G. Yu, Z. M. Su, D. B. Zhu, *Chemical Communications* **2006**, 755-757.
- [18] J. W. Oh, Y. O. Lee, T. H. Kim, K. C. Ko, J. Y. Lee, H. Kim, J. S. Kim, *Angewandte Chemie-International Edition* **2009**, *48*, 2522-2524.
- [19] G. Venkataramana, P. Dongare, L. N. Dawe, D. W. Thompson, Y. M. Zhao, G. J. Bodwell, *Organic Letters* **2011**, *13*, 2240-2243.

- [20] J. Y. Hu, M. Era, M. R. J. Elsegood, T. Yamato, *European Journal of Organic Chemistry* **2010**, 72-79.
- [21] J. S. Seldenthuis, F. Prins, J. M. Thijssen, H. S. J. van der Zant, *Acs Nano* **2010**, *4*, 6681-6686.
- [22] L. X. Wang, B. X. Gao, M. Wang, Y. X. Cheng, X. B. Jing, F. S. Wang, *Journal of the American Chemical Society* **2008**, *130*, 8297-8306.
- [23] M. V. Bhatt, *Tetrahedron* **1964**, *20*, 803-&.
- [24] M. Hanif, P. Lu, M. Li, Y. Zheng, Z. Q. Xie, Y. G. Ma, D. Li, J. H. Li, *Polymer International* **2007**, *56*, 1507-1513.
- [25] K. Müllen, Y. Fogel, M. Kastler, Z. H. Wang, D. Andrienko, G. J. Bodwell, *Journal of the American Chemical Society* **2007**, *129*, 11743-11749.
- [26] X.-F. Wu, P. Anbarasan, H. Neumann, M. Beller, *Angewandte Chemie International Edition* **2010**, *49*, 9047-9050.
- [27] L. Zöphel, D. Beckmann, V. Enkelmann, D. Chercka, R. Rieger, K. Müllen, *Chemical Communications* **2011**, *47*, 6960-6962.
- [28] K. Rajesh, M. Somasundaram, R. Saiganesh, K. K. Balasubramanian, *Journal of Organic Chemistry* **2007**, *72*, 5867-5869.
- [29] S. I. Kawano, M. Baumgarten, D. Chercka, V. Enkelmann, K. Müllen, *to be submitted*.
- [30] N. E. Galanin, E. V. Kudrik, G. P. Shaposhnikov, *Russian Journal of Organic Chemistry* **2006**, *42*, 603-606.
- [31] M. J. Frisch, G. W. Trucks, H. B. Schlegel, G. E. Scuseria, M. A. Rob, J. R. Cheeseman, J. A. Montgomery Jr., T. Vreven, K. N. Kudin, J. C. Burant, J. M. Millam, S. S. Iyengar, J. Tomasi, V. Barone, B. Mennucci, M. Cossi, G. Scalmani, N. Rega, G. A. Petersson, H. Nakatsuji, M. Hada, M. Ehara, K. Toyota, R. Fukuda, J. Hasegawa, M. Ishida, T. Nakajima, Y. Honda, O. Kitao, H. Nakai, M. Klene, X. Li, J. E. Knox, H. P. Hratchian, J. B. Cross, V. Bakken, C. Adamo, J. Jaramillo, R. Gomperts, R. E. Stratmann, O. Yazyev, A. J. Austin, R. Cammi, C. Pomelli, J. W. Ochterski, P. Y. Ayala, K. Morokuma, P. S. G. A. Voth, J. J. Dannenberg, V. G. Zakrzewski, S. Dapprich, A. D. Daniels, M. C. Strain, O. Farkas, D. K. Malick, A. D. Rabuck, K. Raghavachari, J. B. Foresman, J. V. Ortiz, Q. Cui, A. G. Baboul, S. Clifford, J. Cioslowski, B. B. Stefanov, G. Liu, A. Liashenko, P. Piskorz, I. Komaromi, R. L. Martin, D. J. Fox, T. Keith, M. A. Al-Laham, C. Y. Peng, A. Nanayakkara, M. Challacombe, P. M. W. Gill, B. Johnson, W. Chen, M. W. Wong, C. Gonzalez, J. A. Pople, Gaussian 03 ed., Gaussian, Inc., Wallingford CT, **2003**.
- [32] S. Sumalekshmy, K. R. Gopidas, *Journal of Physical Chemistry B* **2004**, *108*, 3705-3712.
- [33] S. Sumalekshmy, K. R. Gopidas, *New Journal of Chemistry* **2005**, *29*, 325-331.

- [34] M. Maus, W. Rettig, D. Bonafoux, R. Lapouyade, *Journal of Physical Chemistry A* **1999**, *103*, 3388-3401.
- [35] B. Valeur, *Molecular Fluorescence: Principles and Applications*, Wiley-VCH Verlag GmbH, **2001**.
- [36] C. Reichardt, *Chemical Reviews* **1994**, *94*, 2319-2358.
- [37] F. Lahmani, E. Breheret, O. B. Dazy, A. Zehnackerrentien, J. F. Delouis, *Journal of Photochemistry and Photobiology a-Chemistry* **1995**, *89*, 191-199.
- [38] D. D. Bao, B. Millare, W. Xia, B. G. Steyer, A. A. Gerasimenko, A. Ferreira, A. Contreras, V. I. Vullev, *Journal of Physical Chemistry A* **2009**, *113*, 1259-1267.
- [39] A. Dey, G. R. Desiraju, *Chemical Communications* **2005**, 2486-2488.
- [40] C. L. Wang, H. L. Dong, H. X. Li, H. P. Zhao, Q. Meng, W. P. Hu, *Crystal Growth & Design* **2010**, *10*, 4155-4160.
- [41] M. R. Bryce, *Chemical Society Reviews* **1991**, *20*, 355-390.
- [42] S. Horiuchi, H. Yamochi, G. Saito, K. Sakaguchi, M. Kusunoki, *Journal of the American Chemical Society* **1996**, *118*, 8604-8622.
- [43] J. M. Williams, A. J. Schultz, U. Geiser, K. D. Carlson, A. M. Kini, H. H. Wang, W. K. Kwok, M. H. Whangbo, J. E. Schirber, *Science* **1991**, *252*, 1501-1508.
- [44] B. J. Powell, R. H. McKenzie, *Journal of Physics-Condensed Matter* **2006**, *18*, R827-R866.
- [45] L. R. Melby, W. Mahler, W. E. Mochel, R. J. Harder, W. R. Hertler, R. E. Benson, *Journal of the American Chemical Society* **1962**, *84*, 3374-&.
- [46] T. Amano, H. Kuroda, H. Akamatu, *Bulletin of the Chemical Society of Japan* **1971**, *44*, 1758-&.
- [47] K. Medjanik, D. Chercka, P. Nagel, M. Merz, S. Schuppler, M. Baumgarten, K. Müllen, S. A. Nepijko, H.-J. Elmers, G. Schönhense, H. O. Jeschke, R. Valenti, *Journal of the American Chemical Society* **2012**.
- [48] R. Rieger, Ph.D. thesis, University of Mainz **2009**.
- [49] P. F. Barbara, T. J. Meyer, M. A. Ratner, *Journal of Physical Chemistry* **1996**, *100*, 13148-13168.
- [50] C. K. Prout, J. D. Wright, *Angewandte Chemie-International Edition* **1968**, *7*, 659-&.
- [51] M. Tashiro, T. Yamato, *Journal of the American Chemical Society* **1982**, *104*, 3701-3707.
- [52] T. Yamato, M. Fujimoto, A. Miyazawa, K. Matsuo, *Journal of the Chemical Society-Perkin Transactions I* **1997**, 1201-1207.
- [53] Q. J. Shen, H. Q. Wei, W. S. Zou, H. L. Sun, W. J. Jin, *Crystengcomm* **2012**, *14*, 1010-1015.

4 Pyrenocyanines

4.1 Introduction

Phthalocyanines (Pcs) constitute an important class of organic dyes and their optical properties and thermal stability have been intensively investigated. Therefore, the application is manifold from organic pigments to semiconductors for electronic devices.^[1-6] The so-called Q-band is unique for Pcs absorption behavior and is referred to the π - π^* -transition at wavelength in the red part of the visible light and the near infrared. A common way to alter the Q-band according to the need of efficient sunlight absorption lies in the extension of the aromatic π -system attached to the tetraazaporphyrin (TAP) core. Benzannulation causes destabilization of the HOMO level and red-shifts the absorption.^[7]

Enlarged aromatic residues moreover affect the tendency for π -stacking and change the processability due to higher sublimation temperatures.^[8] Decoration with alkyl chains of large Pcs provides solubility and enables the control of the intermolecular association by π - π -interaction in solution which is referred to as aggregation.^[9-11] In addition, alkyl substituents have proven to significantly influence the bulk properties. Rigid and disc-like molecules with flexible aliphatic chains attached are known to spontaneously aggregate along a unique

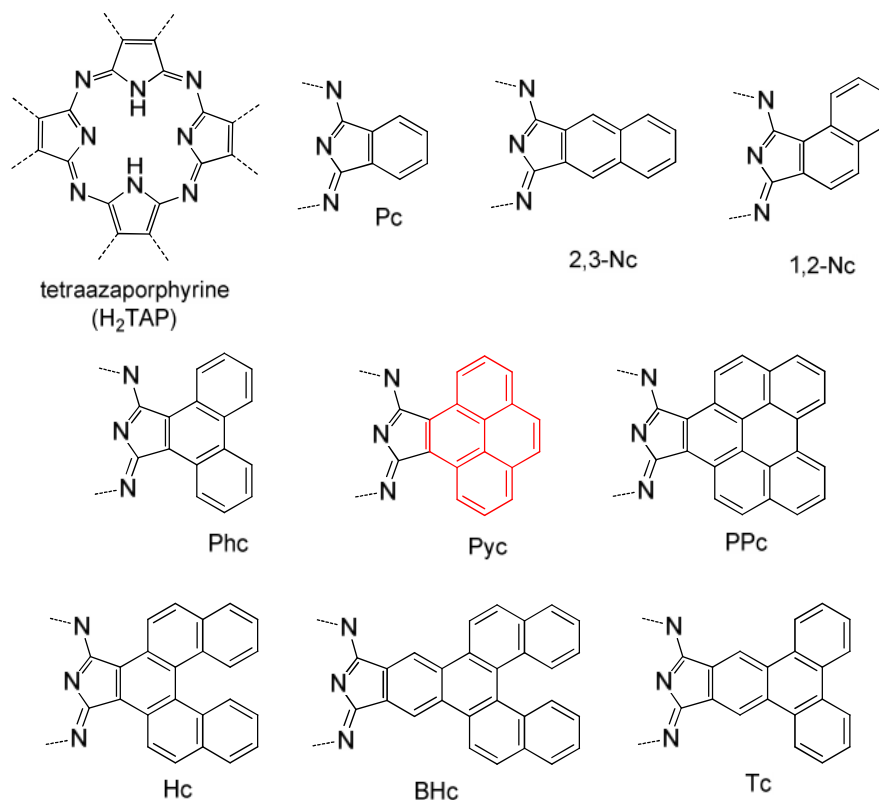
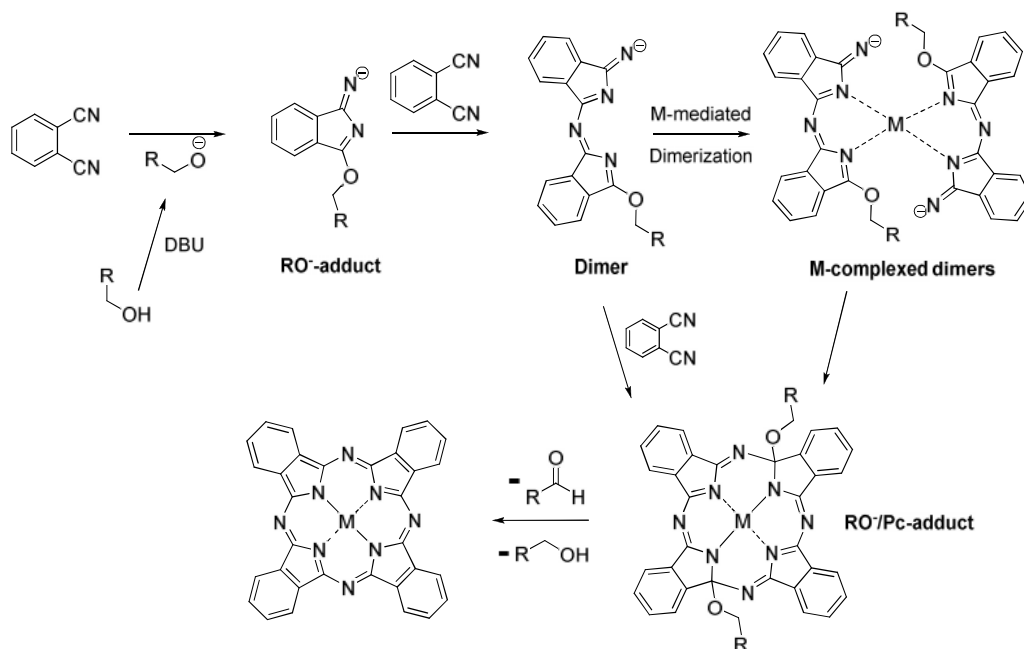


Figure 4.1: Selection of reported phthalocyanines with linearly and angularly extension. So far unknown pyrenocyanine (Pyc) is highlighted in red.

direction and assemble in a one-dimensional molecular stack, which can further organize into higher ordered two-dimensional lattices primarily as the consequence of differences in packing requirements for aromatic cores and aliphatic chains.^[12-13] This phenomenon is generally driven by attractive noncovalent forces like π - π -interaction, hydrogen bonds and van der Waals interactions. Such tendency for self-organization into columnar structures by cofacial stacking of flat and rigid aromatic discs with dangling alkyl chains in the periphery is well known.^[13-15] Fine control over the liquid crystalline thermotropic behavior can be achieved by the variation of the steric demand of the chains.^[16-17]

A major motivation of such studies is the application in field-effect transistors (FETs) and photovoltaic cells (PVCs) due to charge carrier transport along one-dimensional columnar pathways enabled by π -orbital overlap of



Scheme 4.1: Proposed mechanism for the phthalocyanine-forming reaction.^[18]

adjacent molecules.^[19-22] Furthermore, Pcs have been found to self-assemble uniquely which was used for the construction of nanostructures on surfaces including helical fibers.^[23-26]

The synthesis of phthalocyanines is comparatively simple in view of other macrocycles, in case the required precursor is available. Generally spoken, a large number of *ortho*-disubstituted compounds can be applied. *ortho*-Substitution is a definite prerequisite. Just to mention a few phthalocyanine precursors, phthalic acid, phthalonitrile, phthalic anhydride, phthalimide, diiminoindoline, *o*-cyanobenzamide, iminothioamide or dithioimide have been used.^[27] However, most Pcs with extended π -systems have been prepared by the cyclotetramerization reaction of the aromatic *ortho*-dicyano precursor in the presence of a base in high boiling alcohols. The mechanism of the cyclotetramerization has not yet been completely revealed. A proposed mechanism is depicted in Scheme 4.1 which is partly based on isolated intermediates.^[18, 28] After deprotonation of the alcohol a RO^- -adduct is formed which reacts with a second phthalonitrile to the respective dimer. Either by metal-mediated dimerization or sequential addition of phthalonitrile units would

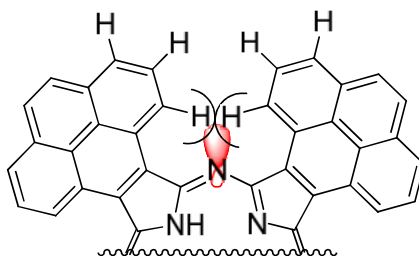


Figure 4.2: Illustration of the steric overcrowding caused by the angularly annulated benzene rings and the electron lone-pair of the TAP skeleton.

give the intermediate RO⁻/Pc-adduct results. The aromatization occurs under elimination of the aldehyde and the respective alcohol. In this proposed mechanism the solvent alcohol is crucial and has three functions at the same time: solvent, nucleophile and reducing agent.

A series of Pcs is shown in Figure 4.1. By name, phenanthrolocyanine (Phc)^[29-30], triphenylenophthalocyanine (Tc)^[31-32], helicenocyanine (Hc)^[33-34], benzohelicenocyanine (BHc)^[35] and perylenophthalocyanine (PPc)^[36] have been built from benzene or naphthalene precursors because protocols are rare for direct *ortho*-functionalization of polycyclic aromatic hydrocarbons (PAHs).

The four phthalocyanines Phc, Hc, PPc and the proposed 4,5-pyrenocyanine (Pyc) bear the structural motif of angular annulation of two benzene rings. The issue of spatial overlap of inner pyrene hydrogen atoms and the TAP nitrogen lone-pairs has solely been addressed for Phcs. The overcrowding illustrated in Figure 4.2 is therein described to be relieved by warping of the TAP ring.^[29] A saddle and propeller conformation is proposed and can be expected for Pycs as well.

The annulation of pyrene to the TAP core and thereof arising non-planar three-dimensional shape holds promise for new optical and self-assembling properties. In this chapter, the synthesis of a series of alkoxy substituted pyrenocyanines is presented and a detailed investigation of the adsorption behavior at the liquid/solid interface and the assembly in bulk in dependency on chain length and spatial demand is described.

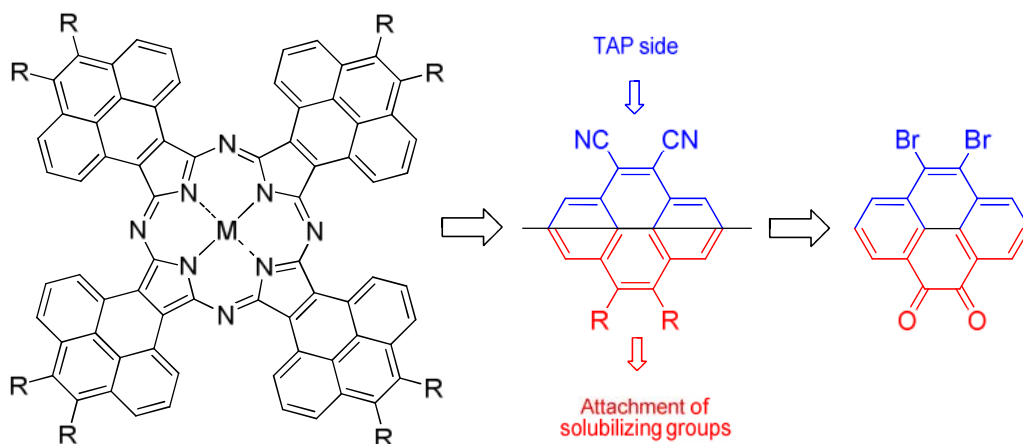
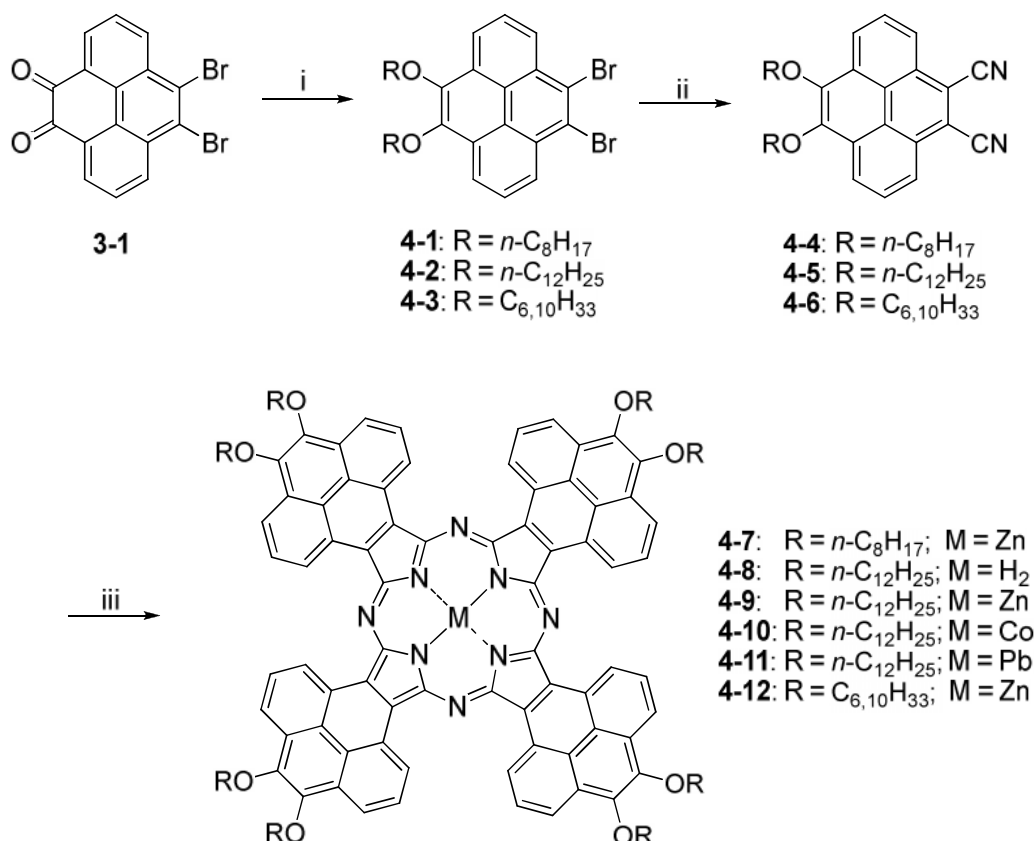


Figure 4.3: Retrosynthesis of 4,5-pyrenocyanines (Pycs).

4.2 Synthesis

Retrosynthetic considerations are depicted in Figure 4.3 and are taking the introduction of solubilizing groups into account. Based on the asymmetrically substituted pyrene building block **3-1**,^[37] reductive methylation with dimethyl sulfate followed by the exchange of bromine has been described in the previous chapter. In the present case, reductive alkylation was achieved by alkyl bromides in the presence of sodium dithionite (Scheme 4.2). With respect to the study of aggregation behavior and self-assembly properties, linear C₈ and C₁₂ as well as branched C_{6,10}^[38] alkoxy chains were attached to obtain 4,5-dibromo-9,10-dialkoxypyrenes **4-1**, **4-2** and **4-3**. The same conditions for the synthesis of **3-6** were applied to yield the *ortho*-dicyano precursors **4-4**, **4-5** and **4-6** in good yields.

Tetramerization reaction was achieved by reflux of 4,5-dialkoxy-9,10-dicyanopyrenes **4-4**, **4-5** and **4-6** in dry isopentanol for two days in the presence of DBU and the respective metal chloride to give a series of Pycs with different alkoxy chains and metals in the cavity.^[39] For workup, the Pycs were precipitated in a one-to-one mixture of methanol/water and purified by repeated



Scheme 4.2: Synthetic route for the preparation of pyrenocyanines **4-7** to **4-12**: *i* RBr, $\text{Na}_2\text{S}_2\text{O}_4$, KOH, Bu_4NBr , THF/ H_2O 1.75:1, 40°C , overnight, **4-1** 72 %, **4-2** 90 %, **4-3** 30 % yield; *ii* CuCN, NMP, 180°C , 3 days, **4-4** 78 %, **4-5** 74 %, **4-6** 79 % yield; *iii* MCl_2 , DBU, 1-pentanol, reflux, 2 d, **4-7** 26 %, **4-8** 6 % (without addition of MCl_2), **4-9** 34 %, **4-10** 18 % (using $\text{Co}(\text{OAc})_2$), **4-11** 34 %, **4-12** 32 % yield.

size exclusion chromatography. Using ZnCl_2 the zinc centered pyrenocyanines **4-7**, **4-9** and **4-12** were isolated in yields around 30 % which is in the same order of other π -extended phthalocyanines. Reflux of **4-5** with PbCl_2 , $\text{Co}(\text{OAc})_2$ or without a metal salt gave the respective lead, cobalt and metal-free pyrenocyanines. The lead centered Pyc **4-11** was formed in 32 % yield, whereas cobalt bearing **4-10** was obtained in 18 % yield. Assumably, the synthesis of the free-base variant **4-8** suffers from the lack of a coordinating metal ion resulting in a poor yield of 6 %.

The newly synthesized pyrenocyanines were characterized by IR spectroscopy which revealed very similar transitions for all Pycs. In case of the non-metalated form **4-8** the characteristic N-H stretching band of the cavity

protons was found at 3298 cm^{-1} and therefore proves the absence of a metal in the cavity. The molecular weights of the protonated molecular ions of all pyrenocyanines were confirmed by high resolution ESI-TOF mass spectrometry in collaboration with Louis Bertschi from the ETH Zürich.

4.3 NMR Investigations

Investigation on π -extended phthalocyanines in solution by nuclear magnetic resonance (NMR) spectroscopy is complicated due to the often found efficient π - π -cofacial interactions leading to the formation of dimers, trimers or higher aggregates.^[40-41] Nevertheless, the concentration dependence of the aromatic signals of disc-like molecules in proton NMR spectra has often been used for the investigation of this phenomenon and is considered as a “signature” of aggregation.^[11, 42] This shift of the resonances is caused by the ring current of adjacent aromatic cores being typically in a face-to-face order.

The proton NMR spectrum of the free-base Pyc **4-8** shows three broadened signals at room temperature in the aromatic region in DCM, which correspond to the pyrene positions 1, 2, and 3 (Figure 4.4). The signals of α -, β - and ω -protons are likewise broadened but resolved. The expected *NH* signal appears as two broad resonances (2 H by integration) at -6.70 ppm and -9.53 ppm (Figure 4.4 inset). It is assumed that the high upfield shift arises from cofacial association of TAP's which promotes a stronger ring current effect.^[29, 43-44] Attributing the splitting into two signals to the dynamic formation of molecular assemblies, the solvent was changed to tetrachloroethane- d_2 and the solution was heated gradually to 393 K. Surprisingly, at room temperature six instead of two resonances appear from -5 ppm to -10 ppm and the aromatic region from 7.0 ppm to 10.5 ppm shows multiple peaks, indicating a pronounced solvent dependency.^[11] Upon heating coalescence was observed for both, aromatic and

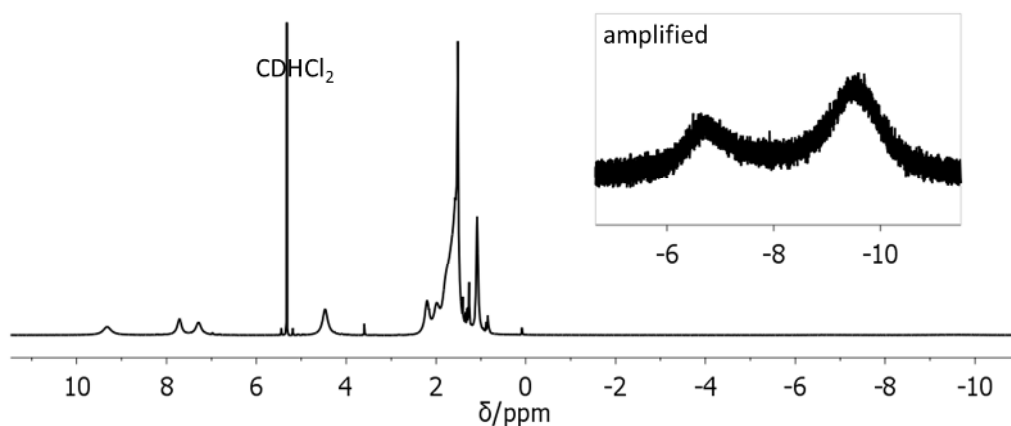


Figure 4.4: ¹H NMR spectrum (700 MHz, RT, 2.5 mg/ml) of **4-8** in CD₂Cl₂.

NH resonances. Additionally performed 2D NOESY exchange experiments at room temperature revealed the complete exchange of the six NH resonances, and thus, strengthen the hypothesis of an aggregation induced phenomenon.

A similar solvent dependency was found for zinc centered Pycs with linear and branched alkoxy chains. The proton NMR spectra of **4-9** and **4-12** in DCM and THF are depicted in Figure 4.5. In the aromatic region three broad signals were observed for **4-9** with linear dodecyl chains, similar to the metal-free Pyc **4-8** in the same solvent. Switching to THF causes multiple resonance splitting and a downfield shift by ~2 ppm. In contrast, **4-12** exhibits multiple aromatic resonances in DCM but sharply resolved peaks in THF which even allowed ¹³C NMR spectroscopy. This finding supports the assumption of monomeric species of **4-12** in THF solution and complex assemblies of the molecules in DCM indicated by the line broadening as consequence of aggregation.^[11] In turn, **4-9** with linear alkoxy chains appears to exhibit aggregated species in both solvents as a consequence the broadened and split resonances in the aromatic region.

Similar observations have already been described for other discotic molecules. Geerts et al. reported solvent dependency for octaalkoxycarbonyl phthalocyanines determined by the nature of the alkyl substituents.^[11] Similarly, proton NMR spectroscopy of alkyl decorated hexa-*peri*-hexabenzocoronenes (HBCs) revealed moderate aggregation in THF compared to benzene and cyclohexane.^[10]

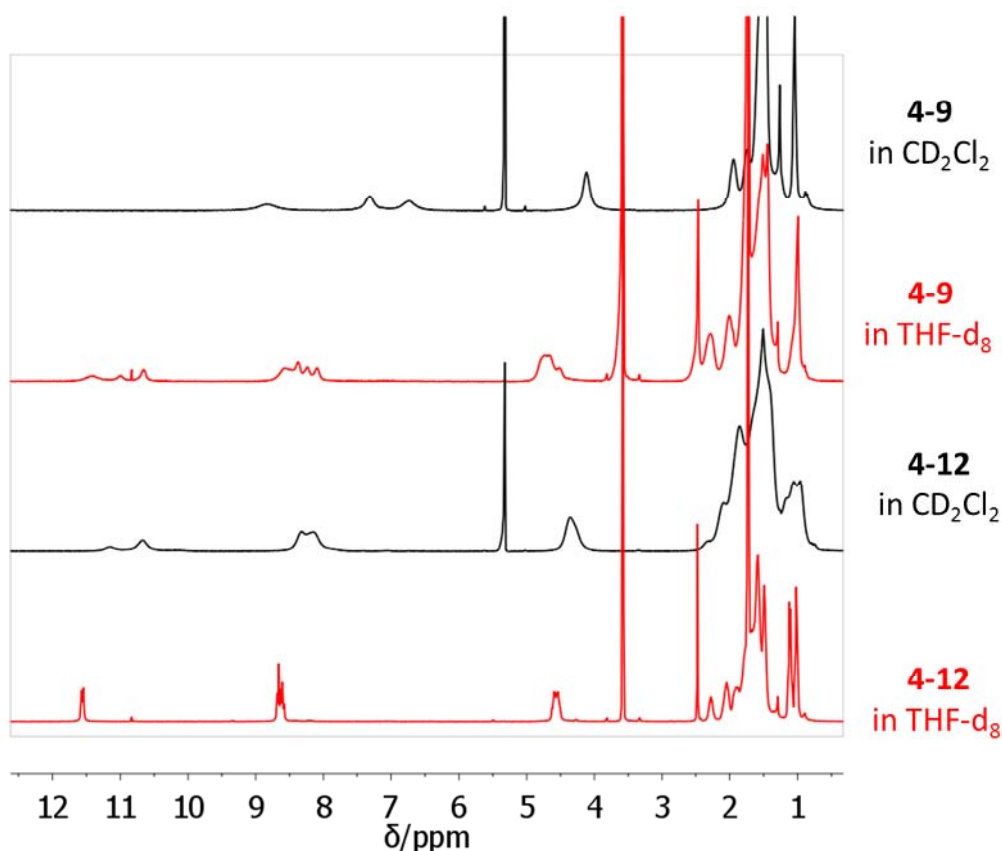


Figure 4.5: ¹H NMR spectra (300 MHz, RT) of **4-9** (9.7 mg/ml) and **4-12** (11.4 mg/ml) in CD₂Cl₂ (black) and THF-d₈ (red).

Therefore, THF was chosen in order to study the aggregation phenomenon of **4-9** and **4-12** by concentration dependent proton NMR spectroscopy. Proton NMR spectra were recorded at 0.1 mg/ml, 1 mg/ml, 10 mg/ml and 25 mg/ml concentration. The spectra of **4-12** show the same pattern of three sharp peaks at the same chemical shift in the aromatic region at all concentrations, and thus, support the presence of only monomeric species (spectra not shown; compare Figure 4.5 **4-12** in THF-d₈). Branched chains have already been used successfully to prevent self-aggregation of phthalocyanines but with benzene instead of pyrene as aromatic moiety.^[9]

The observation of no aggregation of **4-12** is rather surprising in respect to the large aromatic pyrene residue attached to the TAP core because even with branched alkoxy chains large discotic molecules like HBCs start to form

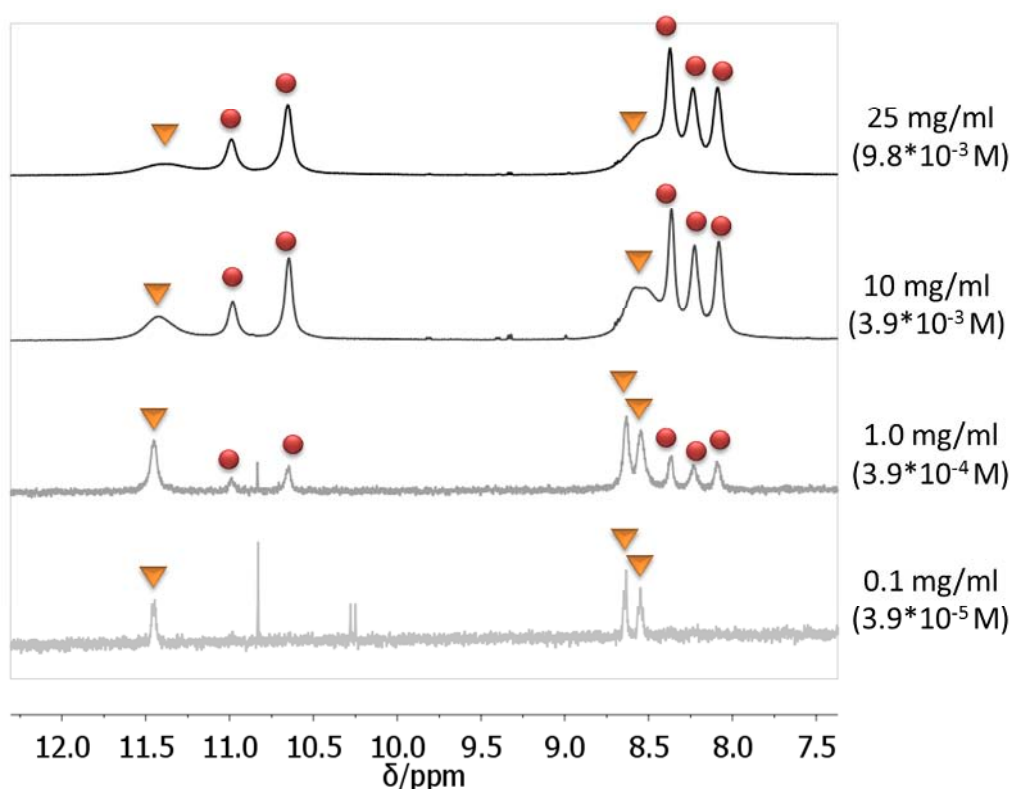


Figure 4.6: ^1H NMR spectra (500 MHz, RT) of **4-9** at different concentrations in THF-d_8 .

aggregates at concentrations between 10^{-5} M to 10^{-4} M.^[10, 29, 36] The deviation from planarity caused by steric crowding between the pyrene residues might be an explanation for reduced aggregation (compare Figure 4.2).

The spectra of **4-9** at different concentrations are depicted in Figure 4.6. At 0.1 mg/ml one set of three sharp signals (▼) appears which can be attributed to the three protons of the pyrene moiety. The signals exhibit the expected multiplicity of two doublets and one triplets and have almost identical chemical shifts (11.45 ppm, 8.64 ppm, 8.55 ppm) with **4-12** in THF (11.56 ppm, 8.67 ppm, 8.60 ppm). With increasing concentration the signals (▼) strongly broaden whereas five new signals (●) arise upfield. Two sets of independent resonances have already been reported for the formation of monomers and dimers of dendronized hexa-*peri*-hexabenzocoronenes with increasing concentration.^[42] In the present case, the set of the three signals (▼) can be assigned to the monomeric species. Most likely, the second set of signals (●)

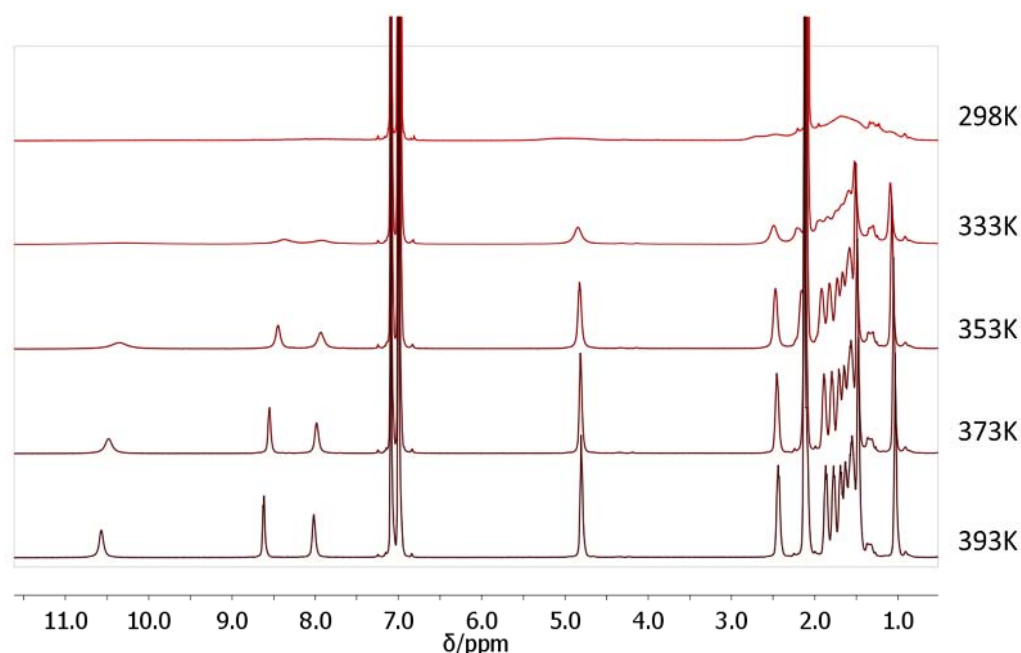


Figure 4.7: ^1H NMR spectra (500 MHz) of **4-11** in toluene- d_8 at 298 K, 333 K, 353 K, 373 K and 393 K.

corresponds to an concentration dependent average over different oligomeric species with a fast self-association equilibration on the NMR time scale.^[42]

As mentioned above, lead centered Pyc **4-11** with linear C_{12} chains shows no solubility in DCM and THF at room temperature. Therefore, temperature dependent proton NMR spectroscopy in deuterated toluene was performed and the spectra are depicted in Figure 4.7. With gradually increasing temperature **4-11** dissolves and the signals rise and sharpen. The expected pattern of three aromatic signals and the alkoxy chains were observed together with a slight downfield shift of aromatic signals. The sharpening can be attributed to the higher equilibration rate of the aggregated species at elevated temperatures.^[45]

The unexpectedly different solubility of **4-11** compared to the other investigated Pycs must be related to the exchange of the metal in the center as the periphery is identical to **4-9**. Earlier investigations by X-ray analysis on the cavity size of phthalocyanines as a function of the metal ion show that the cavity is only slightly widened in case of zinc and lead. Contrary to this, the distance of the metal from the TAP plane differs from zinc (0.075 Å) to lead (>1.2 Å) substantially.^[46] This observation is ascribed to the tremendous

increase of the size from zinc to lead which forces the lead atom far out of the phthalocyanine plane.^[47] In addition, it has been shown from X-ray data that lead phthalocyanines exhibit pseudo-double-decker structure by the binding of the lead atom of one molecule to an aza nitrogen atom of the other.^[48-49] Such binding could be a reason for the reduced solubility.

4.4 Optical Properties

Historically, phthalocyanines have always been associated with their outstanding optical properties. Therefore, the investigation of new Pyc's absorption behavior is of high interest in respect to their potential application as organic dye.

The absorption spectra of pyrenocyanines **4-7** to **4-12** in toluene are depicted in Figure 4.8 and the values are listed in Table 4.1 on page 77. Zinc centered Pycs with different C₈, C₁₂ and C_{10,6} alkoxy chains show similar spectra. The Q-band appears broad from 550 nm to 750 nm and the B-band is found below 400 nm. Similar broad Q-band absorption was reported for structurally related phenanthralocyanines. Therein, the broadening is ascribed to the structural motif of the angularly benzannulated π -system and thereof derived nonplanarity in contrast to the usually planar Pc core.^[29] The change from short and linear to longer and branched alkoxy chains leads to a small increase of the extinction coefficient of the Q-band.

Compared to the free-base anthralocyanine^[50] bearing three linearly annulated benzene rings with a sharp Q-band at 980 nm, Pycs absorb light at substantially shorter wavelength. Orti et al. explain this observation with a destabilization of the HOMO level for angularly benzannulated species to a smaller extent compared to linearly fused Pcs which leads to Q-band absorption at shorter wavelength.^[7] A broadened Q-Band at 703 nm in toluene is reported for helicenocyanine (H₂Hc) as well.^[33-34]

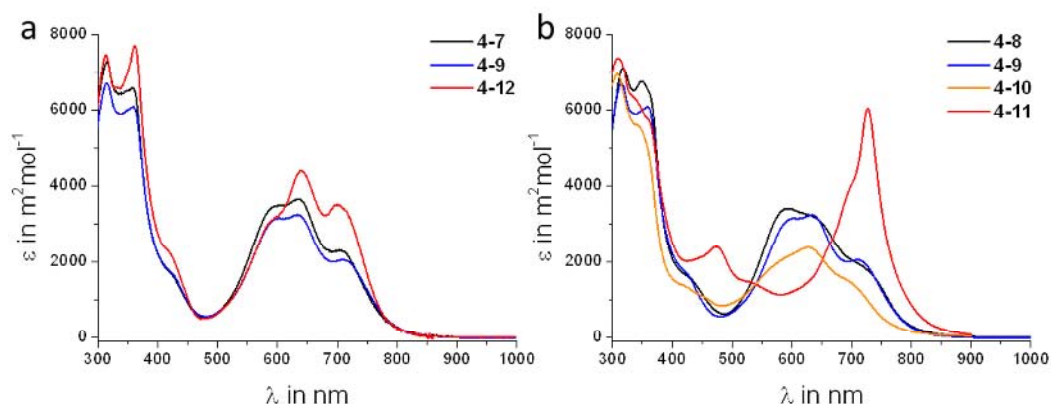


Figure 4.8: UV/vis absorption spectra of pyrenocyanines (a) **4-7**, **4-9**, **4-12** and (b) **4-8**, **4-9**, **4-10** and **4-11** in toluene at room temperature and 10^{-5} M concentration.

Table 4.1: Optical properties of pyrenocyanines.^[a]

| Compound | B-band (ϵ) ^[b] | Q-band (ϵ) ^[b] |
|-------------|--------------------------------------|--------------------------------------|
| 4-7 | 315 nm (7280), 359 nm (6589) | 633 nm (3654), 707 nm (2313) |
| 4-8 | 317 nm (7110), 349 nm (6758) | 592 nm (3401) |
| 4-9 | 315 nm (6711), 359 nm (6081) | 634 nm (3238), 710 nm (2055) |
| 4-10 | 307 nm (6958) | 628 nm (2388) |
| 4-11 | 309 nm (7370) | 727 nm (6036) |
| 4-12 | 314 nm (7471), 361 nm (7704) | 639 nm (4383), 700 nm (3511) |

[a] All absorption and emission spectra are measured in toluene, RT, at a concentration of $1 \cdot 10^{-5}$ M. [b] Extinction coefficients (ϵ) are given in $\text{m}^2\text{mol}^{-1}$.

Figure 4.8 **b** shows the absorption spectra of pyrenocyanines with C_{12} chains but different cavities. The free-base form **4-8** marginally differs from the UV/vis absorption of **4-9**. Cobalt centered Pyc **4-10** exhibits smaller extinction coefficients but a similarly broad shape of the Q-band like **4-8** and **4-9**. In contrast, lead Pyc **4-11** has a narrow Q-band and absorbs light at a maximum of 727 nm with a strongly increased extinction coefficient in comparison to the Q-band absorption of the other Pycs. Similar sharpening and bathochromic shift of the Q-band from the free-base to the lead centered form have also been reported for angularly annulated Hc, BHc^[33] and PbPhc.^[29]

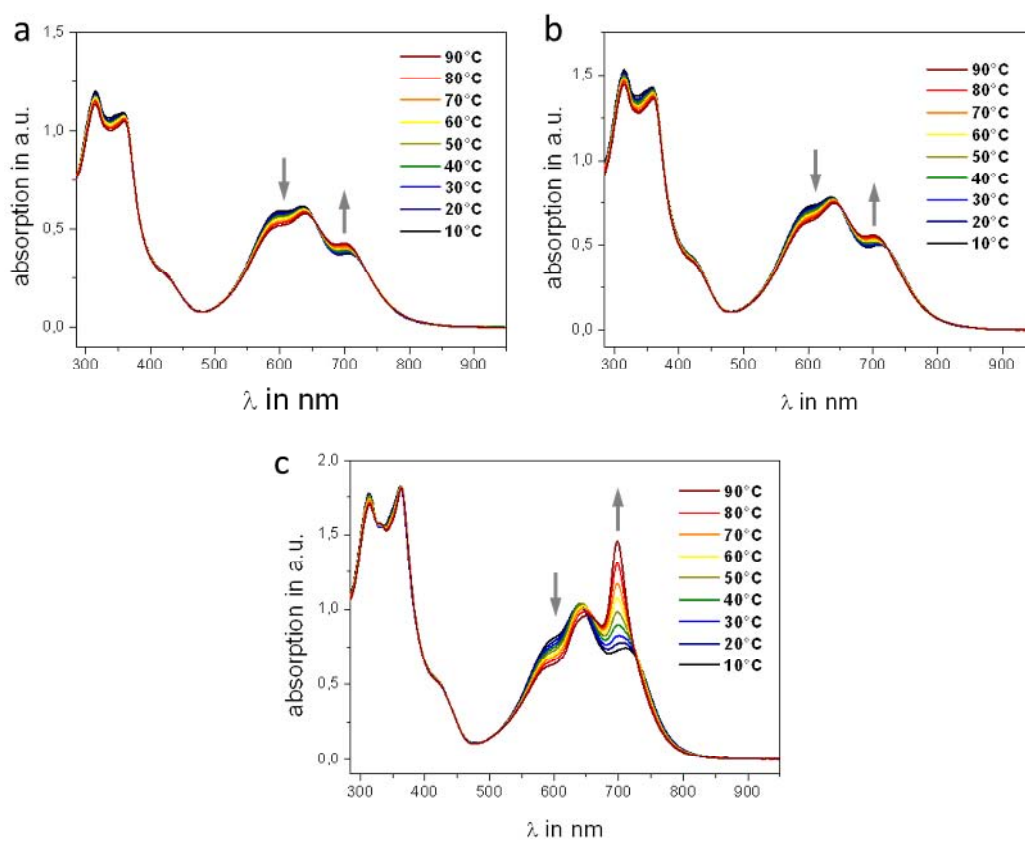


Figure 4.9: Temperature dependent absorption spectra of (a) 4-7, (b) 4-9 and (c) 4-12 in toluene from 10°C to 90°C at 2×10^{-5} M concentration; arrows indicate the change in absorption with increasing temperature.

Beside the strong influence on optical and electronic properties by the annulation of pyrene to the TAP core, a considerable contribution to the aggregation can be expected. It has often been reported that disc-like molecules assemble to dimers, trimers or even higher species in solution which in turn changes the intrinsic properties by intermolecular interactions. Under these premises, temperature dependent UV/vis absorption measurements were performed in order to monitor possible changes at elevated temperature.

The temperature dependent UV/vis spectra of the zinc centered Pycs in toluene are depicted in Figure 4.9. The temperature was increased in steps of 10 degrees from 10°C up to 90°C and again down to 30°C to evaluate the stability of the Pycs by comparison of the spectra before and after heating. The

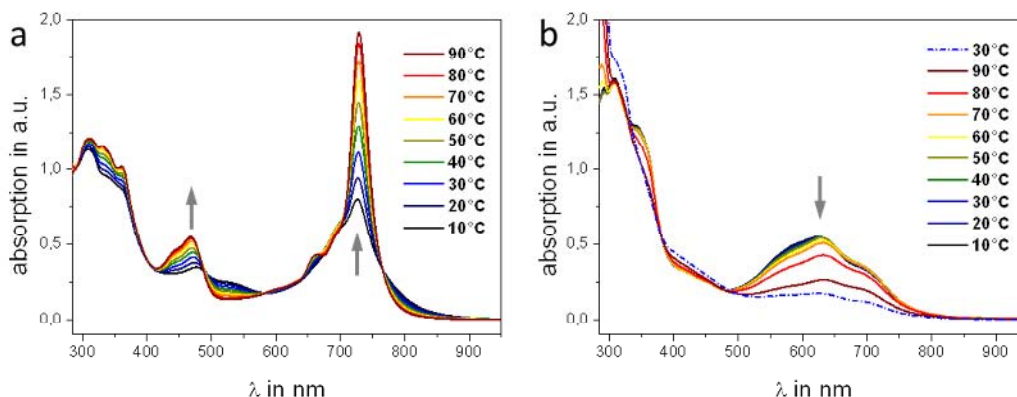


Figure 4.10: Temperature dependent absorption spectra of (a) **4-11** and (b) **4-10** in toluene from 10°C to 90°C at $2 \cdot 10^{-5}$ M concentration; arrows indicate the change in absorption with increasing temperature.

Pycs with linear alkoxy chains **4-7** and **4-9** show only small changes in absorption. In contrast, the absorption band at the longest wavelength of **4-12** distinctively increases. It is well known that self-association processes of phthalocyanines in solution strongly alter the UV/vis absorption behavior in the way of a broadened Q-band with decreased molar extinction.^[51] Presuming that branched chains disfavor cofacial π - π -interaction of disc-like molecules,^[10] the formation of aggregated species of **4-12** is reduced by increasing temperature indicated by the strong change of the Q-band. In case of **4-7** and **4-9** with linear chains the aggregation could not be overcome at the applied temperature and therefore only small changes in the absorption were detected. All zinc centered Pycs showed no change in the absorption spectrum after cooling to 30°C, indicating thermal stability of these Pycs in solution.

The absorption of the Q-band increases most for lead Pyc **4-11** upon heating from 10°C to 90°C by a factor of more than two (Figure 4.10 a). In addition, a second band between 420 nm and 490 nm rises in intensity. It is noteworthy that upon cooling down to 30°C the initial absorption recovers, although lead centered Pcs are known to decompose easily in solution.^[33]

In contrast to all herein described Pycs, fast decomposition of **4-10** was observed in solution (Figure 4.10 b). Absorption intensity decreased gradually upon heating.

4.5 Self-Assembly at the Liquid/Solid Interface (STM)

The results from NMR and UV/vis spectroscopy revealed pronounced effects of the pyrene units attached to the TAP core and the steric demand of alkoxy substituents on the self-association of Pycs in solution. This subchapter focusses on the formation of supramolecular arrays of Pycs at the liquid/solid interface after the deposition of the molecules from solution. In view of the inherently non-planar nature of the molecular frame of Pycs compared to conventional Pcs this issue may provide new perspectives for molecular self-assembly.

Many flat and disc-shaped molecules like macrocycles, HBCs and Pcs have been found to self-organize into monolayers at the liquid/solid interface.^[16, 52-55] In order to achieve well-defined geometries, highly specific communication is required between large numbers of such molecules to form defect-free arrays. In contrast to covalent networks of Pcs,^[56] the non-covalent approach of self-assembly exploits weak but multiple intermolecular interactions to construct supramolecular architectures by hydrogen bonds, π - π -interactions and van der Waals interactions.^[57] In particular, peripheral alkyl chains have been found to interdigitate with the ones of neighboring molecules and thus stabilize the array as well as provide van der Waals interactions with HOPG (highly oriented pyrolytic graphite) substrates due to the high degree of structural matching.^[58-59]

The visualization of the assembly on a molecular level has always been equally fascinating and valuable for scientists. In collaboration with Dr. [REDACTED] and Prof. Dr. [REDACTED] from the Division of Molecular Imaging and Photonics of the K. U. Leuven (Belgium) a detailed investigation of Pycs **4-8**, **4-9** and **4-12** at the liquid/solid interface using Scanning Tunneling

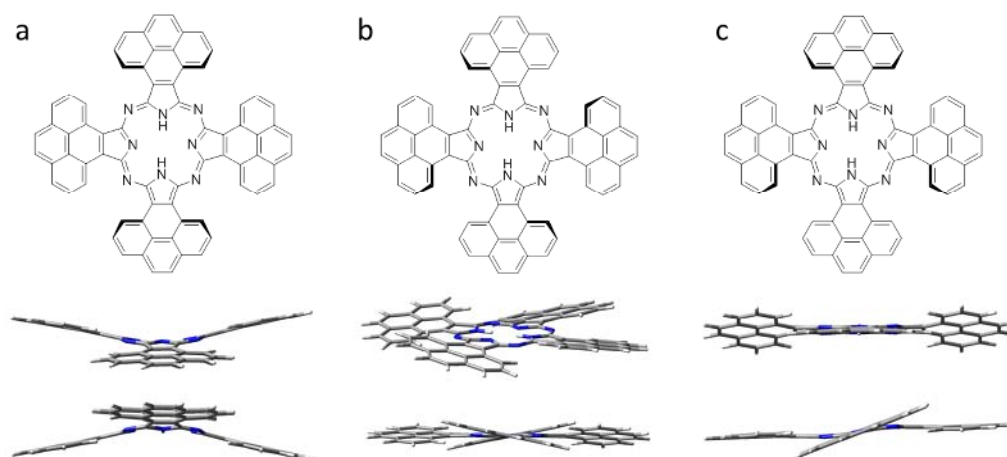


Figure 4.11: DFT/B3LYP/6-31G(d) calculation in vacuum of free-base Pyc core; (a) saddle conformation (lowest energy), (b) propeller conformation (+1.0 kcal/mol) and (c) stair conformation (+1.2 kcal/mol).

Microscopy (STM) has been performed. STM enables real-space visualization of submolecular characteristics of large solution processable molecules being not suitable for ultra-high vacuum deposition. Therefore, the Pycs were dissolved in high boiling alkanes and dropped onto HOPG.

As briefly addressed in Figure 4.2 the angular annulation leads to a non-planar conformation of the Pycs. DFT calculations on B3LYP level using 6-31G(d) basis set were performed by Dr. [REDACTED] and predict the three-dimensional structure of metal-free Pyc core which is illustrated in Figure 4.11. Similar to Phcs, three conformations assigned as propeller, saddle and stair conformation turned out to be favorable for the free-base Pyc. The energy minimum was found for the saddle, whereas the other two are only slightly less favorable by 1 kcal/mol (propeller) and 1.2 kcal/mol (stair). It was expected that this uncommon conformational shape provides new perspectives for the molecular self-assembly compared to other Pcs. All Pycs investigated by STM bear eight alkoxy chains in the periphery of the molecule. Beside the aforementioned solubilizing effect, those facilitate the anchoring of molecules on the surface of HOPG *via* favorable van der Waals interactions.

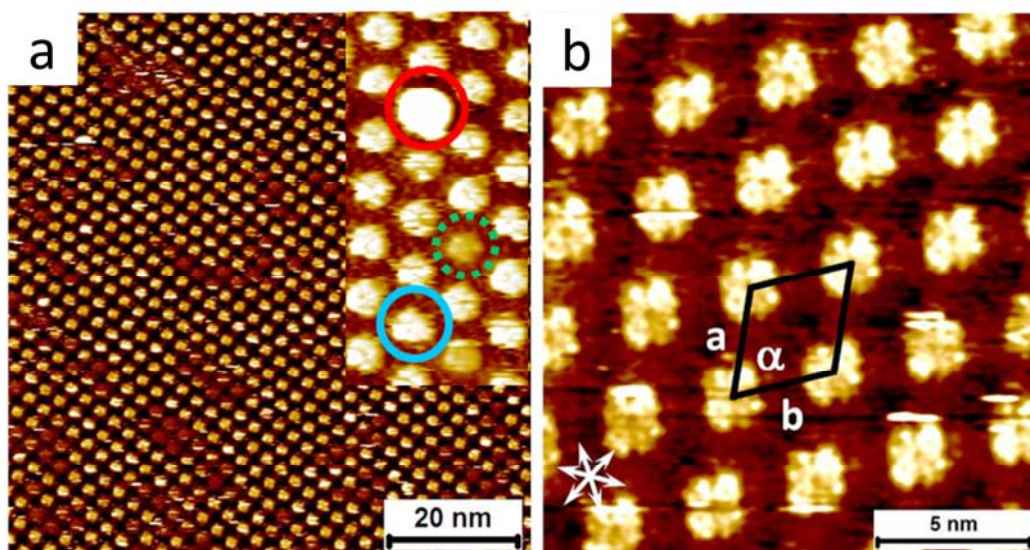


Figure 4.12: Large scale (a) and high resolution (b) STM images of **4-8** adsorbed at the 1-phenyloctane/HOPG interface. The main symmetry axes of the graphite lattice are shown in the lower left corner of **b**. Unit cell parameters: $a = 3.42 \pm 0.08$ nm, $b = 3.48 \pm 0.08$ nm and $\alpha = 66.0 \pm 2.0^\circ$; 1 molecule/unit cell, plane group $p2$. Tunneling conditions: $V_t = -1.0$ V / $I_t = 22$ pA.

At first, metal-free pyrenocyanine **4-8** was adsorbed at the 1-phenyloctane/HOPG interface and the STM images are depicted in Figure 4.12. Well-ordered two-dimensional arrays were found in which the molecules arranged in the form of rows. The unit cell of **4-8** on HOPG surface is drawn in Figure 4.12 **b** in black and the cell parameters are $a = 3.42 \pm 0.08$ nm, $b = 3.48 \pm 0.08$ nm and $\alpha = 66.0 \pm 2.0^\circ$ and belong to the plane group $p2$. The influence of the substrate lattice on the self-assembly is confirmed by the found sixfold symmetry of the network and indicates epitaxial adsorption.

Unfortunately, the presumably interdigitating alkoxy side chains could not be resolved for **4-8**, which are believed to stabilize the molecular network by van der Waals forces. Nevertheless, high resolution could be achieved of the central aromatic core consisting of four separated lobes and a depression hole in the middle which corresponds to the metal-free cavity (Figure 4.12 **b**).

Taking a closer look at the contrast of **4-8**, a conspicuous variation is observed. Three different levels (Figure 4.12 **b** inset; red, blue and green circle)

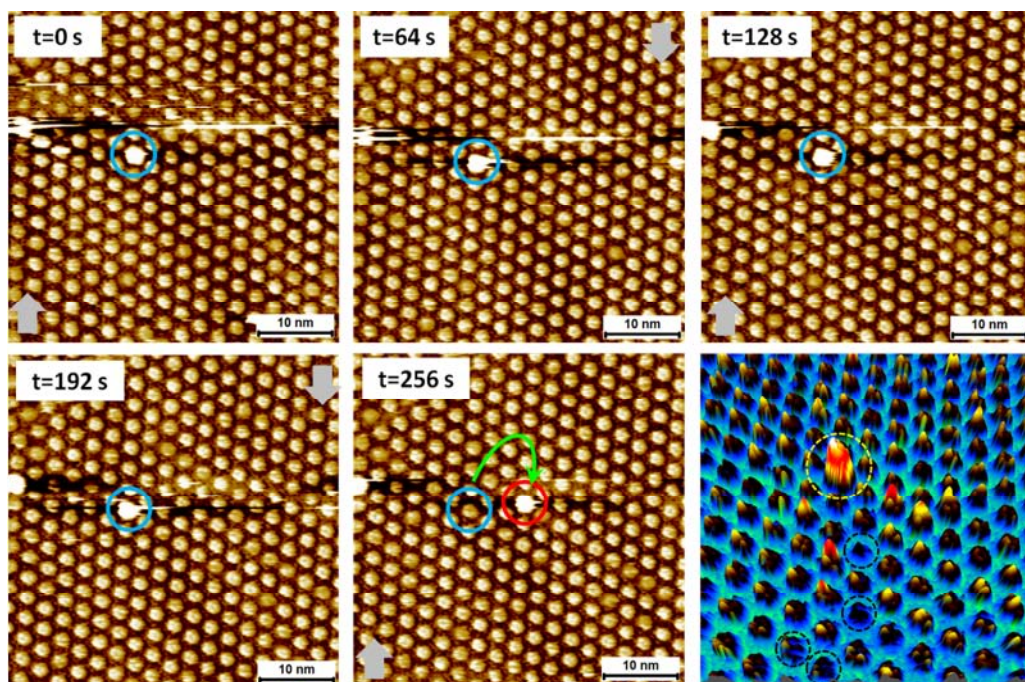


Figure 4.13: Time dependent STM images of **4-8** showing the dynamics of bright features within the monolayer. The bright features are stable over few minutes and tend to migrate over molecules. Tunneling conditions: $V_t = -0.850$ V/ $I_t = 35$ pA. bottom right: 3D representation highlighting the height difference.

can be distinguished from the STM images. Two different experimental events could explain the various levels of contrast: First, more than one molecule is located between tip and substrate. Second, molecules could be adsorbed in different conformations.

To experimentally elucidate the origin of those observed variations, concentration dependent measurements were performed. Decreasing the concentration of the solution led to disappearance of the brighter spots (Figure 4.12 **a** inset, red circle), and thus, suggests the existence of π -stacked dimers. Additional time resolved experiments by scanning the same area of the substrate are depicted in Figure 4.13. Migration within the monolayer seems to take place while the dimers remain stable for three to four minutes.

Concentration dependent investigation could not give an explanation for the dark spots (Figure 4.12 **a** inset, green dashed circle), and thus, the conformational approach seems likely. The inherent non-planar structure of Pycs due to the angular annulation might be the origin of an up or down

adsorption. An example of tin centered phthalocyanines (SnPc) showing different adsorption configurations on Ag(111) under ultra-high vacuum and cryogenic conditions has been reported recently.^[60] Contrary to the distorted molecular frame of **4-8**, the non-planarity of the SnPc arises from the size difference of the cavity and the large tin atom.

Still, the observation of multiple adsorption geometries of **4-8** surprises since the experiments have been performed at room temperature and one would expect a self-healing process to the thermodynamically more stable assembly on the interface. It seems that pinning down the Pyc by attractive van der Waals interactions between the side chains dominates over the contribution of the non-planar adsorption. This is the first example of metal-free Pcs exhibiting multiple adsorption geometries at the liquid/solid interface.^[39]

Regarding the quantity and spatial distribution careful investigation of STM images revealed that molecules with darker contrast appear in a smaller number. Furthermore, a tendency of these dark molecules to adsorb in vicinity of others could be observed and points towards a cooperative effect in the molecular recognition process. This might origin from differing alkoxy chain interactions between up or down adsorbed molecules.

The here described observation of multiplicity in the adsorption geometry could possibly be used for reversible switching between two different conformations on the surface and therefore might be applicable for molecule-based switches.^[61]

The STM images of **4-9** on HOPG surface are depicted in Figure 4.14 **a - c**. **4-9** forms very similar arrays like **4-8** with a unit cell containing one molecule and parameters $a = 3.47 \pm 0.04$ nm, $b = 3.52 \pm 0.08$ nm and $\alpha = 61.5 \pm 1.7^\circ$ (plane group $p2$). The conformity implies that the insertion of the zinc atom does not affect the two-dimensional assembly due to weak interaction between zinc and the HOPG surface. The large scale image displayed in Figure 4.14 **a** shows the cruciform shape of the Pyc. Taking a closer look, the high resolution image Figure 4.14 **b** revealed the core as bright humbs surrounded by regions of darker contrast with linear fine structures. Those were assigned to parallel

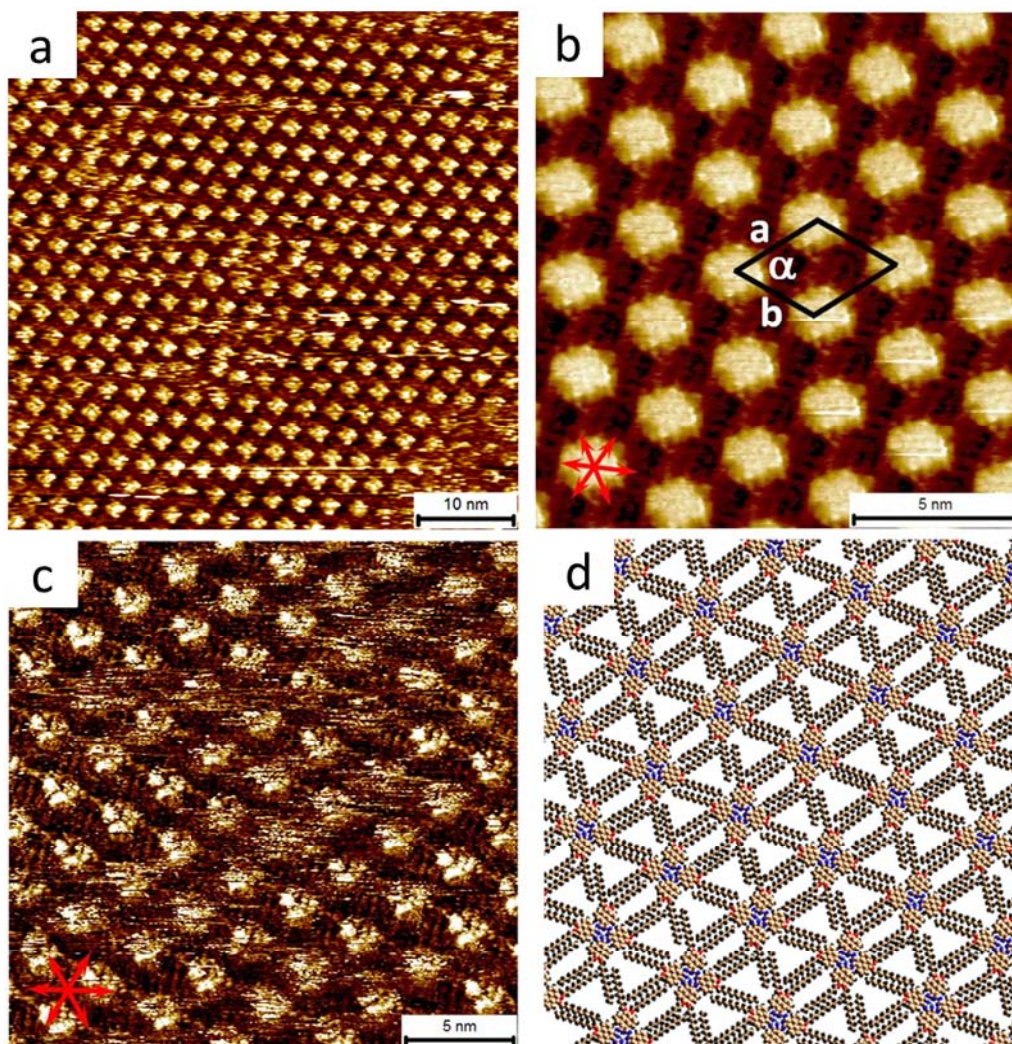


Figure 4.14: Large scale (a) and high resolution (b) STM images of **4-9** adsorbed at the 1-phenyloctane/HOPG interface. The zinc site in the central aromatic cavity appears as a depression in (c) indicating that zinc does not show up in STM images. The main symmetry axes of the graphite lattice are shown in the lower left corner of (b) and (c). Unit cell parameters: $a = 3.47 \pm 0.04$ nm, $b = 3.52 \pm 0.08$ nm and $\alpha = 61.5 \pm 1.7^\circ$; 1 molecule/unit cell, plane group $p2$. Tunneling conditions: $V_t = -1.0$ V/ $I_t = 0.22$ nA; (d) Tentative molecular model which reproduces the observed metrics and symmetry in the STM images.

interdigitated alkoxy chains by van der Waals interactions which dominantly induce the observed self-assembly. Figure 4.14 d depicts the tentative model for the two-dimensional network of **4-9** illustrating the spatial situation on the HOPG surface.

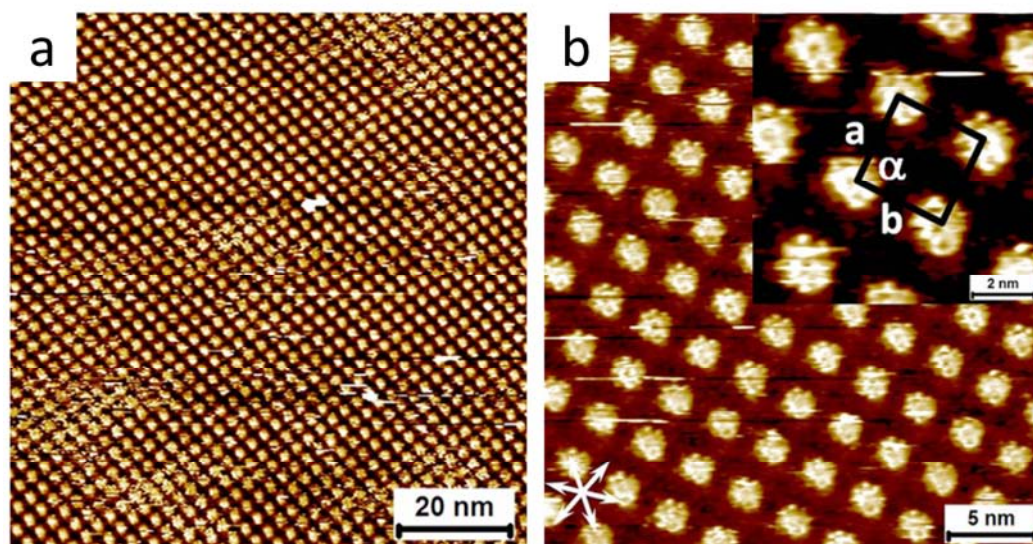


Figure 4.15: Large scale (a) and high resolution (b) STM images of **4-12** adsorbed at the 1-phenyloctane/HOPG interface. The main symmetry axes of the graphite lattice are shown in the lower left corner of **b**. Unit cell parameters: $a = 3.23 \pm 0.05$ nm, $b = 3.26 \pm 0.07$ nm and $\alpha = 88.0 \pm 1.8^\circ$; 1 molecule/unit cell, plane group $p4gm$. Tunneling conditions: $V_t = -1.2$ V / $I_t = 30$ pA.

Although no depression in the center is visible in Figure 4.14 **b**, **c** shows a decrease in the apparent height in the molecular center. This finding is in line with non-appearance of zinc in STM images due to negligible ‘d’-orbital character of frontier orbitals and hence insignificant orbital mediated tunneling.^[39, 62-63]

In contrast to metal-free Pyc **4-8**, the aforementioned contrast variations could not be found in case of **4-9**. A possible explanation lies in the experimental need for this sample of very dilute solutions (10^{-7} M versus 10^{-5} M) and elevated temperatures during the annealing process which could affect the adsorption behavior.

In the previous subchapter it could be shown that the replacement of a linear by a branched alkoxy chain in the periphery of Pycs drastically decreases the aggregation behavior in solution. Investigation of Pyc **4-12** bearing branched $C_{10,6}$ alkoxy chains at the liquid/solid interface, showed a change in the adsorption behavior compared to Pycs **4-8** and **4-9** with linear chains (Figure 4.15). Beside the change to a quadratic unit cell symmetry with the respective

parameters $a = 3.23 \pm 0.05$ nm, $b = 3.26 \pm 0.07$ nm and $\alpha = 88.0 \pm 1.8^\circ$ the deposition time had to be extended to three hours to obtain reasonable images. The prolonged self-assembly process relative to the Pycs with linear chains might also be responsible for the fact that no contrast variations similar to **4-8** could be observed due to sufficient time for molecular self-healing mechanisms in the monolayer.

Likewise **4-9** the characteristic depression in the middle of the Pyc could be resolved in the STM images. Although the alkoxy chains could not be visualized, it can be concluded from the experimentally determined unit cell parameters that the longer C₁₀ chain adsorbs selectively on the HOPG surface, whereas the shorter C₆ chain remains solubilized in the supernatant liquid, not being part of the crystal lattice. This arrangement of the alkoxy chains is responsible for the rather similar unit cell parameters determined for **4-9** and **4-12**.

4.6 Self-Assembly in the Bulk (2D WAXS)

Prior to detailed description of the investigation of pyrenocyanines in bulk using 2D WAXS, it shall be clarified that a comparison of STM and 2D WAXS data is not the aim of this work and not reasonable due to the fundamental difference in the aggregation behavior at the liquid/solid interface and in bulk.

At the liquid/solid interface, molecule-substrate interaction influences the self-assembling process which is obviously not present in bulk. Furthermore, the formation of monolayers is mainly governed by lateral interaction between adjacent molecules at the interface that originates from interdigitation of alkoxy chains (van der Waals forces). In bulk, additional π - π -stacking crucially affects the three-dimensional order. Just to mention one more example, the change from the linear to the branched alkoxy chains merely influenced the monolayer

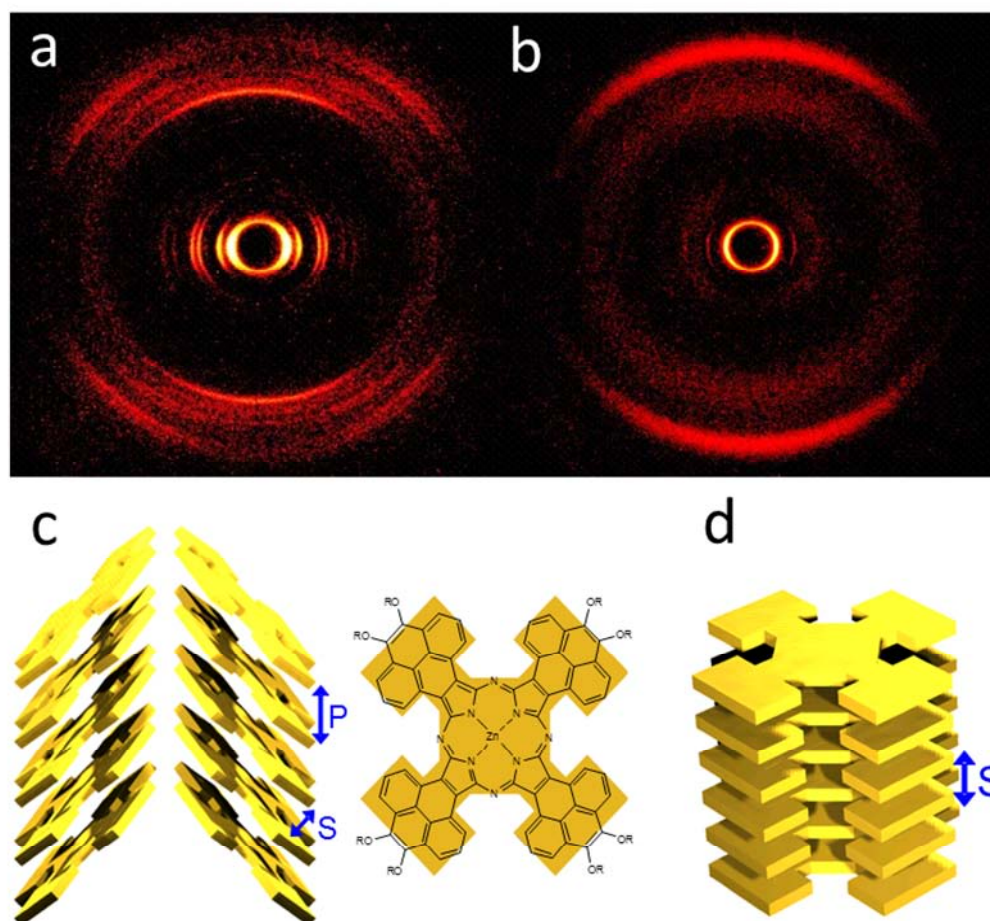


Figure 4.16: 2D WAXS patterns of **4-7** (a) at 30°C (before heating) and (b) 110°C; schematic illustrations of the intracolumnar packing at (c) 30°C in the crystalline and (d) 110°C in the liquid crystalline phase (P = period, S = π -stacking); for simplicity side chains are omitted and the molecular conformation is flat.

pattern as shown above because the second arm of the chain is simply solubilized in the supernatant solvent, whereas a crucial impact on the bulk properties can be expected.^[10, 12, 39]

The 2D WAXS study of bulk properties of pyrenocyanines was performed in collaboration with Dr. [REDACTED], [REDACTED] and Dr. [REDACTED] and were focused on the influence of peripheral alkoxy chains on the bulk properties of zinc centered free-base pyrenocyanines. After extrusion of suitable fibers at elevated temperatures and vertical placement with respect to the incident beam, the Pycs are aligned along the axis of the fiber and

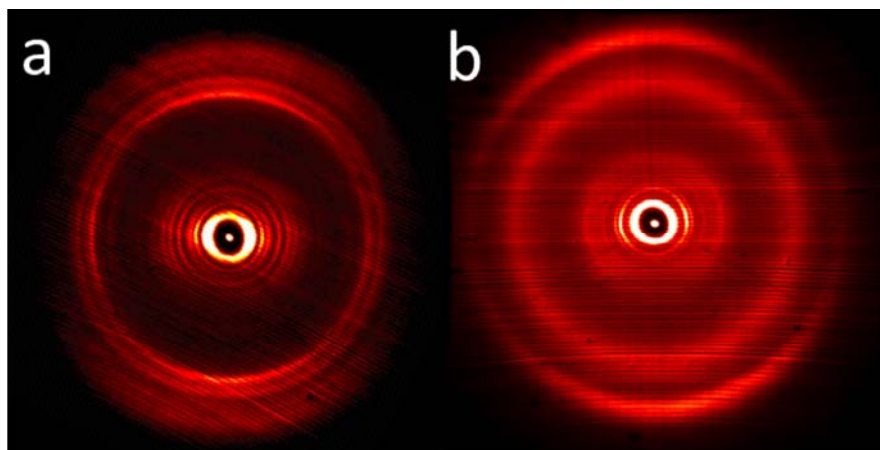


Figure 4.17: 2D WAXS patterns of **4-9** at (a) 30°C (before heating) and at (b) 110°C.

irradiated at different temperature to investigate the thermotropic behavior.^[12, 64] All determined packing parameters are summarized in Table 4.2 on page 91 but will be discussed and illustrated separately in the following.

The 2D WAXS diffraction patterns of **4-7** at 30°C and 110°C are shown in Figure 4.16 **a** and **b**. At low temperature a typical crystalline herringbone organization was observed. From off-meridional reflections a π -stacking distance of 0.35 nm (S) and a tilt by 45° of the molecules within the columns could be derived. Meridional scattering intensity revealed a distance of 0.45 nm (P) between the discs and a schematic illustration for clarity is given in Figure 4.16 **c**. Information about the intermolecular arrangement was gained by the position of the equatorial reflections which indicate a rectangular lattice for **4-7** ($a = 5.34$ nm, $b = 2.38$ nm).

The diffraction pattern at 110°C indicates the transition into a discotic liquid crystalline phase with a non-tilted packing and a π -stacking distance of 0.35 nm (Figure 4.16 **b** and **d**). A hexagonal arrangement of the columns in the unit cell was found with parameter $a_{\text{hex}} = 3.18$ nm. It is noteworthy that after considerable time the liquid crystalline phase remains after cooling down to 30°C.

Similar to **4-7**, **4-9** exists in a crystalline phase at 30°C in a rectangular unit cell but the molecules are less tilted by a value of 15° (Figure 4.17). The linear

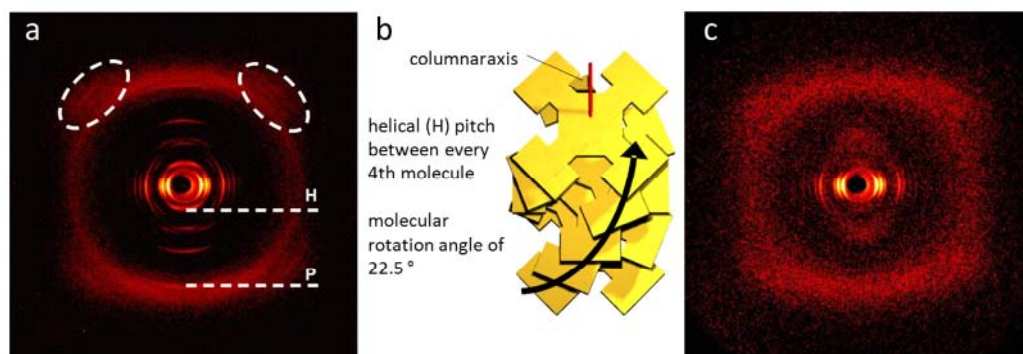


Figure 4.18: 2D WAXS pattern of **4-12** at (a) 30°C (dashed circles indicate the off-meridional reflections related to molecular tilting, P = period, H = helix), (b) schematic illustration for the helical packing within the columnar stack at 30°C and (c) 2D WAXS pattern at 150°C.

elongation of the alkoxy chain by four carbon atoms from C₈ to C₁₂ leads to a slight increase of the cell parameters ($a = 5.72$ nm, $b = 2.40$ nm). The thermotropic behavior is identical with **4-7**, as **4-9** exhibits a liquid crystalline state at 110°C and remains stable after cooling to 30°C with the same π -stacking distance of 0.35 nm but slightly increased unit cell parameter $a_{\text{hex}} = 3.54$ nm.

A stronger effect was expected and found for the Pyc with branched, and thus, sterically demanding C_{10,6} chains **4-12** on the intra- and intercolumnar arrangement. At 30°C a columnar superstructure in a rectangular lattice ($a = 5.82$ nm and $b = 2.18$ nm) was observed but the intracolumnar order differed from those of Pycs with linear chains. Multiple off-meridional reflections encircled in Figure 4.18 **a** correspond to a tilt of **4-12** molecules but point towards further intracolumnar associations and a more complex helical packing.

The reflection indicated as H corresponds to a helical period of 1.92 nm. Divided by the intracolumnar period for tilted discs of 0.48 nm, every fourth molecule in the column has identical orientation with an intermolecular rotation angle of 22.5° (Figure 4.18 **b**). This low temperature phase of **4-12** can be referred to as plastic crystalline because of the high degree of three-dimensional positional order.^[65]

Table 4.2: Packing parameters determined at various temperatures by fiber 2D WAXS.^[a]

| Compound | T | Phase | Unit cell | Parameters in nm | Intracolumnar organization |
|----------|---------------------|---------------------|-------------|----------------------------|--|
| 4-7 | 30°C ^[a] | crystalline | rectangular | $a = 5.34$; $b = 2.38$ | 45° molecular tilt; 0.45 nm period |
| | 110°C | liquid crystalline | hexagonal | $a = 3.18$ | non-tilt; π -stacking 0.35 nm |
| 4-8 | 30°C | plastic crystalline | hexagonal | $a = 3.64$ | non-tilt; 1.75 nm helix period; π -stacking 0.35 nm |
| | 160°C | liquid crystalline | hexagonal | $a = 3.71$ | non-tilt; π -stacking 0.35 nm |
| 4-9 | 30°C ^[a] | crystalline | rectangular | $a = 5.72$; $b = 2.40$ | ca. 15° molecular tilt |
| | 110°C | liquid crystalline | hexagonal | $a = 3.54$ | π -stacking 0.35 nm |
| 4-12 | 30°C | plastic crystalline | rectangular | $a = 5.82$; $b = 2.18$ | 45° molecular tilt; 0.48 nm period; 1.92 nm helical period |
| | 160°C | liquid crystalline | rectangular | $a = 5.82$; $b = 2.18$ | molecular tilt; disordered |

[a] Before heating.

Most likely, the helical packing is caused by the hindered cofacial stacking of the branched and sterically demanding side chains. The rotation of the proximate molecule leads to avoidance of steric overcrowding, and therefore, a favorable room filling. This effect on the arrangement within columns of discotic molecules has been reported to arise either from spatial demand of peripheral substituents or certain disc symmetry.^[66-69] It seems logical that the variation of the steric demand of the peripheral substituents can be utilized to tune the rotation angle.

Heating **4-12** to 150°C meridional and off-meridional reflections became diffuse, whereas equatorial ones almost kept their shape (Figure 4.18 c). This characteristic speaks for the formation of so-called ‘disordered columnar stacks’.^[70-71] The high temperature increases the steric demand of the side chains by their additional motion which leads to a state in which the molecules leave their well-packed order and rather bounce on top of each other.

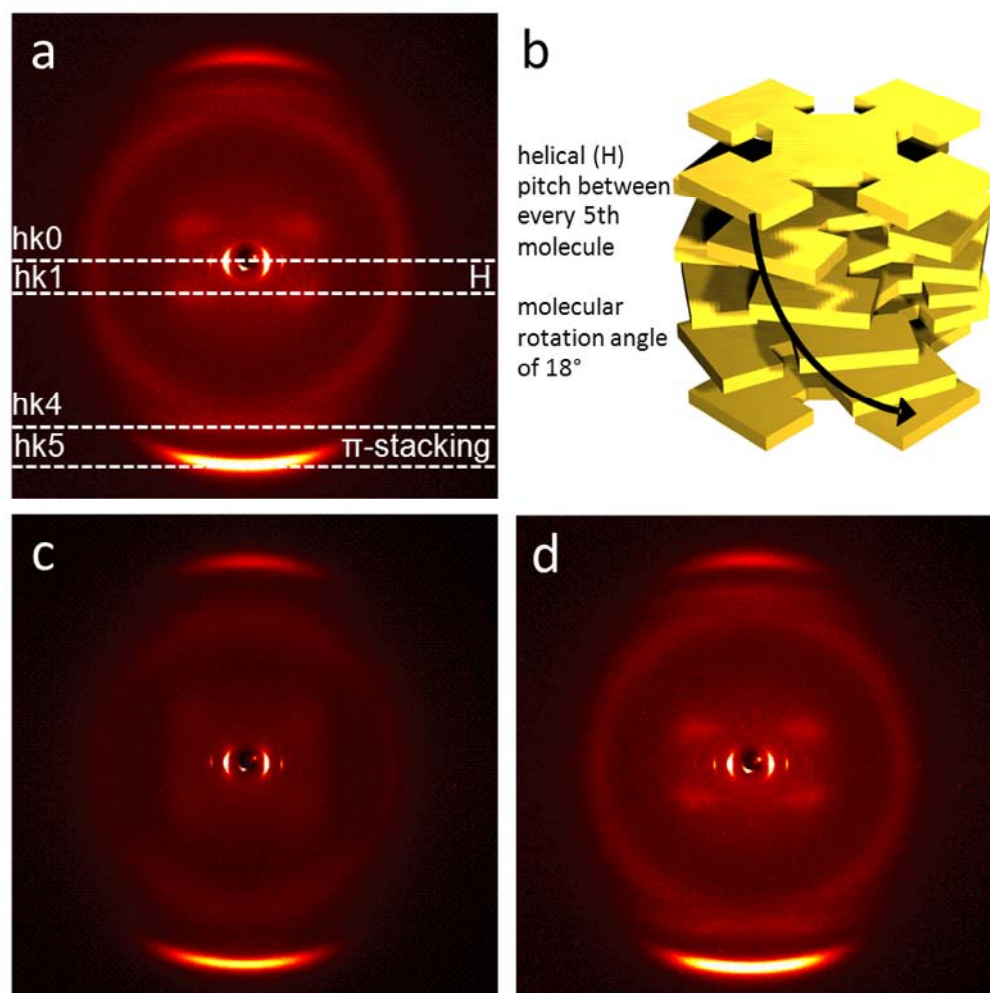
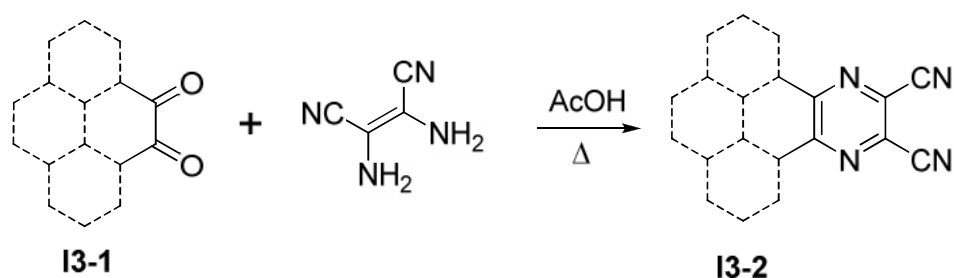


Figure 4.19: 2D WAXS pattern of **4-8** at 30°C (scattering lines and Miller's indices are indicated by dashed lines; H = helix) and (b) schematic illustration for the helical packing within the columnar stack at 30°C; (c) 2D WAXS pattern at 160°C and (d) after cooling back to 30°C.

From the so far described 2D WAXS investigations it can be concluded that while keeping the zinc atom in the cavity branched alkoxy chains induce helicity into the columnar order. For comparison reasons, the metal-free Pyc with linear alkoxy chains **4-8** was studied in respect to the molecular packing.

The thermotropic behavior of **4-8** is strongly altered compared to **4-9** although both are substituted with linear C_{12} chains in the periphery. At first appearance Figure 4.19 a indicates a typical liquid crystalline phase at 30°C with non-tilted molecules and a hexagonal lattice with common parameters



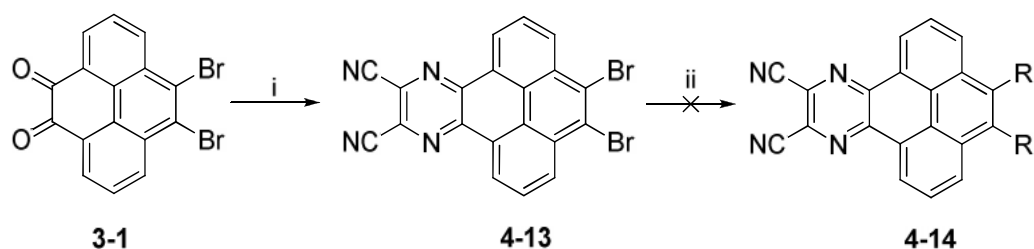
Scheme 4.3: Condensation reaction of an α -diketone **13-1** with diaminomaleonitrile to the pyrazinocyanine precursor **13-2**; Pyrene is insinuated by dashed lines.

(π -stacking distance 0.35 nm; $a_{\text{hex}} = 3.64$ nm). Interestingly, two reflections on scattering lines $hk1$ and $hk4$ give rise to assume a complex intracolumnar organization. $Hk1$ line corresponds to a spacing of 1.75 nm along the stacking direction and indicates a helical pitch (H). Calculated from the π -stacking distance of 0.35 nm every fifth molecule is in an identical order and each molecule is rotated by 18° in respect to its neighbor (Figure 4.19 **b**). Likewise **4-12** this phase is called plastic crystalline.

Elevation of the temperature and therefore an increase of Brownian motion leads to disorganization of the helix into a liquid crystalline phase. The initial plastic crystallinity was recovered again by cooling to 30°C (Figure 4.19 **d**)

4.7 Pyrenopyrazinocyanines

In the previous section the synthesis of new pyrenocyanines and a careful study of their properties have been described. Therefore, the core of Pycs was substituted differently and the occupancy of the central cavity was altered. The object of this subchapter is to develop a synthetic strategy for further extension of the Pyc π -system in order to tune the optical properties.



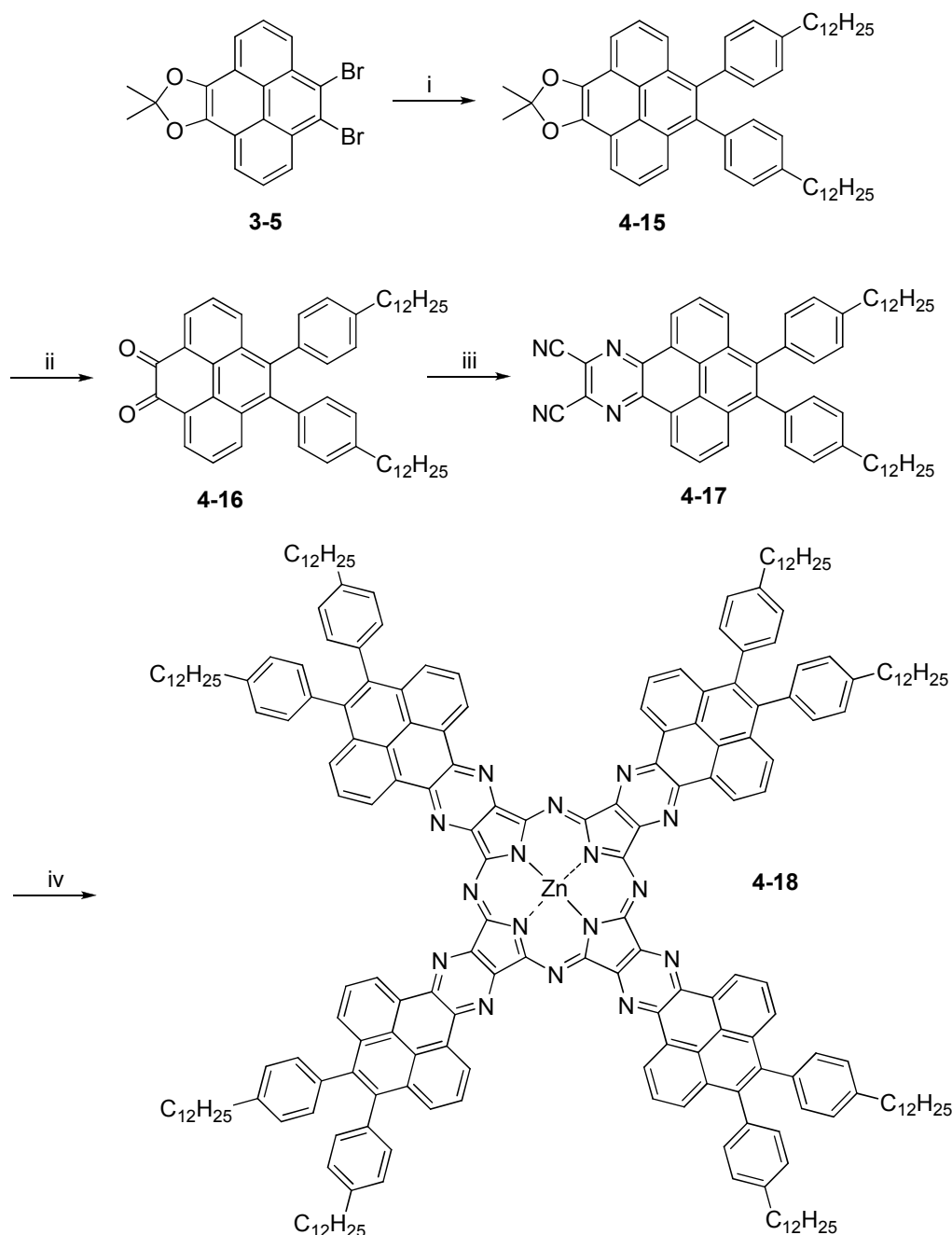
Scheme 4.4: First approach towards **4-14**. Conditions: *i* diaminomaleonitrile, *o*-dichlorobenzene/AcOH 1:1, reflux, 3.5 h, 75 % *ii* e.g. 4-dodecylphenylboronic acid, Pd(OAc)₂, SPhos, K₃PO₄, THF, RT, 16 h.

The extension of the conjugated π -system of phthalocyanines has often been accomplished by the insertion of pyrazine units and many examples of pyrazinocyanines (also referred to as aza-phthalocyanines) were reported.^[72-78] The condensation reaction of an α -diketone with diaminomaleonitrile is a powerful tool in Pc chemistry and affords the precursor for the tetramerization reaction in one step (Scheme 4.3). From a synthetic point of view, pyrene is an obvious candidate for extended pyrazinocyanines due to the availability of the α -diketone.

4.7.1 Synthesis

The first approach towards pyrenopyrazinocyanines shown in Scheme 4.4 was chosen with respect to the smallest number of steps. Treatment of diketone **3-1** with diaminomaleonitrile gave **4-13** in 75 % yield. The condensation product is badly soluble even at elevated temperature, and thus, only proton NMR spectroscopy and mass spectrometry could be performed revealing the anticipated signals and molecular weight, respectively.

Unfortunately, any attempt for the introduction of solubilizing groups *via* palladium catalyzed cross-coupling reaction (Suzuki, Negishi, Hagihara) failed or only traces of the expected molecular mass of the product could be detected by mass spectrometry. Possible explanation can be the lack of solubility or the electronic nature of the respective aryl bromide **4-13**.



Scheme 4.5: Synthetic route for the preparation of pyrenopyrazinocyanines **4-18**. Conditions: *i* 4-dodecylphenylboronic acid, $\text{Pd}(\text{OAc})_2$, SPhos, K_3PO_4 , THF, RT, 16 h, 73 %; *ii* TFA/ CHCl_3 1:1, air, 50°C , 4 h, 68 %; *iii* diaminomaleonitrile, *o*-dichlorobenzene/AcOH 1:2, reflux, 6 h, 55 %; *iv* ZnCl_2 , DBU, 1-pentanol, reflux, overnight, 13 %.

Nevertheless, the route was changed to the use of acetonide **3-5** involving two additional steps (Scheme 4.5). In contrast to **4-13**, Suzuki coupling of **3-5** ran smoothly and yielded **4-15** in 73 %. The acetonide acts as protecting group

for the ketone and was cleaved in the next step under acidic conditions and oxidized while air was bubbled through the reaction mixture.^[79] Condensation reaction analog to the synthesis of **4-13** was accomplished to give the *ortho*-dicyano precursor **4-17** in 55 % yield. Established conditions for the synthesis and purification *via* GPC column chromatography of Pycs were likewise effective for the isolation of pyrenopyrazinocyanine **4-18** in 13 %.

Characterization of **4-18** appeared to be difficult as proton NMR shows only broad and unresolved signals even at elevated temperature at 413 K. Nevertheless, the structure could be confirmed by high resolution MALDI MS by the detection of the protonated molecular ion at 3237.9956 m/z (A+3) with a divergence of 0.0006 m/z.

4.7.2 Optical Properties

The absorption spectrum of pyrenopyrazinocyanine **4-18** is depicted in Figure 4.20 a at room temperature. Broad absorption was observed, gradually decreasing to longer wavelength with a maximum at 697 nm ($\epsilon = 2404 \text{ m}^2\text{mol}^{-1}$) corresponding to the Q-band. The B-band appears badly resolved around ~450 nm. Compared to zinc centered pyrenocyanine **4-9** with linear C₁₂ side chains the Q-band is even slightly blue shifted with a similar extinction coefficient. For evaluation of the shape of the spectrum and comparison to **4-9** the structural differences have to be pointed out:

First, the insertion of an additional pyrazine unit between the TAP core and the pyrene moieties relieves the steric strain from the angular annulation illustrated in Figure 4.2. Planarization of the molecule is the consequence and π - π -stacking and aggregation should increase. Second, the enlargement of the π -systems itself favors the intermolecular association to dimer, trimers or higher aggregates. Third, the replacement of the oxygen by a phenyl ring is known to

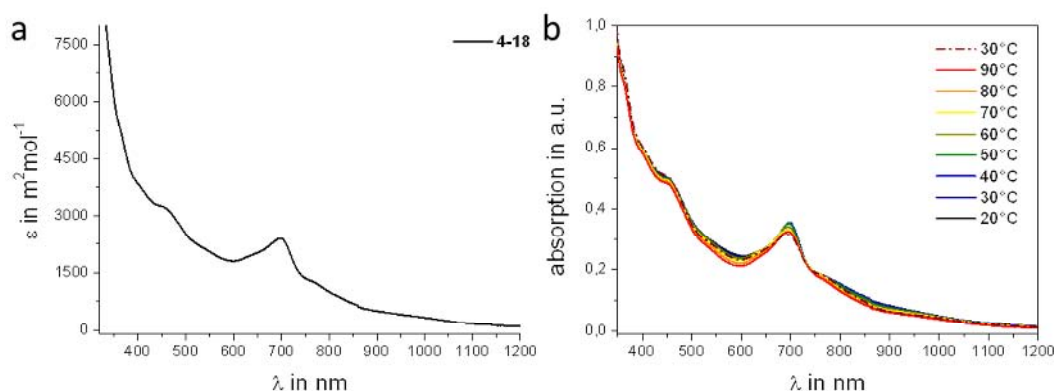


Figure 4.20: UV/vis absorption spectrum of pyrenopyrazinocyanine **4-18** (a) at room temperature and (b) temperature dependent from 20°C to 90°C in toluene and 10^{-5} M concentration.

enhance the aggregation on hexa-*peri*-benzocoronene, which should apply for Pcs as well.^[80] Fourth, although the annulated π -system is increased linearly the pyrazine unit is known to ineffectively contribute to the conjugation in Pcs and therefore leads to a Q-band at shorter wavelength compared to the pure carbon analogon.^[33-34, 81]

Upon increasing temperature to 90°C of **4-18** in toluene the absorption spectrum merely changed (Figure 4.20 b). It is assumed that the strong aggregation tendency cannot be overcome under these conditions.

In order to counteract aggregate formation in the case of pyrenopyrazinocyanines the synthesis could be started from *tert*-butylated asymmetric pyrene **3-2**. The additional pyrazine ring between TAP core and the pyrene unit makes room for sterically demanding *tert*-butyl groups at pyrene positions 2 and 7.

Nevertheless, the example of pyrenopyrazinocyanine **4-18** highlights the synthetic feasibility for the extension of the pyrenocyanine structure by pyrazine units and promises to be a versatile method by the choice of other *ortho*-diamines.^[76]

4.8 Summary

In this chapter, the synthesis and characterization of novel pyrenocyanines and π -extended pyrenopyrazinocyanines have been presented. Based on asymmetrically substituted pyrene building block 9,10-dibromopyrene-4,5-dione the *ortho*-dicyano precursors with linear alkoxy chains of different length and branched chains were obtained *via* reductive alkylation and bromine/cyano exchange in two steps. The cyclotetramerization reaction under standard conditions yielded the pyrenocyanines as metal-free, zinc-, cobalt- and lead centered version. The synthesis of zinc centered pyrenopyrazinocyanines turned out to be more challenging due to the necessity of protection and deprotection of the ketones for the palladium catalyzed introduction of solubilizing groups.

DFT calculations on the aromatic Pyc core revealed non-planarity owing to the steric demand of the angularly fused aromatic residue being a unique feature of this class of core extended Pcs. Similar to structurally related phenanthralocyanine, the characteristic Q-band was found to be strongly broadened, most likely due to distortion of the molecule.^[29] The bathochromic shift of the Q-band is not as distinctive as expected for the linearly annulated aromatic systems with the same number of benzene rings. This finding could be explained by the pronounced destabilization of the HOMO in the linear case. The peripheral alkoxy substitution provided good solubility of Pycs in organic solvents like dichloromethane, THF or toluene and influences the temperature dependence of the absorption in solution. Solely the lead centered Pyc exhibited a rather narrow Q-band assumably owing the symmetry change caused by the large lead atom of the three-dimensional shape.

The self-assembling properties at the liquid/solid interface were investigated by STM on HOPG. Well-ordered arrays of Pyc rows in monolayers were observed with the alkoxy chains adsorbed on the surface. Those facilitate the anchoring of the non-planar molecules on the surface and provide

intermolecular contact of neighboring molecules by interdigitation and van der Waals forces.

It has also been found that only the metal-free Pyc exhibits non-periodic contrast variation which can be attributed to the adsorption of Pycs in different conformations due to the inherent non-planar nature of the Pyc skeleton. This observation was rather surprising since a uniform and energetically optimized adsorption was expected at room temperature.

The self-assembly of Pycs in bulk was studied by 2D WAXS after extrusion of the material into fibers and thermotropic columnar arrangement for all investigated Pycs was found with a liquid crystalline phase at elevated temperatures. It was further revealed that changing the side-chains from linear to branched induces a helical arrangement within the columnar stacks at 30°C for zinc centered Pycs. Thus, it was assumed that tuneability of the rotation angle of zinc centered Pycs exists by the simple alteration of the steric demand of peripheral substituents.

Regarding the occupation of the central cavity, dependency was found for the thermotropic behavior and the intracolumnar arrangement. Similar to the strongly deviating results of the metal-free and metal-centered Pycs at the liquid/solid interface, the metal-free Pyc with linear alkoxy chains formed a helical columnar arrangement in bulk whereas the zinc centered analogs did not. Apparently, the central atom is an additional factor for the control of the intracolumnar organization for discotic liquid crystals and will further be investigated.

4.9 Bibliography

- [1] C. C. Leznoff, A. B. P. Lever, *Phthalocyanines: properties and applications, Vol. 1-4*, Wiley, New York, **1989-1996**.
- [2] G. de la Torre, C. G. Claessens, T. Torres, *Chemical Communications* **2007**, 2000-2015.
- [3] M. V. Martinez-Diaz, G. de la Torrea, T. Torres, *Chemical Communications* **2010**, 46, 7090-7108.
- [4] J. Mack, N. Kobayashi, *Chemical Reviews* **2011**, 111, 281-321.
- [5] G. de la Torre, P. Vaquez, F. Agullo-Lopez, T. Torres, *Chemical Reviews* **2004**, 104, 3723-3750.
- [6] N. B. McKeown, *Phthalocyanine Materials: Synthesis, Structure and Function*, **1998**.
- [7] E. Orti, M. C. Piqueras, R. Crespo, J. L. Bredas, *Chemistry of Materials* **1990**, 2, 110-116.
- [8] A. W. Snow, *Phthalocyanines: properties and materials* **2003**, 129-176.
- [9] B. Tylleman, G. Gbabode, C. Amato, C. Buess-Herman, V. Lemaure, J. Cornil, R. G. Aspe, Y. H. Geerts, S. Sergeyev, *Chemistry of Materials* **2009**, 21, 2789-2797.
- [10] M. Kastler, W. Pisula, D. Wasserfallen, T. Pakula, K. Müllen, *Journal of the American Chemical Society* **2005**, 127, 4286-4296.
- [11] S. Sergeyev, E. Pouzet, O. Debever, J. Levin, J. Gierschner, J. Cornil, R. G. Aspe, Y. H. Geerts, *Journal of Materials Chemistry* **2007**, 17, 1777-1784.
- [12] W. Pisula, Z. Tomovic, C. Simpson, M. Kastler, T. Pakula, K. Müllen, *Chemistry of Materials* **2005**, 17, 4296-4303.
- [13] S. Sergeyev, W. Pisula, Y. H. Geerts, *Chemical Society Reviews* **2007**, 36, 1902-1929.
- [14] B. R. Kaafarani, *Chemistry of Materials* **2011**, 23, 378-396.
- [15] S. Laschat, A. Baro, N. Steinke, F. Giesselmann, C. Hagele, G. Scalia, R. Judele, E. Kapatsina, S. Sauer, A. Schreivogel, M. Tosoni, *Angewandte Chemie-International Edition* **2007**, 46, 4832-4887.
- [16] X. L. Feng, W. Pisula, T. Kudernac, D. Q. Wu, L. J. Zhi, S. De Feyter, K. Müllen, *Journal of the American Chemical Society* **2009**, 131, 4439-4448.
- [17] N. B. McKeown, M. Helliwell, B. M. Hassan, D. Hayhurst, H. Li, N. Thompson, S. L. Teat, *Chemistry-a European Journal* **2007**, 13, 228-234.
- [18] K. M. Kadish, K. M. Smith, R. Guillard, *The Porphyrin Handbook - Phthalocyanines: Synthesis, Vol. 15, 63-68*, Academic Press, San Diego, **2003**.
- [19] H. N. Tsao, W. Pisula, Z. H. Liu, W. Osikowicz, W. R. Salaneck, K. Müllen, *Advanced Materials* **2008**, 20, 2715-+.

- [20] W. W. H. Wong, T. B. Singh, D. Vak, W. Pisula, C. Yan, X. L. Feng, E. L. Williams, K. L. Chan, Q. H. Mao, D. J. Jones, C. Q. Ma, K. Müllen, P. Bauerle, A. B. Holmes, *Advanced Functional Materials* **2010**, *20*, 927-938.
- [21] W. Pisula, A. Menon, M. Stepputat, I. Lieberwirth, U. Kolb, A. Tracz, H. Sirringhaus, T. Pakula, K. Müllen, *Advanced Materials* **2005**, *17*, 684-+.
- [22] J. Li, M. Kastler, W. Pisula, J. W. F. Robertson, D. Wasserfallen, A. C. Grimsdale, J. Wu, K. Müllen, *Advanced Functional Materials* **2007**, *17*, 2528-2533.
- [23] A. Tracz, T. Makowski, S. Masirek, W. Pisula, Y. H. Geerts, *Nanotechnology* **2007**, *18*, -.
- [24] P. O. Mouthuy, S. Melinte, Y. H. Geerts, B. Nysten, A. M. Jonas, *Small* **2008**, *4*, 728-732.
- [25] R. J. M. Nolte, H. Engelkamp, S. Middelbeek, *Science* **1999**, *284*, 785-788.
- [26] T. J. Katz, J. M. Fox, S. Van Elshocht, T. Verbiest, M. Kauranen, A. Persoons, T. Thongpanchang, T. Krauss, L. Brus, *Journal of the American Chemical Society* **1999**, *121*, 3453-3459.
- [27] K. M. Kadish, K. M. Smith, R. Guilard, *The Porphyrin Handbook - Phthalocyanines: Synthesis, Vol. 15, 4-5*, Academic Press, San Diego, **2003**.
- [28] R. M. Christie, D. D. Deans, *Journal of the Chemical Society-Perkin Transactions 2* **1989**, 193-198.
- [29] E. M. Maya, A. W. Snow, A. W. Snow, J. S. Shirk, S. R. Flom, R. G. S. Pong, J. H. Callahan, *Journal of Porphyrins and Phthalocyanines* **2002**, *6*, 463-475.
- [30] Blackbur.Ev, C. J. Timmons, *Journal of the Chemical Society C-Organic* **1970**, 175.
- [31] A. N. Cammidge, H. Gopee, *Chemical Communications* **2002**, 966-967.
- [32] M. Ichihara, M. Miida, B. Mohr, K. Ohta, *Journal of Porphyrins and Phthalocyanines* **2006**, *10*, 1145-1155.
- [33] B. K. Mandal, T. Sooksimuang, *Journal of Porphyrins and Phthalocyanines* **2002**, *6*, 66-72.
- [34] B. K. Mandal, T. Sooksimuang, C. H. Lee, R. Wang, *Journal of Porphyrins and Phthalocyanines* **2006**, *10*, 140-146.
- [35] T. Sooksimuang, B. K. Mandal, *Journal of Organic Chemistry* **2003**, *68*, 652-655.
- [36] A. N. Cammidge, H. Gopee, *Chemistry-a European Journal* **2006**, *12*, 8609-8613.
- [37] L. Zöphel, D. Beckmann, V. Enkelmann, D. Chercka, R. Rieger, K. Müllen, *Chemical Communications* **2011**, *47*, 6960-6962.
- [38] R. N. Hurd, G. Delamater, G. C. Mcelheny, V. H. Wallingford, R. J. Turner, *Journal of Organic Chemistry* **1961**, *26*, 3980-&.
- [39] L. Zöphel, K. S. Mali, P. S. Reddy, M. Wagner, S. De Feyter, W. Pisula, K. Müllen, *Chemistry-a European Journal* **2012**, *18*, 3264-3276.

- [40] K. Kadish, K. Smith, R. Guilard, *The Porphyrin Handbook*, Vol. 17, Academic Press, San Diego, **2003**.
- [41] K. M. Kadish, K. M. Smith, R. Guilard, *The Porphyrin Handbook - Phthalocyanines: Synthesis*, Vol. 15, 69, Academic Press, San Diego, **2003**.
- [42] J. S. Wu, A. Fechtenkötter, J. Gauss, M. D. Watson, M. Kastler, C. Fechtenkötter, M. Wagner, K. Müllen, *Journal of the American Chemical Society* **2004**, 126, 11311-11321.
- [43] A. W. Snow, J. R. Griffith, N. P. Marullo, *Macromolecules* **1984**, 17, 1614-1624.
- [44] R. B. Martin, *Chemical Reviews* **1996**, 96, 3043-3064.
- [45] M. J. Chen, J. W. Rathke, *Journal of Porphyrins and Phthalocyanines* **2001**, 5, 528-536.
- [46] D. R. Tackley, G. Dent, W. E. Smith, *Physical Chemistry Chemical Physics* **2001**, 3, 1419-1426.
- [47] K. M. Kadish, K. M. Smith, R. Guilard, *The Porphyrin Handbook - Phthalocyanines: Synthesis*, Vol. 15, 70-71, Academic Press, San Diego, **2003**.
- [48] Y. Z. Bian, L. Li, J. M. Dou, D. Y. Y. Cheng, R. J. Li, C. Q. Ma, D. K. P. Ng, N. Kobayashi, J. Z. Jiang, *Inorganic Chemistry* **2004**, 43, 7539-7544.
- [49] P. M. Burnham, M. J. Cook, L. A. Gerrard, M. J. Heeney, D. L. Hughes, *Chemical Communications* **2003**, 2064-2065.
- [50] P. V. Bedworth, J. W. Perry, S. R. Marder, *Chemical Communications* **1997**, 1353-1354.
- [51] W. J. Schutte, M. Sluytersrehabach, J. H. Sluyters, *Journal of Physical Chemistry* **1993**, 97, 6069-6073.
- [52] M. G. Schwab, Ph.D. thesis, University of Mainz **2011**.
- [53] S. B. Lei, K. Tahara, X. L. Feng, S. H. Furukawa, F. C. De Schryver, K. Müllen, Y. Tobe, S. De Feyter, *Journal of the American Chemical Society* **2008**, 130, 7119-7129.
- [54] S. De Feyter, F. C. De Schryver, *Chemical Society Reviews* **2003**, 32, 139-150.
- [55] L. Dössel, Ph.D. thesis, University of Mainz **2011**.
- [56] M. Abel, S. Clair, O. Ourdjini, M. Mossoyan, L. Porte, *Journal of the American Chemical Society* **2011**, 133, 1203-1205.
- [57] S. B. Lei, C. Wang, S. X. Yin, H. N. Wang, F. Xi, H. W. Liu, B. Xu, L. J. Wan, C. L. Bai, *Journal of Physical Chemistry B* **2001**, 105, 10838-10841.
- [58] J. A. A. W. Elemans, S. B. Lei, S. De Feyter, *Angewandte Chemie-International Edition* **2009**, 48, 7298-7332.
- [59] J. P. Rabe, S. Buchholz, *Science* **1991**, 253, 424-427.
- [60] M. Toader, M. Hietschold, *Journal of Physical Chemistry C* **2011**, 115, 12494-12500.
- [61] M. Toader, M. Hietschold, *Journal of Physical Chemistry C* **2011**, 115, 3099-3105.
- [62] M. S. Liao, S. Scheiner, *Journal of Computational Chemistry* **2002**, 23, 1391-1403.

- [63] K. Nilson, P. Palmgren, J. Ahlund, J. Schiessling, E. Gothelid, N. Martensson, C. Puglia, M. Gothelid, *Surface Science* **2008**, *602*, 452-459.
- [64] W. Pisula, X. A. Feng, K. Müllen, *Advanced Materials* **2010**, *22*, 3634-3649.
- [65] J. Simmerer, B. Glusen, W. Paulus, A. Kettner, P. Schuhmacher, D. Adam, K. H. Etzbach, K. Siemensmeyer, J. H. Wendorff, H. Ringsdorf, D. Haarer, *Advanced Materials* **1996**, *8*, 815-&.
- [66] M. Lehmann, *Chemistry-a European Journal* **2009**, *15*, 3638-3651.
- [67] M. Peterca, M. R. Imam, C. H. Ahn, V. S. K. Balagurusamy, D. A. Wilson, B. M. Rosen, V. Percec, *Journal of the American Chemical Society* **2011**, *133*, 2311-2328.
- [68] X. Feng, W. Pisula, K. Müllen, *Journal of the American Chemical Society* **2007**, *129*, 14116-+.
- [69] T. Sierra, F. Vera, J. L. Serrano, *Chemical Society Reviews* **2009**, *38*, 781-796.
- [70] K. Müllen, W. Pisula, M. Kastler, D. Wasserfallen, M. Mondeshki, J. Piris, I. Schnell, *Chemistry of Materials* **2006**, *18*, 3634-3640.
- [71] M. Lehmann, G. Kestemont, R. G. Aspe, C. Buess-Herman, M. H. J. Koch, M. G. Debije, J. Piris, M. P. de Haas, J. M. Warman, M. D. Watson, V. Lemaure, J. Cornil, Y. H. Geerts, R. Gearba, D. A. Ivanov, *Chemistry-a European Journal* **2005**, *11*, 3349-3362.
- [72] J. M. Fox, T. J. Katz, S. Van Elshocht, T. Verbiest, M. Kauranen, A. Persoons, T. Thongpanchang, T. Krauss, L. Brus, *Journal of the American Chemical Society* **1999**, *121*, 3453-3459.
- [73] T. C. Wen, S. P. Chen, C. Y. Tsai, *Synthetic Metals* **1998**, *97*, 105-112.
- [74] R. Faust, C. Weber, *Journal of Organic Chemistry* **1999**, *64*, 2571-2573.
- [75] C. S. Wang, M. R. Bryce, A. S. Batsanov, J. A. K. Howard, *Chemistry-a European Journal* **1997**, *3*, 1679-1690.
- [76] K. Müllen, Y. Fogel, M. Kastler, Z. H. Wang, D. Andrienko, G. J. Bodwell, *Journal of the American Chemical Society* **2007**, *129*, 11743-11749.
- [77] B. Mohr, G. Wegner, K. Ohta, *Journal of the Chemical Society-Chemical Communications* **1995**, 995-996.
- [78] K. M. Kadish, K. M. Smith, R. Guilard, *The Porphyrin Handbook - Phthalocyanines: Synthesis, Vol. 15, 191-205*, Academic Press, San Diego, **2003**.
- [79] J. Frey, T. Kraus, V. Heitz, J. P. Sauvage, *Chemistry-a European Journal* **2007**, *13*, 7584-7594.
- [80] X. L. Feng, W. Pisula, T. Kudernac, D. Q. Wu, L. J. Zhi, S. De Feyter, K. Müllen, *Journal of the American Chemical Society* **2009**, *131*, 4439-4448.
- [81] K. M. Kadish, K. M. Smith, R. Guilard, *The Porphyrin Handbook - Phthalocyanines: Synthesis, Vol. 15, 199-204*, Academic Press, San Diego, **2003**.

5 Dithienobenzo[e]pyrenes

5.1 Introduction

The usage of polycyclic aromatic hydrocarbons in combination with thiophene, either fused or simply attached *via* a single bond, is popular among material chemists and often pursued. Both motifs contribute unique properties that are believed to be essential for active materials in organic field-effect transistors. At first, large and flat aromatic molecules show high tendency for π - π -stacking and thereby induced self-organization.^[1-2] A short π - π -distance is believed to enhance charge carrier transport. Secondly, the five-membered ring of thiophene contains sulfur which is known to help charges hopping by its diffuse orbitals. Moreover, the motif of thiophene is probably the most used unit in polymeric organic semiconducting material and is widely applied in small molecule organic transistor.^[3-6]

The majority of reports on pyrene and its derivatives are related to the emission of light and the optical properties.^[7-11] Examples of OFETs based on pyrene derivatives have rarely been reported and a selection is depicted in Figure 5.1.^[12] An explanation is obviously the limited availability of methods for the functionalization of the pyrene core. Most syntheses found in literature start from single or multiple bromination at the active sites 1, 3, 6 and 8. **I5-1**

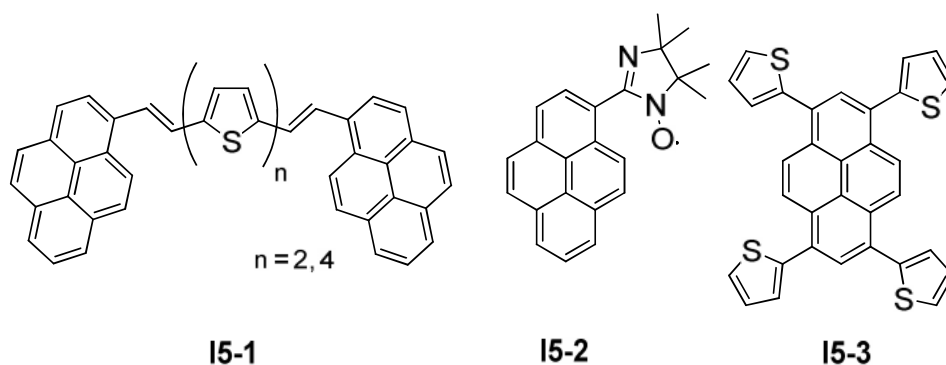


Figure 5.1: Examples of pyrene-based materials used in OFETs.

has been prepared from 1-bromopyrene and *p*-type transistors with hole mobilities between 10^{-5} to $10^{-3} \text{ cm}^2 \text{V}^{-1} \text{s}^{-1}$.^[11, 13] Starting from the same reagent, the pyrene organic radical **I5-2** gives hole mobilities of $0.1 \text{ cm}^2 \text{V}^{-1} \text{s}^{-1}$.^[14] The Suzuki coupling of thiophen-2-ylboronic acid with 1,3,6,8-tetrabromopyrene yielded **I5-3** with a *p*-type performance of $3.7 \cdot 10^{-3} \text{ cm}^2 \text{V}^{-1} \text{s}^{-1}$.^[15] It has to be noted that these values are obtained from devices with vacuum deposited layers of organic molecules.

Overviewing so far known semiconductive pyrene derived materials the class of 4,5,9,10-functionalized pyrenes is sparsely represented. Conspicuously and as outlined in the introduction, the chemical accessibility of these positions is complicated and is believed to be the reason for the lack of such materials. Nevertheless, expectations on this class of compounds are high with good reasons. The combination of thiophene and pyrene has already been proven to show semiconductivity in OFETs.^[15-17] Especially an *ortho*-dithienyl substitution would enable subsequent planarization to a benzodithiophene subunit, a well-known motif in organic electronics.^[18-19] However, the opened and closed structures are potential materials for solution processed OFETs. Starting from the asymmetrically substituted pyrene building block **3-1**, the substitution with thiophene at positions 4 and 5 and aliphatic groups at 9 and 10 leads to a new “head-tail” geometry with a rear for adjustment of solution-processability and the sulfur containing front.

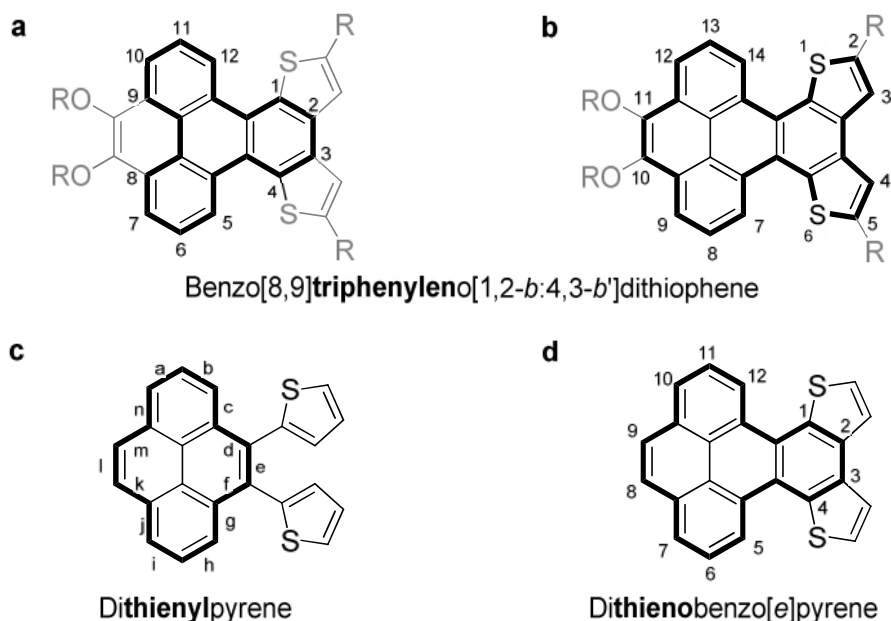
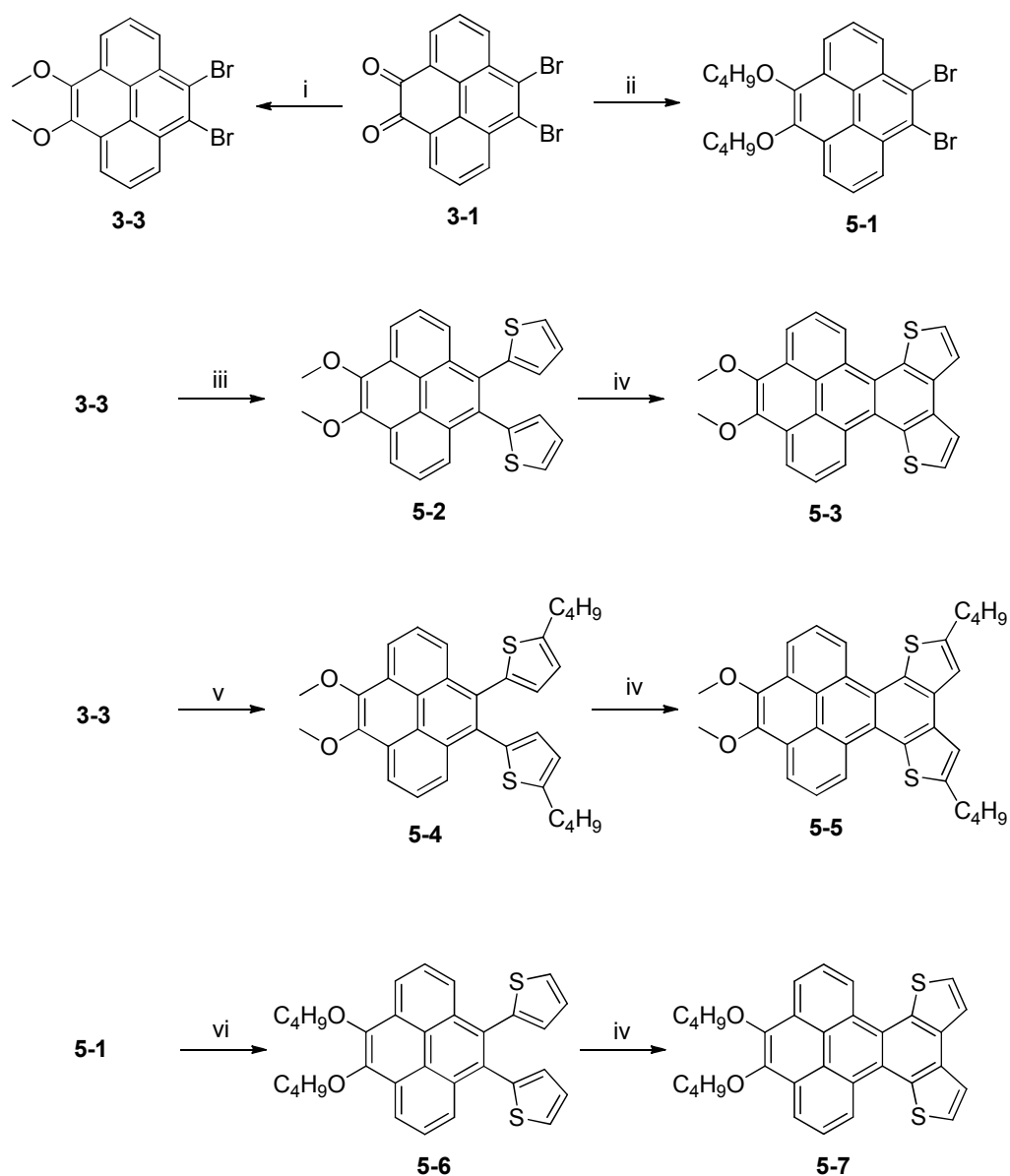


Figure 5.2: Nomenclature of benzo[8,9]triphenyleno[1,2-*b*:4,3-*b'*]dithiophenes (**a** and **b**), dithienylpyrene (**c**) and dithienobenzo[*e*]pyrene (**d**).

5.2 Synthesis

As known from previous studies, alkyl side chains play an important role for the performance of organic materials as semiconductor. Both, length and the position of the attached alkyl chains have a deep impact on solubility, the degree of crystallinity and the molecular packing of “small molecule” materials. These three parameters strongly influence the processing ability of the material and in turn the performance within the organic field-effect transistor. Finding the right balance between solubility and crystallinity is not trivial as the length of the chains influences both, solubility and the packing. Unfortunately, predictions are hard to make and the optimization of the structure underlies “trial and error” to some extent.^[20] For this reason, chemists are asked for series of compounds simply altered by the alkyl chains to find the right balance.

In this context, a series of dithienylpyrenes and dithienobenzo[*e*]pyrenes with methoxy and butoxy chains was synthesized.^[21] It seems helpful to give a



Scheme 5.1: Synthesis of dithienobenzo[*e*]pyrenes **5-3**, **5-5** and **5-7**. Conditions: *i* Na₂S₂O₄, Me₂SO₄, KOH, Bu₄NBr, H₂O/THF, 40°C, overnight, 65 %; *ii* Na₂S₂O₄, 1-bromobutane, KOH, Bu₄NBr, H₂O/THF, 40°C, overnight, 50 %; *iii* 2-tributylstannylthiophene, Pd(PPh₃)₄, toluene, reflux, overnight, 69 %; *iv* I₂, hv at 300 nm, toluene, overnight, **5-3** 47 %, **5-5** 61 %, **5-7** 72 %; *v* tributyl(5-butylthiophen-2-yl)stannane, Pd(PPh₃)₄, toluene, reflux, overnight, 80 %; *vi* 2-tributylstannylthiophene, Pd(PPh₃)₄, toluene, reflux, overnight, 63 %.

remark concerning the nomenclature at this point (Figure 5.2). IUPAC suggests a triphenylene based naming which is used in the experimental part (Figure 5.2

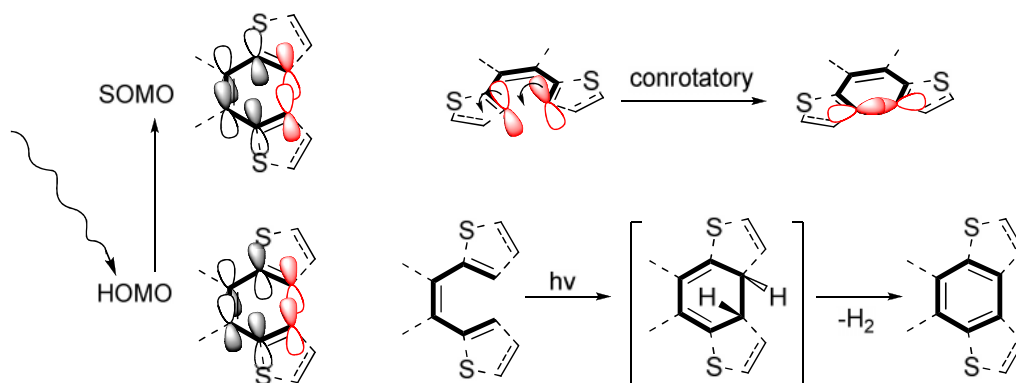
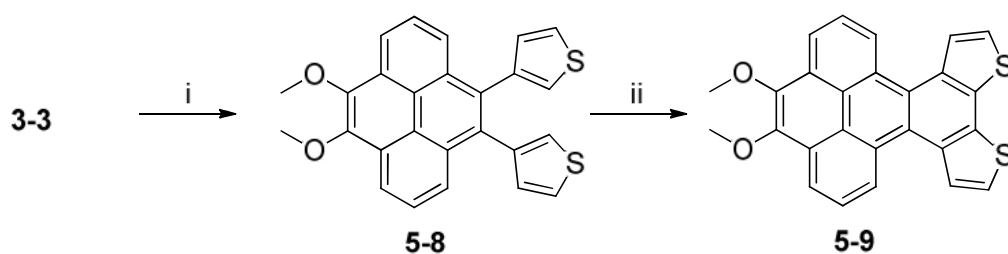


Figure 5.3: Orbital description of light-induced cyclization of conrotatory 6 π -electron processes.

a and **b**). Nevertheless, for the sake of simplicity the opened and closed species are named in this text as dithienylpyrene and dithienobenzo[*e*]pyrene, respectively, referring to the derivation from pyrene.

Based on asymmetrically substituted 9,10-dibromopyrene-4,5-dione **3-1**, **3-3** and **5-1** were obtained after reduction with sodium dithionite ($\text{Na}_2\text{S}_2\text{O}_4$) and alkylation with dimethyl sulfate and 1-bromobutane, respectively (Scheme 5.1). Subsequent Stille coupling of *ortho*-dibromopyrenes **3-3** and **5-1** with the respective 2-(tributylstannyl)thiophene gave di(thien-2-yl)pyrenes **5-2**, **5-4** and **5-6** in 63 % to 80 % yield. To afford the closure between the thienyl rings, convenient light induced ring-closure reaction was carried out in toluene in the presence of iodine. The solution was irradiated in a quartz reactor with light of a wavelength of 300 nm (40 W) overnight. The dithienobenzo[*e*]pyrenes **5-3**, **5-5** and **5-7** were obtained in yields from 47 % to 80 %.

This photo-induced electrocyclic reaction is well known for 6 π -electron systems and has extensively been studied on tetraarylethenes between phenyl and thienyl rings.^[22-24] One electron from the HOMO is excited by irradiation to the LUMO which is now called singly occupied molecular orbital (SOMO). The SOMO has three nodal planes and according to the Woodward-Hoffmann rules the reaction of the π -orbitals occurs conrotatory.^[25] This step is followed by rearomatization and elimination of H_2 as hydrogen iodide (HI) to give the fully aromatic product.



Scheme 5.2: Synthesis of dithienobenzo[*e*]pyrene **5-9**. Conditions: *i* 3-thiophenebionic acid, Pd(PPh₃)₄, Na₂CO₃, toluene/ethanol/water, reflux, overnight, 80 %; *ii* 2.1 eq. FeCl₃, MeNO₂, DCM, RT, 15 min, 51 %.

In order to relate the electronic properties and the performance in devices with the position of the sulfur moiety, thiophene was coupled to **3-3** *via* its β -position (Scheme 5.2). Thus, Suzuki coupling of 3-thiophenebionic acid and **3-3** yielded **5-8** in 80 %. Irradiation in the presence of iodine led to an inseparable mixture of compounds. However, oxidative cyclodehydrogenation using 2.1 equivalents of iron(III)chloride in nitromethane gave **5-9** and respective dimers of **5-8** which could be easily separated from the product.^[26] The dimers were formed because of open α -positions of the thiophenes. In this regard, dilute solutions were essential to suppress the oligomerization as side reaction. The mechanism of the reaction involving FeCl₃ proceeds over oxidative coupling and has earlier been used for the polymerization of thiophene-based monomers with open α -positions.^[27-28]

5.3 Optical and Electronic Properties

The absorption and emission spectra of di(thien-2-yl)pyrenes and the corresponding planarized species are depicted in Figure 5.4 **a** and **b** and the values are listed in Table 5.1 on page 114. Differently alkyl substituted di(thien-2-yl)pyrenes show similarly shaped absorption spectra with two broad absorption bands at ~280 nm and ~360 nm. Emission spectra of **5-2** and **5-6** are

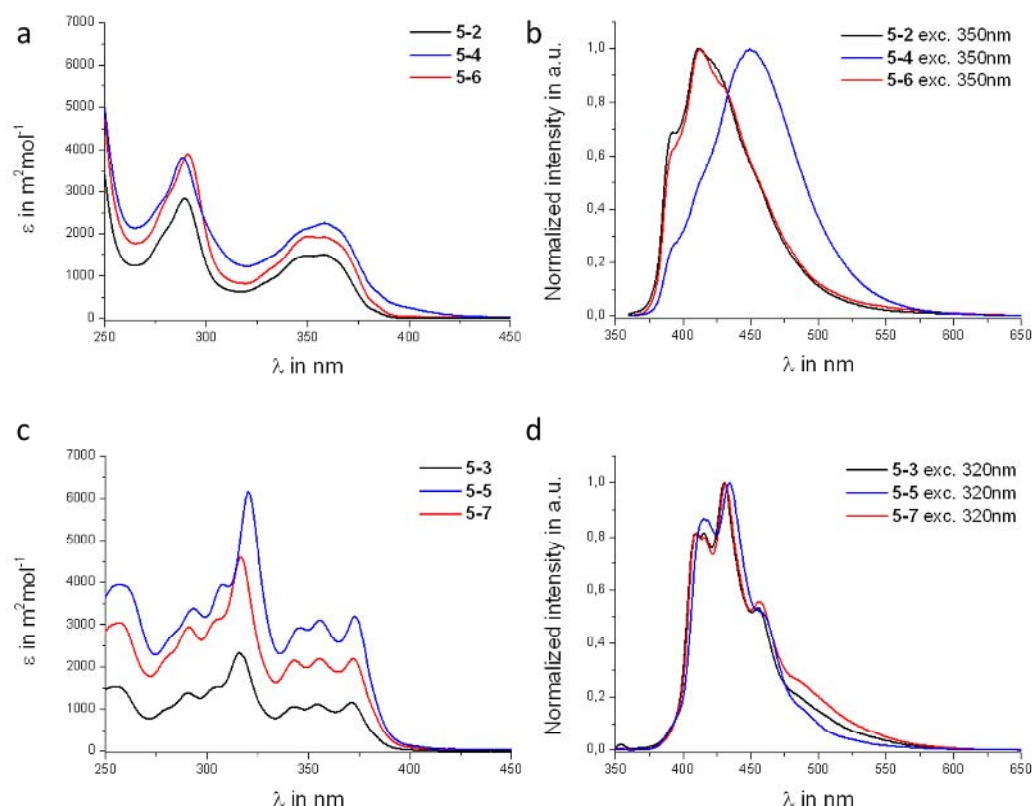


Figure 5.4: UV/vis absorption and emission spectra of di(thien-2-yl)pyrenes **5-2**, **5-4** and **5-6** (a and b) and dithienobenzo[*e*]pyrenes **5-3**, **5-5** and **5-7** (c and d) in THF at 10^{-5} M concentration.

almost identical, indicating minor influence of longer alkoxy chains. Instead, the maximum of **5-4** is red-shifted as an effect of alkylation of the free α -position at the thienyl moiety. Intramolecular ring-closure between adjacent thienyl rings to the dithienobenzo[*e*]pyrene scaffold led to distinctive splitting of the absorption bands and emission spectra appear sharpened compared to the opened form. As Brusso et al. reported for the transition from 1,2,4,5-tetrathienylbenzene to tetrathienoanthracene, the fused species exhibits pronounced vibronic structure introduced by enhanced rigidity of the molecules.^[22, 29] Furthermore, the closure between the thiophenes should lead to a considerable increase of the conjugation length and thereof a bathochromic shift of the absorption. In contrast, only minor changes between 0.02 eV and 0.05 eV of the optical energy gap could be observed. These small variations

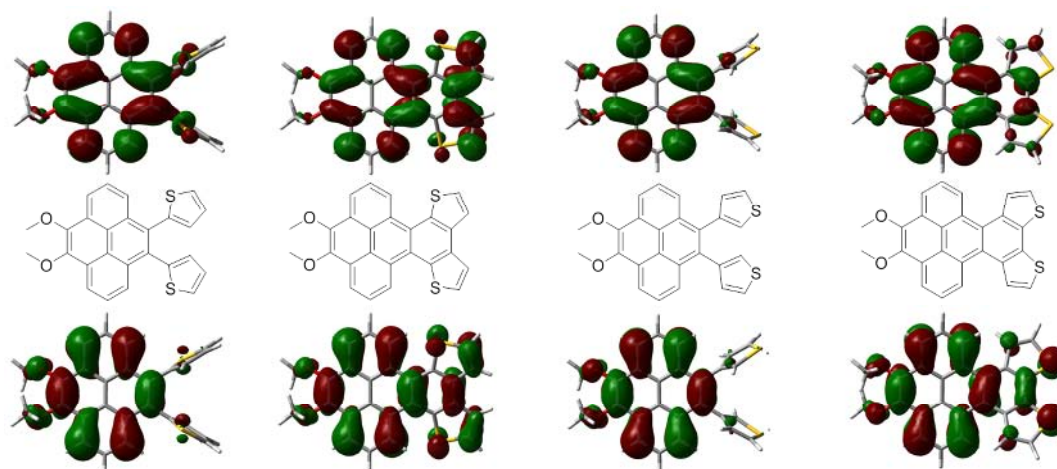


Figure 5.5: Orbital surfaces of the HOMO (below the formulae) and LUMO (above the formulae) of **5-2**, **5-3**, **5-8** and **5-9** (from left to right) determined by DFT calculations on 6-31G basis.

indicate that no acene-like conjugation can be found for dithienobenzo[*e*]pyrenes as described for the formation of tetrathienoanthracene from tetrathienylbenzene.^[29]

To gain further insight into the electronic structure, quantum mechanical calculations using Gaussian 03 were performed.^[30] The orbital surfaces of the HOMO and the LUMO of **5-2** and **5-3** are shown in Figure 5.5 and the values are listed in Table 5.1. The calculations confirm the trend of a slight decrease of the energy gap after ring-closure. The frontier orbitals of the pyrene unit show only slight changes from the opened to the fused species, but orbital coefficients on thiophenes are significantly increased after planarization. Nevertheless, the frontier orbitals are dominated by the 2-7 nodal plane which is missing for asymmetric substituted donor/acceptor pyrenes **3-6** and **3-7** (Figure 3.8). These nodals seem to hinder effective conjugation and could be an explanation for small decrease of the energy gap.

Due to the weak electron-donating effect of alkyl chains, alteration of the position and the chain length of alkyl substitution only slightly influenced the absorption maxima and thus the optical energy gap. Even though values differ minimally in the range of 0.05 eV, a trend could be observed for decreasing

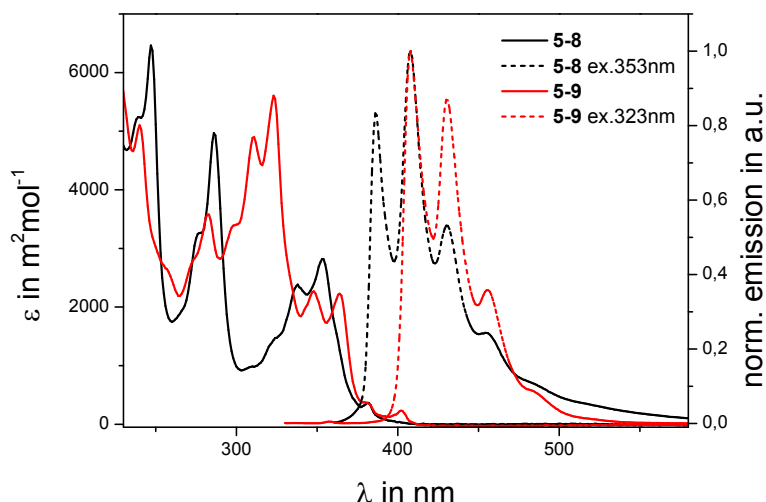


Figure 5.6: UV/vis absorption (solid line) and emission spectra (dashed line) of di(thien-3-yl)pyrene **5-8** and the planarized species **5-9** in THF at 10^{-5} M concentration.

$E_{g(opt)}$ from **5-2**, **5-6**, to **5-4** and **5-3**, **5-7** to **5-5**, respectively. The decrease of the energy gap can presumably be attributed to a raised HOMO level, caused by increased inductive effect of longer and a larger number of inductive substituents.^[31] The destabilizing effect on the HOMO level appears highest for **5-4/ 5-5**, which bear two additional electron-donating groups and is further investigated by cyclic voltammetry in the next subchapter.

The attachment of thiophene at its less reactive 3-position to pyrene did not drastically change the absorption compared to the 2-position isomers (Figure 5.6). For the thienyl derivative **5-8** absorption and emission spectrum exhibit sharp peaks compared to broad bands in the case of **5-2**. An explanation could be the decreased rotational freedom of the 3-thienyl moiety due to two hydrogens in *ortho*-position instead of one hydrogen and one sulfur atom.

Comparing the isomers, the absorption onset is shifted hypsochromically by 11 nm for **5-2** to **5-8** and 13 nm for **5-3** to **5-9**. The energy gap decreases by 0.03 eV from the opened to the closed form (**5-8** to **5-9**) which is in accordance with the calculations. Furthermore, smaller orbital coefficients with one additional nodal plane were computed for the HOMO of the thiophene subunit of **5-9** (Figure 5.5). The reason for the reduction of conjugation might be

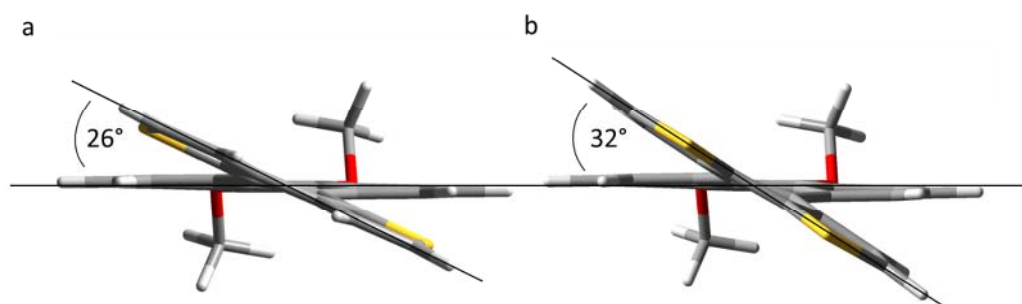


Figure 5.7: Side view of optimized structures of **5-3** (a) and **5-9** (b) and measured angle between the pyrene plane and benzodithiophene plane.

Table 5.1: Optical properties of dithienyl- and dithienobenzo[e]pyrenes.^[a]

| | λ_{abs} ^[b] | λ_{em} ^[c] (λ_{ex}) ^[d] | λ_{edge} | $E_{\text{g(opt)}}$ ^[e] | $E_{\text{g(cal)}}$ ^[f] |
|------------|---------------------------------------|---|-------------------------|------------------------------------|------------------------------------|
| 5-2 | 358 nm | 392 nm (350 nm) | 382 nm | 3.25 eV | 3.62 eV |
| 5-3 | 371 nm | 409 nm (320 nm) | 388 nm | 3.20 eV | 3.51 eV |
| 5-4 | 358 nm | 449 nm (350 nm) | 388 nm | 3.20 eV | ^[g] |
| 5-5 | 373 nm | 415 nm (320 nm) | 390 nm | 3.18 eV | ^[g] |
| 5-6 | 358 nm | 412 nm (350 nm) | 384 nm | 3.23 eV | ^[g] |
| 5-7 | 372 nm | 409 nm (320 nm) | 389 nm | 3.19 eV | ^[g] |
| 5-8 | 353 nm | 386 nm (353 nm) | 371 nm | 3.34 eV | 3.67 eV |
| 5-9 | 364 nm | 408 nm (323 nm) | 375 nm | 3.31 eV | 3.70 eV |

[a] All absorption and emission spectra were measured in THF. [b] λ_{abs} is the absorption band appearing at the longest wavelength. [c] λ_{em} is the fluorescence band appearing at the shortest wavelength. [d] λ_{ex} wavelength of excitation. [e] Calculated from λ_{edge} [f] Calculated DFT/B3LYP/6-31G using Gaussian. [g] not calculated.

derived from distortion of the molecules. Figure 5.7 shows the optimized three-dimensional structure of **5-3** and the isomer **5-9** in side view and the measured angle between the pyrene plane and the benzodithiophene plane. An angle of 26° for **5-8** and 32° for **5-9** was predicted. The higher degree of distortion of **5-9** derives from the steric overcrowding in the *cove* region of one hydrogen atom and the sulfur lone pairs (**5-3**) versus two hydrogen atoms (**5-9**). A similar spatial configuration dominates the three-dimensional structure of tetrabenzo[*de,hi,mn,qr*]naphthacene with two hydrogens within the *cove* region and a distortion similar to dithienobenzo[e]pyrenes was reported.^[32]

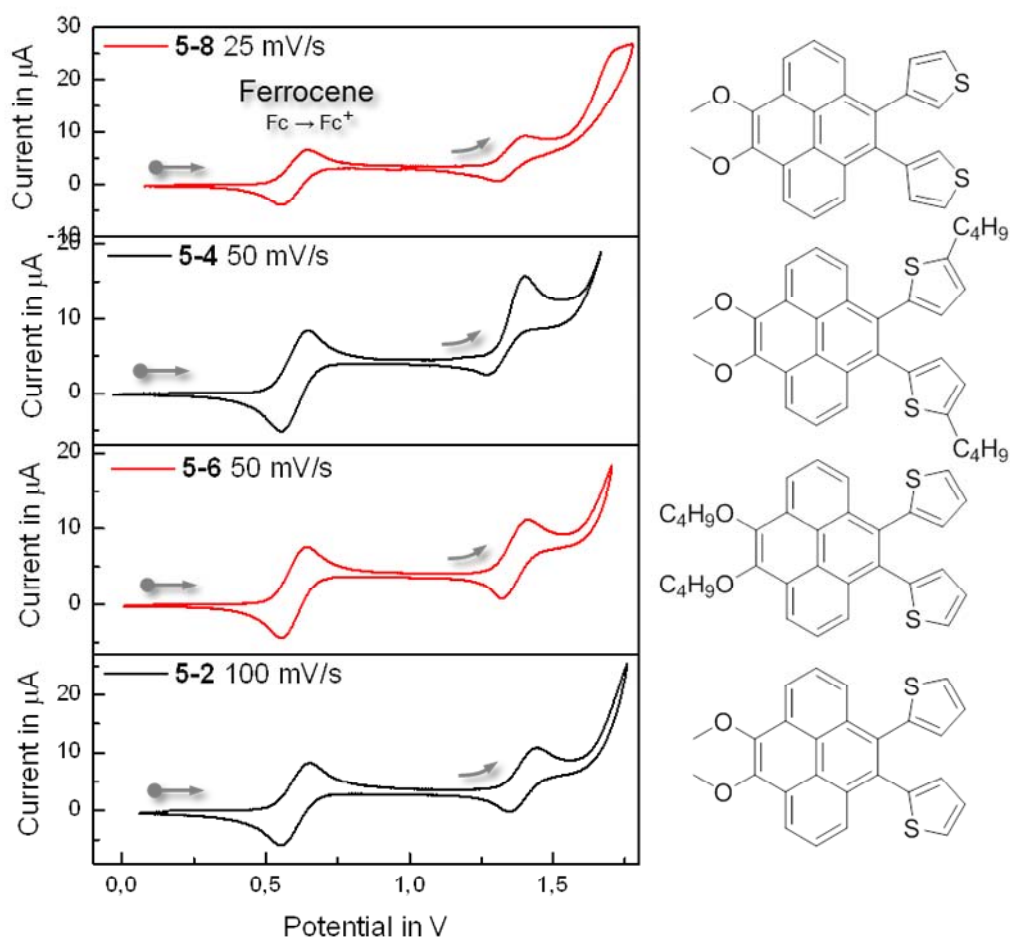


Figure 5.8: Cyclic voltammograms of dithienylpyrenes **5-2**, **5-4**, **5-6** and **5-8**. Ferrocene oxidation and reduction wave is set to half-wave potential of 0.6 V.

Cyclic Voltammetry

The energy levels of active materials play an important role in organic field-effect transistors, especially at the junction between semiconductive material and the electrodes. Therefore, cyclic voltammetry (CV) was applied to determine the position of the frontier orbitals of dithienyl- and dithienobenzo[*e*]pyrenes. In all measurements ferrocene (0.1 mM) was used as internal standard to reference all values according to the ferrocene half-wave potential (0.600 V versus SCE).^[33]

Table 5.2: Electronic properties of dithienyl- and dithienobenzo[e]pyrenes.^[a]

| Compound | E _{HOMO(CV)} ^[b] | E _{HOMO(cal)} ^[c] |
|------------|--------------------------------------|---------------------------------------|
| 5-2 | -5.52 eV | -5.55 eV |
| 5-3 | -5.49 eV | -5.47 eV |
| 5-4 | -5.51 eV | ^[d] |
| 5-5 | -5.43 eV | ^[d] |
| 5-6 | -5.50 eV | ^[d] |
| 5-7 | -5.47 eV | ^[d] |
| 5-8 | -5.48 eV | -5.52 eV |
| 5-9 | -5.46 eV | -5.52 eV |

[a] Values of the HOMO determined by cyclic voltammetry and calculated. [b] CV measured in 0.1 M n-Bu₄NPF₆/DCM with scan rates between 25 mV/s and 100 mV/s; values calculated using the ferrocene HOMO level: E_{HOMO(CV)} = - (E_{ox,onset} - E^(1/2)_{Fc/Fc+} + 4.8) eV [c] Calculated DFT/B3LYP/6-31G using Gaussian; [d] not calculated.

The cyclic voltammograms of dithienylpyrenes are depicted in Figure 5.8 and the obtained values are listed in Table 5.2. For evaluation of the data the onset of oxidation waves and the half-wave potential of the ferrocene as internal standard was used. All compounds show a first oxidation wave with an onset between 1.28 V and 1.33 V (vs SCE), which indicates the HOMO level and corresponds to the formation of a radical cation. Except **5-4**, the oxidation process seems to be reversible.

A second irreversible oxidation could only be observed for **5-8** at 0.3 V higher potential. It was found that applying potentials higher than 2 V leads to the loss of reversibility of the first oxidation process in all cases and additional irreversible oxidation waves. These can be ascribed to the formation of oligomeric and polymeric species.^[22, 29, 34] Swager et al. reported tandem cyclization-polymerization of 4,5-bis(2-thienyl)-1,2-didecyloxybenzene electrochemically, monitored by cyclic voltammetry.^[34] Therein, two oxidation processes were observed and assigned to the subsequent formation of the respective polymer.

Cyclic voltammetry of the dithienobenzo[e]pyrenes revealed a small rise of the HOMO level by 0.02 eV and 0.03 eV for **5-3**, **5-7** and **5-9** (Figure 5.9). For

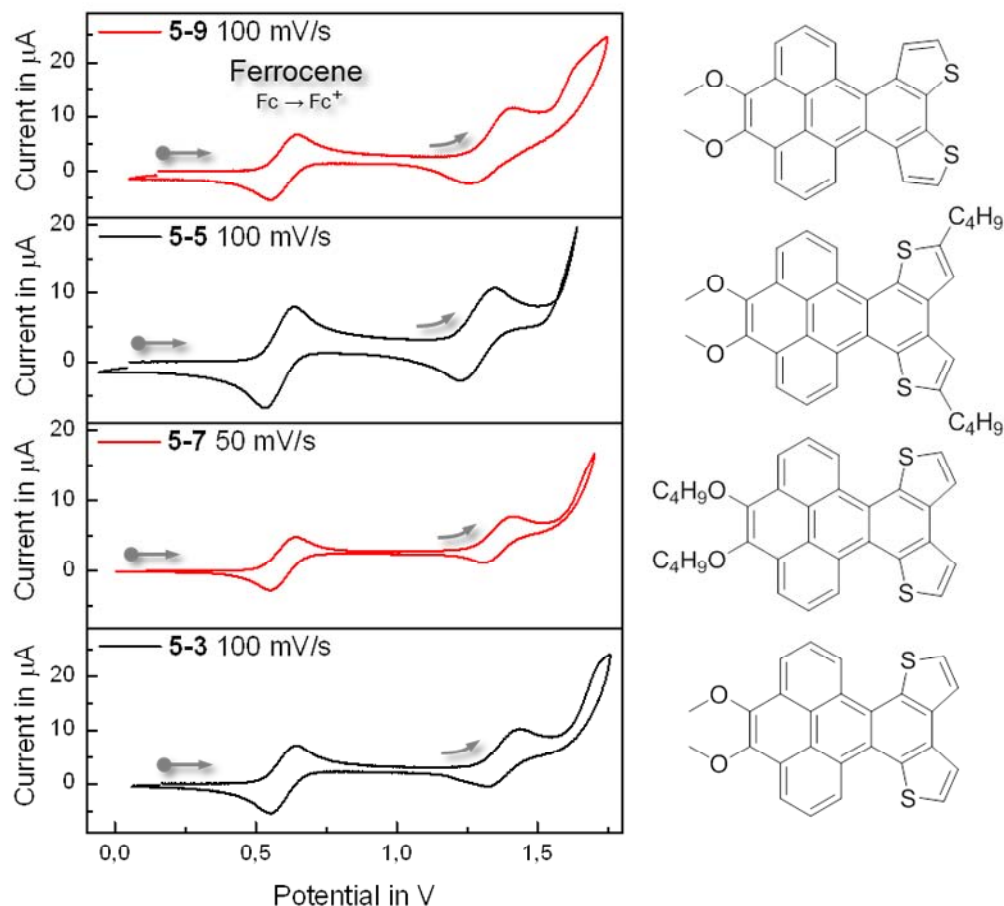


Figure 5.9: Cyclic voltammogram of dithienobenzo[*e*]pyrenes **5-3**, **5-5**, **5-7** and **5-9**. Ferrocene oxidation and reduction wave is set to half-wave potential of 0.6 V.

the HOMO level of **5-5** an increase of 0.08 eV was determined. This large shift, compared to the other dithienobenzo[*e*]pyrenes, could be explained by the additional electron donating effect of the butyl chains that influences the HOMO to a greater extent in the planarized conformation. The experimental observation of a slight destabilization of the HOMO level by ring-closure and the determined values for the HOMO level are supported by Density Functional Theory (DFT, B3LYP/6-31G) calculations.

The electrochemical data on dithienylpyrenes and dithienobenzo[*e*]pyrenes with HOMO levels between -5.43 eV and -5.52 eV indicate that these new sulfur-containing heterocycles are not particularly strong donors. Even though

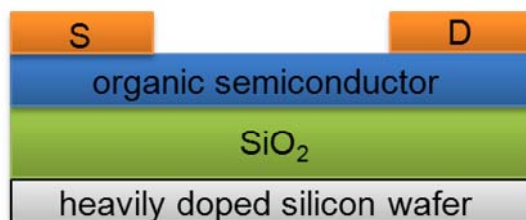


Figure 5.10: OFET geometry: top contact/ bottom gate. S: source and D: drain electrodes are from gold, dielectric from silicon dioxide. Gate electrode: heavily doped silicon wafer.

only minor effects on the frontier orbitals can be observed for the ring-closure, the impact on the spatial shape of the molecules and resulting packing properties is expected to be crucial of the performance in OFET devices.^[2]

5.4 OFET Performance

The semiconductive properties of dithienylpyrenes and dithienobenzo[e]-pyrenes in organic field-effect transistors (OFETs) were tested in collaboration with [REDACTED] in the institute. Beside the active material, the performance of the devices strongly depends on other factors like the transistor design, the electrode material, the presence of oxygen, the processing, the substrate and its surface modifications.^[2] However, the impact of all of these factors could hardly be investigated in this study and it has clearly been focused on the semiconductive material. To retain comparability, all transistors in this investigation were fabricated in a top contact/ bottom gate configuration using heavily doped silicon wafers as gate electrode and run under nitrogen atmosphere (Figure 5.10).^[35]

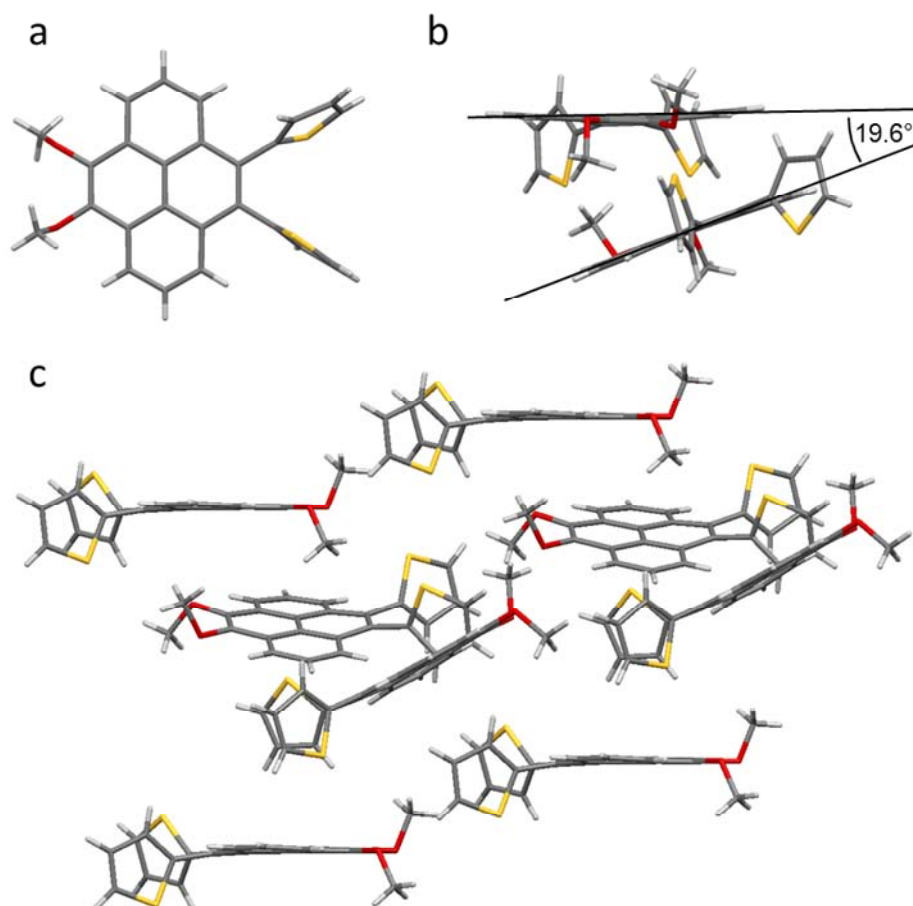


Figure 5.11: X-ray structure of **5-2** in (a) front view, (b) nonparallel pair of **5-2** and (c) the arrangement in the crystal; for clarity, due to conformational isomerism of thienyl rings only the majority component is shown.

The potential organic semiconductor was either processed from toluene solution by drop casting, spin coating or by vacuum deposition. The transistors were completed by evaporating source and drain electrodes from gold using shadow mask. Gold electrodes were used as the source and the drain since the gold Fermi level perfectly matches the HOMO energy of the dithienylpyrenes and dithienobenzo[*e*]pyrenes, thus holding promise for hole injection and low contact resistance.^[36]

At first, dithienylpyrenes **5-2** and the isomer **5-8** were solution processed by drop casting and dip coating on silicon oxide, but no field-effect could be detected. We reasoned that the twisted thienyl rings do not induce a favorable stacking for charge carrier transport. To provide this statement with

experimental proof, crystals were grown from both isomers suitable for X-ray diffraction. Crystal structures could be resolved for both compounds (Figure 5.11 and Figure 5.12). The methoxy groups stick out of the pyrenyl plane oppositely. Within the asymmetric unit of **5-2**, two molecules pack in a nonparallel way with an angle of 19.6° and a π - π -distance of 3.73 Å to 4.66 Å. Between pyrene and thienyl rings, torsion angles from 69.0° to 87.0° were observed.

The investigation of the impact of the crystal packing on the device performance is important in order to develop and refine structural concepts on the molecular level. Despite great efforts that have been made in this area the structure-performance relationship is yet not well understood. One reason might be the observation that the “best” packing motif for charge transport does not exist. Common arrangements found for small molecular semiconducting molecules are either dominated by face-to-edge ($\text{C-H}\cdots\pi$) or face-to-face ($\pi\cdots\pi$) in the herringbone or brick-like motif, respectively.^[2] As an example, (trialkylsilyl)ethynyl substituted anthradithiophenes were characterized in FET devices in dependence of different alkyl residues which led to a brick-like order for isopropyl and to herringbone motif for methyl. Very high charge carrier mobilities were measured for the anthradithiophene derivative in the brick-like and no performance in the herringbone arrangement.^[37] It was assumed that the face-to-face arrangement enhances the π - π -overlap which maximizes the electronic coupling for efficient charge carrier mobility. In contrast, similar mobilities have been reported for molecules that pack in the herringbone motif.^[38-39]

In case of **5-2** the found skew packing and the non-parallel pyrenyl units lead to large π - π -distance which hinder efficient π - π -overlap, and thus, disfavor charge carrier transport in organic materials.^[2, 40]

Like **5-2**, **5-8** shows conformational isomers within the crystal due to the rotational freedom of the single bond linkage between the pyrenyl and thienyl moiety. Both thienyl units are similarly rotated by 65.8° and 67.6° , respectively. As depicted in Figure 5.12, the stacks of di(thien-3-yl)pyrenes are laterally

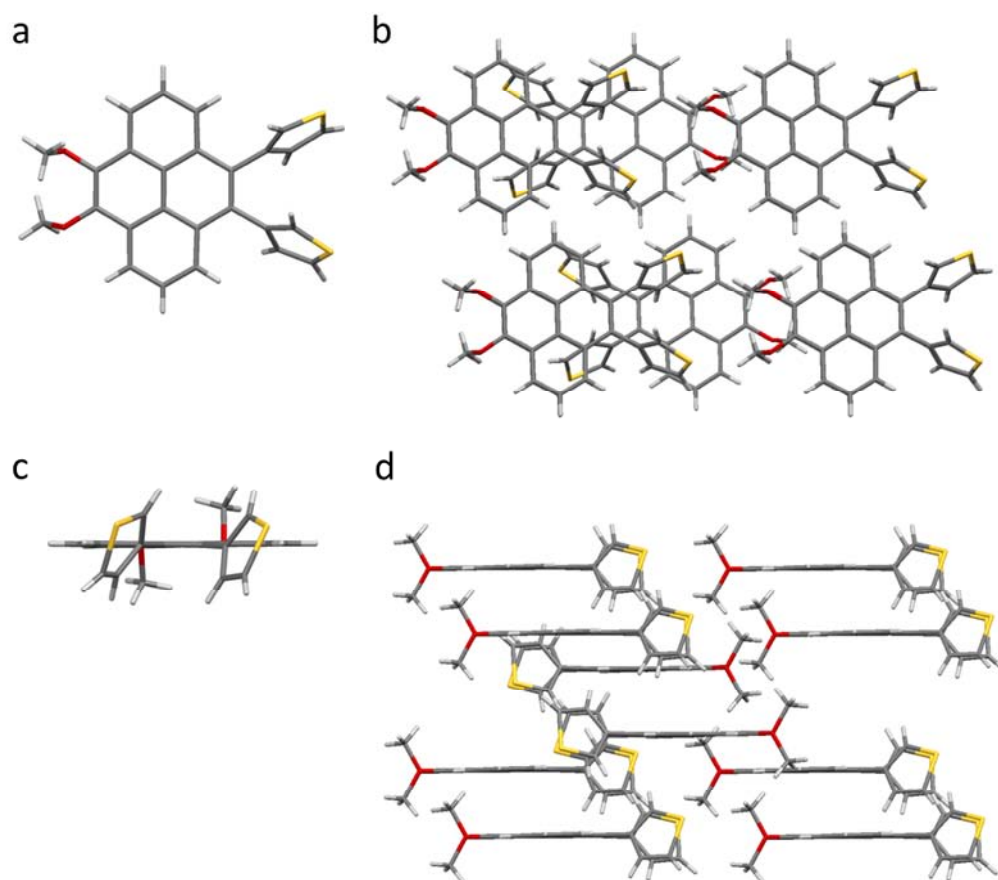


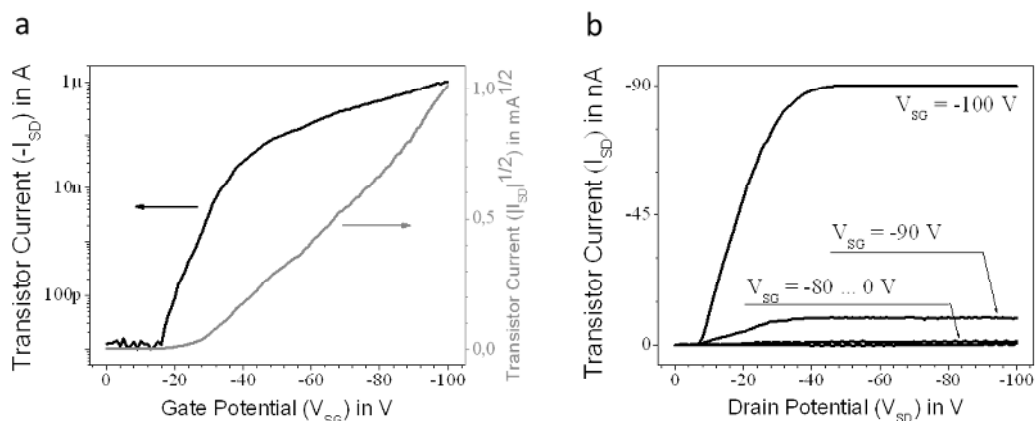
Figure 5.12: X-ray structure of **5-8** in (a) front view, (c) side view and (b) the arrangement in the crystal from side and (d) front view; due to conformational isomerism of thienyl rings only the majority component is shown.

shifted and the thienyl moieties are located in between pyrenes. In contrast to **5-2**, pyrene molecules of **5-8** are parallel aligned. The distance from one pyrene plane to another was determined as 4.61 Å which is too far for π - π -stacking. Efficient π - π -interaction of adjacent pyrene moieties is hence inhibited by bulky thiophenes (Figure 5.12 d). Nevertheless, it shall be noted that **5-8** easily crystallizes in large crystals just by slow solvent evaporation of the solvent.

In a few words, crystal packing of dithienylpyrenes is mainly coined by twisted thienyl moieties and large π - π -distances, which could be the reason for the missing semiconductive properties of the materials. Expecting in turn a closer packing after ring-closure, dithienobenzo[*e*]pyrenes **5-3**, **5-5**, **5-7** and **5-9** were applied as active material in field-effect transistors as well. At first, drop

Table 5.3: Device performance of dithienobenzo[e]pyrenes.

| | Processing | Substrate | Charge carrier mobility/ $\text{cm}^2\text{V}^{-1}\text{s}^{-1}$ |
|------------|--------------|----------------|--|
| 5-3 | Drop casting | SiO_2 | $2.7 \cdot 10^{-5}$ |
| | Dip coating | HMDS | $2.5 (\pm 0.7) \cdot 10^{-3}$ |
| | Sublimed | HMDS | $2 \cdot 10^{-5}$ |
| 5-5 | Drop casting | SiO_2 | No performance |
| 5-7 | Drop casting | SiO_2 | $3.5 \cdot 10^{-4}$ |
| 5-9 | Drop casting | SiO_2 | No performance |
| | Dip coating | HMDS | No performance |
| | Sublimed | HMDS | $3.4 \cdot 10^{-5}$ |

**Figure 5.13:** Typical transfer (a) and output (b) characteristics of dip-coated **5-3** transistors.

casting was used to process dithienobenzo[e]pyrenes from toluene solution on silicon wafers. Measured charge carrier mobilities of the devices are listed in Table 5.3. Very low values for hole transport around $10^{-4} \text{ cm}^2\text{V}^{-1}\text{s}^{-1}$ to $10^{-5} \text{ cm}^2\text{V}^{-1}\text{s}^{-1}$ were obtained for **5-3** and **5-7** and no field-effect for **5-5** and **5-9** could be detected. Looking at the films after solution deposition no homogenous films could be observed.

Recently, Brusso et al. reported the FET performance of tetrathieno[*a,c,h,j*]anthracenes made from 1,2,4,5-tetra(thien-2-yl)benzene and 1,2,4,5-tetra(thien-3-yl)benzene.^[29] It was found that either processed from solution or vacuum, the tetrathieno[*a,c,h,j*]anthracene isomer obtained from the thien-3-yl precursor gives higher hole mobilities. The authors argue that the

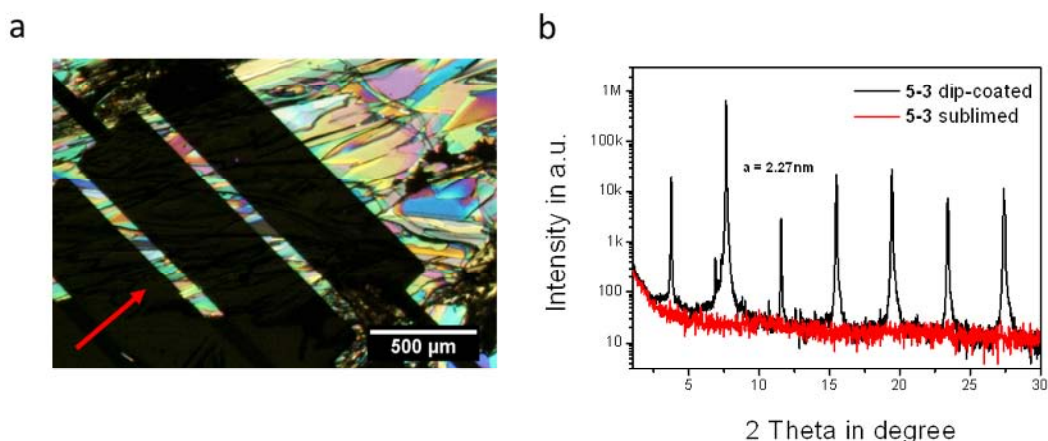


Figure 5.14: (a) Film formation of dip-coated **5-3** on HMDS-treated silicon dioxide insulator in a top contact/ bottom gate transistor configuration. The image is taken at crossed polarizer/analyzer; the arrow indicates the dip-coating direction; (b) X-ray diffraction in reflection mode for the dip-coated (black) and the sublimed (red) film of **5-3**. $2\Theta_{\text{dip-coated}} = 3.66 - 3.89^\circ$ corresponds to an out-of-plane spacing $d_{\text{dip-coated}} = 2.27 - 2.41$ nm in the **5-3** based film.

sulfur is more exposed which enhances the S-S contact with surrounding molecules. In order to study the effect of the position of the sulfur on dithienobenzo[*e*]pyrenes, the devices of **5-3** and **5-9** are optimized. The surface of the dielectric (SiO_2) was modified by using hexamethyldisilazane (HMDS) in order to avoid interface trapping by silanol groups.^[41] Both materials were processed by dip coating, but solely **5-3** formed a uniform film. The transistor transfer curve is given in Figure 5.13. Charge carrier mobilities of $\mu_{\text{sat}} = 2.5 (\pm 0.7) \times 10^{-3} \text{ cm}^2 \text{V}^{-1} \text{s}^{-1}$ (mean value and 90 % confidence region) were achieved, which represent today's highest values for solution-processed, pyrene-based field-effect transistors reported by journal articles.^[17] An on-off ratio of $I_{\text{on}}/I_{\text{off}} = 1.1 (\pm 0.4) \times 10^4$ was obtained.

For the sake of comparison, devices prepared by vacuum deposition of the isomers **5-3** and **5-9** yielded hole mobilities in the range 2 to $3 \times 10^{-5} \text{ cm}^2 \text{V}^{-1} \text{s}^{-1}$ for both compounds. Thus, no general conclusion about the position of sulfur could be drawn. In order to understand the improvement of performance of dip-coated transistors of **5-3** better, the films of the transistors were studied in more

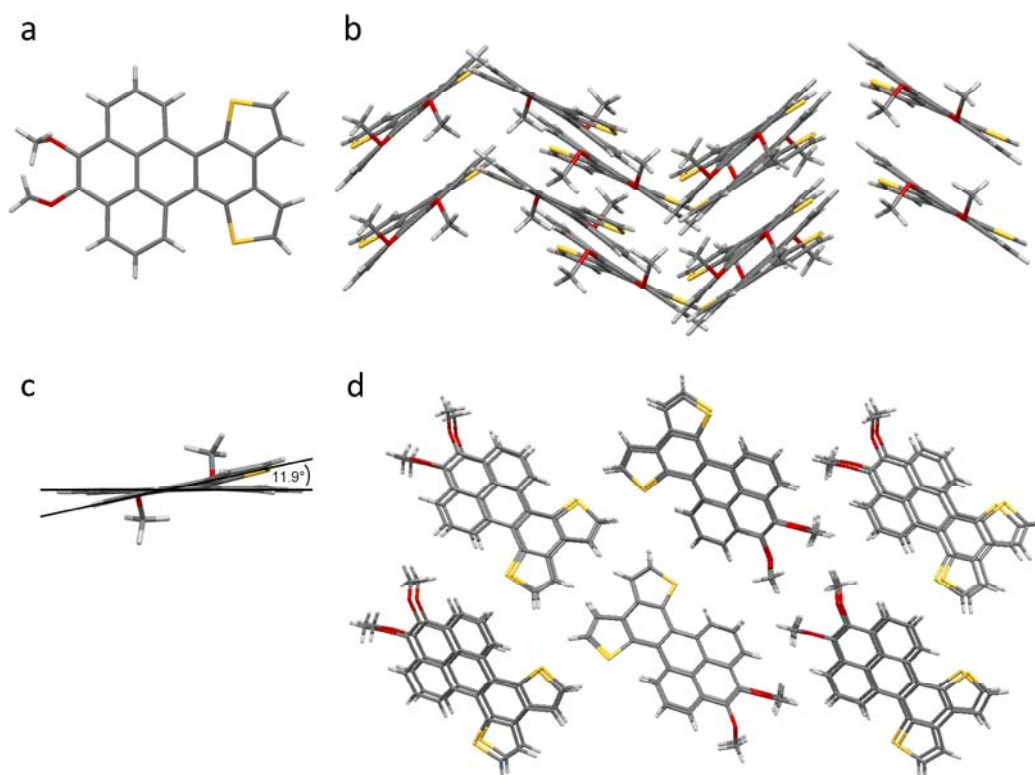


Figure 5.15: X-ray structure of **5-3** in (a) front view, (c) side view and the herringbone packing motif from (c) side and (d) front view.

detail. Optical microscopy was performed and high crystallinity of large domains in the film of **5-3** were verified (Figure 5.14 a). Film X-ray (Bragg reflection) revealed a high crystallinity for the drop-casted film as well, but no clear reflection could be observed in case of the sublimed layer of **5-3** (Figure 5.14 b). This high order within the film seems to be crucial for the mobility of the charge carriers. Therefore, single crystals of **5-3** were analyzed by X-ray crystallography and the crystal packing is depicted in Figure 5.15. Dithienobenzo[*e*]pyrene **5-3** arranges in a herringbone motif with an average π - π -stacking distance of 3.35 Å and thus reveals a smaller spacing than for **5-2** induced by the planarization. Due to steric effects **5-3** was found to be distorted by 11.9° between the pyrene plane and the benzodithieno plane (Figure 5.15 c). The distortion found in the crystalline state is smaller by 15° compared to the calculated value in vacuum (Figure 5.7 a).

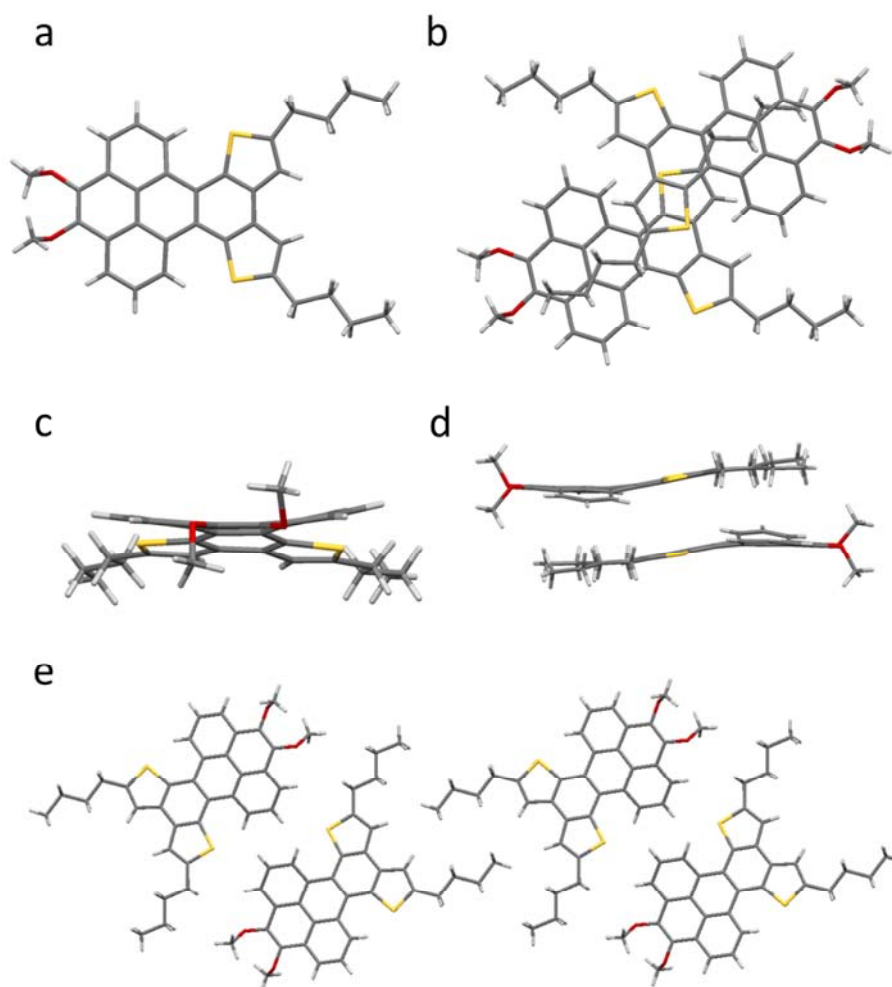


Figure 5.16: X-ray structure of **5-5** in (a) front view, (c) side view, (f) the 2D arrangement in one plane and the stacking in (b) front and (d) side view.

Unfortunately, crystals of **5-9** large enough for X-ray analysis could not be grown and therefore a detailed comparison of the packing and stacking properties between **5-3** and **5-9** is missing. However, **5-5** yielded suitable crystals and the structure could be solved (Figure 5.16). While the pyrene plane is twisted against the dithienobenzo plane in case of **5-3**, the pyrene moiety within **5-5** is bent by 15.0° (Figure 5.16 c). Figure 5.16 e displays the arrangement of the molecules in one layer of molecules. Three-dimensional order is coined by the overlap of the thieno moiety with a π - π -distance of 3.48 \AA (Figure 5.16 b and d). Only a small part of the π -systems is participating

in the π - π -interaction as a layer-by-layer structure is formed consisting of alternately stacked butyl chains and the pyrene core.

Besides the crystal packing, other before mentioned factors like the film morphology or the source and drain contact to the active layer can be brought up as explanations for low or no field-effects. Respective **5-5**, the unsatisfactory processing properties seem to dominate the performance of this material.

5.5 Summary

In summary, it could be shown that asymmetrically substituted, pyrene derived semiconductors dithieno[1,2-*b'*;4,3-*b''*]benzo[*e*]pyrenes were suitable for the application in organic field-effect transistors as p-type material reaching charge carrier mobilities in the range of $10^{-3} \text{ cm}^2 \text{ V}^{-1} \text{ s}^{-1}$. This value ranks three magnitudes lower than the current state of the art field-effect transistor, but represents today's highest values for solution-processed, pyrene-based field-effect transistors reported by journal articles.^[17]

The transition from the dithienylpyrenes to the flattened form only slightly changes the optical energy gap and the height of the HOMO level but stiffens the molecules, clearly recognizable by the pronounced vibronic bands in the UV/vis absorption spectra. Therefore, the crystal packing and in particular the contact to neighboring molecules is deeply altered by the planarization. A close π - π -stacking in combination with a parallel arrangement has been pointed out to be crucial for the utilization in OFETs. Best OFETs were obtained from short methoxy instead of butoxy chains attached to pyrene, confirming the important role of high crystallinity for these molecules in the film.

For the reason of comparison, the isomer di(thien-3-yl)pyrene and the planarized dithieno[2,1-*b'*;3,4-*b''*]benzo[*e*]pyrene were synthesized to investigate differences in performance as a function of the position of the sulfur atom within the molecule. Working OFETs could not be built by solution processing. Vacuum deposition of the dithienobenzo[*e*]pyrene isomers gave mobilities in the magnitude of $10^{-5} \text{ cm}^2 \text{ V}^{-1} \text{ s}^{-1}$ for both of them and no significant difference could be measured. Suitable crystals for X-ray analysis could not be grown for dithieno[2,1-*b'*;3,4-*b''*]benzo[*e*]pyrene, which left a detailed study of the impact on the crystals packing still open.

The in-depth analysis of dithienobenzo[*e*]pyrenes inevitably asks for the development of the here presented structural concept in order to improve the material performance, always keeping the synthetic feasibility in mind. In

respect to the strong linkage between sulfur containing aromatic hydrocarbons and the semiconductivity in organic materials, doubling the benzodithiophene motif to both pyrene sides appears obvious and will be targeted in the next chapter. It has to be noted that the non-planarity found for dithienobenzo[*e*]pyrenes due to the *cove* regions might force the molecules into a distorted conformation unfavorably for efficient charge transport.

5.6 Bibliography

- [1] C. A. Hunter, K. R. Lawson, J. Perkins, C. J. Urch, *Journal of the Chemical Society-Perkin Transactions 2* **2001**, 651-669.
- [2] M. Mas-Torrent, C. Rovira, *Chemical Reviews* **2011**, *111*, 4833-4856.
- [3] A. R. Murphy, J. M. J. Frechet, *Chemical Reviews* **2007**, *107*, 1066-1096.
- [4] J. E. Anthony, *Angewandte Chemie-International Edition* **2008**, *47*, 452-483.
- [5] A. Mishra, C. Q. Ma, P. Bauerle, *Chemical Reviews* **2009**, *109*, 1141-1276.
- [6] A. Pron, P. Gawrys, M. Zagorska, D. Djurado, R. Demadrille, *Chemical Society Reviews* **2010**, *39*, 2577-2632.
- [7] W. L. Jia, T. McCormick, Q. D. Liu, H. Fukutani, M. Motala, R. Y. Wang, Y. Tao, S. N. Wang, *Journal of Materials Chemistry* **2004**, *14*, 3344-3350.
- [8] J. N. Moorthy, P. Natarajan, P. Venkatakrishnan, D. F. Huang, T. J. Chow, *Organic Letters* **2007**, *9*, 5215-5218.
- [9] J. Y. Hu, M. Era, M. R. J. Elsegood, T. Yamato, *European Journal of Organic Chemistry* **2010**, 72-79.
- [10] K. R. J. Thomas, M. Velusamy, J. T. Lin, C. H. Chuen, Y. T. Tao, *Journal of Materials Chemistry* **2005**, *15*, 4453-4459.
- [11] T. M. Figueira-Duarte, K. Müllen, *Chemical Reviews* **2011**, *111*, 7260-7314.
- [12] C. Wang, H. Dong, W. Hu, Y. Liu, D. Zhu, *Chemical Reviews* **2012**, *112*, 2208-2267.
- [13] F. Moggia, C. Videlot-Ackermann, J. Ackermann, P. Raynal, H. Brisset, F. Fages, *Journal of Materials Chemistry* **2006**, *16*, 2380-2386.
- [14] Y. Wang, H. M. Wang, Y. Q. Liu, C. A. Di, Y. M. Sun, W. P. Wu, G. Yu, D. Q. Zhang, D. B. Zhu, *Journal of the American Chemical Society* **2006**, *128*, 13058-13059.
- [15] H. J. Zhang, Y. Wang, K. Z. Shao, Y. Q. Liu, S. Y. Chen, W. F. Qiu, X. B. Sun, T. Qi, Y. Q. Ma, G. Yu, Z. M. Su, D. B. Zhu, *Chemical Communications* **2006**, 755-757.
- [16] M. Ashizawa, K. Yamada, A. Fukaya, R. Kato, K. Hara, J. Takeya, *Chemistry of Materials* **2008**, *20*, 4883-4890.
- [17] P. Anant, N. T. Lucas, J. M. Ball, T. D. Anthopoulos, J. Jacob, *Synthetic Metals* **2010**, *160*, 1987-1993.
- [18] J. G. Laquindanum, H. E. Katz, A. J. Lovinger, A. Dodabalapur, *Advanced Materials* **1997**, *9*, 36-&.
- [19] R. Rieger, D. Beckmann, A. Mavrinskiy, M. Kastler, K. Müllen, *Chemistry of Materials* **2010**, *22*, 5314-5318.
- [20] P. Gao, D. Beckmann, H. N. Tsao, X. L. Feng, V. Enkelmann, M. Baumgarten, W. Pisula, K. Mullen, *Advanced Materials* **2009**, *21*, 213-+.

- [21] L. Zöphel, D. Beckmann, V. Enkelmann, D. Chercka, R. Rieger, K. Müllen, *Chemical Communications* **2011**, 47, 6960–6962.
- [22] E. Fischer, J. Larsen, J. B. Christensen, M. Fourmigue, H. G. Madsen, N. Harrit, *Journal of Organic Chemistry* **1996**, 61, 6997–7005.
- [23] R. B. Woodward, R. Hoffmann, *The Conservation of Orbital Symmetry*, VCH: Weinheim 1970.
- [24] M. Irie, *Chemical Reviews* **2000**, 100, 1685–1716.
- [25] I. Fleming, *Frontier Orbitals and Organic Chemical Reactions* John Wiley & Sons Ltd **1976**.
- [26] T. Chen, G. B. Pan, H. Wettach, M. Fritzsche, S. Hoyer, L. J. Wan, H. B. Yang, B. H. Northrop, P. J. Stang, *Journal of the American Chemical Society* **2010**, 132, 1328–1333.
- [27] M. S. A. Abdou, X. T. Lu, Z. W. Xie, F. Orfino, M. J. Deen, S. Holdcroft, *Chemistry of Materials* **1995**, 7, 631–641.
- [28] R. Rieger, D. Beckmann, W. Pisula, W. Steffen, M. Kastler, K. Müllen, *Advanced Materials* **2010**, 22, 83–+.
- [29] J. L. Brusso, O. D. Hirst, A. Dadvand, S. Ganesan, F. Cicoira, C. M. Robertson, R. T. Oakley, F. Rosei, D. F. Perepichkat, *Chemistry of Materials* **2008**, 20, 2484–2494.
- [30] M. J. Frisch, G. W. Trucks, H. B. Schlegel, G. E. Scuseria, M. A. Rob, J. R. Cheeseman, J. A. Montgomery Jr., T. Vreven, K. N. Kudin, J. C. Burant, J. M. Millam, S. S. Iyengar, J. Tomasi, V. Barone, B. Mennucci, M. Cossi, G. Scalmani, N. Rega, G. A. Petersson, H. Nakatsuji, M. Hada, M. Ehara, K. Toyota, R. Fukuda, J. Hasegawa, M. Ishida, T. Nakajima, Y. Honda, O. Kitao, H. Nakai, M. Klene, X. Li, J. E. Knox, H. P. Hratchian, J. B. Cross, V. Bakken, C. Adamo, J. Jaramillo, R. Gomperts, R. E. Stratmann, O. Yazyev, A. J. Austin, R. Cammi, C. Pomelli, J. W. Ochterski, P. Y. Ayala, K. Morokuma, P. S. G. A. Voth, J. J. Dannenberg, V. G. Zakrzewski, S. Dapprich, A. D. Daniels, M. C. Strain, O. Farkas, D. K. Malick, A. D. Rabuck, K. Raghavachari, J. B. Foresman, J. V. Ortiz, Q. Cui, A. G. Baboul, S. Clifford, J. Cioslowski, B. B. Stefanov, G. Liu, A. Liashenko, P. Piskorz, I. Komaromi, R. L. Martin, D. J. Fox, T. Keith, M. A. Al-Laham, C. Y. Peng, A. Nanayakkara, M. Challacombe, P. M. W. Gill, B. Johnson, W. Chen, M. W. Wong, C. Gonzalez, J. A. Pople, Gaussian 03 ed., Gaussian, Inc., Wallingford CT, **2003**.
- [31] X. Guo, S. Wang, V. Enkelmann, M. Baumgarten, K. Müllen, *Organic Letters* **2011**, 13, 6062–6065.
- [32] A. Mukherjee, K. Pati, R. S. Liu, *Journal of Organic Chemistry* **2009**, 74, 6311–6314.
- [33] D. D. Bao, B. Millare, W. Xia, B. G. Steyer, A. A. Gerasimenko, A. Ferreira, A. Contreras, V. I. Vullev, *Journal of Physical Chemistry A* **2009**, 113, 1259–1267.
- [34] J. D. Tovar, T. M. Swager, *Advanced Materials* **2001**, 13, 1775–1780.

- [35] A. Facchetti, M. H. Yoon, T. J. Marks, *Advanced Materials* **2005**, *17*, 1705-1725.
- [36] D. R. Lide, *CRC handbook of chemistry and physics: a ready-reference book of chemical and physical data*, CRC Press, **2006**.
- [37] M. M. Payne, S. R. Parkin, J. E. Anthony, C. C. Kuo, T. N. Jackson, *Journal of the American Chemical Society* **2005**, *127*, 4986-4987.
- [38] T. Yamamoto, K. Takimiya, *Journal of the American Chemical Society* **2007**, *129*, 2224-+.
- [39] K. Takimiya, S. Shinamura, I. Osaka, E. Miyazaki, *Advanced Materials* **2011**, *23*, 4347-4370.
- [40] J. E. Anthony, B. Purushothaman, *Organic Field-Effect Transistors Vi* **2007**, 6658, L6580-L6580.
- [41] M. H. Yoon, C. Kim, A. Facchetti, T. J. Marks, *Journal of the American Chemical Society* **2006**, *128*, 12851-12869.

6 Hexaaryl[*a,c,fg,j,l,op*]tetracenes

6.1 Introduction

The interest in non-planar polycyclic aromatic hydrocarbons among theoreticians, physicists and chemists exists longer than the discovery of fullerenes and carbon nanotubes.^[1] Nevertheless, cyclophanes and bowl shaped molecules have attracted particular attention as cut outs of carbon nanotubes in recent years, mimicking the uniquely bent shape and hemispheres at the ends.^[2-4] Being a great challenge in organic synthesis, strong arguments are needed to convince PAHs to leave their low-energy conformation. Chemists have therefore developed a number of strategies, wet-chemically and pyrolytically.^[5] For instance, corannulene **I6-1** can be obtained from 7,10-divinylfluoranthene derivatives *via* flash vacuum pyrolysis (FVP), which requires temperatures above 1000 °C.^[3] Prominent examples for a wet-chemical approach are cyclophanes and molecule **I6-2** in Figure 6-1 reported by Bertozzi et al.^[6] and Bodwell et al.^[7], respectively, whose syntheses started from cyclic precursors containing sp³-hybridized carbon junction which are aromatized in the last step to build up the strain within the hydrocarbon entities.

Not endangering the world record for non-planar molecules, many pyrene derivatives have been reported in the last years that are twisted and/or bent in

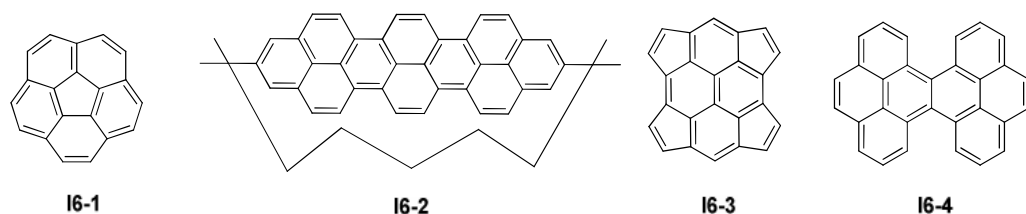


Figure 6-1: Examples of non-planar molecules.

various ways. Whereas fourfold pentannulation of pyrene leads to bowl shaped cyclopentapyrenes **I6-3**^[8-10], tetrabenzo[*de,hi,mn,qr*]tetracene **I6-4**^[11-12] exhibits a twist of the tetracene moiety. The molecular distortion is triggered by two different effects: (1) introduction of five-membered rings that have to go out of plane to retain proper bond length (compare **I6-3**); (2) overcrowding of hydrogen in *cove* regions (compare **I6-4**).^[13-14]

As described in the previous chapter, the overcrowding of one hydrogen and one of sulfurs lone pairs in a *cove* drives the dithienobenzo[*e*]pyrenes out of a planar conformation. The hydrocarbon case can be simplified to accumulation of four [4]helicene structure motifs.^[15] Among the homologous series of helicenes and its hetero analogous, helical chirality and its stability have synthetically^[16-18] and theoretically^[19] been explored. A crucial value for the conformational stability is the activation enthalpy for the racemization process (also reported as racemization barrier) which is mainly dependent on the number of angularly annulated benzene rings and the steric demand of substituents in the curve.

For the series of unsubstituted [4]helicene to [6]helicene increasing values^[19] of 3.5 kcal/mol, 22.7 kcal/mol and 35.2 kcal/mol have been calculated. Introduction of a methyl group and a fluorine atom into the *cove* of [4]helicene led to an experimentally determinable racemization barrier of 31.3 kcal/mol and yielded stable conformers at room temperature.^[20] The list of *cove*-substituted [4]helicenes is long and multi-step syntheses of enantiopure products are reported.^[21-22] However, the single chlorine substituted *cove* motif has often been used as precursor for the syntheses of non-planar PAHs applying flash vacuum pyrolysis.^[23-26]

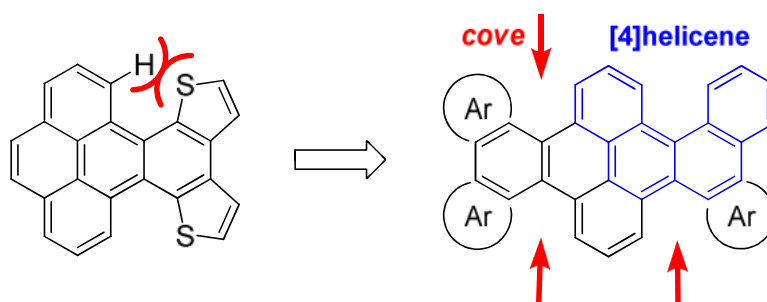


Figure 6-2: Schematic depiction of the design from a two cove (left) to a four cove scaffold; [4]helicene moiety highlighted in blue.

In this context, the accumulation of four *coves* should synthetically be realized in one molecule using pyrene as a core structure (see Figure 6-2).^[27] The investigation of the curvature might open new ways for molecular engineering and is of importance as the three-dimensional shape of molecules is closely related to the properties. The outer aryl rings could either be thiophene or benzene ring. First attempts were focused on thiophene moieties as the ring-closure has already been realized at one side.^[28] However, higher distortion can be expected for benzene rings and was targeted in a second part.

6.2 Synthesis

Retrosynthetic considerations on the synthesis of hexaaryl[*a,c,fg,j,l,op*]-tetracenes (HATs) led to the need of a 4,5,9,10-tetafunctionalized pyrene precursor (Figure 6-3). In contrast to already reported inconvenient five-step synthesis of 4,5,9,10-tetraphenylpyrene^[29] the aryl groups should be attached *via* palladium-catalyzed cross-coupling reactions.

A well-established method for addressing pyrene's K-region is the bromination of 2,7-di-*tert*-butylpyrene **I-19** to **I-24** using Br₂ in the presence of iron. Unfortunately, the *tert*-butyl groups are synthetically required (Scheme 6.1).^[30] With respect to the high impact of such bulky groups on the crystal

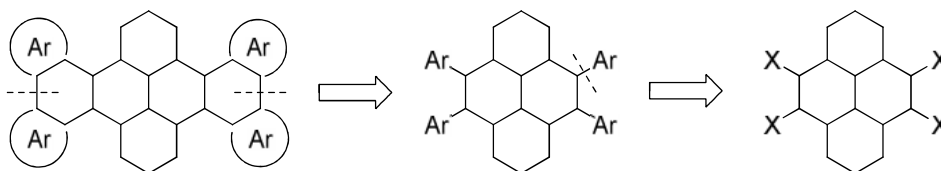
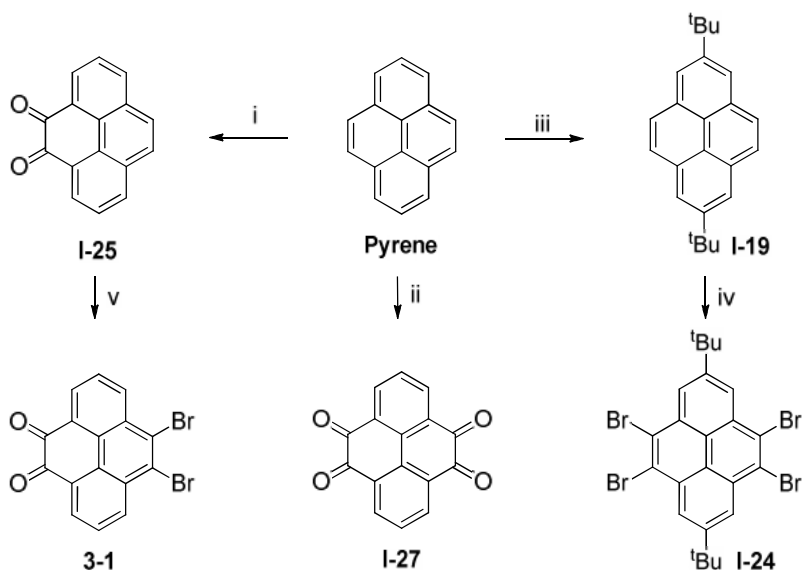


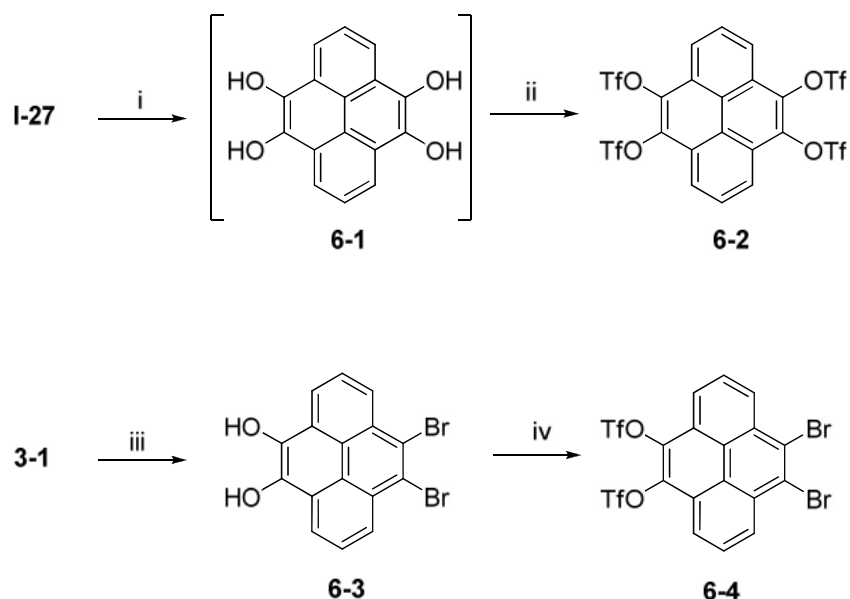
Figure 6-3: Retrosynthesis of a fourfold cove structure. Ar: thiophene or benzene; X: halogen or halogen analog for palladium-catalyzed cross-coupling reactions.



Scheme 6.1: Synthesis of 4, 5, 9, 10 tetrafold functionalized pyrene derivatives **3-1**, **I-27** and **I-24**; Conditions: *i* RuCl_3 , 4.7 eq. NaIO_4 , H_2O /DCM/ MeCN, RT, overnight, 45 % (lit.^[31]); *ii* RuCl_3 , 8.2 eq. NaIO_4 , H_2O /DCM/ MeCN, 40 °C, overnight, 36 % (lit.^[31]); *iii* $t\text{BuCl}$, AlCl_3 , RT, overnight, 61 % (lit.^[30]); *iv* Br_2 , Fe, CCl_4 , RT, 4 h, 79 % (lit.^[32]); *v* 2 eq. NBS, conc. H_2SO_4 , 4 h, quantitative.

packing, the syntheses of HATs should be started preferentially from unsubstituted pyrene. Thus, the already introduced ruthenium-catalyzed oxidation yielding pyrene-4,5-dione **I-25** and pyrene-4,5,9,10-tetraone **I-27** played a key role in the synthesis described here.^[31]

Triflates can be used in palladium-catalyzed cross-coupling reactions like Suzuki and Stille coupling.^[33-36] Therefore, the conversion of ketones **I-27** and **3-1** (obtained after bromination with NBS) to the corresponding triflates were



Scheme 6.2: Synthesis of 4, 5, 9 and 10 tetrafold halogen and triflate functionalized pyrenes **6-2** and **6-4**. Conditions: *i* H₂, Pd-C, THF, 2 h; *ii* Tf₂O, pyridine, THF, -78°C, overnight; 5 % (for two steps); *iii* Na₂S₂O₄, THF/ H₂O, RT, 4 h, 82 %; *iv* Tf₂O, pyridine, THF, -78°C, overnight; 23 %.

chosen to provide a promising access to fourfold aryl-aryl coupling at these positions. At first, **I-27** was treated with an aqueous solution of sodium dithionite but isolation of **6-1** did not succeed as the tetraol seems to be instable in the presence of oxygen and the absence of Na₂S₂O₄. Thus, a water free reduction was needed because the following quenching with trifluoromethanesulfonic anhydride (Tf₂O) requires anhydrous conditions (Scheme 6.2). Palladium on carbon with hydrogen atmosphere in anhydrous THF followed by the addition of Tf₂O/pyridine at -78 °C finally gave tetratriflatopyrene **6-2** in 5 % yield.

Varying temperature, reaction time and concentration showed no increase of the yield although the formation of triflates from aromatic alcohols is well established and described in high yields. Obviously, the intermediate **6-3** is more stable than tetraol **6-1**. Reports on the reduction of halogenated phenanthrene-9,10-dione describe easy handling and yields above 90 % for the corresponding phenanthrene-9,10-diol.^[37-38]

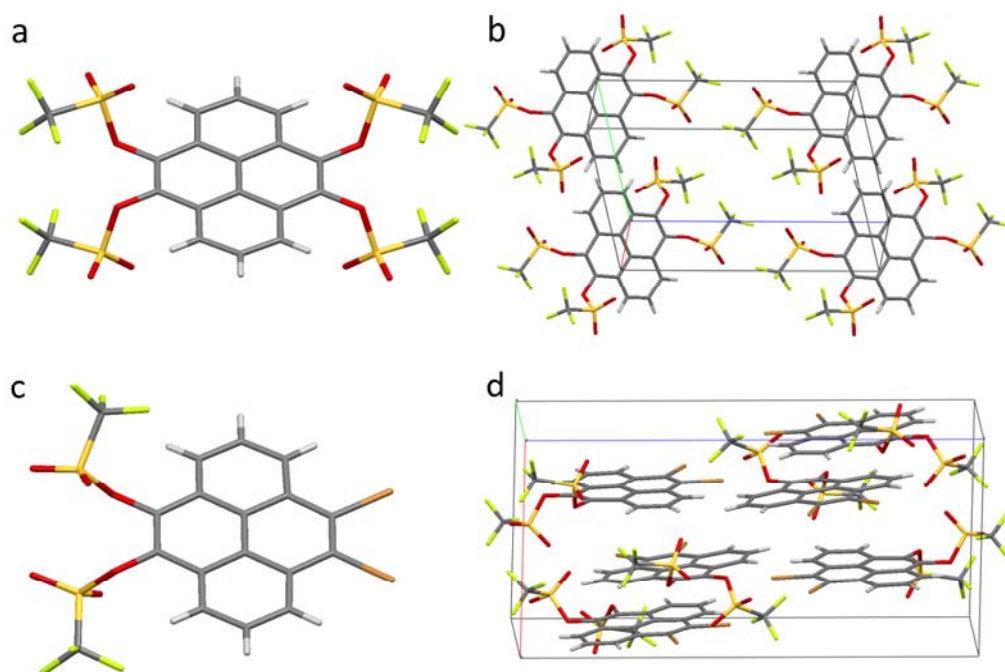
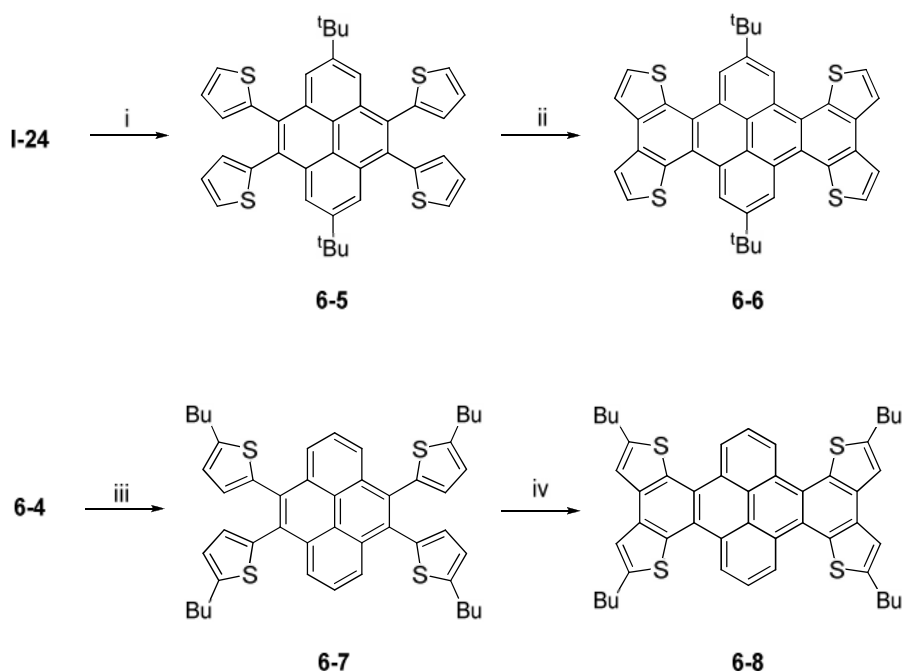


Figure 6-4: Crystal structure of 4,5,9,10-tetratriflatopyrene **6-2** (**a** front view, **b** unit cell) and 4,5-dibromo-9,10-ditriflatopyrene **6-4** (**c** front view, **d** unit cell).

Likewise phenanthrene, 9,10-dibromopyrene-4,5-diol **6-3** could be isolated simply by extraction from the reaction mixture on air after reduction with aqueous $\text{Na}_2\text{S}_2\text{O}_4$ solution. The complete reduction of the diketone was proven in ^1H -NMR experiments by the exchange of the alcohol proton to deuterium after D_2O addition. **6-3** was further treated with Tf_2O to give **6-4** in 23 % and the reaction was scaled up to 7 g batches providing sufficient amounts of 4,5-dibromo-9,10-ditriflatopyrene. The structure of **6-2** and **6-4** could be confirmed by single crystal X-ray analysis (Figure 6-4).

The availability of **I-24** and **6-4** in considerable amounts provided the basis for HATs with and without *tert*-butyl groups. Both substitution patterns with alkyl chains were targeted because most likely the crystal packing and the three-dimensional shape strongly differ due to the bulkiness of the side group.

The synthesis and characterization of dibenzo[*fg,op*]tetrathieno[*a,c,j,l*]-tetracenes (DBTTTs) and hexabenzo[*a,c,fg,j,l,op*]tetracenes (HBTs) will be addressed separately followed by a detailed study and comparison of the spatial shape of DBTTTs and HBTs in subchapter 6.3.



Scheme 6.3: Synthesis of hexaaryl[*a,c,fg,j,l,op*]tetracenes **6-6** and **6-8**. Conditions: *i* 2-Tributylstannylthiophene, Pd(PPh₃)₄, toluene, reflux, overnight, 48 %; *ii* I₂, *hν* at 300 nm, toluene, overnight, 60 %; *iii* tributyl(5-butyl-2-thienyl)-stannane, Pd(PPh₃)₄, toluene, reflux, overnight, 42 %; *iv* 4.5 eq. FeCl₃, MeNO₂, DCM, RT, 30 min, 17 %.

6.2.1 Dibenzo[*fg,op*]tetrathieno[*a,c,j,l*]tetracenes

At first the syntheses of DBTTTs were targeted. In order to introduce four thienyl units to the K-region fourfold Stille coupling was performed between pyrene derivatives **I-24** and **6-4** and tin organyls tributylstannylthiophene and tributyl(5-butyl-2-thienyl)-stannane (Scheme 6.3). Yields of 42 % and 48 %, respectively, were obtained which is reasonable for a fourfold Stille reaction.

Crystallization of **6-7** from THF afforded single crystals suitable for X-ray crystallography and the crystal structure is depicted in Figure 6-5. Similar to dithienylpyrenes, the thienyl rings of **6-7** are twisted out of the pyrenyl plane and the stacks are laterally shifted, whereas the thienyl moieties are located in between pyrenes.

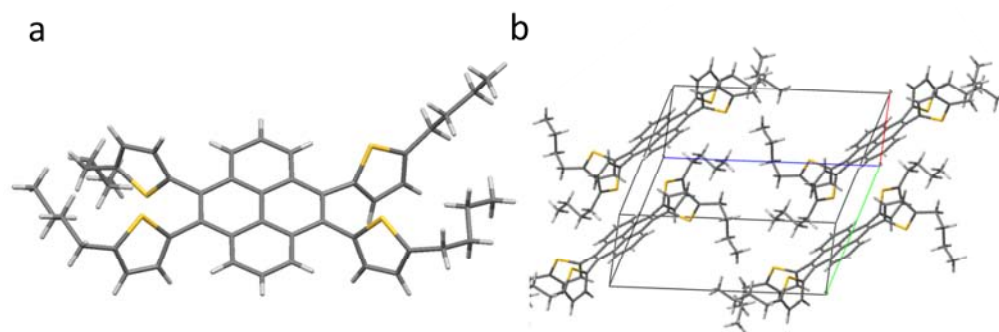


Figure 6-5: Crystal structure of 4,5,9,10-tetrakis-(5-*n*-butylthien-2-yl)pyrene **6-7** (a front view, b unit cell).

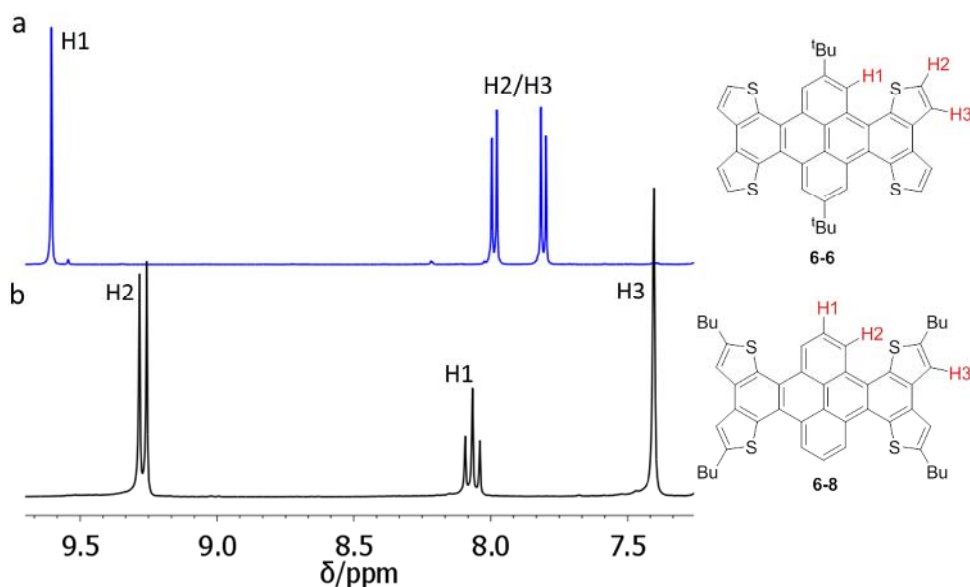


Figure 6-6: ^1H NMR spectra (300 MHz, RT) of (a) **6-6** and (b) **6-8a** in deuterated chloroform.

Subsequent ring closure to the DBTTT **6-8** was achieved by treatment with iron(III)chloride, which is commonly applied in cyclodehydrogenation reactions.^[39-41] Assumably, the low yield of 17 % was most likely caused by the side reactions of the β -thienyl position with pyrene active sites 1, 3, 6 and 8. However, in case of **6-5** iron(III)chloride could not be used. The free α -positions of the thienyl rings are known to undergo oligomerization and polymerization, respectively. Instead, irradiation of **6-5** in the presence of iodine as oxidant yielded 8,17-di-*tert*-butyl-dibenzo[*fg,op*]tetrathieno[*a,c,j,l*]-tetracene **6-6** via light induced cyclization reaction in 60 % yield.^[42] The proton NMR spectra of the aromatic region in Figure 6-6 show the expected pattern for DBTTTs **6-6** and **6-8**.

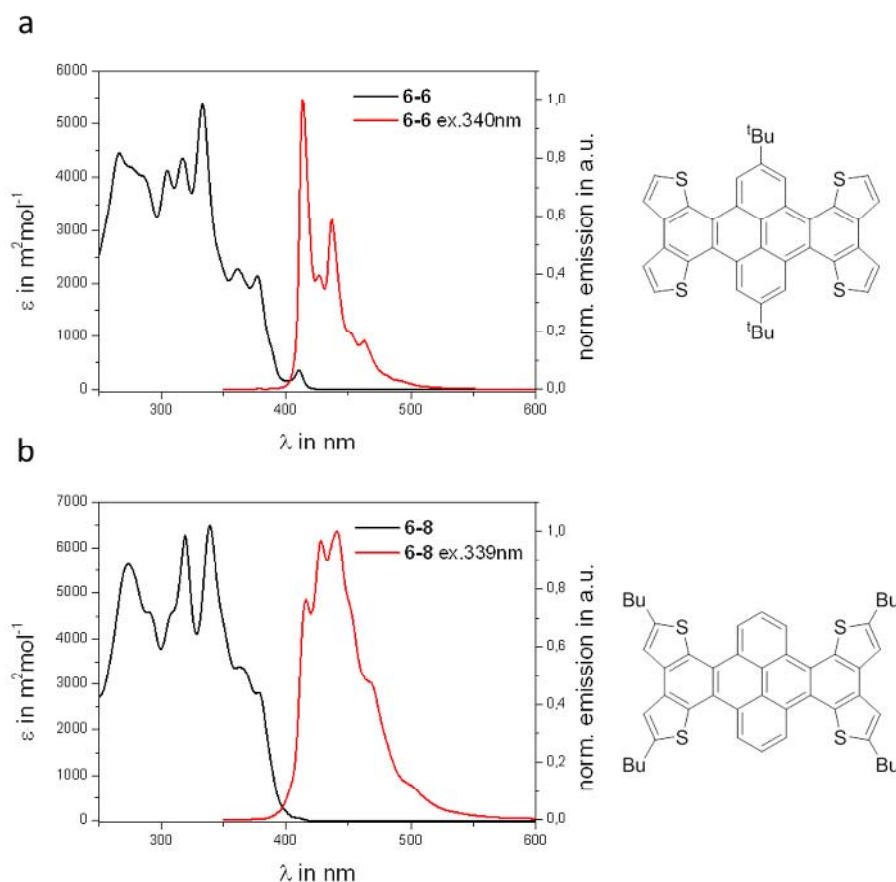


Figure 6-7: UV/vis absorption and emission spectra of dibenzo[*fg,op*]tetrathieno[*a,c,j,l*]-tetracenes **6-6** (a) and **6-8** (b) in THF at 10^{-5} M concentration.

6.2.1.1 Optical and Electronic Properties

The absorption and emission spectra of **6-6** and **6-8** are depicted in Figure 6-7 and the values are listed in Table 6.1. The absorption and emission spectra of **6-6** and **6-8** reveal fine splitting of the bands due to a rigid molecular structure after ring-closure.^[28, 41] Judging by the onset, a decrease of the $E_{g(opt)}$ by 0.11 eV (**6-5**→**6-6**) and 0.07 eV (**6-7**→**6-8**) could be observed due to the extension of the π -conjugated system as result of the ring-closure. This trend fits to the observation from dithieno[*e*]benzopyrenes discussed in the previous chapter. In comparison to the transition of the energy gap from naphthalene to tetracene,

Table 6.1: Optical and electronic properties of compounds **6-5**, **6-6**, **6-7** and **6-8**.^[a]

| | λ_{abs} ^[b] | λ_{em} ^[c] (λ_{ex}) ^[d] | λ_{edge} | $E_{\text{g(opt)}}$ ^[e] | $E_{\text{HOMO(CV)}}$ ^[f] |
|------------|---------------------------------------|---|-------------------------|------------------------------------|--------------------------------------|
| 6-5 | 361 nm | 396 nm (350 nm) | 383 nm | 3.24 eV | -5.56 eV |
| 6-6 | 377 nm | 413 nm (340 nm) | 396 nm | 3.13 eV | -5.54 eV |
| 6-7 | 359 nm | 435 nm (358 nm) | 389 nm | 3.19 eV | -5.53 eV |
| 6-8 | 378 nm | 416 nm (339 nm) | 397 nm | 3.12 eV | -5.34 eV |

[a] All absorption and emission spectra were measured in THF. [b] λ_{abs} is the absorption band appearing at the longest wavelength. [c] λ_{em} is the fluorescence band appearing at the shortest wavelength. [d] λ_{ex} wavelength of excitation. [e] Calculated from λ_{edge} [f] CV measured in 0.1 M n-Bu₄NPF₆/DCM with a scan rate of 100 mV/s; values calculated using the ferrocene HOMO level: $E_{\text{HOMO(CV)}} = -(E_{\text{ox,onset}} - E_{\text{Fc/Fc}^+}^{(1/2)} + 4.8)$ eV.

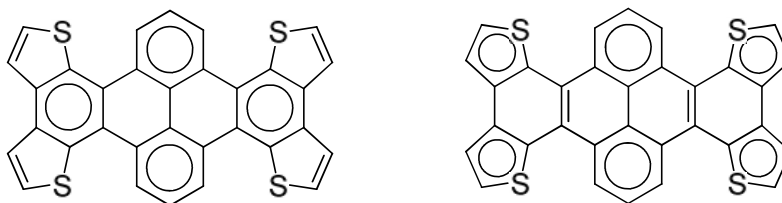


Figure 6-8: Depiction of resonance structures of dibenzo[*fg,op*]tetrathieno[*a,c,j,l*]tetracene core structure according to Clar's suggestion of four (left) and six (right) electron sextets. The formally incorrect use of double bonds together with Clar sextets is made to indicate the stability arising from the dibenzo[*e,l*]pyrene and that no acene like conjugation is present.

only a small change occurred in this system.^[43] According to Clar's sextet rule the resonance structure with the highest number of separated aromatic π -sextets is the most important for the properties, and thus, acene like delocalization of π -electrons obviously could not be found for DBTTTs **6-6** and **6-8** (Figure 6-8). It shall be mentioned here that terming compounds **6-6** and **6-8** "tetracenes" is due to IUPAC nomenclature and is not correlated to the properties of tetracene.

CV revealed only small changes in HOMO levels for *tert*-butylated species **6-5** and **6-6** (Figure 6-9). In contrast, a rise of the HOMO was observed from **6-7** to **6-8** by 0.19 eV. This destabilization can be attributed to the pronounced impact of the inductive effect of linear butyl chains being directly attached to

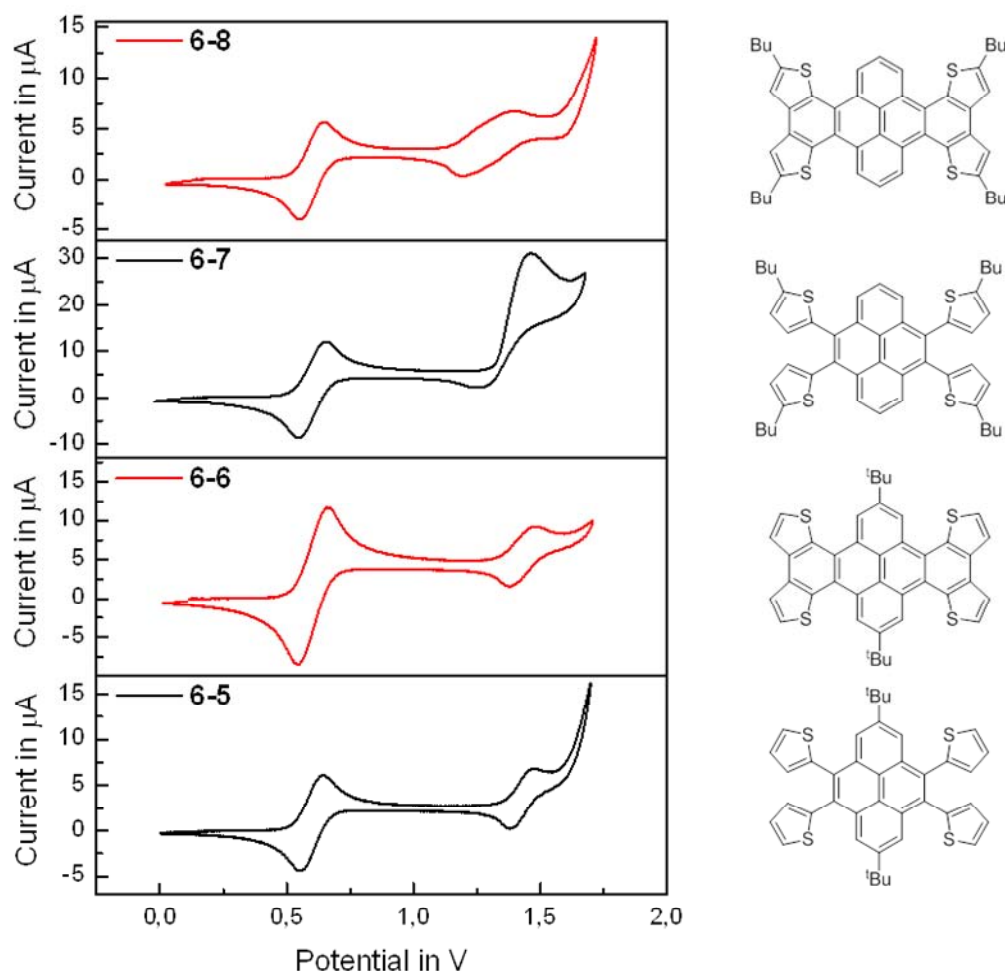
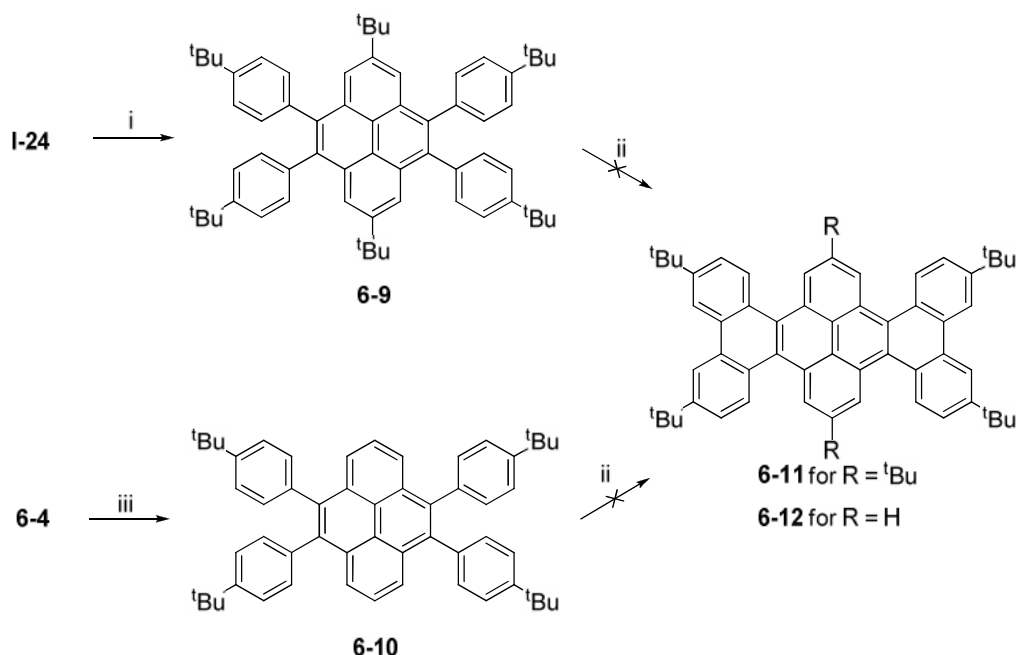


Figure 6-9: Cyclic voltammograms of **6-5**, **6-6**, **6-7** and **6-8** are recorded at scan rate of 100 mV/s. Ferrocene oxidation and reduction wave is set to half-wave potential of 0.6 V.

flattened core and has also been found for thiophene-alkylated dithienobenzo[*e*]pyrene **5-5**. The oxidation process of **6-5** and **6-6** seems to be reversible despite free α -positions on thienyl and thieno moieties, respectively, which is known to allow electropolymerization.^[41]

In contrast, **6-7** shows an irreversible oxidation wave. In case of **6-8**, the broadening of the wave indicates two oxidation processes taking place close behind one other. No reduction of compounds **6-5** to **6-8** could be observed under the measurement conditions.

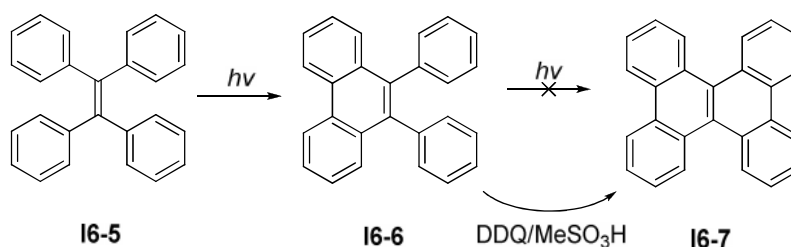


Scheme 6.4: Synthesis of hexabenzo[*a,c,fg,j,l,op*]tetracenes **6-11** and **6-12**. Conditions: *i* 4-*tert*-butylphenylbromic acid, Pd(PPh₃)₄, Na₂CO₃, toluene/ water, reflux, 4d, 64 %, *ii* 10 eq. FeCl₃, MeNO₂, DCM, RT, 30 min to overnight, *iii* 4-*tert*-butylphenylbromic acid, Pd(PPh₃)₄, Na₂CO₃, toluene/ water, reflux, overnight, 72 %.

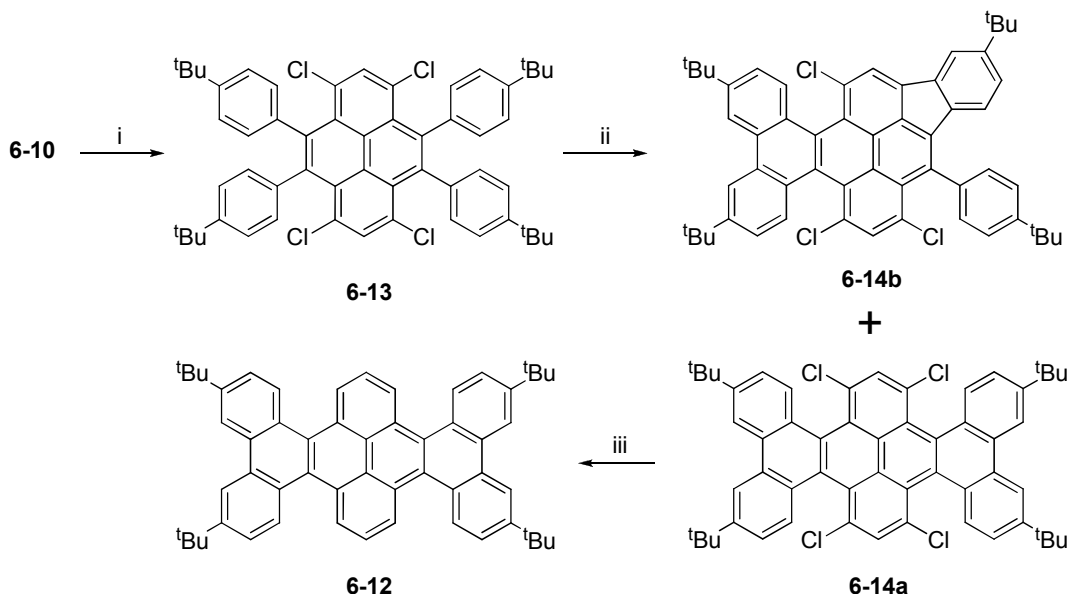
6.2.2 Hexabenzo[*a,c,fg,j,l,op*]tetracenes

In comparison to DBTTTs the use of benzene instead of thiophene units is believed to drastically enhance the distortion within HBTs due to the steric demand of the additional hydrogen atom in the *coves* (compare Figure 6-2 page 135). For the synthesis the versatile 4,5,9,10-tetrafunctionalized precursors **I-24** and **6-4** were used like for DBTTTs. As mentioned above, precursor **6-4** leaves space for introduction of substituents at pyrene positions 1, 3, 6 and 8 and therefore enhancement of the steric strain within the *cove*.

In place of Stille reaction for DBTTTs, Suzuki coupling with 4-*tert*-butylphenylbromic acid was applied. **6-9** and **6-10** were obtained in yield above 60 % (Scheme 6.4). It is noteworthy that both tetraarylpyrenes showed very low



Scheme 6.5: Synthesis of dibenzo[*g,p*]chrysene **16-7**.^[42, 44-46]



Scheme 6.6: Synthesis of highly bent structure **6-14**. Conditions *i* SO_2Cl_2 , AcOH, CHCl_3 , 65 %, *ii* 10 eq. FeCl_3 , MeNO_2 , DCM, RT, 50 min, 32 %; *iii* Bu_3SnH , AIBN, toluene, 100 °C, overnight.

solubility in DCM and THF although *tert*-butyl side groups are known for their distinct solubilizing effect. Thus, characterization by NMR spectroscopy had to be carried out in tetrachloroethane at elevated temperature.

The oxidative ring-closure between peripheral phenyl rings turned out to be challenging. Linking the *ortho*-phenyls of 9,10-diphenylphenanthrene **16-6** has been described not to proceed photochemically upon irradiation (Scheme 6.5).^[42, 44-45] Whereas tetraphenylethylene **16-5** gives 9,10-diphenylphenanthrene **16-6**, the reaction stops before the second oxidative cyclization to dibenzo[*g,p*]chrysene **16-7**. It is argued that the electronic distribution in the excited state exhibits low electron availability at the carbon atoms which are

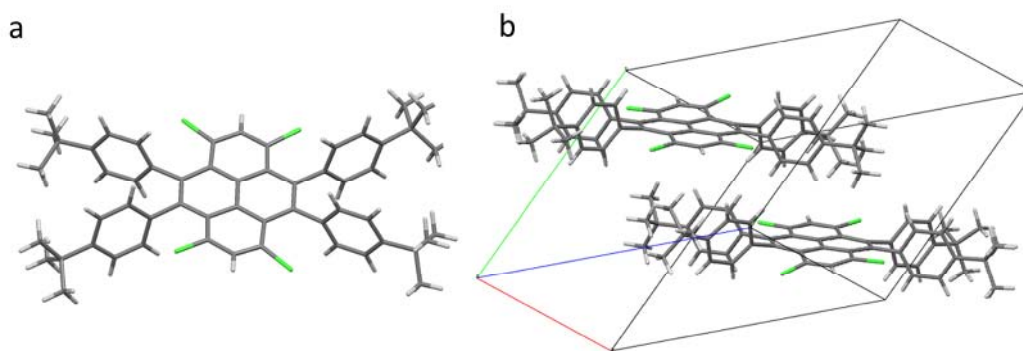


Figure 6-10: Crystal structure of 4,5,9,10-tetrakis(4-*tert*-butylphenyl)-1,3,6,8-tetrachloropyrene **6-13** (a front view, b unit cell).

responsible for the formation of the new bond.^[45] Accordingly, often utilized iron(III)chloride for the so called *Scholl* reaction was used but neither **6-11** nor **6-12** could be obtained.

Recently, DDQ/ MeSO₃H has been reported as new oxidation system for the synthesis of dibenzo[*g,p*]chrysene **I6-7** (14 % yield for the last step).^[46] Unfortunately, treatment of **6-10** under these conditions resulted in a complex mixture of compounds. Besides formation of five-membered rings with pyrenes active positions 1, 3, 6 and 8, aryl migration could possibly occur.^[47-48] To exclude side reactions with pyrene positions 1, 3, 6 and 8, a method to selectively block these sites was needed.

Therefore, **6-10** was treated with bromine but the unwanted bromination of the phenyl rings was observed. Going for milder conditions, sulfuryl chloride exclusively chlorinated sites 1, 3, 6 and 8 at room temperature to give **6-13** as yellow and well soluble solid (Scheme 6.6). The selectivity of this key reaction was proven by proton NMR spectroscopy and X-ray crystal analysis (Figure 6-10).

In the next step, cyclodehydrogenation with iron(III)chloride was applied. Target compound **6-14a** was obtained in 32 % yield, but additionally byproduct **6-14b** was formed in 46 %. The structure of **6-14b** was identified by mass spectrometry, ¹H and ¹³C one-dimensional and two-dimensional proton correlation NMR spectroscopy.

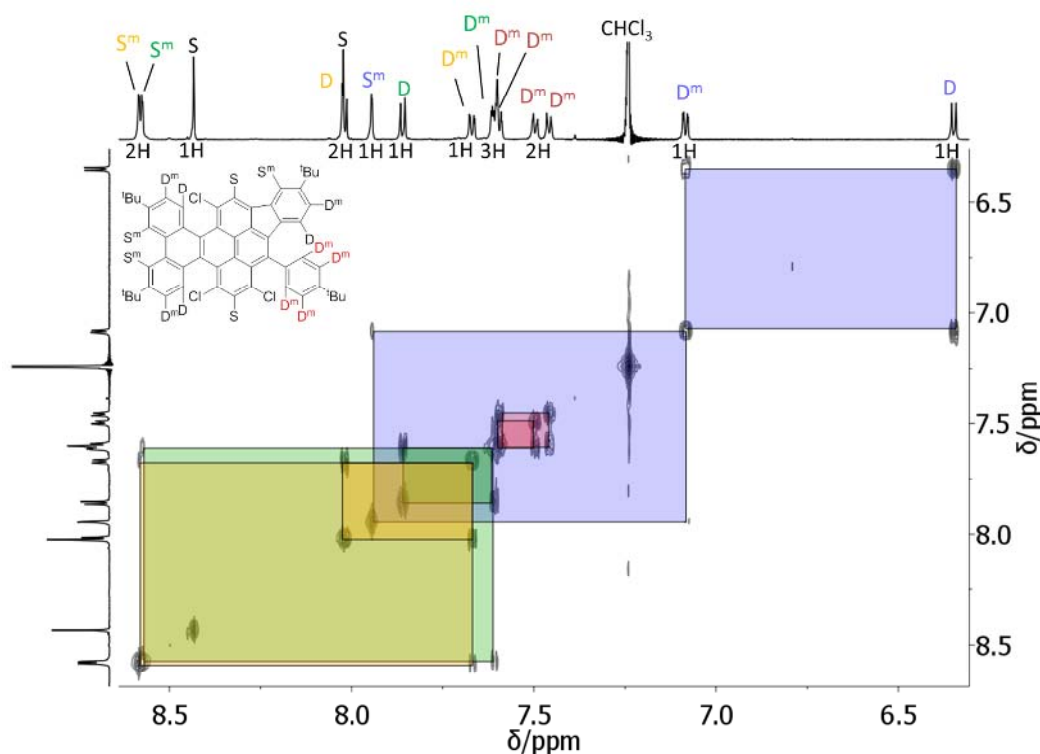


Figure 6-11: Two-dimensional proton correlation NMR spectroscopy (^1H , ^1H COSY) of side product **6-14b** in chloroform (700 MHz, RT): Three signal groups each consisting of S^m , D^m and D (yellow, green and blue), four D^m (red) of the rotatable phenyl ring and two singlet. S: singlet, D: doublet, m : with meta coupling.

As shown in Figure 6-11, three independent groups of cross-coupling signals (yellow, green and blue) consisting of one meta-coupling singlet, one meta-coupling doublet and one doublet (S^m , D^m and D) match with three phenyl ring that underwent cyclodehydrogenation. Furthermore, the two pyrene singlets give signals at 8.02 ppm and 8.43 ppm. The signals of the rotatable phenyl ring partially overlap, being part of an AA'BB' system.

To obtain the pure hydrocarbon, removal of chlorine atoms could be accomplished only in analytical scale by reductive dehalogenation reaction using tributyltin hydride in the presence of the radical initiator AIBN (Scheme 6.6 page 145). **6-12** was verified by proton NMR spectroscopy and high resolution ESI MS but suitable amounts for carbon NMR spectroscopy or crystal growth could not be isolated. Anyhow, due to the four times larger

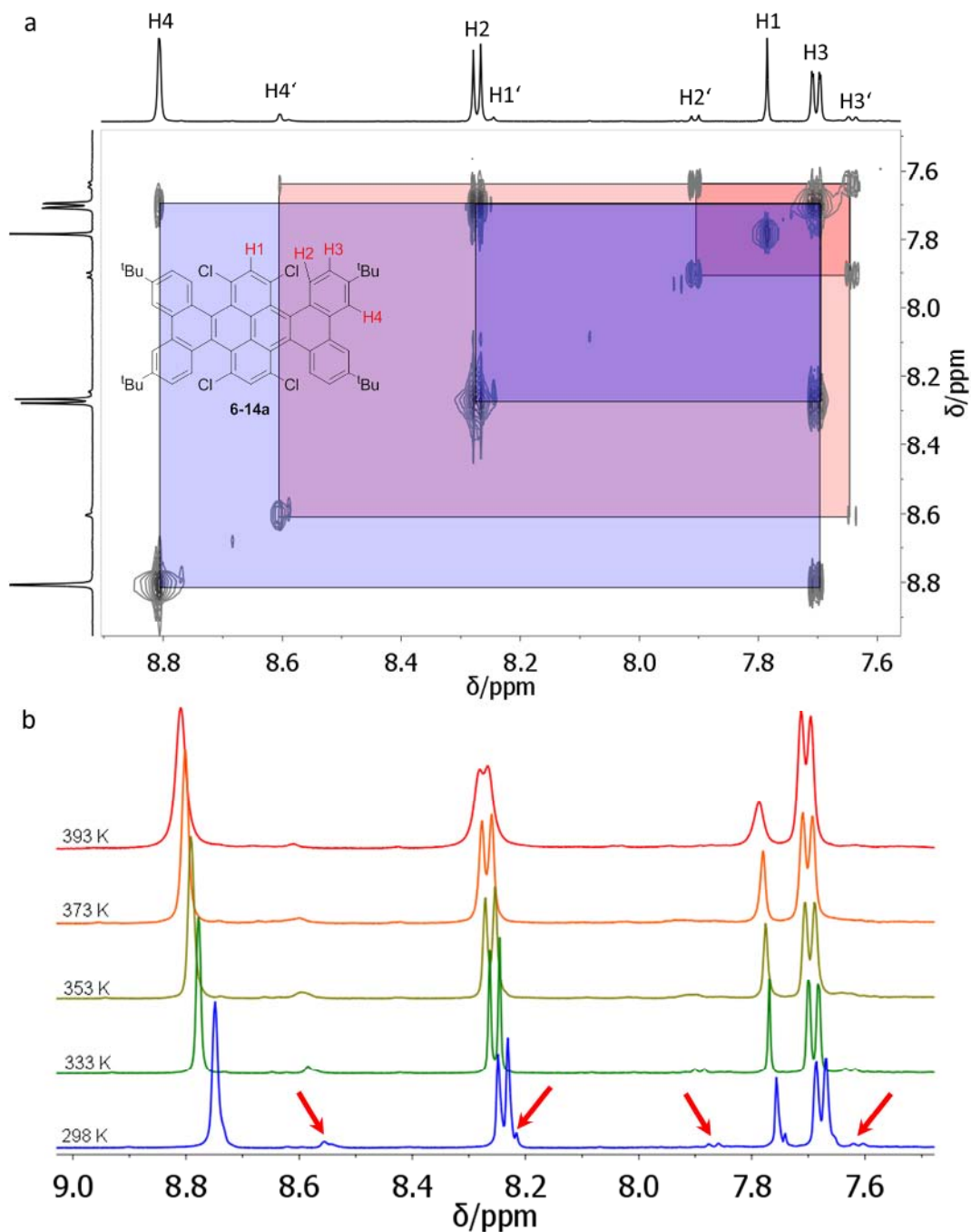


Figure 6-12: NMR spectroscopic investigation of **6-14a**; (a) Two-dimensional proton correlation NMR spectrum (^1H , ^1H COSY) at 298 K (700 MHz); major conformer: blue boxes; minor conformer: red boxes (b) Temperature dependent proton NMR spectroscopy from 298 K to 393 K in deuterated 1,1,2,2-tetrachloroethane (500 MHz).

atomic radius^[49] of chlorine atoms (1.00 Å) compared to hydrogen (0.25 Å), the four chlorine atoms in the *coves* cause additional strain compared to **6-12** and therefore **6-14a** is certainly valuable for this study.

In contrast to the DBTTTs (compare Figure 6-6 page 140), proton NMR spectroscopy revealed conformational isomers in solution for **6-14a** in a ratio of 9:1 determined by integration (Figure 6-12). In order to prove conformational isomerism, two-dimensional correlated proton NMR spectroscopy (¹H,¹H COSY) was performed. The spectrum shows identical cross-signals for the minor and major species which strongly supports the coexistence of conformational isomers.

Upon heating gradually from 298 K to 393 K in C₂D₂Cl₄, coalescence of the signals of the minor and major isomer occurred (Figure 6-12 **b**). After cooling back to room temperature, the initial state of an isomeric mixture was recovered. In addition, NOESY experiments show chemical exchange peaks between protons H2 and H2' which supports the assumption of an equilibrium of conformers at room temperature.

6.2.2.1 Optical and Electronic Properties

Investigation of UV/vis absorption and emission of tetraphenylpyrenes **6-10** and **6-13** and HBT **6-14a** shows distinct influence upon the introduction of chlorine atoms and the ring-closure step (Figure 6-13). The optical energy gap calculated from the edge decreases by 0.33 eV upon chlorination and by another 0.22 eV as consequence of the cyclodehydrogenation. Likewise, the fluorescence maximum is shifted bathochromically by 46 nm and 35 nm, respectively. All data are summarized in Table 6.2 on page 150.

Cyclic voltammetry in DCM of **6-10**, **6-13** and **6-14a** shows no reduction wave under the measurement conditions, and thus, no direct information about the LUMO level could be obtained. Instead, going to higher potentials **6-10** was

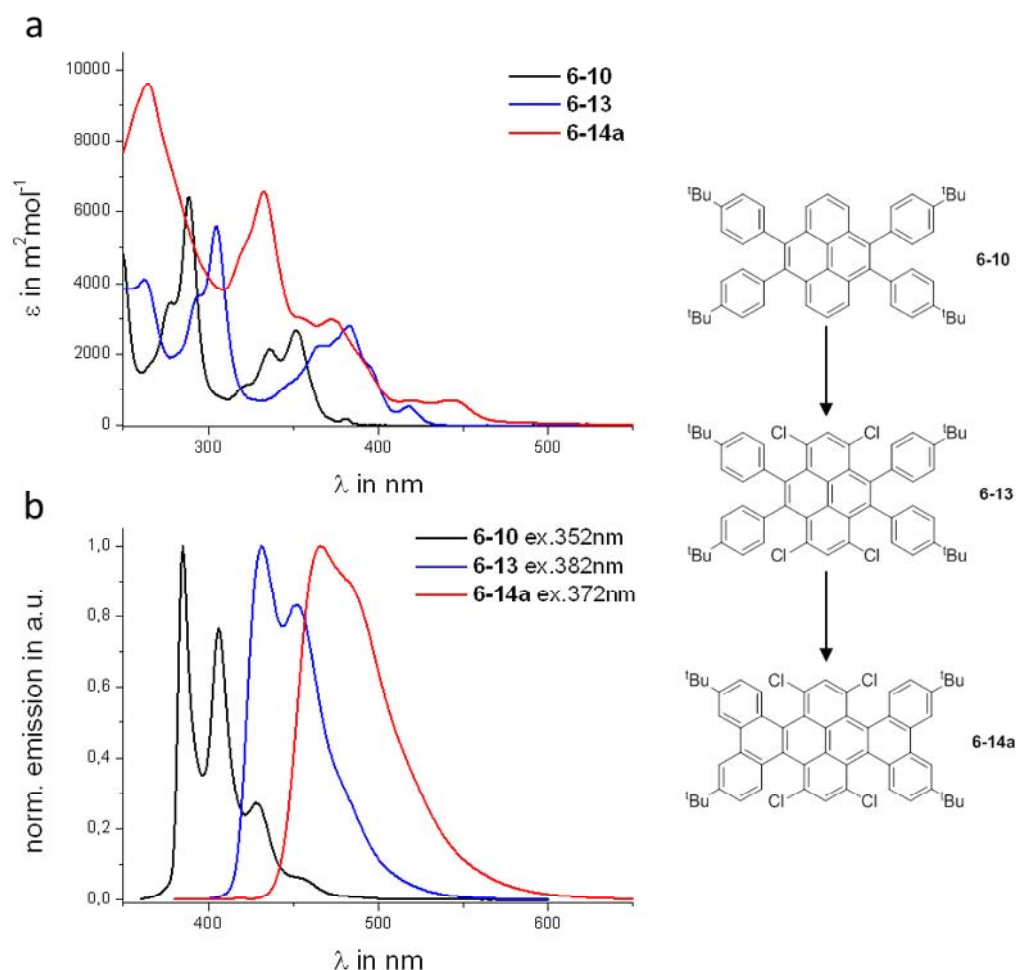


Figure 6-13: UV/vis absorption (a) and emission spectra (b) of tetraphenylpyrenes **6-10** (black) and **6-13** (blue) and hexabenzotetracene **6-14a** (red) in THF at 10^{-5} M concentration.

Table 6.2: Optical and electronic properties of compounds **6-10**, **6-13** and **6-14a**.^[a]

| | λ_{abs} ^[b] | λ_{em} ^[c] (λ_{ex}) ^[d] | λ_{edge} | $E_{\text{g(opt)}}$ ^[e] | $E_{\text{HOMO(CV)}}$ ^[f] |
|--------------|---------------------------------------|---|-------------------------|------------------------------------|--------------------------------------|
| 6-10 | 352 nm | 385 nm (352 nm) | 386 nm | 3.21 eV | - 5.51 eV |
| 6-13 | 383 nm | 431 nm (382 nm) | 430 nm | 2.88 eV | - 5.66 eV |
| 6-14a | 442 nm | 466 nm (372 nm) | 466 nm | 2.66 eV | - 5.68 eV |

[a] All absorption and emission spectra were measured in THF. [b] λ_{abs} is the absorption band appearing at the longest wavelength. [c] λ_{em} is the fluorescence band appearing at the shortest wavelength. [d] λ_{ex} wavelength of excitation. [e] Calculated from λ_{edge} [f] CV measured in 0.1 M n-Bu₄NPF₆/DCM with a scan rate of 25 mV/s; values calculated using the ferrocene HOMO level: $E_{\text{HOMO(CV)}} = - (E_{\text{ox,onset}} - E^{(1/2)}_{\text{Fc/Fc}^+} + 4.8) \text{ eV}$.

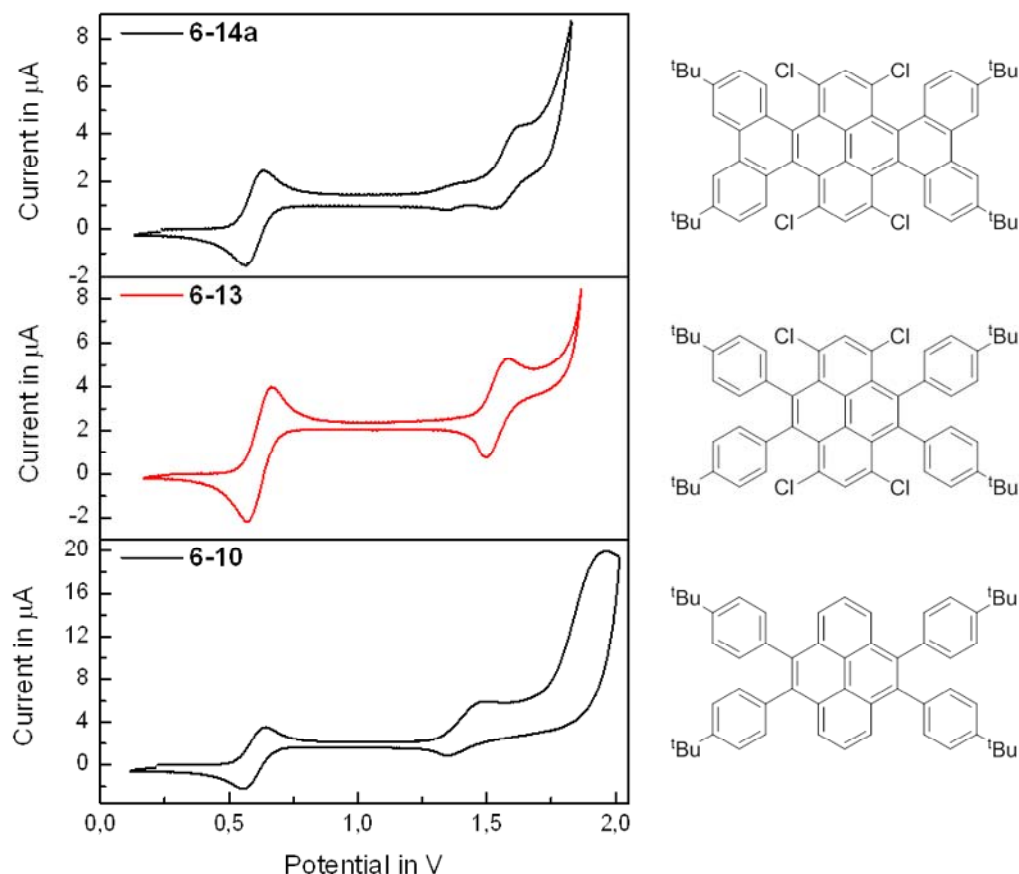


Figure 6-14: Cyclic voltammograms of **6-10**, **6-13** and **6-14a** are recorded at scan rate of 25 mV/s in dry DCM. Ferrocene oxidation and reduction wave is set to half-wave potential of 0.6 V.

oxidized at 1.31 V corresponding to a HOMO level at -5.51 eV. Oxidation of **6-13** and **6-14a** occurred at higher potentials of 1.46 V and 1.48 V. A very small wave could be observed prior to the major oxidation process of **6-14a** and was assigned to minor impurity of dehalogenated species of **6-14a** after the cyclization with FeCl_3 .

According to CV the HOMO is lowered by 0.15 eV upon chlorination. The following ring-closure (**6-13**→**6-14a**) merely influenced the HOMO level of **6-14a** by 0.02 eV which is within the error of the measurement. Keeping in mind the bathochromic shift of absorption and the decrease of the optical energy gap, mainly the energetic position of the LUMO is lowered by the ring-closure between the peripheral phenyl rings.

6.3 Crystal Structure Analysis

The coexistence of conformers of **6-14a** in solution revealed by proton NMR spectroscopy investigations in chapter 6.2.2 already points towards a different steric situation in the *cove* in comparison to DBTTTs. As described in the introduction of this chapter a non-planar shape can be expected for HATs due to the steric overcrowding.

In order to prove the approach of curved structures *via* four *coves*, crystals for X-ray analysis were grown from highly concentrated solutions of the respective compounds and the structures were solved for all target molecules **6-6**, **6-8** and **6-14a**. The front and side views are depicted in Figure 6-15, nicely showing the curved shape. All three molecules exhibit saddle shaped conformation consisting of an oppositely bent pyrene and tetracene moiety. For clear definition and comparison of structural data, nearly planar benzene rings A and B have been defined and used for determination of angles α and β which are listed in Table 6.3 (see Figure 6-15 **f**, **g** and **h**).

Rings A are tilted against each other by the angle α of 35.4° (**6-8**) and 36.0° (**6-6**), respectively. For rings B the angle β was measured as 26.2° (**6-8**) and 30.4° (**6-6**). The higher value of angle β for compound **6-6** is most likely due to the steric demand of the *tert*-butyl groups. **6-14a** shows by far the biggest angles within this series. Angle α is ~ 1.5 times and $\beta \sim 2$ times higher than for the DBTTTs **6-6** and **6-8**. The distortion is obviously governed by the protruding chlorine and hydrogen atoms into the *cove*.

Moreover, the C-C distances were determined. Within rings A and B the values range from 1.39 Å to 1.44 Å, whereas 1.46 Å to 1.47 Å was found for the bonds between rings A and B and 1.45 Å between B and B for all three compounds. These findings suggest enhanced single bond character for A-B and B-B bonds.^[50]

The crystal packing of **6-6**, **6-8** and **6-14a** is depicted in Figure 6-16. **6-6** and

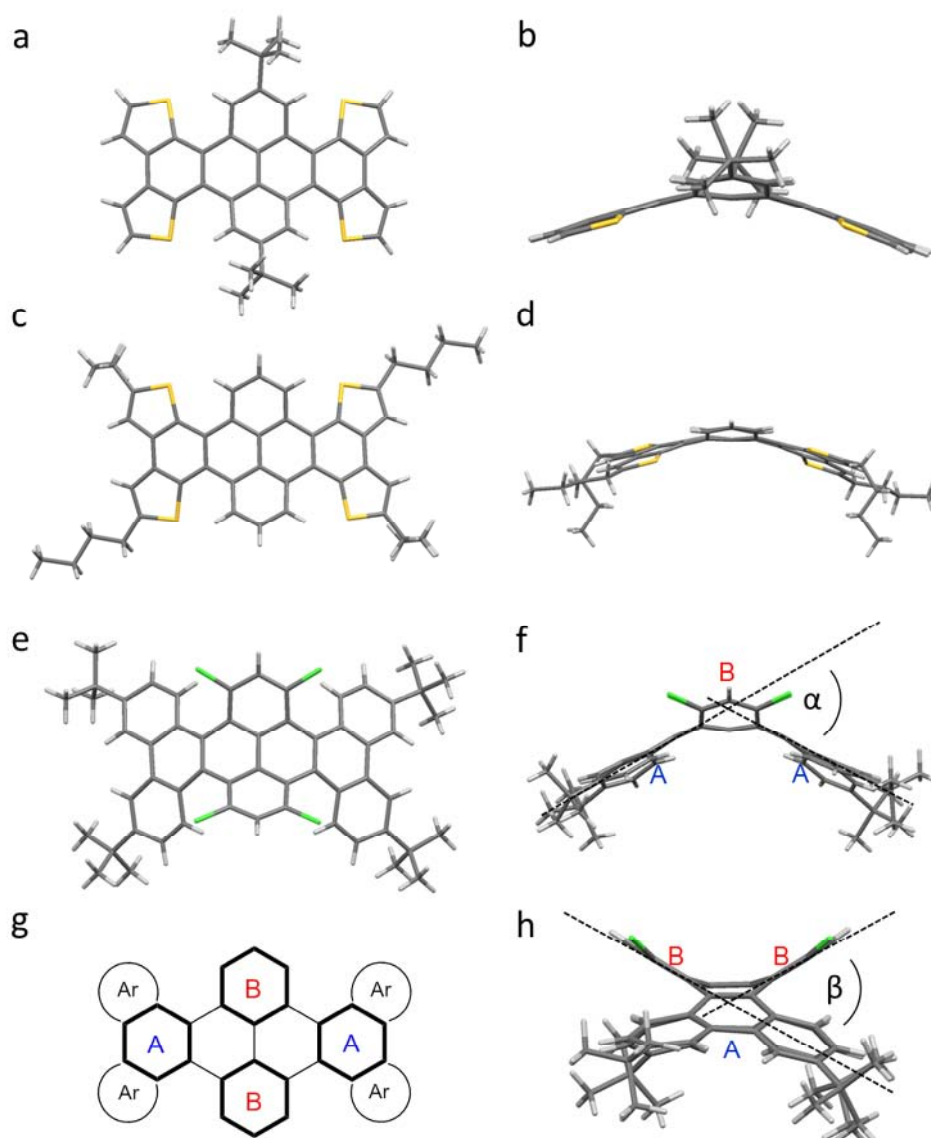


Figure 6-15: Crystal structures of distorted hexaaryl[*a,c,fg,j,l,op*]tetracenes **6-6** (a and b), **6-8** (c and d), **6-14a** (e, f and h); (g) Illustration of planar benzene rings A and B; used for calculation of curving angles α and β ; Two of four *n*-butyl of **6-8** and one *tert*-butyl side group of **6-14a** are disordered - for clarity, only the majority component is shown.

Table 6.3: Structural parameter of hexaaryl[*a,c,fg,j,l,op*]tetracenes **6-6**, **6-8** and **6-14a**.

| | angle α | angle β |
|--------------|----------------|---------------|
| 6-6 | 36.0 ° | 30.4 ° |
| 6-8 | 35.4 ° | 26.2 ° |
| 6-14a | 54.4 ° | 57.4 ° |

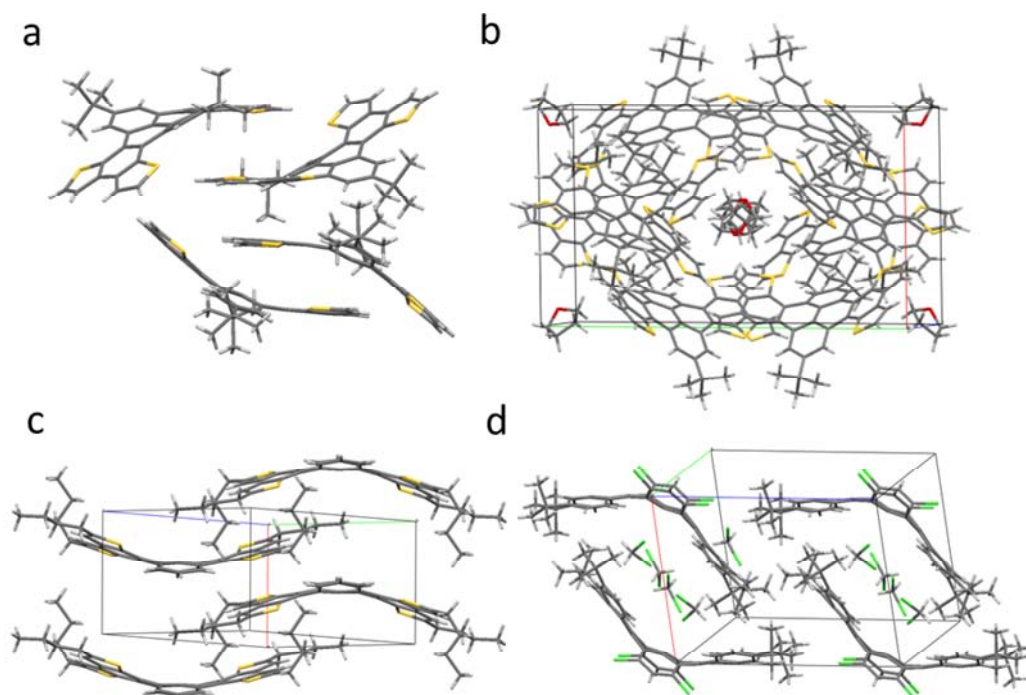


Figure 6-16: Crystal packing of hexaaryl[*a,c,fg,j,l,op*]tetracenes **6-6** (a and b), **6-8** (c) and **6-14a** (d); solvate molecules are THF for **6-6** and DCM for **6-14a**, respectively.

6-14a form solvates with THF and DCM, respectively. The arrangement of **6-6** in the crystal is dominated by the bulky side groups. Some benzodithiophene units of adjacent molecules π - π -interact with a distance of 3.3 Å but *tert*-butyl groups prohibit the formation of stacks. The packing is complex as eight molecules are located in the unit cell and are positioned around THF filled channels (Figure 6-16 b). Likewise **6-6**, π - π -stacking is absent for **6-14a**. Four solvate molecules of dichloromethane fill the cavity in between dimers of **6-14a**. Clearly, non-planarity and *tert*-butyl groups disfavor π - π -interaction in both cases and prevent commonly found motifs for PAHs like herringbone arrangement.^[51]

In contrast, a wavelike brick order was found for **6-8** in which the benzodithiophene units are located above each other with an A-A' ring distance of 3.45 Å to 3.75 Å.^[27] Flexibility of *n*-butyl chains enable this overlap by their alternate conformation from angled to all-*trans*. No solvate molecules were found for **6-8** crystals pointing towards space-filling of the alkyl chains.

Due to the promising packing characteristics, the structural similarity to **5-3** and in total four annulated thieno moieties, **6-8** was tested for its performance in field-effect transistors. Disappointingly, no field-effect could be measured in a top contact/ bottom gate FET prepared by drop casting (same setup was used which was described in the previous chapter). Investigation of the organic layer disclosed small and separated crystallites which provide good a reason since an intact network is needed. For the use as organic semiconductor, **6-8** may be altered in the length of alkyl chains to achieve homogenous films.

Structural Calculations

Very recently King et al. described the synthesis of HBTs *via* biphenylation of *p*-dibromoarenes, in particular using 4,5,9,10-tetrabromo-2,7-di-*tert*-butylpyrene.^[52] Surprisingly, the crystal structure revealed an alternate structure of phenanthryl and pyrenyl moieties, contrary to the here found saddle shape containing bent tetracene backbone and no comments were made regarding conformers in the ¹H NMR spectrum. It should be emphasized that annulated “acenes” mainly exhibit a twist in contrast to the here found bent shape within the “acene” backbone, which indicates the need of a theoretical study of HBT conformers.^[1]

Therefore, calculations using DFT/B3LYP method on 6-31G(d) basis set were performed in collaboration with Dr. [REDACTED] from this institute. The energy difference (ΔE) between the possible conformers and the corresponding fourfold chlorinated derivative in vacuum at room temperature was determined in order to provide the experimentally found conformation with theoretical background. The four most likely conformers and their conformational energy differences are depicted in Figure 6-17.

In the hydrocarbon case (see Figure 6-17 **a**) the twisted and alternating conformation show only minor difference in energy (0.9 kcal/mol). The energy for the saddle is increased by 4.3 kcal/mol whereas the stair is not likely to exist

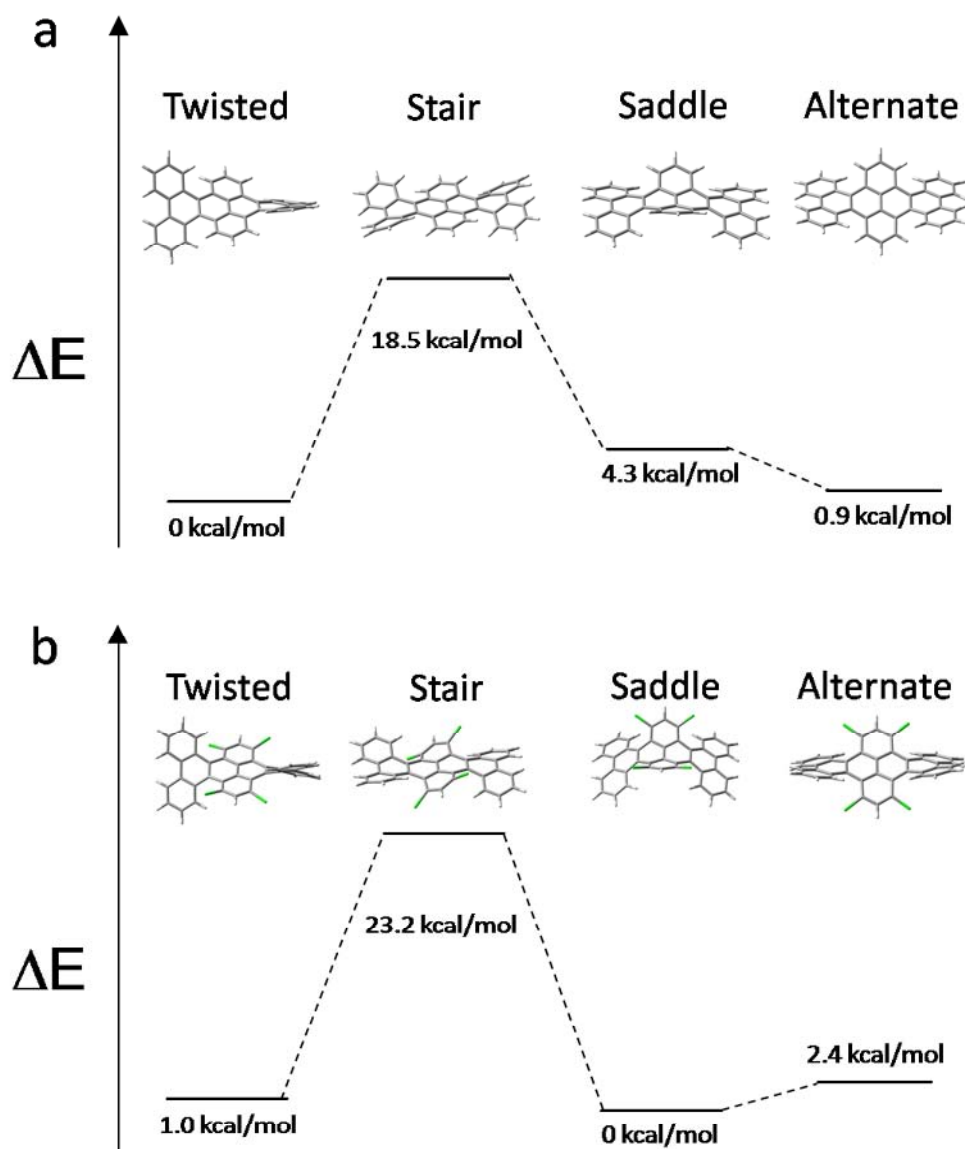


Figure 6-17: B3LYP/6-31G(d) calculations in vacuum of the energy differences ΔE in kcal/mol between four conformers of hexabenzo[*a,c,fg,j,l,op*]tetracene (a) and 9,11,20,22-tetrachlorohexabenzo[*a,c,fg,j,l,op*]tetracene (b).

with 18.5 kcal/mol. King et al. reported alternate conformations for two differently *tert*-butylated HBTs which matches with the calculated low energy value. In respect to the small energy difference to the twisted form, the coexistence of both conformers in solution is probable in case of a small transition barrier. Due to the fact that no isomers are detected by NMR

spectroscopy, either the conformer transition appears too fast for NMR or only enantiomeric conformers, and thus, indistinguishable for NMR are present.

Calculations on the chlorinated HBT (see Figure 6-17 **b**) revealed likewise unfavorable stair conformation (23.2 kcal/mol) but the saddle was predicted to be the energy minimum. The energy for the twisted form was determined to be only 1 kcal/mol higher than the saddle. As saddle shape was found experimentally for HBTs **6-14a** in the solid state, it may be assumed that the twisted conformer forms crystals badly and constantly converts to the saddle within the equilibrium as the saddle solidifies. This conclusion is in accordance with a low transition barrier observed from temperature dependent NMR. Furthermore, only a slightly higher energy of 2.4 kcal/mol was calculated for the alternate conformation. Assignment of the two NMR signal groups to the conformers could only be guessed.

6.4 Summary

In this chapter the concept of pyrene extension at the K-region by arylation and subsequent cyclodehydrogenation was successfully extended to both sides of pyrene and used to synthesize non-planar hexaarylated tetracenes.

Therefore, novel 4,5-dibromo-9,10-ditriflatopyrene and literature known 2,7-di-*tert*-butyl-4,5,9,10-tetrabromopyrene were applied in palladium-catalyzed cross-coupling reactions to prepare a series of tetrathienyl and tetraphenyl pyrenes, with and without *tert*-butyl groups at pyrene positions 2 and 7. For *ortho*-thienyl derivatives, ring-closure is easily realized either using irradiation with light or iron(III)chloride. Cyclodehydrogenation between benzene rings is found to be difficult as the photochemical approach failed and treatment with iron(III)chloride gave a mixture of non-separable byproducts. Chlorination under mild conditions with sulfuryl chloride at pyrene positions 1, 3, 6 and 8 and therefore blocking these sites was found to offer a way for the synthesis of HBTs. Consequently, ring-closure between phenyl rings of the chlorinated precursor succeeded, bearing an additional bulky substituent in the *coves*.

Single crystal X-ray analysis revealed saddle conformation for all HATs. The deviation from planarity arises from steric overcrowding in the four *coves*. In more detail, each *cove* of DBTTT hosts one hydrogen atom and one sulfur lone pair which force the conjugated skeleton to deform. In contrast, the saddle of chlorinated HBT exhibits angles twice as big caused by additional steric strain from chlorine atoms in the *cove*. Calculations on B3LYP/6-31G(d) level in vacuum confirmed the saddle shape as energetically favored conformation for chlorinated HBT.

In solution, the coexistence of at least two conformers of chlorinated HBT was proved by proton NMR spectroscopy at room temperature. Temperature dependent NMR experiments revealed coalescence of the signal groups at elevated temperature. Recovery of the initial ratio after cooling is pointing towards an equilibrium with a transition energy barriers between conformers

that is overcome at room temperature. This observation could neither be made for DBTTT nor is it reported for HBTs by King et al.

From a synthetic point of view the *cove*-chlorinated HBT is a versatile compound for further research. Replacement of chlorine in the *cove* with bulky substituents holds promise for tuning the transition energy barrier and therefore the spatial shape at last. Furthermore, the chlorine atom in the *cove* makes this molecule a potential precursor for bowl shaped PAHs *via* FVP.^[24]

6.5 Bibliography

- [1] R. A. Pascal, *Chemical Reviews* **2006**, *106*, 4809-4819.
- [2] D. J. Cram, J. M. Cram, *Accounts of Chemical Research* **1971**, *4*, 204-&.
- [3] P. W. Rabideau, A. Sygula, *Accounts of Chemical Research* **1996**, *29*, 235-242.
- [4] L. T. Scott, *Pure and Applied Chemistry* **1996**, *68*, 291-300.
- [5] B. D. Steinberg, L. T. Scott, *Angewandte Chemie-International Edition* **2009**, *48*, 5400-5402.
- [6] R. Jasti, J. Bhattacharjee, J. B. Neaton, C. R. Bertozzi, *Journal of the American Chemical Society* **2008**, *130*, 17646-+.
- [7] B. L. Merner, L. N. Dawe, G. J. Bodwell, *Angewandte Chemie-International Edition* **2009**, *48*, 5487-5491.
- [8] H. A. Wegner, H. Reisch, K. Rauch, A. Demeter, K. A. Zachariasse, A. de Meijere, L. T. Scott, *Journal of Organic Chemistry* **2006**, *71*, 9080-9087.
- [9] R. W. A. Havenith, J. H. van Lenthe, F. Dijkstra, L. W. Jenneskens, *Journal of Physical Chemistry A* **2001**, *105*, 3838-3845.
- [10] R. W. A. Havenith, H. J. Jiao, L. W. Jenneskens, J. H. van Lenthe, M. Sarobe, P. V. Schleyer, M. Kataoka, A. Necula, L. T. Scott, *Journal of the American Chemical Society* **2002**, *124*, 2363-2370.
- [11] K. W. Muir, J. M. Robertson, *Acta Crystallographica, Sect. B* **1972**, 879-884.
- [12] A. Mukherjee, K. Pati, R. S. Liu, *Journal of Organic Chemistry* **2009**, *74*, 6311-6314.
- [13] C. J. Carrell, H. L. Carrell, J. P. Glusker, E. Abushaqara, C. Cortez, R. G. Harvey, *Carcinogenesis* **1994**, *15*, 2931-2936.
- [14] A. K. Katz, H. L. Carrell, J. P. Glusker, *Carcinogenesis* **1998**, *19*, 1641-1648.
- [15] F. H. Herbstein, G. M. J. Schmidt, *Journal of the Chemical Society* **1954**, 3302-3313.
- [16] R. Amemiya, M. Yamaguchi, *Chemical Record* **2008**, *8*, 116-127.
- [17] R. H. Martin, *Angewandte Chemie-International Edition in English* **1974**, *13*, 649-659.
- [18] Y. Shen, C.-F. Chen, *Chemical Reviews* **2011**.
- [19] S. Grimme, S. D. Peyerimhoff, *Chemical Physics* **1996**, *204*, 411-417.
- [20] M. S. Newman, R. G. Mentzer, G. Slomp, *Journal of the American Chemical Society* **1963**, *85*, 4018-&.
- [21] M. C. Carreno, A. Enriquez, S. Garcia-Cerrada, M. J. Sanz-Cuesta, A. Urbano, F. Maseras, A. Nonell-Canals, *Chemistry-a European Journal* **2008**, *14*, 603-620.
- [22] H. Scherubl, U. Fritzsche, A. Mannschreck, *Chemische Berichte-Recueil* **1984**, *117*, 336-343.
- [23] T. J. Hill, R. K. Hughes, L. T. Scott, *Tetrahedron* **2008**, *64*, 11360-11369.

- [24] A. C. Whalley, K. N. Plunkett, A. A. Gorodetsky, C. L. Schenck, C. Y. Chiu, M. L. Steigerwald, C. Nuckolls, *Chemical Science* **2011**, *2*, 132-135.
- [25] M. J. Plater, *Journal of the Chemical Society-Perkin Transactions 1* **1997**, 2903-2909.
- [26] M. J. Plater, *Tetrahedron Letters* **1994**, *35*, 6147-6150.
- [27] L. Zöphel, V. Enkelmann, R. Rieger, K. Müllen, *Organic Letters* **2011**, *13*, 4506-4509.
- [28] L. Zöphel, D. Beckmann, V. Enkelmann, D. Chercka, R. Rieger, K. Müllen, *Chemical Communications* **2011**, *47*, 6960-6962.
- [29] S. I. Kawano, C. Yang, M. Ribas, S. Balushev, M. Baumgarten, K. Müllen, *Macromolecules* **2008**, *41*, 7933-7937.
- [30] Y. Miura, E. Yamano, A. Miyazawa, M. Tashiro, *Journal of the Chemical Society-Perkin Transactions 2* **1996**, 359-364.
- [31] J. Hu, D. Zhang, F. W. Harris, *Journal of Organic Chemistry* **2005**, *70*, 707-708.
- [32] M. Tashiro, T. Yamato, *Journal of the American Chemical Society* **1982**, *104*, 3701-3707.
- [33] T. Ohe, N. Miyaoura, A. Suzuki, *Synlett* **1990**, 221-223.
- [34] T. Ohe, N. Miyaoura, A. Suzuki, *Journal of Organic Chemistry* **1993**, *58*, 2201-2208.
- [35] N. Miyaoura, A. Suzuki, *Chemical Reviews* **1995**, *95*, 2457-2483.
- [36] K. Ritter, *Synthesis-Stuttgart* **1993**, 735-762.
- [37] D. J. Hong, E. Lee, J. K. Lee, W. C. Zin, M. Han, E. Sim, M. Lee, *Journal of the American Chemical Society* **2008**, *130*, 14448-+.
- [38] H. J. Kim, E. Lee, H. S. Park, M. Lee, *Journal of the American Chemical Society* **2007**, *129*, 10994-+.
- [39] P. Rempala, J. Kroulik, B. T. King, *Journal of Organic Chemistry* **2006**, *71*, 5067-5081.
- [40] M. Müller, C. Kübel, K. Müllen, *Chemistry-a European Journal* **1998**, *4*, 2099-2109.
- [41] J. L. Brusso, O. D. Hirst, A. Dadvand, S. Ganesan, F. Cicoira, C. M. Robertson, R. T. Oakley, F. Rosei, D. F. Perepichkat, *Chemistry of Materials* **2008**, *20*, 2484-2494.
- [42] E. Fischer, J. Larsen, J. B. Christensen, M. Fourmigue, H. G. Madsen, N. Harrit, *Journal of Organic Chemistry* **1996**, *61*, 6997-7005.
- [43] R. Rieger, K. Müllen, *Journal of Physical Organic Chemistry* **2010**, *23*, 315-325.
- [44] R. J. Olsen, R. E. Buckles, *Journal of Photochemistry* **1979**, *10*, 215-220.
- [45] F. B. Mallory, C. S. Wood, J. T. Gordon, *Journal of the American Chemical Society* **1964**, *86*, 3094-&.
- [46] T. S. Navale, K. Thakur, R. Rathore, *Organic Letters* **2011**, *13*, 1634-1637.
- [47] M. Müller, V. S. Iyer, C. Kübel, V. Enkelmann, K. Müllen, *Angewandte Chemie-International Edition in English* **1997**, *36*, 1607-1610.
- [48] B. T. King, J. Kroulik, C. R. Robertson, P. Rempala, C. L. Hilton, J. D. Korinek, L. M. Gortari, *Journal of Organic Chemistry* **2007**, *72*, 2279-2288.

- [49] J. C. Slater, *Journal of Chemical Physics* **1964**, *41*, 3199-&.
- [50] F. H. Allen, O. Kennard, D. G. Watson, L. Brammer, A. G. Orpen, R. Taylor, *Journal of the Chemical Society-Perkin Transactions 2* **1987**, S1-S19.
- [51] C. A. Hunter, K. R. Lawson, J. Perkins, C. J. Urch, *Journal of the Chemical Society-Perkin Transactions 2* **2001**, 651-669.
- [52] B. Kumar, C. E. Strasser, B. T. King, *Journal of Organic Chemistry* **2012**, *77*, 311-316.

7 *Peri*-Pentacene

7.1 Introduction

Acenes consist of linearly fused benzene rings and hold an outstanding position among the family of polycyclic aromatic hydrocarbons (PAHs). Today, acenes, heteroacenes and their derivatives constitute an important class of active materials for organic field-effect transistors and light emitting diodes.^[1-3] Acene's properties derive from their linear shape and length. According to Clar's sextet rule only one electron sextet can be drawn which explains the low aromatic stabilization. In comparison to other PAHs with the same number of benzene rings, acenes show the smallest energy gap and the highest reactivity.^[4] Whereas the smaller members naphthalene and anthracene are stable under ambient conditions, tetracene and pentacene are easily oxidized to the quinone or undergo Diels-Alder cycloaddition between an inner acene diene and dienophiles like oxygen.^[5-8] The substitution with tri(alkyl)silyl ethynyl substituents has become famous in their role at pentacene positions 6 and 13, making pentacene **I7-1** solution processable, more air resistant and one of the most frequently used small molecule semiconductors.^[1-2, 9]

The arising instability and insolubility with increasing length only allows detection of octacene and nonacene spectroscopically in PMMA matrix and at

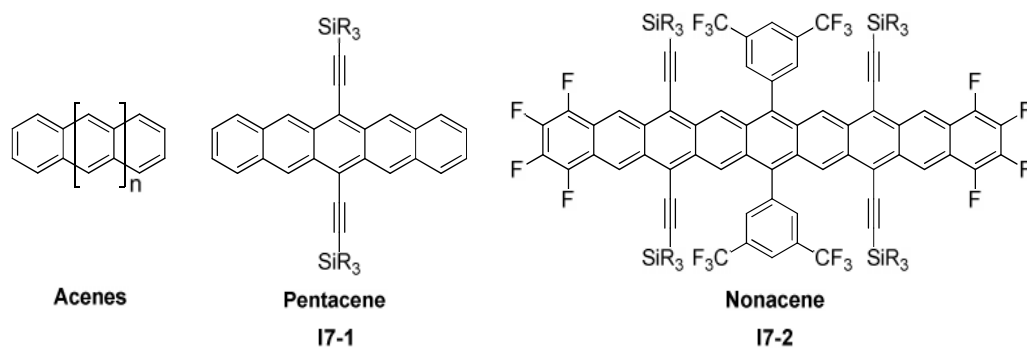


Figure 7.1: Chemical structure of acenes. Solutions processable pentacene **17-1** and larges acene **17-2**.

30 K.^[10] However, characterization in solution could be performed on substituted nonacene derivatives, which are the highest acenes reported so far. The tremendous scientific challenge becomes clear when Miller et al.^[11-12] reported the synthesis of “persistent” nonacene in 2010 but was corrected one year later by Anthony et al. proving that actually endoperoxide of nonacene has been investigated.^[13] The latter group published the highly decorated nonacene derivative **17-2** supported by X-crystal analysis. Out of available 22 $\text{C}_{\text{ar}}\text{H}$ sites 14 are substituted providing stability and solubility.

So called *peri*-acenes are conceptionally built by formation of single bonds between two acenes, and thus, two *armchair* and two *zig-zag* edges shape the rectangular aromatic skeleton (Figure 7.2). Gradually increasing their size, *peri*-acenes are of high interest due to the use as model compounds to experimentally verify predicted properties of infinite nanographenes.^[14-15] Many theoretical studies on *peri*-acenes exist and predict properties like a very small band gap, a significant biradical character, high reactivity due to high HOMO levels and their strong size dependence.^[4, 14, 16-18] For larger *zig-zag* edged nanographenes singlet open-shell ground state is predicted.^[15, 17, 19] Wang et al. reported that such biradical character is strongly determined by the length of the edges. In particular, elongation of the *zig-zag* edge results in an increase, whereas elongation of the *armchair* edge leads to a decrease of biradical character. A prominent example constitutes the substituted teranthene

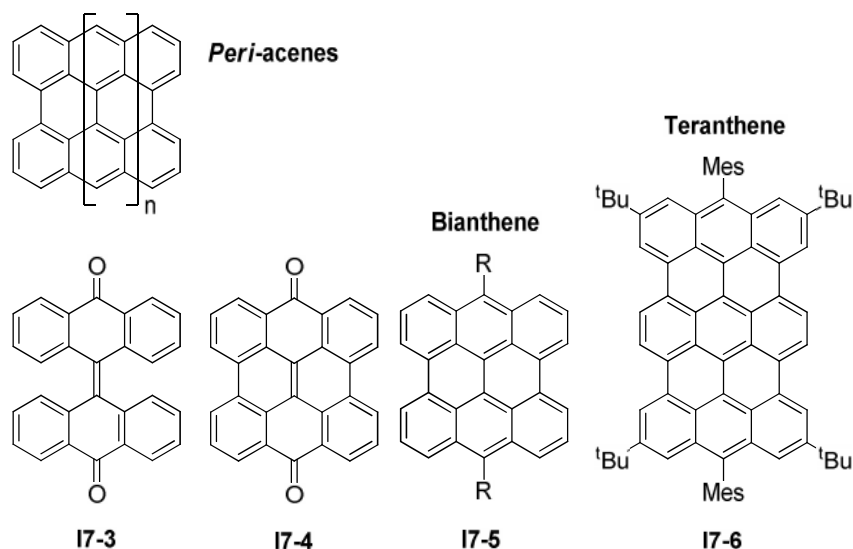
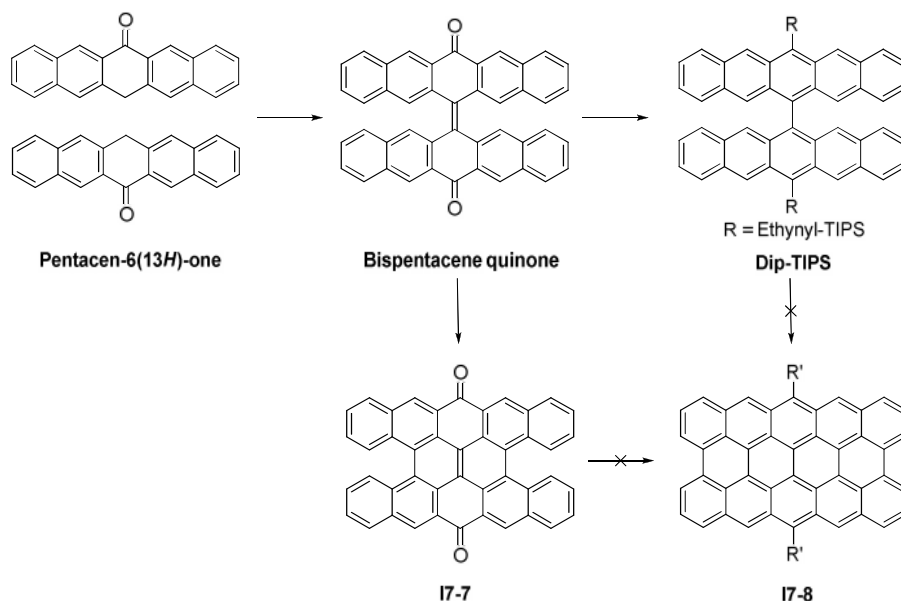


Figure 7.2: General structure of *peri*-acenes and literature known derivatives **I7-2** to **I7-5**.

derivative **I7-6** by Kubo et al. which shows singlet biradical character experimentally (Figure 7.2).^[20-21] Furthermore, balanced ambipolar charge carrier transport has been found for a delocalized singlet biradical hydrocarbon.^[22-23]

The smallest *peri*-acene is perylene ($n=0$) which came to fame as mono- or diimide due to its outstanding optical properties and stability.^[24] Extension to $n=1$ results in bisanthene, which has been functionalized with electron withdrawing imide groups or phenyl rings at its *zig/zag* edges like **I7-5** (Figure 7.2).^[25-26]

Higher *peri*-acenes like *peri*-tetracene ($n=2$) or *peri*-pentacene ($n=3$) have not been reported so far. Reasons could be the high reactivity concomitant with a low stability and bad solubility without appropriate substitution.^[27] Possible approaches might utilize quinone forms as stable precursors for the last step of reductive aromatization. This strategy has already been followed for the synthesis of compounds **I7-5** via **I7-3** and **I7-4** depicted in Figure 7.2. Another advantage is the convenient substitution of the quinone with nucleophiles like above mentioned tri(alkyl)silyl ethynyl lithium, aryl lithium or aryl Grignard reagents which yields the substituted PAH after reduction.



Scheme 7.1: Approaches towards *peri*-pentacene derivative **17-6**.

In parallel to this work, Wu and coworkers described the synthesis of quinone structures **17-7** and bispentacene quinone on their way to new NIR dyes (Scheme 7.1).^[28-29] Starting from pentacen-6(13*H*)-one, bispentacene quinone could be obtained. Treatment with TIPS ethynyl lithum and subsequent reduction gives cruciform 6,6'-dipentacenyl derivative **Dip-TIPS**. Fully fused *peri*-pentacene **17-8** is not reported by this route. Instead, bispentacene quinone converts into **17-7** upon irradiation analogously to the light induced reaction of bisanthracene quinone (**17-3**) to bisanthene quinone (**17-4**).^[30-31] Crucially, only the inner two bonds are formed and the reaction stops at tetrabenzobisanthene quinone **17-7** not further proceeding towards *peri*-pentacene quinone. Treatment with organometallic reagents leads unexpectedly to Michael 1,4-addition instead of an derivatization at the ketone function.^[29]

The approach towards *peri*-pentacene presented in the following uses pyrene chemistry to build the PAH skeleton instead of the *peri*-fusion of pentacenes. Such a completely different synthetic strategy seems to be required in order to evade the abovementioned experimental difficulties.

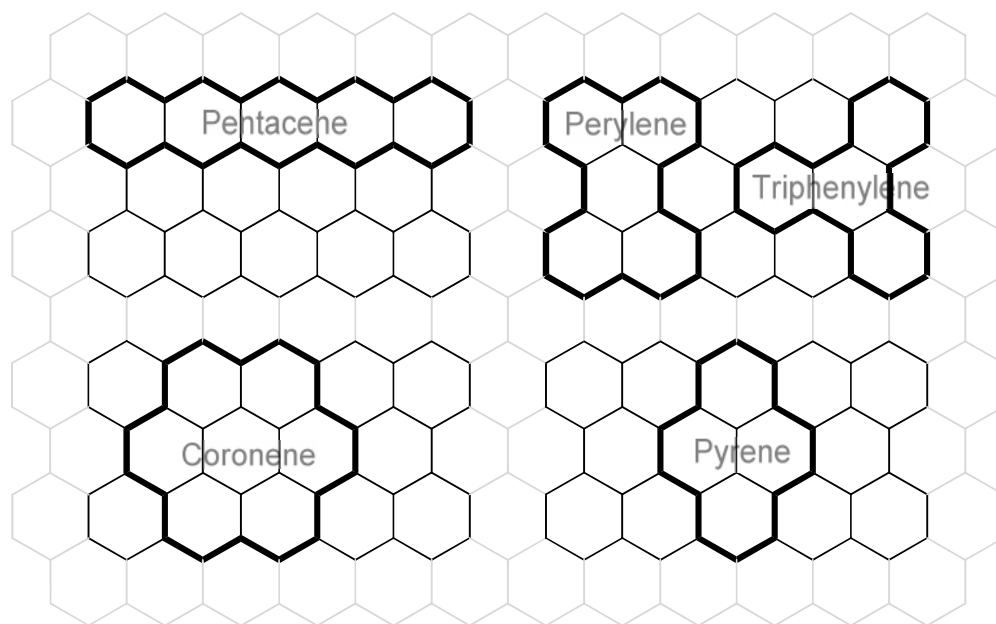


Figure 7.3: Selected PAHs drawn into the *peri*-pentacene scaffold.

7.2 Synthesis

Above described disadvantages of the *peri*-fusion of two pentacenes gave rise to the development of an alternative and more versatile synthetic approach. Therefore, a selection of PAHs are drawn into the *peri*-pentacene sketch to identify potential building blocks (Figure 7.3). Coronene and triphenylene nicely mimic parts of the edges of the target molecule but cannot be fitted symmetrically, and thus, require multi-step synthesis for asymmetric substitution. Perylene can be excluded due to missing protocols for its one-sided substitution.^[24] Owing to its shape and symmetry pyrene fits advantageously into the given mask.

Retrosynthetic considerations are depicted in Figure 7.4 leading to a less reactive tetraketone precursor structure. 4,5,9,10-Tetraphenylpyrene already consists of 40 carbon atoms out of 44 carbon atoms of *peri*-pentacene. Those missing four carbons can be introduced either with the peripheral phenyl rings

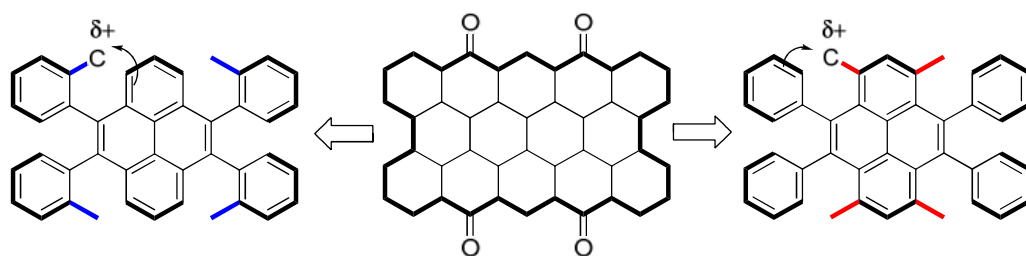
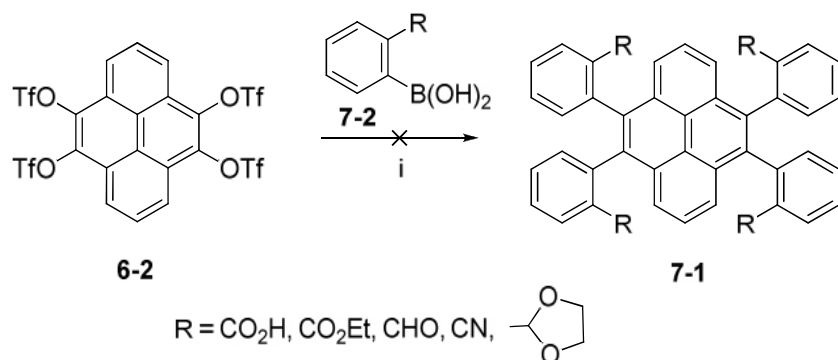


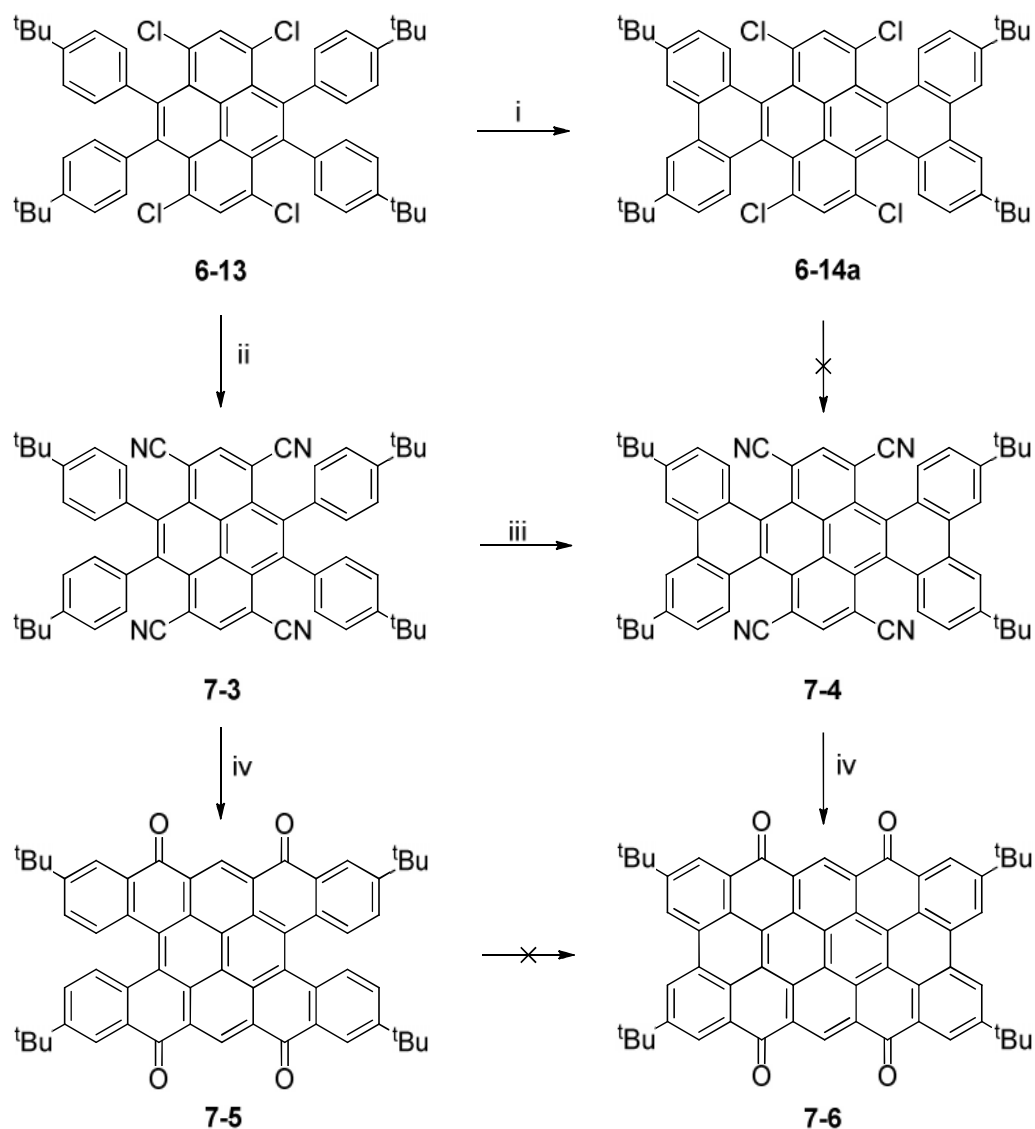
Figure 7.4: Retrosynthetic considerations for pyrene based synthesis of the *peri*-pentacene scaffold by electrophilic aromatic substitution at the peripheral phenyl rings (red) or onto pyrene (blue).



Scheme 7.2: Reaction scheme for the Suzuki coupling reaction of **6-2** to 4,5,9,10-tetraphenylpyrene derivatives **7-1**. Conditions: *i* 8 eq. phenyl boronic acid (**7-2**), 12 eq. K_3PO_4 , 0.05 eq. $\text{Pd}_2(\text{dba})_3$, 0.1 eq. SPhos, toluene, 80°C , 3 d.^[32]

(Figure 7.4, blue) or at the pyrene core (Figure 7.4, red). One way or the other, a functional group with one carbon has to be introduced which undergoes Friedel-Crafts-like electrophilic aromatic substitution to form the ketone bridge.

Starting from previously mentioned tetratriflatopyrene **6-2**, Suzuki coupling reaction of *ortho*-substituted phenyl boronic acids **7-2** failed although the ligand SPhos is reported for palladium catalyzed aryl-aryl coupling reactions of sterically hindered aryl boronic acids and halogens (Scheme 7.2).^[32] Hence, it was switched to the second approach shown in Figure 7.4 (red), which proves additional advantageous: The Suzuki coupling works well with *para*-substituted phenyl boronic acids as shown in the previous chapter; Solubilizing and spatially protecting alkyl groups are introduced easily and are commercially



Scheme 7.3: Synthesis of planar and non-planar tetraketones **7-6** and **7-5**. Conditions; *i* FeCl₃ in MeNO₂, DCM, 50 min, RT, 16 %; *ii* CuCN, NMP, 180°C, 3 days, 55 %; *iii* PIFA/BF₃·Et₂O, DCM, -40°C to RT overnight, 12 %; *iv* H₂SO₄ (60 % v/v), 160°C, overnight, 65 % for **7-5**, traces for **7-6**.

available; Incremental ketone bridging does not decrease the reactivity of the phenyl rings during electrophilic aromatic substitution.

The synthesis of **6-13** and **6-14a** has already been described in the previous chapter. The fastest route towards **7-6** lies in the treatment of **6-14a** with copper(I)cyanide to exchange chlorine atoms by cyano groups (Scheme 7.3).^[33] The nitrile function constitutes a precursor for acid induced ring-closure

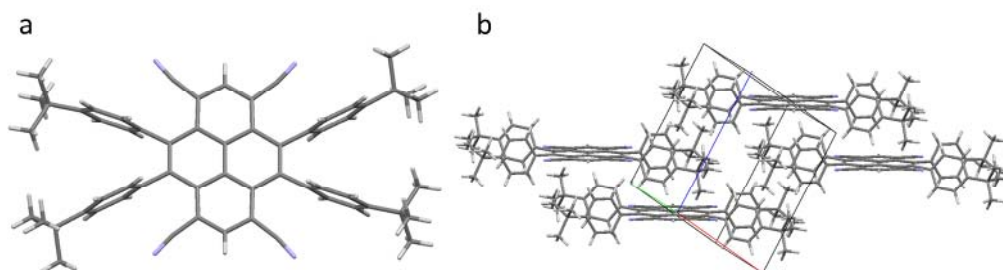


Figure 7.5: Crystal structure of 4,5,9,10-tetrakis(4-*tert*-butylphenyl)pyrene-1,3,6,8-tetracarbonitrile **7-3** (**a** front view, **b** unit cell).

after hydrolysis to the carboxylic acid.^[34] Surprisingly, after three days only the starting material **6-14a** was recovered. Neither extension of the reaction time up to 7 days nor increased temperature to boiling NMP (bp: 203°C) gave **7-4**, although the Rosenmund-von Braun reaction is a well-established method for the synthesis of aryl nitriles from aryl halides.^[33, 35-36]

Alternatively, **6-13** underwent fourfold chlorine cyanide exchange smoothly in 55 % yield and the structure of **7-3** was confirmed by single crystal analysis (Figure 7.5). The phenyl rings are rotated against the pyrenyl plane by angles between 72° and 82°. Furthermore, the cyano groups deviated by 10° from ideal 180° and are bent apart from bulky phenyl rings.

Conceptionally, the two bonds between the peripheral phenyl rings can be closed oxidatively before (**7-3**→**7-4**→**7-6**) or after (**7-3**→**7-5**→**7-6**) ketone bridging. The latter approach has been pursued at first.

Attempts to hydrolyze **7-3** to the corresponding carboxylic acid for the ring-closure failed under basic conditions. Instead, heating **7-3** in dilute H₂SO₄ to 160°C overnight allowed the isolation of a dark-violet solid by extraction with DCM.^[37] Purification and characterization revealed the direct formation of **7-3** to the tetraketone **7-5** in 65 % yield upon acid activation of the cyano group. **7-5** exhibits good solubility in common organic solvents due to non-planarity and alkyl side groups. Proton NMR shows doubled set of expected signals pointing towards the existence of conformers. A detailed characterization of the non-planar molecule is presented in subchapter 7.3.

Aiming for the planar tetraketone **7-6**, oxidative light induced cyclization was applied first on **7-5**. Upon irradiation at 300 nm, 350 nm and 420 nm in the

presence of iodine in deuterated toluene for 18 hours shows zero conversion by proton NMR spectroscopy. Changing power and wavelength to a 150 W middle pressure lamp for three days or 12 hours of daylight did not result in the formation of **7-6**. Trying the wet-chemical approach with iron(III) chloride/nitromethane in DCM gives the starting material with a small amount of chlorinated species. Harsher conditions using a 1:1 mixture from phenyliod(III)bis(trifluoroacetate) (PIFA) and boron trifluoride etherate ($\text{BF}_3 \cdot \text{Et}_2\text{O}$) from -40°C to room temperature lead to decomposition of **7-5** over time.^[38-39] Similar to the oxidative cyclodehydrogenation of **17-7**, the last bond in the *ffords* cannot be formed under the conditions described here.

Hence, the second route (**7-3**→**7-4**→**7-6**) was investigated. Initial attempts of oxidative bond formation between peripheral phenyl rings of **7-3** to **7-4** failed with iron(III) chloride, assumably due to electron poverty of the precursor.

Unexpectedly, treatment of **7-3** with PIFA/ BF_3 gave **7-4**, although in very low yield. Whereas no reaction was observed from -40°C to -10°C by TLC, **7-3** converts to **7-4** upon slow warming to room temperature. It has to be noted that this reaction could only be reproduced twice and all in all a few milligram of **7-4** could be obtained. That is why a careful characterization is presented in the following to unambiguously prove the structure of **7-4**.

High resolution ESI mass spectrometry confirmed the expected monoisotopic mass with a variance from the calculated value of 0.0004 m/z.

The recorded spectrum of two-dimensional proton correlation NMR spectroscopy is depicted in Figure 7.6 a. The one-dimensional spectrum shows the coexistence of conformers in the NMR timescale. The ratio of H2 to H2' was determined by integration to be 3.8 to 1. Further, NOESY was performed to clarify whether the bulky cyano group in the *cove* still allows transition between the conformers likewise **6-14a**. Beside expected NOE signals for H2/H3 and H2'/H3', Figure 7.7 shows a weak cross peak for H2/H2' indicating the conversion of one species into the other within NMR time scale and proves an equilibrium for conformers of **7-4** at room temperature. It has to be noted

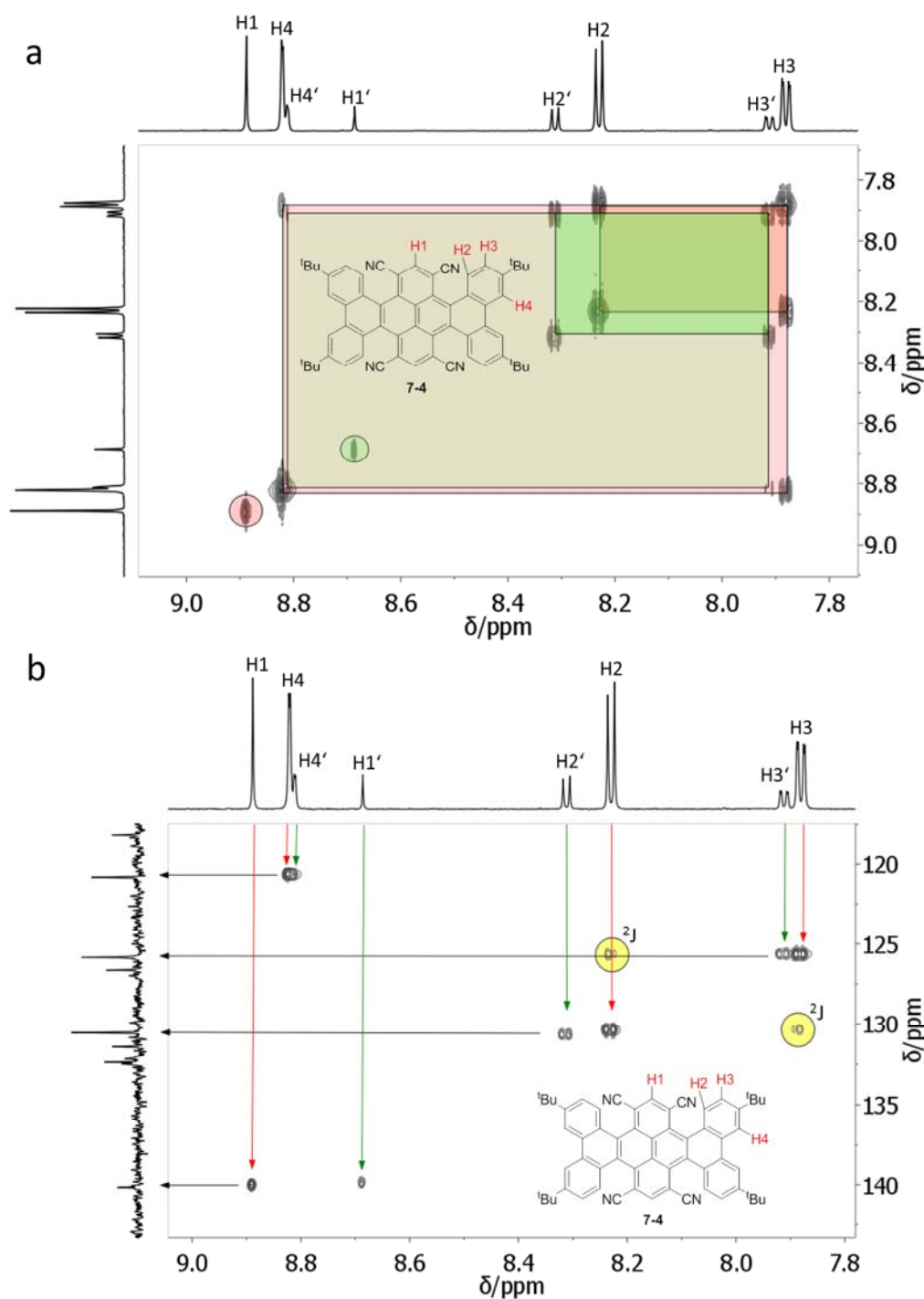


Figure 7.6: (a) Two-dimensional proton correlation NMR spectrum (^1H , ^1H COSY) of **7-4** in CD_2Cl_2 at 298 K (700 MHz); major conformer: red boxes; minor conformer: green boxes; (b) Heteronuclear Single Quantum Coherence NMR experiment (^1H , ^{13}C HSQC) of **7-4** in CD_2Cl_2 at 298 K (500 MHz); major conformer: red arrow; minor conformer: green arrow; ^2J coupling: yellow circle.

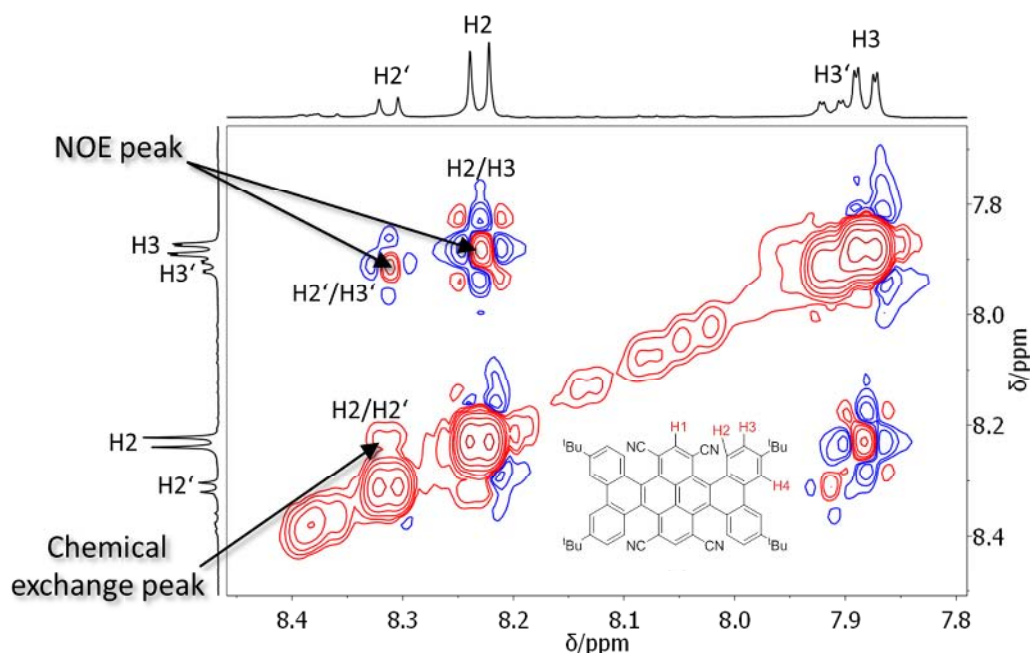


Figure 7.7: Nuclear Overhauser Effect Spectroscopy (NOESY) of **7-4** in CD_2Cl_2 at 298 K (500 MHz); NOE and chemical exchange peaks are highlighted by arrows.

that the resolution of chemical exchange peaks is challenging due to low intensity compared to NOE signals and small chemical shifts between the signal pairs of interest.

^1H , ^{13}C Heteronuclear single quantum coherence (HSQC) NMR spectroscopy was performed to identify proton bearing carbon atoms. In this experiment ^1J coupling over one bond between protons and carbon was detected and the result is shown in Figure 7.6 b. Only half of the expected doubled sets signals were revealed by one-dimensional ^{13}C NMR spectroscopy due to low concentration of the sample. The HSQC experiment proves overlay of the signals due to very little difference in the chemical shifts. In addition, H2 and H3 give a second less intense cross-peak which is attributed to ^2J coupling (over two bonds) and underlines the adjacent position of these protons.

Having carefully proven the structure of **7-4**, the tetranitrile precursor was treated with diluted sulfuric acid (60 %) at 160°C for 2 hours to give **7-6**. Purification and characterization **7-6** turned out to be difficult. Despite four *tert*-butyl groups the planar tetraketone does not dissolve in common organic

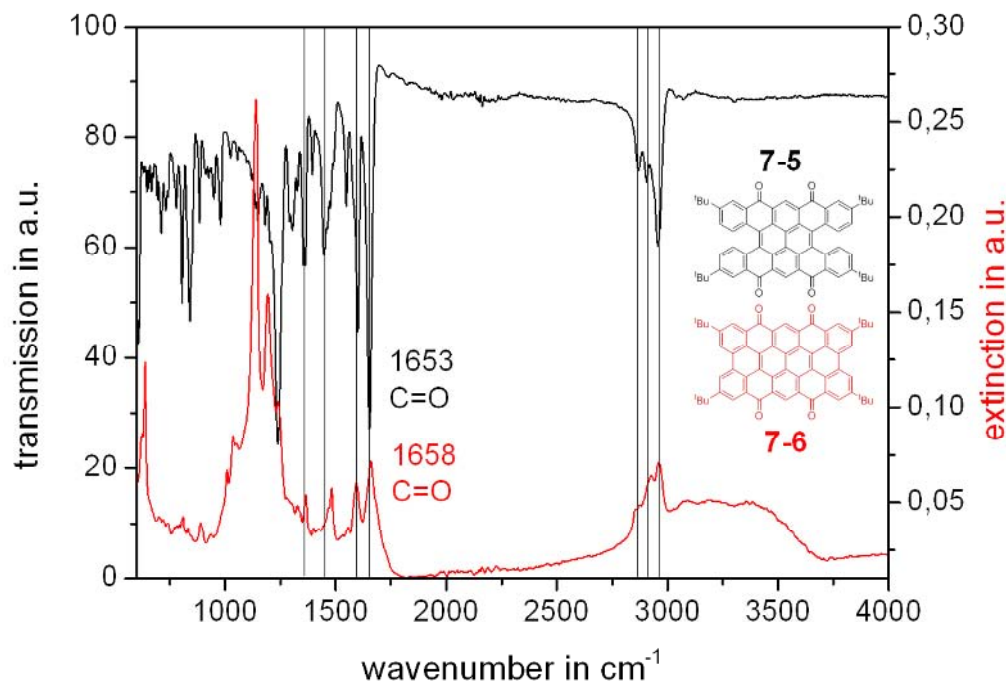


Figure 7.8: IR spectra of **7-5** and **7-6**. **7-6** has been measured on Teflon filter.

solvents, even not in boiling dichlorobenzene. Nothing but concentrated acids like H₂SO₄ or TFA dissolve **7-6**, most likely by protonation of the ketones. Investigation by proton NMR in D₂SO₄ or TFA-D₁ failed due to dilution of the sample and overlapping solvent signal. Thus, mass spectrometry, IR and UV/vis absorption spectroscopy were performed.

The IR spectrum of **7-6** was difficult to obtain due to the small amounts available. Therefore, the compound was dissolved in conc. H₂SO₄, diluted with ice and filtered over a teflon filter. IR absorption was measured directly from the film on the filter which is the reason for the bad quality of the recorded spectrum. The spectra of **7-6** and **7-5** for comparison are depicted in Figure 7.8. Nevertheless, similar vibrational bands can be observed below 3000 cm⁻¹ (C_{Ar}-H stretching vibration) and at 1653 cm⁻¹ and 1658 cm⁻¹ (C=O), respectively. Crucially, no characteristic CN band can be observed which was found as a strong signal at 2217 cm⁻¹ for the precursor **7-3**. Thus, the IR

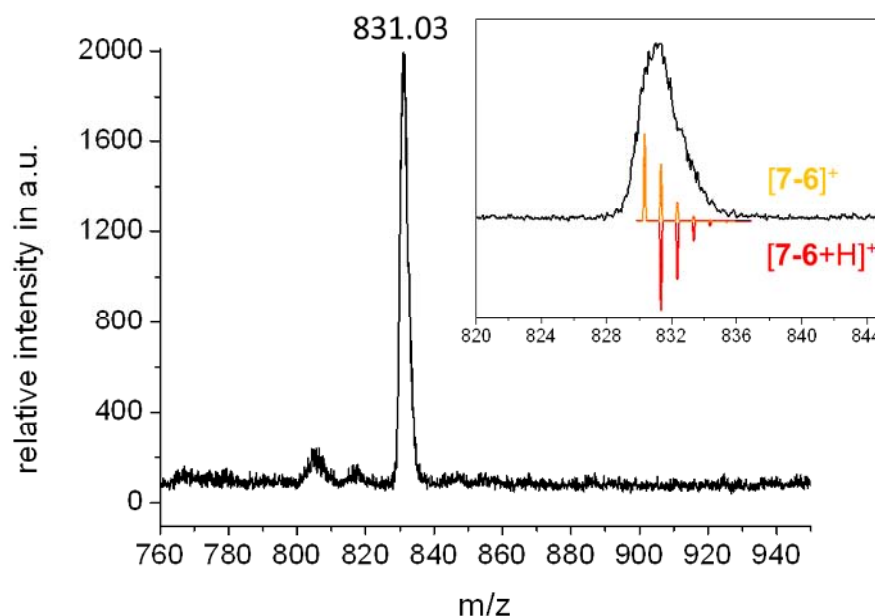


Figure 7.9: MALDI-TOF spectrum of **7-6**. Inset: product signal with calculated isotopic distribution of $[7-6]^+$ and $[7-6+H]^+$.

investigations support the complete conversion of the nitrile precursor to the ketone structure **7-6**.

Acid solubility further complicated mass spectrometrical investigations of **7-6**. For the preparation of the sample a few drops of the analyte in conc. TFA were given to a large excess of DCTB and extensively blended. The obtained spectrum is shown in Figure 7.9 with the magnified product signal in the inset. Better resolution of the isotopic pattern could neither be achieved by different the laser intensities nor by the use of various matrices. A reasonable explanation for the width of the signal lies in the assumption of two ionization mechanisms taking place at the same time. The calculated isotopic patterns of the radical cation $[7-6]^+$ (orange) generated by photoionization and the protonated species $[7-6+H]^+$ (red) are depicted in the inset and fit to the experimental data.

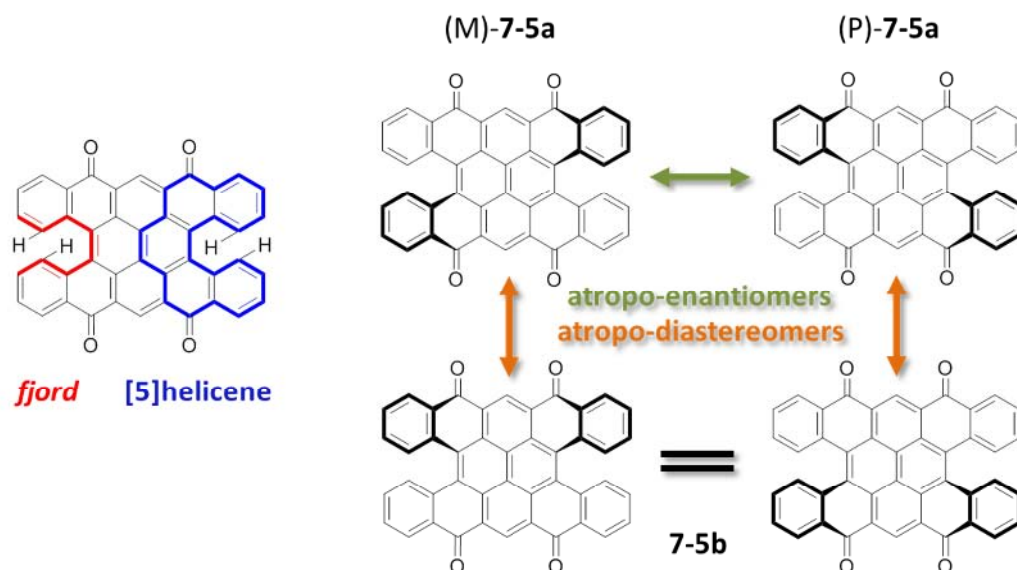


Figure 7.10: Illustrative depiction of the non-planar core and the conformers of **7-5**; left: [5]Helicene moiety and *fjord* highlighted in blue and red; right: atropo-enantiomers (M)-**7-5a** and (P)-**7-5a** and atropo-diastereomer **7-5b**.

7.3 Conformational Investigations of 7-5

The molecular structure of **7-5** is coined by two *fjords* that are formed by two [5]helicene moieties (Figure 7.10). Within the *fjord* two hydrogen atoms are facing each other and force the [5]helicene motif out of the plane into a dragonfly-like shape. Helicenes are prominent examples for helical chirality and can exist in a (M) and (P) helical form. Figure 7.10 illustrates the possible isomers: one pair of atropo-enantiomers (M)-**7-5a**, (P)-**7-5a** and the corresponding atropo-diastereomer **7-5b**.

Recently, a core-extended terrylene tetracarboxdiimide has been synthesized in our group which contains a similar aromatic core structure like **7-5** with two *fjords*.^[40] Therein, Eversloh et al. reported the separation of diastereomers by silica column chromatography and the atropo-enantiomers using chiral HPLC. Circular dichroism measurements revealed low degree of racemization even at elevated temperatures. Surprisingly, Wu et al. did not mention conformers for

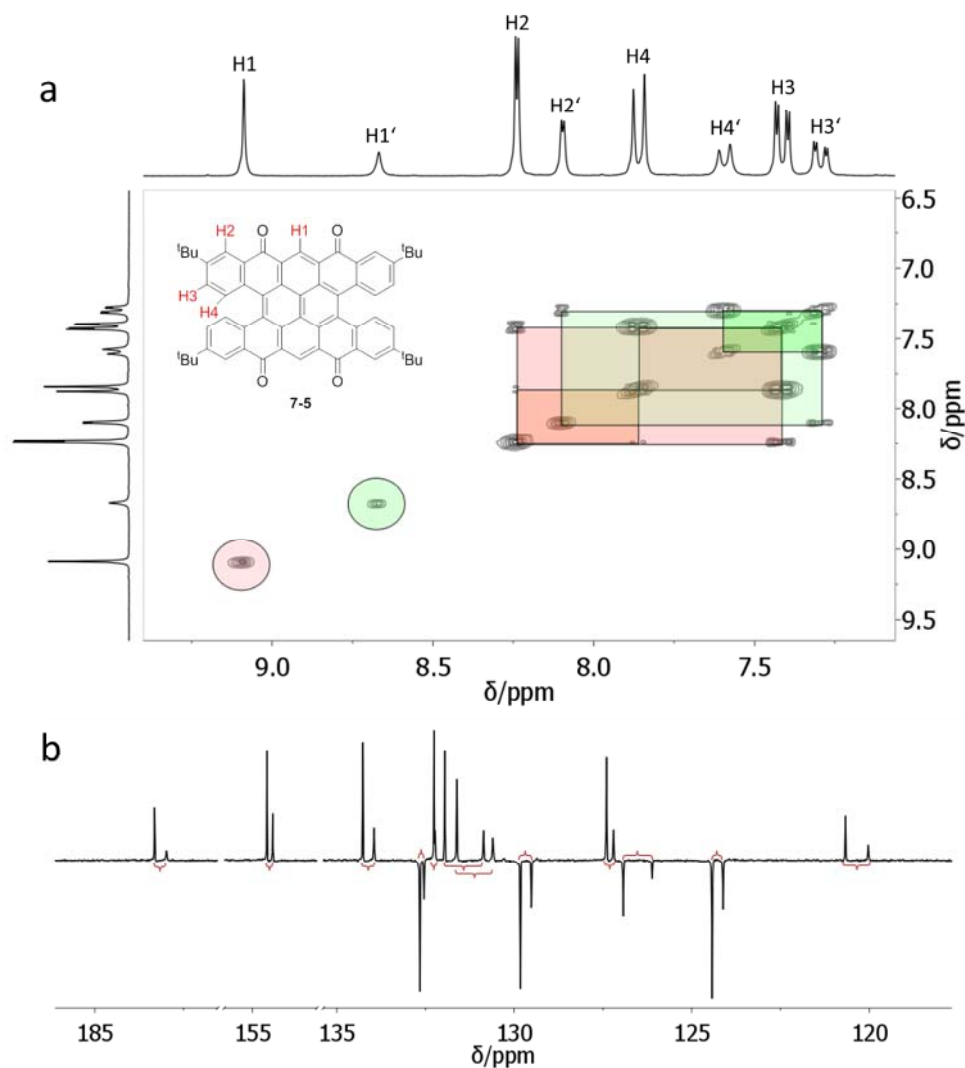


Figure 7.11: (a) Two-dimensional proton correlation NMR spectrum (^1H , ^1H COSY) of **7-5** in CD_2Cl_2 at 298 K (250 MHz); major conformer: red boxes; minor conformer: green boxes; (b) Spin-Echo ^{13}C NMR spectrum of **7-5** in CD_2Cl_2 at 298 K (175 MHz).

I7-7 neither detected by NMR spectroscopy nor other analytical methods.^[29] In the following a detailed study on the spatial shape of **7-5** is presented.

NMR Investigation

One-dimensional proton NMR spectroscopy of **7-5** in DCM-d_2 shows two sets of four signals in a ratio of 2 to 1 in the aromatic region of the spectrum (Figure 7.11 a). ^1H , ^1H COSY indicates two atropo-isomers coexisting in NMR time

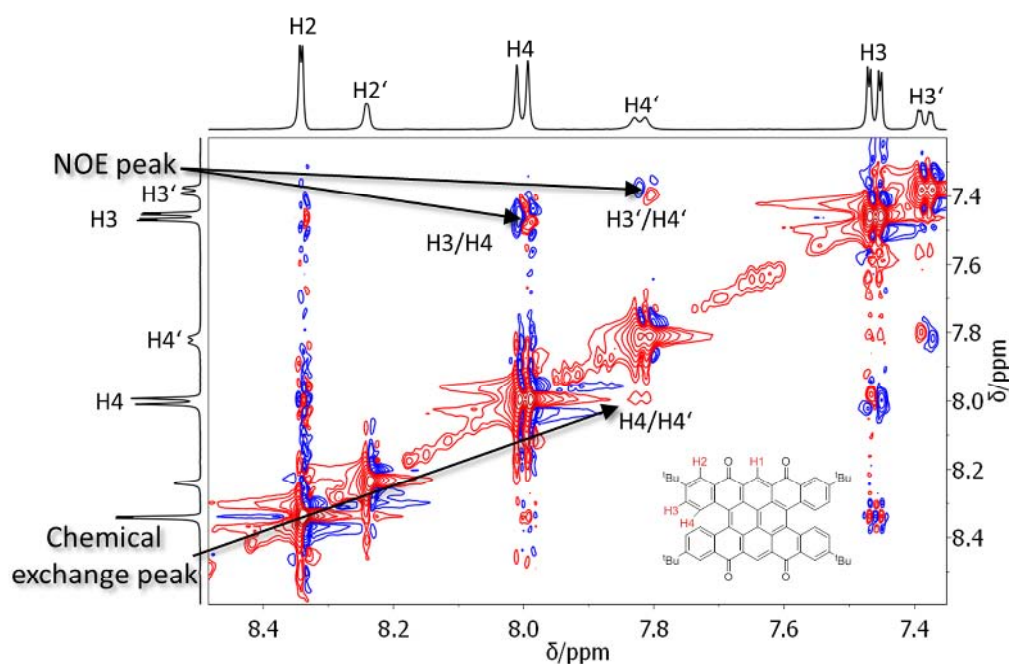


Figure 7.12: Nuclear Overhauser Effect Spectroscopy (NOESY) of **7-5** in CD_2Cl_2 at 298 K (500 MHz); NOE and chemical exchange peaks are highlighted by arrows.

scale. Signals of both sets can easily be assigned to the corresponding protons (H1-H4 ; H1'-H4') and cross-peaks are exclusively found among the respective isomer. Spin-echo carbon NMR revealed two sets of signals as well (Figure 7.11 **b**). Presuming that atropo-enantiomers (*M*)-**7-5a** and (*P*)-**7-5a** are undistinguishable by NMR spectroscopy, one set of protons refers to **7-5a** and the other one to **7-5b**. Calculations using Gaussian 03W (DFT/B3LYP/6-31G(d)) on the core structure of **7-5** give a 10.46 kcal/mol higher energy for atropo-diastereomer **7-5b** than atropo-enantiomers **7-5a**. Thus, it seems likely that the major set of signals (H1-H4) corresponds to the energetically favored atropo-enantiomers **7-5a**.

To answer the question of interconversion between the three conformers of **7-5**, NOESY experiments were performed (Figure 7.12). Similar to **7-4**, a weak chemical exchange peak of H4/H4' could be resolved beside the expected NOE signals and proves an equilibrium at room temperature. In literature, different mechanisms for the racemization of [5]helicene are proposed, proceeding over a coplanar or twisted non-chiral transition state, respectively.^[41-42] Either way, the

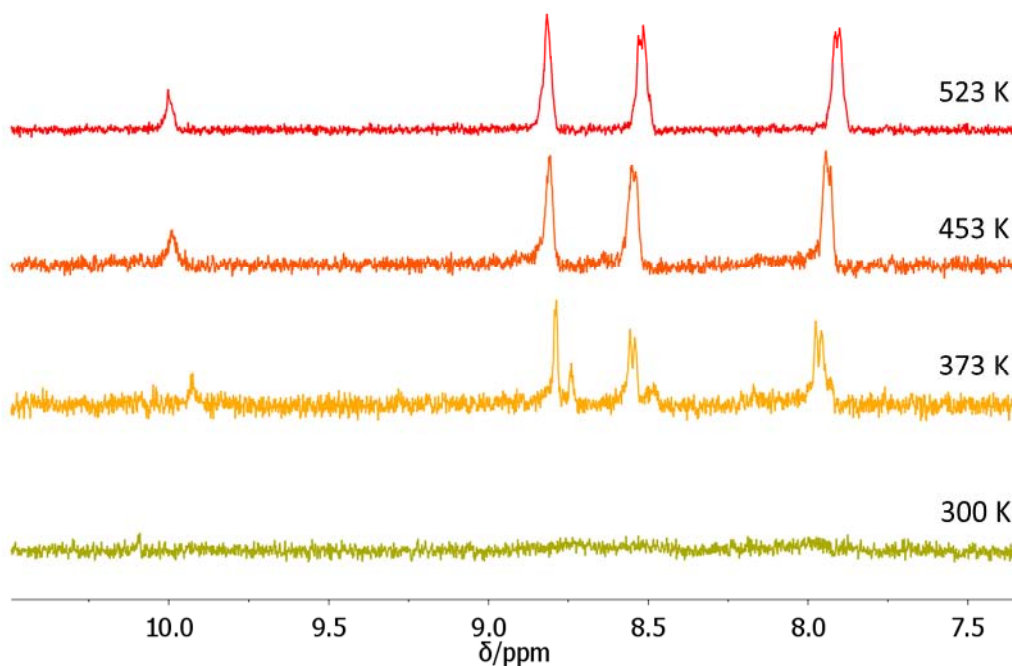


Figure 7.13: Temperature dependent proton NMR of **7-5** in sulfolane- d_8 from 300 K to 523 K (500MHz).

transition should show temperature dependence due to an energetically unfavorable transition state.

Therefore, temperature dependent proton NMR spectroscopy was performed to shift the equilibrium between the conformers. First attempts heating **7-5** in $C_2D_2Cl_4$ up to 393 K only slightly shifted all signals by less than 0.1 ppm downfield but the ratio between conformers remained unchanged. Therefore, sulfolane- d_8 was chosen because of the high boiling point at 558 K (Figure 7.13). At 300 K no signals are resolved due to the bad solubility of **7-5** in the solvent. Increasing temperature to 373 K showed both signal groups whereas at 523 K only the major one remains. From this experiment the conclusion can be drawn that the transition barrier is overcome by temperatures above 373 K. A precise transition temperature could not be determined as the high background noise makes exact determination of disappearance of a signal by integration difficult. The initial equilibrium recovers and both signal groups are observed by cooling back to 373 K.

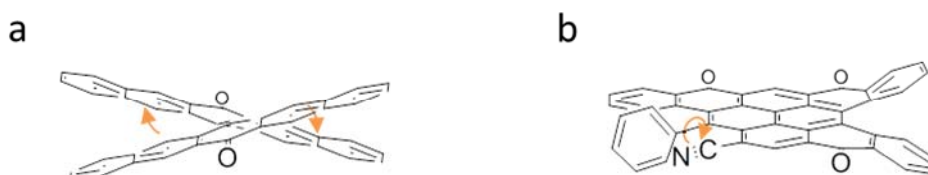


Figure 7.14: Depiction of the spatial state during the formation of **17-7** (a) and **7-5** (b).

All experiments and observations clearly support that a mixture of atropo-isomers **7-5** exists in solutions but still the question remains open why no atropo-diastereomers are reported for the structural closely related compound **17-7**.^[29] A possible explanation is related to the difference of the synthesis route. Presuming that the fourfold electrophilic attack proceeds stepwise, the last ring-closure determines whether **7-5a** or **7-5b** is formed (Figure 7.14 b). In contrast, the X-form of bispentacene quinone presets the two possible atropo-enantiomeric species. Apparently, no equilibrium exists with an atropo-diastereomeric form because proton signals of only one species were found by ¹H NMR spectroscopy.

Chiral HPLC

So far gained insights into conformational properties strongly ask for the separation of the conformers. Common silica column chromatography with DCM did not enable the fractionation of any isomer from the mixture although TLC shows two badly separated spots. Therefore, HPLC on a Kromasil Chiral DMB column was performed in collaboration with [REDACTED] from this institute.

Carefully optimized gradient of THF/*n*-heptane from 10:90 to 12.5:87.5 was used and three signals were observed and the fractions collected. It is assumed that of the three signals correspond with the three conformers (M)-**7-5a**, (P)-**7-5a** and **7-5b**. Unfortunately, analytical reinjection on the next day did not display separated peaks. Instead, an elugram with the respective enriched signal

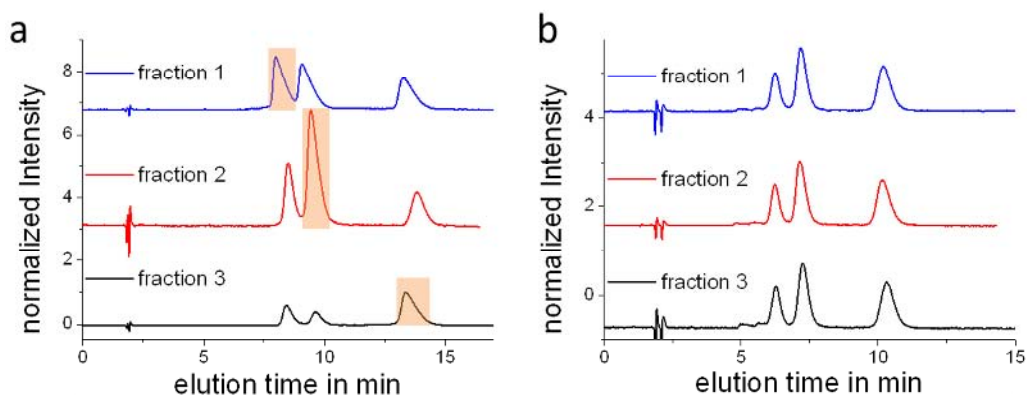


Figure 7.15: Elugrams of HPLC on Kromasil Chiral DMB column using THF/*n*-heptane gradient from 10:90 to 12.5:87.5; **(a)** analytical injection of separated fractions 1 to 3 after one day (enriched conformer is shaded in orange); **(b)** analytical injection of separated fractions 1 to 3 after four weeks.

was obtained (Figure 7.15 **a**). After four weeks the initial state was recovered and all fractions showed the same elugram (Figure 7.15 **b**). Proton NMR spectroscopy confirmed the initial ratio between sets of signals. These observations fit to an equilibrium even at room temperature between all three conformers.

A three-dimensional plot of intensity and elution time against absorption spectrum is depicted in Figure 7.16 **a**. Extraction of absorption spectra from the plot at the respective maxima enables comparison of the absorption of all conformers. The absorption spectra at elution times 06'21 min, 07'13 min and 10'14 min are shown in Figure 7.16 **b** and have been normalized to the longest wavelength transition. Although resolution is rather poor due to only one data point per 4 nm the spectrum of 06'21 min slightly deviates from 07'13 min and 10'14 min. It can only be speculated that the firstly eluted molecule is **7-5b** followed by the two atropo-enantiomers.

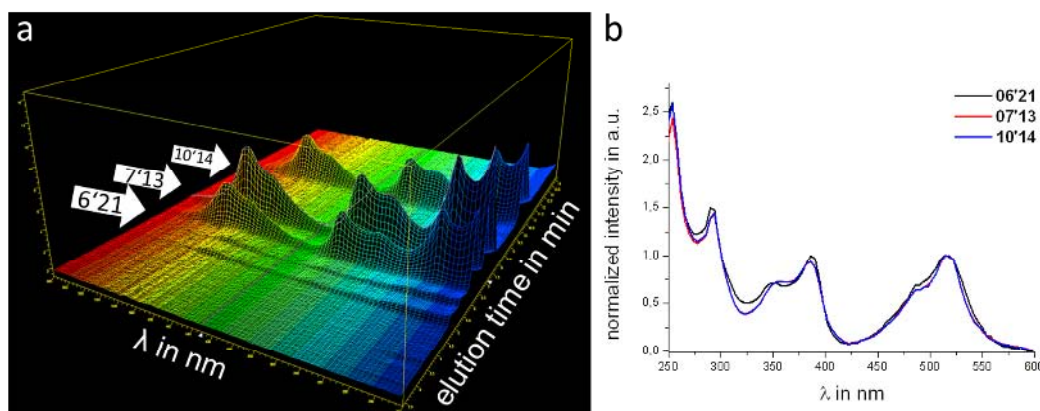


Figure 7.16: (a) Three-dimensional plot of the elution time against the absorption spectrum of chiral HPLC run of **7-5**; (b) spectra at elution times 6'12, 07'13 and 10'14 normalized to the longest wavelength absorption.

7.4 Optical and Electronic Properties

UV/vis Spectroscopy

The UV/vis absorption and emission spectra of the series of octa-substituted pyrene derivatives is depicted in Figure 7.17 **a-c** and the values are summarized in Table 7.1 on page 186. Compounds **6-10** and **6-13** have been included to present the effect of substitution of pyrene within the whole series.

The absorption maximum at the longest wavelength is bathochromically shifted starting from 352 nm to 524 nm (**6-10**→**7-5**) and comes along with a decrease of the optical energy gap by 0.98 eV, which has been determined from the onset of absorption. Whereas the chlorination of tetraphenylpyrene **6-10** decreases $E_{g(opt)}$ by 0.33 eV, the exchange to cyano groups leads to a drop by 0.17 eV. The biggest change is observed for the last step to the tetraketone **7-5** by 0.48 eV and a color change from bright yellow to red in THF solution (Figure 7.17 **c**). The ring-closure extends the π -conjugation, but more important, significantly lowers the LUMO level by the influence the

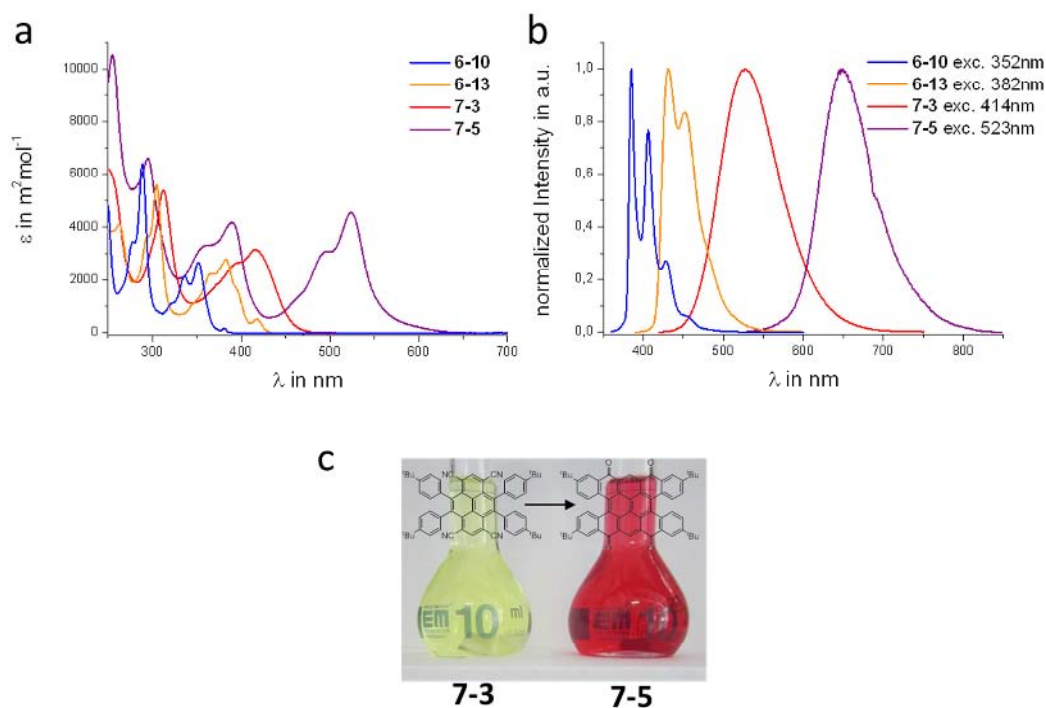


Figure 7.17: UV/vis absorption (a) and emission spectra (b) **6-10**, **6-13**, **7-3** and **7-5** in THF at 10^{-5} M concentration; (c) picture from THF solutions of **7-3** and **7-5**.

stronger electron-withdrawing character of the ketone substituents. The latter statement cannot be concluded from optical spectroscopy. Instead, CV was used to determine the position frontier orbitals and is discussed in the following subchapter.

Compared to the optical properties of **17-7** ($\lambda_{\text{abs}} = 493$ nm; $E_{\text{g(opt)}} = 2.44$ eV; measured in CHCl_3),^[29] the energy gap of **7-5** is decreased by 0.21 eV which can be attributed to a decreased LUMO level by the double number of electron withdrawing ketone groups.

Similar to the absorption, gradual red-shift of the emission maxima was observed. The normalized spectra are depicted in Figure 7.17 b. **7-5** emits at longest wavelength (649 nm), even 264 nm bathochromically shifted compared to tetraphenylpyrene **6-10**.

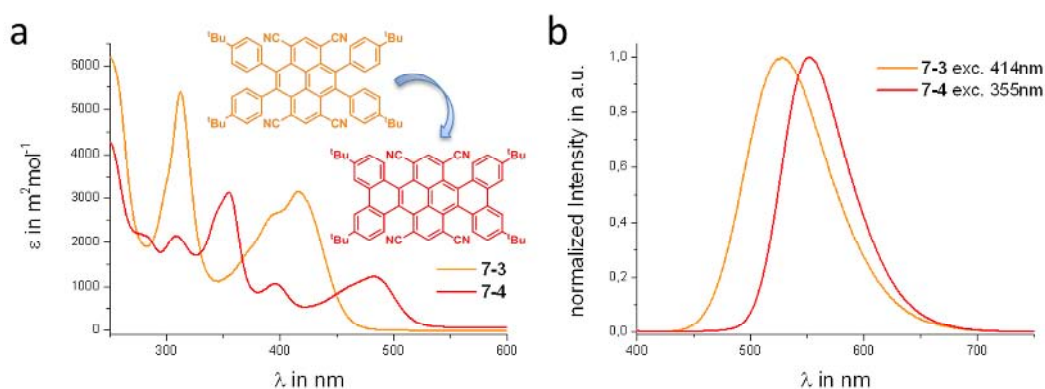


Figure 7.18: UV/vis absorption (a) and emission spectra (b) of **7-3** and **7-4** in THF at 10^{-5} M concentration.

The absorption and emission spectrum of **7-4** is shown in Figure 7.18 along with its precursor **7-3** for comparison. The fusion between peripheral rings leads to a red-shift of the absorption and emission maximum by 66 nm and 25 nm, respectively, and the optical energy gap decreases by 0.33 eV. The narrowing can be ascribed to the planarization and increased conjugation and has also been found for the conversion from **6-13** to **6-14a** (0.22 eV) in the previous chapter.

Due to its above mentioned poor solubility, UV/vis absorption of **7-6** and **7-5** for comparison was recorded in concentrated sulfuric acid (Figure 7.19). A distinct color change of both compounds in the strongly acidic environment was observed which can be attributed to the protonation at the oxygen atoms.^[43] **7-5** exhibits dark green color whereas **7-6** is dark purple.

Despite the expected enhanced conjugation of **7-6** by its planar structure, the maximum of the longest wavelength absorption was found to be hypsochromically shifted by 51 nm compared to dragonfly shaped **7-5**. The same trend was reported for the structurally related helianthrone derivative (**I7-3** with one additional bond between anthraquinone moieties) which exhibits a red-shifted absorption maximum by 42 nm compared to hexyl substituted **I7-4** in conc. H_2SO_4 .^[30, 43]

Likewise, protonation of **7-5** shifts the absorption maximum by 216 nm in

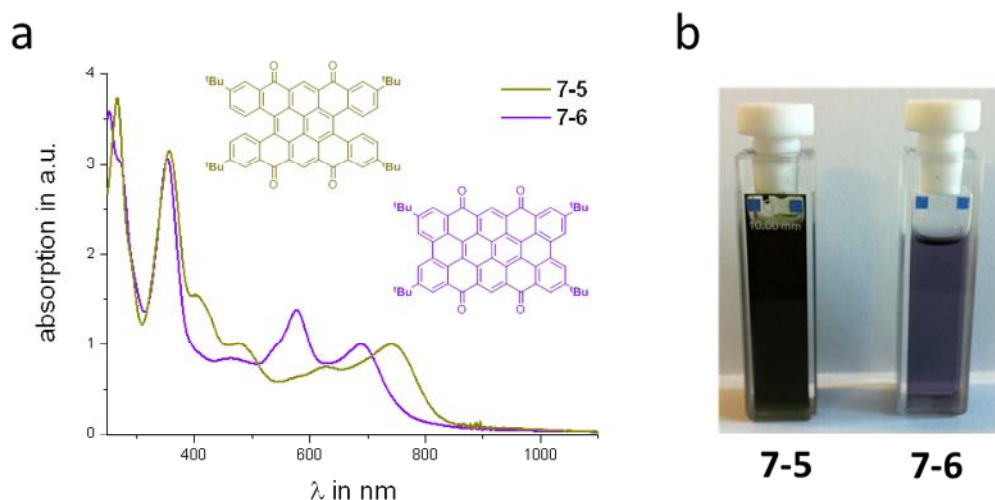


Figure 7.19: (a) UV/vis absorption spectra of tetraketones **7-5** and **7-6** in concentrated sulfuric acid; (b) cuvettes with **7-5** and **7-6** in concentrated sulfuric acid.

comparison to its solution in THF. For comparison, the absorption maximum of the just mentioned helianthrone derivative is shifted by 181 nm to longer wavelength (DCM \rightarrow conc. H_2SO_4). In conc. H_2SO_4 earlier reported diketone **I7-7** exhibits a similarly shaped spectrum like tetraketone **7-5** as well as the characteristic red-shift of the longest wavelength absorption maximum upon protonation by 216 nm to the maximum at 709 nm.^[29]

In order to quantify the protonation occurring at **7-5** and **7-6** attempts to observe the C=O-H proton resonance by proton NMR spectroscopy were carried out at 213 K in $\text{FSO}_3\text{H-SbF}_5$, so-called magic acid. It has been reported that in strongly acidic media at sufficiently low temperature, the C=O-H proton exchange becomes slow enough to permit NMR observation.^[44] The experiment failed most probably due to the overlap of the very broad solvent signal and the expected C=O-H signal. Whether mono-, di-, tri- or even tetrafold protonation of **7-5** takes place can thus only be guessed.^[30]

The dilution of **7-5** and **7-6** in conc. H_2SO_4 with water led to the recovery of the initial color and precipitation which indicates the reversibility of the protonation process. Even after several weeks in conc. H_2SO_4 no degradation of **7-5** could be observed, and thus, demonstrates high stability against acidic and oxidative media. No degradation of quinone **I7-4** was reported either.^[30]

Table 7.1: Optical properties of compounds **7-3** to **7-6**.^[a]

| | λ_{abs} ^[b] | λ_{em} ^[c] (λ_{ex}) ^[d] | λ_{edge} | $E_{\text{g(opt)}}$ ^[e] |
|------------|---------------------------------------|---|-------------------------|------------------------------------|
| 7-3 | 416 nm | 527 nm (414 nm) | 457 nm | 2.71 eV |
| 7-4 | 482 nm | 552 nm (355 nm) | 521 nm | 2.38 eV |
| 7-5 | 524 nm | 649 nm (523 nm) | 555 nm | 2.23 eV |
| 7-5 | 740 nm ^[f] | - | - | - |
| 7-6 | 689 nm ^[f] | - | - | - |

[a] All absorption and emission spectra were measured in THF; [b] λ_{abs} is the absorption band appearing at the longest wavelength; [c] λ_{em} is the fluorescence band appearing at the shortest wavelength; [d] λ_{ex} wavelength of excitation; [e] calculated from λ_{edge} ; [f] measured in concentrated sulfuric acid.

Cyclic Voltammetry and DFT Calculations

CV was performed from compounds **7-3** and **7-5** in DCM and ferrocenes half-wave potential was set to 0.6 eV as internal standard (Figure 7.20 a). Due to the lack of sufficient material and solubility **7-4** and **7-6** could not be investigated.

Under the measurement conditions **7-3** shows no oxidation wave but a reversible reduction process takes place with an onset at -0.57 V corresponding to the LUMO at -3.63 eV (values summarized in Table 7.2 on page 188).

Two closely following and reversible reduction waves were found at -0.15 V and -0.38 V for **7-5** corresponding to the radical anion and dianion.^[29] The LUMO level was calculated at -4.05 eV from the first reduction process and proves the stronger acceptor properties for **7-5** compared to **7-3**. In comparison to diketone **I7-7** (LUMO level at -3.18 eV) the two additional ketone groups of **7-5** exhibit strong impact on the LUMO by a decrease of 0.87 eV. Differential pulse voltammetry (DPV) further proves two one-electron reduction processes for **7-5** (Figure 7.20 b).

In contrast to the reversible reduction behavior, **7-5** oxidizes irreversibly. For comparison the onset potential at 1.84 V was used to estimate the HOMO level at -6.04 eV and the energy gap from CV ($E_{\text{g(CV)}}$) to be 1.99 eV although irreversible processes are not thermodynamically defined.^[29, 45]

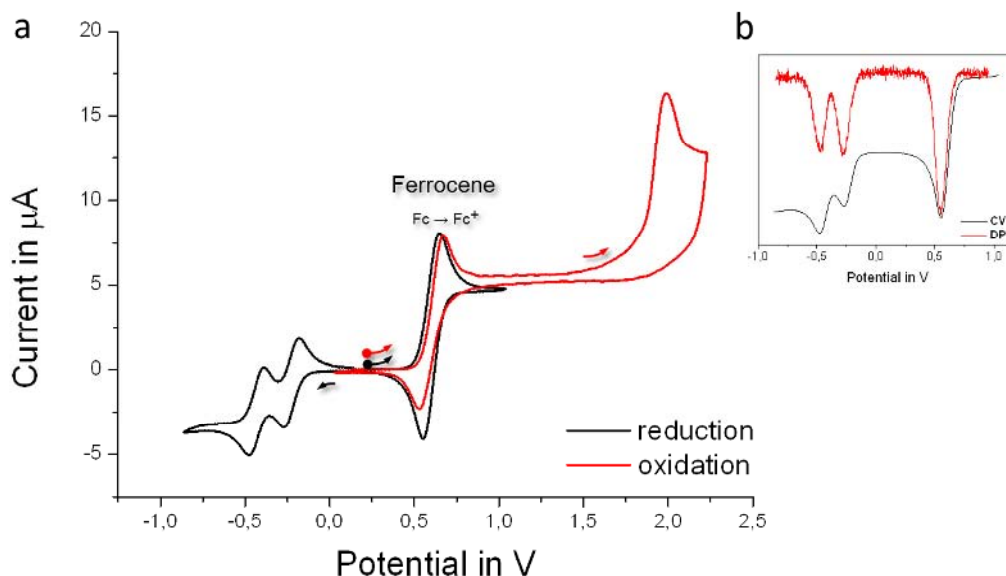


Figure 7.20: (a) Cyclic voltammograms of **7-5**, oxidation and reduction are recorded separately in 0.1 M n-Bu₄NPF₆/DCM with a scan rate of at 50 mV/s. Ferrocene oxidation and reduction wave is set to half-wave potential of 0.6 V; (b) Differential pulse voltammetry of **7-5** in 0.1 M n-Bu₄NPF₆/DCM calibrated to ferrocene signal from CV experiment.

The experimental results for **7-5** from CV are supported by DFT calculations of the core structure without alkyl substituents and the orbital surfaces of the frontier orbitals are shown in Figure 7.21. In addition, **7-6** has been simulated because no experimental data are available.

All three molecules exhibit a nodal plane at the pyrene-2,7-axis in the HOMO and LUMO. Large orbital coefficients are predicted for all LUMOs at the carbonyl group pointing towards a strong influence on the LUMO level. Nevertheless, **7-5** cannot be ranged with super-strong acceptors like TCNQ, but is in the range of pyrene-4,5,9,10-tetraone.^[46] The energy gaps determined by UV/vis absorption (2.23 eV) and CV (1.99 eV) fit quite well to the calculated value of 2.44 eV, keeping in mind that the four electron donating *tert*-butyl groups are not considered in the calculation. For **7-6** an increase of the energy gap was computed by 0.25 eV, which is in line with the trend reported for helianthrone and **I7-4**.^[30]

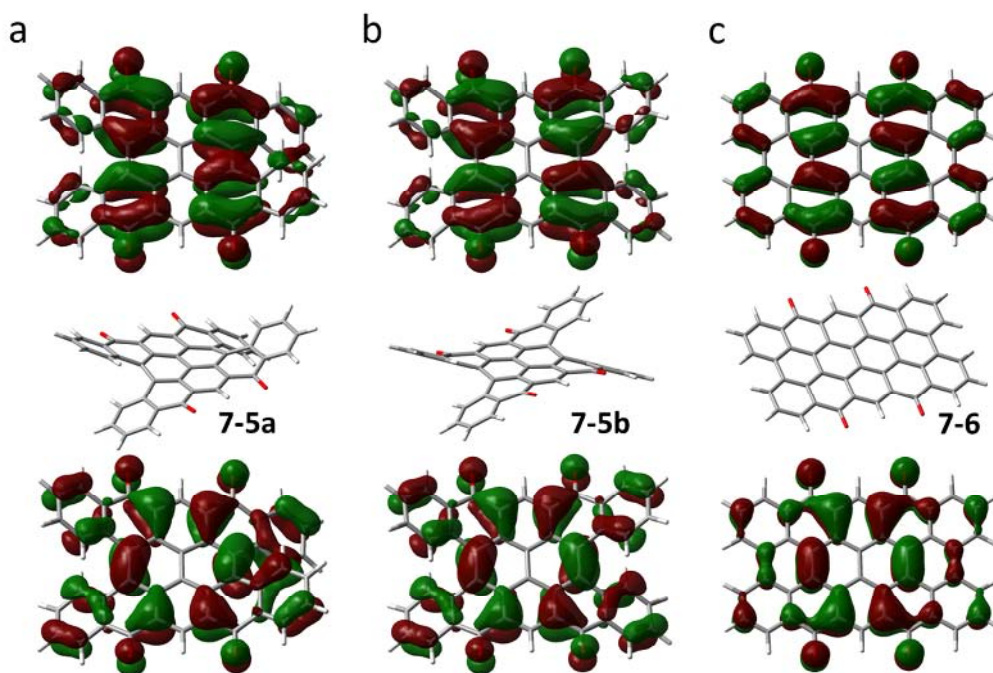


Figure 7.21: Orbital surfaces of the HOMO (below) and LUMO (above) of core structures of **7-5a** (a), **7-5b** (b) and **7-6** (c) (from left to right) determined by DFT/B3LYP calculations using 6-31G(d) basis set.

Table 7.2: Electronic properties of compounds **7-3**, **7-5** and **7-6**.^[a]

| | $E_{\text{red1,onset}}$ | $E_{\text{red2,onset}}$ | $E_{\text{ox1,onset}}$ | $E_{\text{HOMO(CV)}}^{[b]}$ | $E_{\text{LUMO(CV)}}^{[c]}$ | $E_{\text{HOMO(cal)}}^{[d]}$ | $E_{\text{LUMO(cal)}}^{[d]}$ |
|------------|-------------------------|-------------------------|------------------------|-----------------------------|-----------------------------|------------------------------|------------------------------|
| 7-3 | - 0.57 V | - | * | * | - 3.63 eV | - | - |
| 7-5 | - 0.15 V | - 0.38 V | + 1.84 V | - 6.04 eV | - 4.05 eV | - 6.06 eV ^[e] | - 3.62 eV ^[e] |
| 7-6 | - | - | - | - | - | - 6.24 eV | - 3.55 eV |

[a] CV is measured in 0.1 M $n\text{-Bu}_4\text{NPF}_6/\text{DCM}$ with a scan rates between of 25 mV/s and 50 mV/s; values calculated using the ferrocene as internal standard: [b] $E_{\text{HOMO(CV)}} = -(E_{\text{ox,onset}} - E^{(1/2)}_{\text{Fc/Fc}^+} + 4.8) \text{ eV}$; [c] $E_{\text{LUMO(CV)}} = -(E_{\text{red,onset}} - E^{(1/2)}_{\text{Fc/Fc}^+} + 4.8) \text{ eV}$; [d] Calculated DFT/B3LYP/6-31G(d) using Gaussian 03 W; [e] the value for **7-5a** is given; * could not be observed under experiment conditions.

7.5 Transformation of the Tetraketone Structure

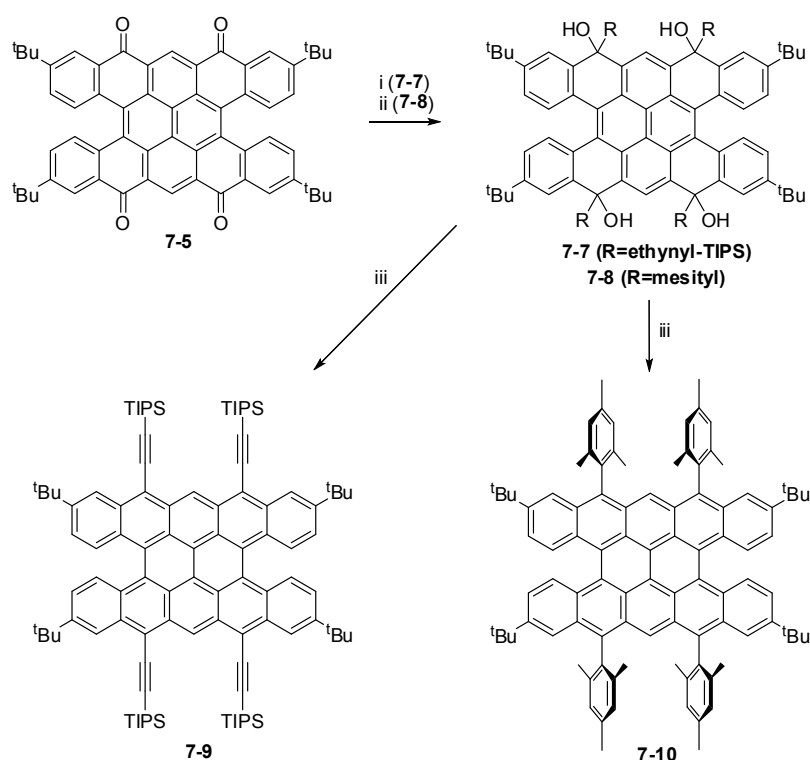
The transformation of the four ketone functions of **7-5** is a critical and highly challenging step on the herein selected path towards *peri*-pentacene. One has to be aware that the aromatization of **7-5** to the fully conjugated PAH comes along with the difficulties like instability and high reactivity as described in the beginning of this chapter. Nevertheless, efforts were made to approach the target molecule although characterization was mainly limited to mass spectrometry or optical methods.

Nucleophilic Attack onto the Carbonyl Function

The attack of aryl Grignard reagents on **I7-7** (Scheme 7.1 page 166) leads to Michael 1,4-addition followed by oxidative rearomatization.^[29] No reaction on the carbonyls of **I7-7** has so far been reported. Therefore, nucleophilic attack onto **7-5** was investigated (Scheme 7.4).

At first, well-established TIPS-ethynyl lithium attack was chosen as this protocol has often been used for the synthesis of TIPS-ethynyl pentacene. Excess (25 eq.) of the lithium nucleophile gave a mixture of two-, three- and fourfold substituted species **7-7** judged from MS (Figure 7.22). The most intense signal fits to threefold substitution. Increasing the excess of the lithium reagent did not drive the reaction to the fully substituted species. The MALDI-TOF mass spectrum already indicated the loss of OH-groups which might have happened during the ionization process.

In order to reduce the alcohol **7-7** to **7-9** the crude reaction mixture was treated with sodium iodine, sodium hypophosphite and degassed acetic acid under reflux for two hours. The mass analysis with MALDI-TOF MS showed successful reduction of partially and fully substituted species (Figure 7.22).



Scheme 7.4: Nucleophilic attacked followed by reduction. Conditions: *i* TIPS-acetylene, *n*-BuLi, THF, 0°C, 40 min; *ii* mesityl-MgBr, CeCl₃, THF, -30°C, 2h; *iii* NaI, NaH₂PO₂·H₂O, THF, AcOH, reflux, 2h.^[20, 47]

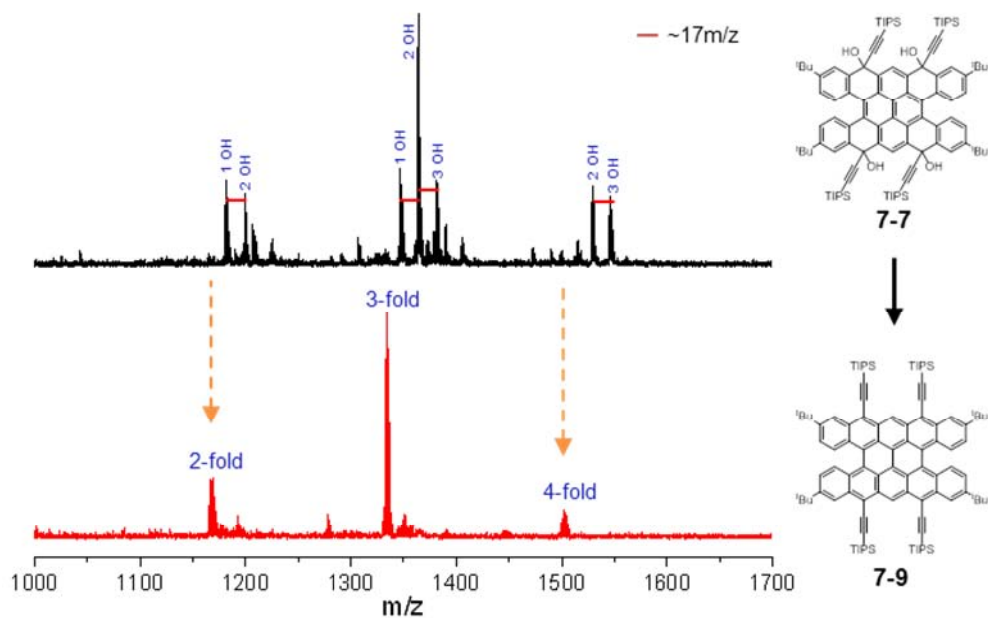


Figure 7.22: MALDI-TOF MS spectra of **7-7** (above) and **7-9** (below).

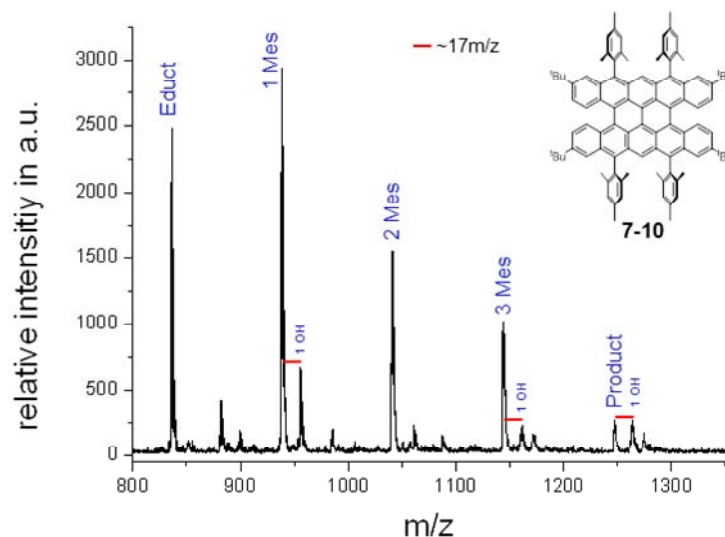
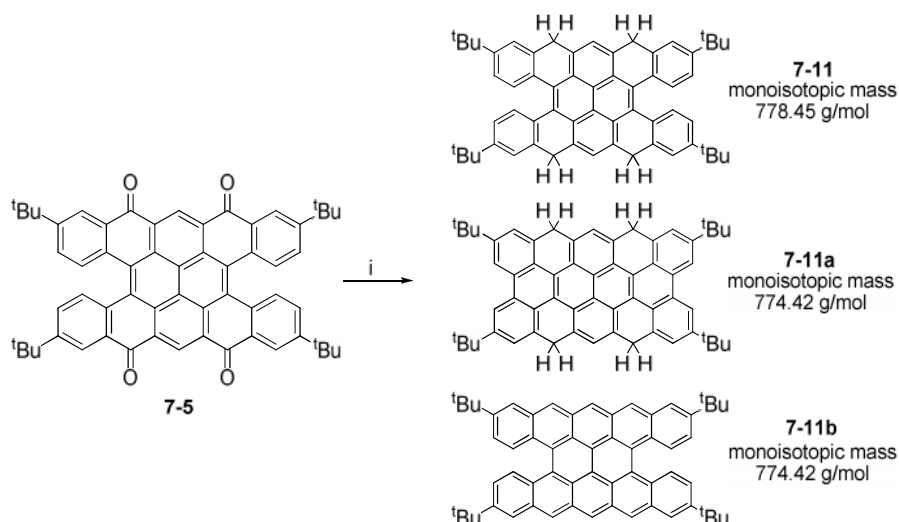


Figure 7.23: MALDI-TOF MS spectrum of **7-10** with enhanced depiction of the product signal with calculated isotopic distribution.

Purification after the nucleophilic attack or the reduction step by chromatography failed most probably due to instability of the product and the small amount of actually fourfold substituted **7-9**.

During the synthesis of teranthene **17-6** successful decoration with mesityl moieties was reported.^[20] Those conditions with cerium(III) chloride and 56 eq. of mesityl-MgBr were also applied on **7-5**. For reduction NaI and NaH₂PO₂ were used in AcOH at elevated temperature and MALDI-TOF MS was performed from the crude mixture to minimize the contact with air (Figure 7.23). Beside the starting material and the product **7-10** the peak pattern shows all three intermediates bearing one, two and three mesityl groups. The intensity decreases towards multiple substitutions and partially incomplete reduction was also found.

Although neither **7-9** nor **7-10** could be isolated from the reaction mixture these results prove the nucleophilic attack onto ketone functions and highlight the strength and weakness of the pyrene-based approach at the same time: on the one hand the ketone functions of **7-5** are accessible *via* nucleophiles, on the other hand the fourfold reaction suffers from incompleteness, and thus, low yields.



Scheme 7.5: Reduction of tetraketone **7-5** with hydroiodic acid to the hydrogen protected PAH **7-11**. Conditions: *i* HI, AcOH, reflux, 5 d.

Reduction

In order to find alternative ways to approach the fully aromatic *peri*-pentacene structure the investigations were focused on the reduction of the ketone groups of precursor **7-5**. As described in literature, acenes or their quinone form can be partially reduced to the hydrogen protected species.^[48] In addition, the conversion of the electron withdrawing ketone to an electron donating or neutral group would possibly enable cyclodehydrogenation between outer ends of the molecule. Thus, **7-5** was treated with HI in acetic acid under reflux for five days to explore the reaction towards the hydrogen protected compound **7-11** (Scheme 7.5). The progress of the reduction was monitored by mass spectrometry and revealed stepwise reduction of the ketone groups by the loss of the oxygen atom over time.

The mass spectrum from the crude reaction mixture after five days is depicted in Figure 7.24. The main signal at 775.77 m/z differs by 4 m/z from the expected -mass of **7-11**. Thus, the formation of **7-11a** or **7-11b** instead of **7-11** seems likely (Figure 7.24 inset). In respect to their identical monoisotopic

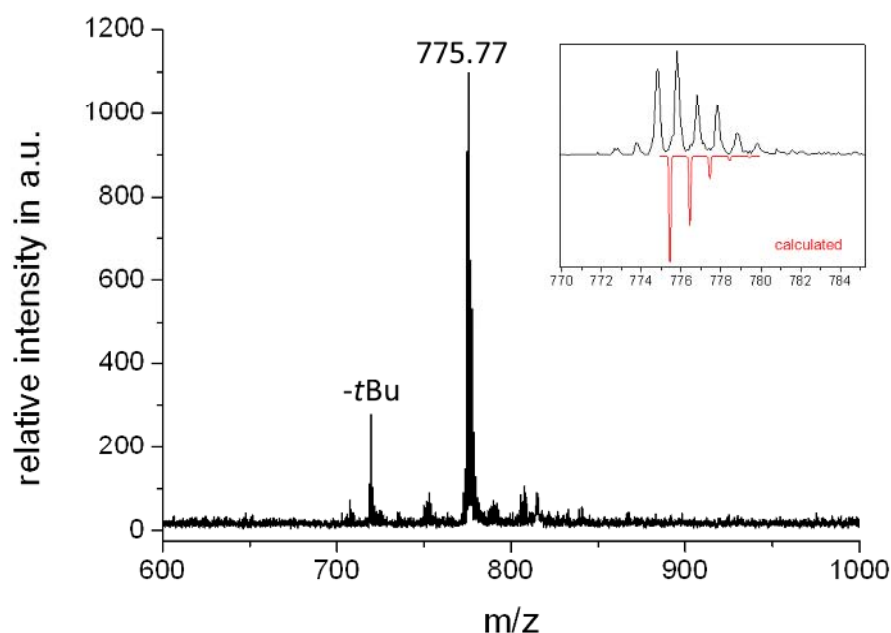


Figure 7.24: MALDI-TOF MS spectrum of **7-11**. Inset: product signal with calculated isotopic distribution $[\mathbf{7-11a/b}+\text{H}]^+$.

mass it can only be guessed whether reduction stopped at the fully aromatic PAH (**7-11b**) or the ring-closure occurred light or laser induced (**7-11a**) because neither **7-11a** nor **7-11b** could be isolated.

At second, the reductive loading of **7-5** with electrons in solution was tested under in situ visualization by UV/vis spectroscopy. Tetrabutylammonium borohydride (TBABH_4) is known as one-electron reduction agent and has already been used for stepwise reduction of PAHs.^[49-52]

Initial experiments with an excess of TBABH_4 in dry DCM led to a color change of the solution from purple to yellow and motivates for a careful study.

The titration spectra are depicted in Figure 7.25 in steps of 0.2 equivalents. The two strong bands at 393 nm 530 nm of the starting compound incrementally vanish whereas new bands in the near IR arise (major bands at 829 nm and 1096 nm). After the addition of roughly four equivalents no further change in the spectrum can be observed. The initial color totally recovers upon exposure to air indicating the reversibility of the reduction process.

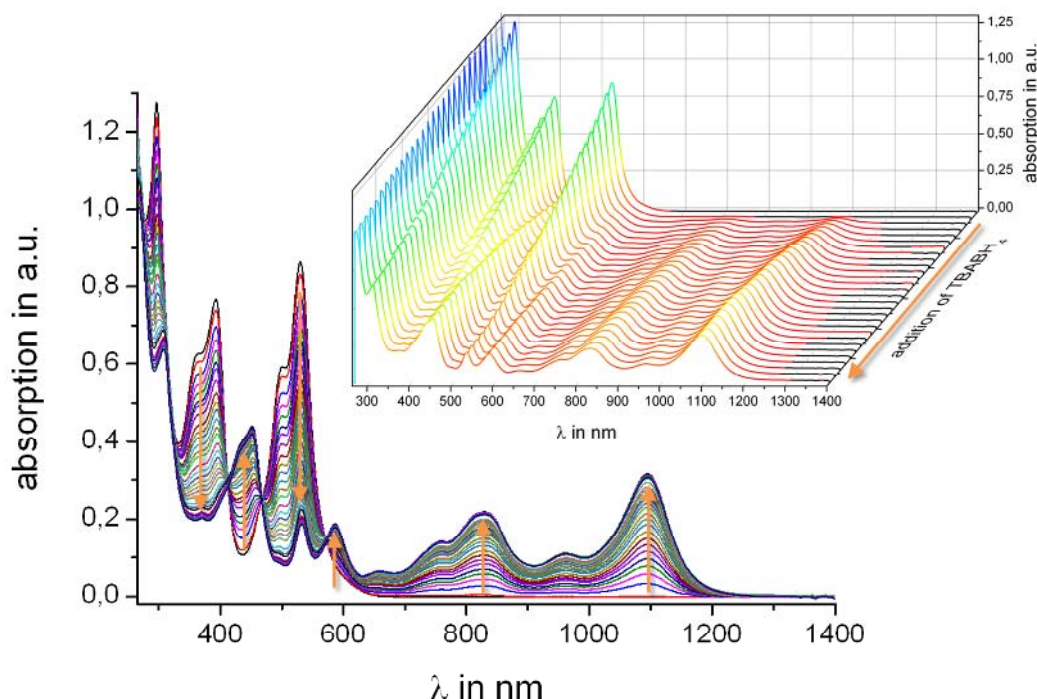


Figure 7.25: Reduction of **7-5** with stepwise addition of TBABH₄ monitored by UV/vis spectroscopy (inset: 3D depiction). Orange arrows indicate direction of changes upon addition of reduction agent.

It is assumed that only one species is obtained upon reduction with TBABH₄ because UV/vis spectroscopy could not resolve an intermediate species. In respect to the saturation of the titration experiment and two reduction processes observed by cyclic voltammetry the formation of the radical anion [7-5]^{•-} or the dianion [7-5]²⁻ in one step is proposed. Consequently, the proposed one- or twofold reduction of **7-5** can either result in a paramagnetic or diamagnetic species, respectively.

Electron Spin Resonance (ESR) spectroscopy was performed to probe the magnetic character of the reduced species. The addition of one equivalent reducing agent to a 10⁻⁴ M solution of **7-5** in degassed THF resulted in a weak ESR signal. Upon increasing excess (2 to 6 eq.) a strong signal was detected which remains stable for several days (Figure 7.26). Thus, the ESR experiment strongly supports the formation of the radical anion [7-5]^{•-}.

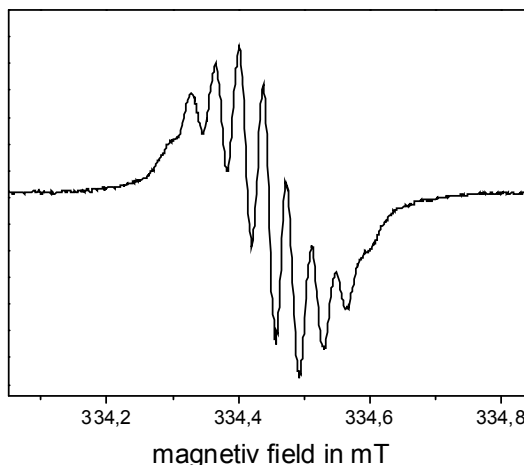


Figure 7.26: ESR spectrum of the proposed radical anion $[7-5]^{•-}$ after reduction of **7-5** with $TBABH_4$ in dilute (10^{-4} M) dry THF solution and argon atmosphere at 298 K. Experimental parameters: 9.4 (9.3941) GHz, 100 kHz modulation frequency, $g_{iso}=2.0035\pm0.0003$, $A_{iso}\sim0.035$ mT.

In addition, NMR spectroscopy was applied to monitor the reduction at $5\cdot10^{-3}$ M concentration in CD_2Cl_2 . All initial signals of **7-5** vanished upon the addition of one equivalent $TBABH_4$ which speaks for the formation of paramagnetic radical anion $[7-5]^{•-}$.

Because of the stability of the radical $[7-5]^{•-}$ MALDI-TOF mass spectrometry was used in negative mode to detect the anionic species. Therefore, the sample of the NMR experiment was mixed with DCTB and quickly applied to the measurement to minimize potential oxidation. Beside an intense signal of $[(DCTB)_3BH_4]^-$ the spectrum depicted in Figure 7.27 shows the radical anion $[7-5]^{•-}$ at 834.45 m/z which matches with the calculated isotopic distribution (Figure 7.27 inset). In positive mode only the cation $[Bu_4N]^+$ at 242.25 m/z was observed.

In order to achieve multiply reduced species of **7-5** the reduction at extremely reactive metal surfaces like potassium or lithium constitutes a promising approach.^[53-56] Higher charged anions are expected to be highly sensitive to moisture and oxygen. Such investigation are planned to be conducted with collaborators.

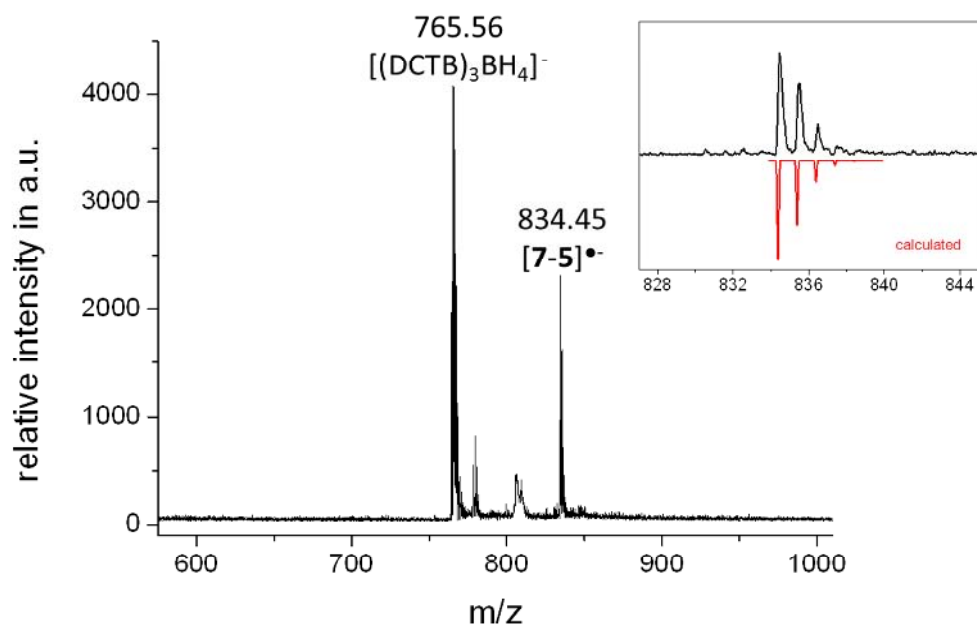


Figure 7.27: MALDI-TOF MS spectrum of **7-5** after reduction with TBABH₄ measured in negative mode (Matrix: DCTB; sample from NMR experiment was used). Inset: product signal with calculated isotopic distribution of [7-5]•⁻.

Furthermore, surface-controlled reaction under UHV conditions and simultaneous STM imaging shall be used to convert stable precursor **7-5** to the planar and fully aromatized PAH by collaborators.^[57-59]

7.6 Summary

An extensive work on approaches towards *peri*-pentacene has been presented in this chapter. 1,3,6,8-Tetrachlorinated 4,5,9,10-tetraphenylpyrene described in the previous chapter was used as basis for the synthesis of stable tetraketo precursors of the target *peri*-acene. The exchange of chlorine with cyano groups smoothed the way for acid-catalyzed fourfold ring-closure from pyrene positions 1, 3, 6 and 8 to the outer phenyl rings. In this way, a planar and a non-planar tetraketo *peri*-pentacene could be isolated.

The non-planar species is well soluble in organic solvents which arises from dragonfly shape due to a spatial overlap of the inner hydrogens in the *ffords* at each side of the molecule. NMR experiments revealed the coexistence of at least two atropo-isomers at room temperature, whereas coalescence of the signals occurs at elevated temperature. HPLC using a chiral stationary phase enabled differentiation of three signals which interconvert even at room temperature into the initial atropo-isomeric mixture.

The optical and electronic properties of both tetraketo compounds have further been studied. The dragonfly shaped form shows two intense absorption bands at 389 nm and 524 nm as well as an optical energy gap of 2.23 eV. Despite four *tert*-butyl groups the planar tetraketo *peri*-pentacene could only be dissolved in concentrated acids by protonation. Because DFT calculations predict only small differences for the energy levels of the frontier orbitals, the non-planar precursor has been carefully investigated in place of the planar form.

Cyclic voltammetry revealed two reversible reduction waves at - 0.15 V and - 0.38 V and one irreversible oxidation process at 1.84 V corresponding to an energy gap of 1.99 eV. Differential pulse voltammetry further clarified two one-electron processes for the reduction.

Transformation of the carbonyl functions was conducted to approach the fully conjugated *peri*-pentacene. Therefore, two strategies have been pursued:

the nucleophilic attack on the ketones and the reductive electron loading of the *peri*-pentacene scaffold.

The reaction of nucleophiles TIPS-ethynyl lithium and mesityl-MgBr yielded incomplete ketone attack in both cases and the respective substituted compounds could not be isolated. Nevertheless, MS analysis clearly indicated that no 1,4-Michael addition occurred as described for **17-7**.^[29] This result fulfills a major motivation for the here presented pyrene based synthetic approach.

For electron loading the rather mild one-electron transfer reducing agent TBABH₄ was used. The radical anion was formed which exhibits two strong absorption bands in the NIR. ESR spectroscopy proved the paramagnetic character. The onefold reduction was found to be reversible by reoxidation in air which is in accordance with reversibility of the reduction processes observed from cyclic voltammetry.

Perspectively, higher charged anions shall be generated using alkali metals as highly reactive electron sources under the strict exclusion of oxygen and moisture. The tetraanionic species is of particular interest because the four additional electrons lead to the desired acene-like conjugation and would be the synthetically closest approach towards the electronic structure of *peri*-pentacene so far.

7.7 Bibliography

- [1] J. E. Anthony, *Angewandte Chemie-International Edition* **2008**, *47*, 452-483.
- [2] J. E. Anthony, *Chemical Reviews* **2006**, *106*, 5028-5048.
- [3] R. Rieger, K. Müllen, *Journal of Physical Organic Chemistry* **2010**, *23*, 315-325.
- [4] J.-i. Aihara, *Physical Chemistry Chemical Physics* **1999**, *1*, 3193-3197.
- [5] A. Maliakal, K. Raghavachari, H. Katz, E. Chandross, T. Siegrist, *Chemistry of Materials* **2004**, *16*, 4980-4986.
- [6] C. R. Kagan, A. Afzali, T. O. Graham, *Applied Physics Letters* **2005**, *86*.
- [7] D. Biermann, W. Schmidt, *Journal of the American Chemical Society* **1980**, *102*, 3163-3173.
- [8] J. Sauer, R. Sustmann, *Angewandte Chemie-International Edition in English* **1980**, *19*, 779-807.
- [9] J. E. Anthony, J. S. Brooks, D. L. Eaton, S. R. Parkin, *Journal of the American Chemical Society* **2001**, *123*, 9482-9483.
- [10] C. Tonshoff, H. F. Bettinger, *Angewandte Chemie-International Edition* **2010**, *49*, 4125-4128.
- [11] I. Kaur, M. Jazdyk, N. N. Stein, P. Prusevich, G. P. Miller, *Journal of the American Chemical Society* **2010**, *132*, 1261-+.
- [12] S. S. Zade, M. Bendikov, *Angewandte Chemie-International Edition* **2010**, *49*, 4012-4015.
- [13] B. Purushothaman, M. Bruzek, S. R. Parkin, A. F. Miller, J. E. Anthony, *Angewandte Chemie-International Edition* **2011**, *50*, 7013-7017.
- [14] D. E. Jiang, B. G. Sumpter, S. Dai, *Journal of Chemical Physics* **2007**, *127*.
- [15] Z. Sun, J. S. Wu, *Journal of Materials Chemistry* **2012**, *22*, 4151-4160.
- [16] D. E. Jiang, S. Dai, *Chemical Physics Letters* **2008**, *466*, 72-75.
- [17] J. H. Wang, D. Y. Zubarev, M. R. Philpott, S. Vukovic, W. A. Lester, T. A. Cui, Y. Kawazoe, *Physical Chemistry Chemical Physics* **2010**, *12*, 9839-9844.
- [18] F. Moscardo, E. San-Fabian, *Chemical Physics Letters* **2009**, *480*, 26-30.
- [19] Y. Kobayashi, K. Fukui, T. Enoki, K. Kusakabe, Y. Kaburagi, *Physical Review B* **2005**, *71*.
- [20] A. Konishi, Y. Hirao, M. Nakano, A. Shimizu, E. Botek, B. Champagne, D. Shiomi, K. Sato, T. Takui, K. Matsumoto, H. Kurata, T. Kubo, *Journal of the American Chemical Society* **2010**, *132*, 11021-11023.
- [21] C. Lambert, *Angewandte Chemie-International Edition* **2011**, *50*, 1756-1758.

- [22] M. Chikamatsu, T. Mikami, J. Chisaka, Y. Yoshida, R. Azumi, K. Yase, A. Shimizu, T. Kubo, Y. Morita, K. Nakasuji, *Applied Physics Letters* **2007**, *91*.
- [23] T. Kubo, A. Shimizu, M. Uruichi, K. Yakushi, M. Nakano, D. Shiomi, K. Sato, T. Takui, Y. Morita, K. Nakasuji, *Organic Letters* **2007**, *9*, 81-84.
- [24] C. Li, H. Wonneberger, *Advanced Materials* **2012**, *24*, 613–636.
- [25] J. H. Yao, C. Y. Chi, J. S. Wu, K. P. Loh, *Chemistry-a European Journal* **2009**, *15*, 9299-9302.
- [26] K. Zhang, K. W. Huang, J. L. Li, J. Luo, C. Y. Chi, J. S. Wu, *Organic Letters* **2009**, *11*, 4854-4857.
- [27] J. Aihara, *Physical Chemistry Chemical Physics* **1999**, *1*, 3193-3197.
- [28] X. J. Zhang, X. X. Jiang, J. Luo, C. Y. Chi, H. Z. Chen, J. S. Wu, *Chemistry-a European Journal* **2010**, *16*, 464-468.
- [29] X. J. Zhang, J. L. Li, H. Qu, C. Y. Chi, J. S. Wu, *Organic Letters* **2010**, *12*, 3946-3949.
- [30] U. Müller, V. Enkelmann, M. Adam, K. Müllen, *Chemische Berichte-Recueil* **1993**, *126*, 1217-1225.
- [31] P. M. Donovan, L. T. Scott, *Polycyclic Aromatic Compounds* **2008**, *28*, 128-135.
- [32] S. D. Walker, T. E. Barder, J. R. Martinelli, S. L. Buchwald, *Angewandte Chemie-International Edition* **2004**, *43*, 1871-1876.
- [33] L. H. Schwartz, C. Koukotas, P. Kukkola, C. S. Yu, *Journal of Organic Chemistry* **1986**, *51*, 995-999.
- [34] C. H. Kuo, M. H. Tsau, D. T. C. Weng, G. H. Lee, S. M. Peng, T. Y. Luh, P. U. Biedermann, I. Agranat, *Journal of Organic Chemistry* **1995**, *60*, 7380-7381.
- [35] G. Pawlowski, M. Hanack, *Synthesis-Stuttgart* **1980**, 287-289.
- [36] C. A. Strassert, L. E. Dicelio, J. Awruch, *Synthesis-Stuttgart* **2006**, 799-802.
- [37] J. S. Yang, H. H. Huang, S. H. Lin, *Journal of Organic Chemistry* **2009**, *74*, 3974-3977.
- [38] T. Takada, M. Arisawa, M. Gyoten, R. Hamada, H. Tohma, Y. Kita, *Journal of Organic Chemistry* **1998**, *63*, 7698-7706.
- [39] P. Rempala, J. Kroulik, B. T. King, *Journal of Organic Chemistry* **2006**, *71*, 5067-5081.
- [40] C. L. Eversloh, Z. H. Liu, B. Müller, M. Stangl, C. Li, K. Müllen, *Organic Letters* **2011**, *13*, 5528-5531.
- [41] H. J. Lindner, *Tetrahedron* **1975**, *31*, 281-284.
- [42] Y. Shen, C.-F. Chen, *Chemical Reviews* **2011**.
- [43] H. Brockmann, R. Randebrock, *Chemische Berichte-Recueil* **1951**, *84*, 533-545.
- [44] Brookhar.M, G. C. Levy, S. Winstein, *Journal of the American Chemical Society* **1967**, *89*, 1735-&.
- [45] C. Y. Chi, G. Wegner, *Macromolecular Rapid Communications* **2005**, *26*, 1532-1537.

- [46] R. Rieger, Ph.D. thesis, University of Mainz **2009**.
- [47] T. Imamoto, N. Takiyama, K. Nakamura, T. Hatajima, Y. Kamiya, *Journal of the American Chemical Society* **1989**, *111*, 4392-4398.
- [48] A. J. Athans, J. B. Briggs, W. L. Jia, G. P. Miller, *Journal of Materials Chemistry* **2007**, *17*, 2636-2641.
- [49] X. Z. Zhu, H. Tsuji, K. Nakabayashi, S. Ohkoshi, E. Nakamura, *Journal of the American Chemical Society* **2011**, *133*, 16342-16345.
- [50] T. M. Pappenfus, J. D. Raff, E. J. Hukkanen, J. R. Burney, J. Casado, S. M. Drew, L. L. Miller, K. R. Mann, *Journal of Organic Chemistry* **2002**, *67*, 6015-6024.
- [51] M. Lucarini, G. F. Pedulli, *Journal of Organometallic Chemistry* **1995**, *494*, 123-131.
- [52] M. Lucarini, G. F. Pedulli, A. Alberti, C. Paradisi, S. Roffia, *Journal of the Chemical Society-Perkin Transactions 2* **1993**, 2083-2087.
- [53] Y. Cohen, A. Y. Meyer, M. Rabinovitz, *Journal of the American Chemical Society* **1986**, *108*, 7039-7044.
- [54] R. Benshafrut, R. E. Hoffman, M. Rabinovitz, K. Müllen, *Journal of Organic Chemistry* **1999**, *64*, 644-647.
- [55] I. Aprahamian, D. V. Preda, M. Bancu, A. P. Belanger, T. Sheradsky, L. T. Scott, M. Rabinovitz, *Journal of Organic Chemistry* **2006**, *71*, 290-298.
- [56] I. Aprahamian, H. A. Wegner, T. Sternfeld, K. Rauch, A. De Meijere, T. Sheradsky, L. T. Scott, M. Rabinovitz, *Chemistry-an Asian Journal* **2006**, *1*, 678-685.
- [57] J. M. Cai, P. Ruffieux, R. Jaafar, M. Bieri, T. Braun, S. Blankenburg, M. Muoth, A. P. Seitsonen, M. Saleh, X. L. Feng, K. Müllen, R. Fasel, *Nature* **2010**, *466*, 470-473.
- [58] G. Otero, G. Biddau, C. Sanchez-Sanchez, R. Caillard, M. F. Lopez, C. Rogero, F. J. Palomares, N. Cabello, M. A. Basanta, J. Ortega, J. Mendez, A. M. Echavarren, R. Perez, B. Gomez-Lor, J. A. Martin-Gago, *Nature* **2008**, *454*, 865-U819.
- [59] K. T. Rim, M. Sij, S. X. Xiao, M. Myers, V. D. Carpentier, L. Liu, C. C. Su, M. L. Steigerwald, M. S. Hybertsen, P. H. McBreen, G. W. Flynn, C. Nuckolls, *Angewandte Chemie-International Edition* **2007**, *46*, 7891-7895.

8 Conclusion and Outlook

This work describes the asymmetric functionalization of pyrene in the K-region and the thereby enabled design and synthesis of novel pyrene based materials. Various patterns of substitution have been successfully accomplished in order to tailor the properties for the respective application.

The bromination of 4,5-diketopyrene in the opposite K-region constitutes the key step and extends the toolbox of pyrene chemistry. The choice of these two functions with orthogonal reactivity enabled the introduction of asymmetric substitution patterns and opened the way for new pyrene derived materials (Figure 8.1).

In the first part of this work (Chapter 3), the asymmetrically substituted precursor has been used to induce a permanent dipole from one to the other K-region of pyrene by donor and acceptor units (Figure 8.1 left). Thus, an alternating donor-above-acceptor order of the molecules in stacks results from the favorable antiparallel arrangement of the dipoles in the solid state. In solution strong dependency of the fluorescence on the solvent polarity was observed which allows the use as solvent polarity sensor. According of the strength of the attached donor or acceptor moiety the level of the frontier orbitals can be controlled.

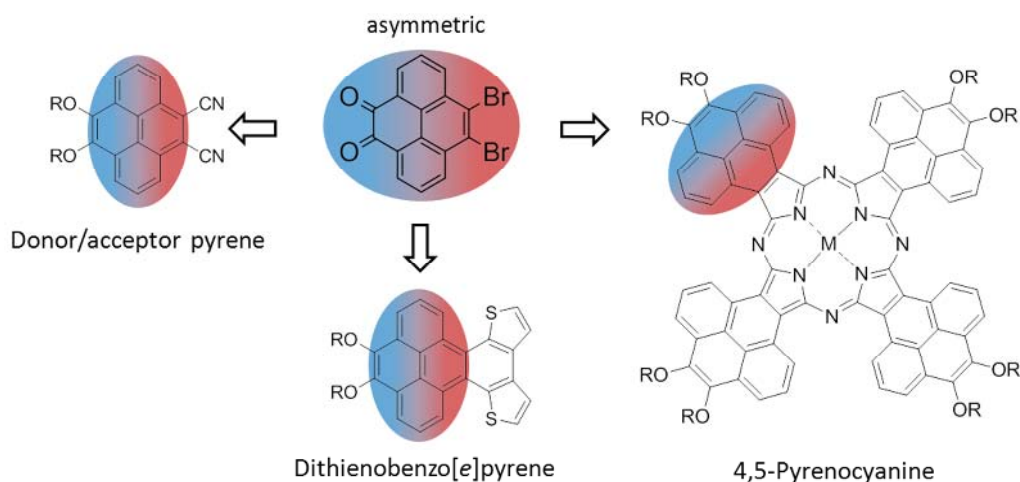


Figure 8.1: Schematic illustration of pyrene based new materials derived from asymmetrically substituted pyrene building block.

At second (Chapter 4), the unique shape of pyrene has been used for the synthesis of non-planar 4,5-pyrenocyanines (Pycs) (Figure 8.1 right). The distortion of Pycs arises from the twofold angularly annulated rings and leads to a broad Q-band absorption. The peripheral substitution with alkyl chains provides solubility for the large aromatic molecules and induces self-organizing behavior. At the liquid/solid interface STM revealed the self-assembly into two-dimensional layers on HOPG. For the metal-free pyrenocyanine contrast variations were observed which are attributed to multiplicity in the adsorption geometry. The STM data support the assumption of a cooperative effect during the annealing process which offers the possibility of reversible switching between two different conformations on the surface and could be of potential interest for building molecule-based switches.

The investigation of zinc pyrenocyanines in bulk by 2D WAXS revealed a transition from a columnar to a helical columnar arrangement on changing the spatial demand of the side chains from linear to branched ones. It is assumed that changing the degree of branching and length of the side chains can be used to tune the molecular rotation angle being a straightforward way to control the intracolumnar packing by molecular design.

Thirdly (Chapter 5), two thiophene moieties have been introduced to the pyrene core in *ortho*-position by palladium-catalyzed Stille reaction (Figure 8.1 bottom). Oxidative ring-closure between adjacent thienyl rings to dithienobenzo[*e*]pyrenes crucially influence the molecular order in the solid state towards parallel and close π -contact herringbone packing motif. Alkoxy chains at the opposite K-region contribute sufficient solubility of the molecules, and thus, allow the fabrication of organic field-effect transistors from solution. Hole transport could be measured with charge carrier mobilities in the range of $10^{-3} \text{ cm}^2 \text{ V}^{-1} \text{ s}^{-1}$ being a top value for pyrene derived semiconductors. Differing from commonly used rod-like and star-shaped molecular symmetries, this is the first example of new “head-tail” shaped organic semiconductors.

At fourth (Chapter 6), the asymmetric pyrene has been converted into a chemically symmetric building block by reductive triflatization of the α -diketone group (Figure 8.2). Thus, fourfold Suzuki coupling to 4,5,9,10-tetraarylpyrene is made possible and forms the synthetic basis for differently shaped PAHs.

Oxidative ring-closure between outer phenyl ring required prior blocking of positions 1, 3, 6 and 8 by chlorination to yield hexaaryl[*a,c,fg,j,l,op*]tetracene. Although the nomenclature refers to tetracene the sixfold arylation strongly stabilizes the molecule and no acene-like properties can be found. The four *cove* regions force the molecule into a saddle conformation due to the steric demand of inner chlorine and hydrogen atoms. Hence, such accumulation of *coves* is a promising structural motif to mimic curved PAHs. Furthermore, the chlorine substitution in the *cove* makes this molecule a precursor for the synthesis of bowl-shaped molecules *via* flash-vacuum pyrolysis.

In the last part (Chapter 7), so far developed protocols for the functionalization of pyrene provided the experimental basis for the synthetic approach towards *peri*-pentacene. The route pursued in this work focused on stable precursors whose acene-like π -conjugation is interrupted by ketone groups. The challenging synthesis of the two long *zig-zag* edges could be accomplished by the sequence of four intramolecular Friedel-Crafts-like

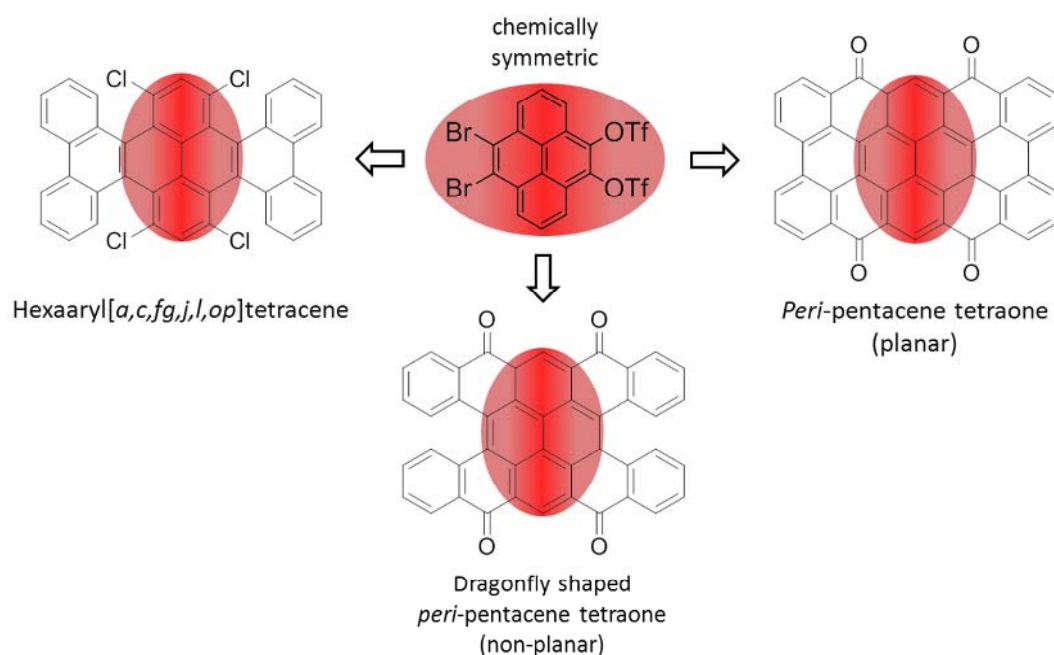


Figure 8.2: Schematic illustration of PAHs with different shape derived from chemically symmetric pyrene K-region building block.

electrophilic aromatic substitutions. One planar and one non-planar tetraketo form could be obtained (Figure 8.2 right and bottom). Despite peripheral fourfold substitution with *tert*-butyl groups the planar species solely dissolved in concentrated acids by protonation of the ketones which precluded further steps. Instead, the non-planar species with two *ffjords* is forced into a dragonfly form by the twist of the peripheral benzo units, and thus, facilitates solubility. The dragonfly shaped ketone precursor is easy to handle and opens the way to approach the fully aromatic *peri*-pentacene exhibiting acene-like conjugation.

Electron loading could be achieved with one electron to the radical anion which has been studied by UV/vis, NMR and ESR spectroscopy and mass spectrometry. Further reduction with alkali metals holds promise for higher charged anions. Beside the wet chemical approaches, surface mediated chemistry shall be used for the sequential planarization and reduction to the fully conjugated species after deposition.

The herein described syntheses, structural diversity and properties of the new molecules can only give a first impression of the scope of this asymmetric and

symmetric K-region substitution of pyrene. In fact, peripherally alkyl substituted macrocycles by 4,5-linkage with ethynyl or phenyl bridging promise interesting optical and self-assembling properties. The asymmetric substitution might further be used as fluorescent core for two-faced dendritic structures in order to design trackable and functional drug carriers.

So far, the issue of asymmetric substituted and *tert*-butylated pyrene derivatives has been left aside in respect to synthetic reasons, structural design and device requirements. But indeed, the bulky *tert*-butyl groups are favorable for materials in organic light-emitting diodes to minimize the red-shift of the fluorescence in the solid state. Beside the small molecular approach, homo- or copolymerization with phenyl spacers at positions 4 and 5 should yield highly twisted, and thus, well soluble and electronically decoupled poly(4,5-pyrenylene)s for blue emission.

9 Experimental Part

9.1 General Methods

9.1.1 Chemicals and Solvents

All used chemicals and solvents were obtained from the companies ABCR, Acros Organics, Alpha-Aesar, Bio-Rad Laboratories Inc., Fluka, Merck, Sigma-Aldrich, Strem Chemicals and TCI Europe. Unless otherwise mentioned, they were used as received without further purification.

9.1.2 Inert Atmosphere

Oxygen or moisture sensitive reactions were carried out under argon atmosphere (Linde). Reactions were degassed by bubbling a stream of argon through the reaction mixture.

9.1.3 UV Reactions

UV reactions were carried out in a Rayonet RPR-100 with up to six lamps (20 W each) of 300 nm. The lamps possess a half width wavelength distribution of 40 nm. The apparatus is equipped with a 15 W air fan and a magnetic stirrer. Reaction vessels of quartz glass were used to provide transparency for the UV light.

9.2 Analytical Techniques

9.2.1 Melting points

Melting points were determined on a Büchi Melting Point B-545 apparatus and are uncorrected.

9.2.2 Mass Spectrometry

Field-desorption mass spectra were obtained on a VG Instruments ZAB 2-SE-FPD spectrometer.

MALDI-TOF spectrometry was conducted on a Bruker Reflex II TOF spectrometer. If not specifically mentioned, dithranol was used as the matrix substance.

MALDI-FTMS measurements were performed on a IonSpec Ultima 4.7T MALDI-FTMS (IonSpec Ltd., Lake Forest California), with a Diode-Pumped laser (Spectra-Physics, Germany). The system was external calibrated in positive mode.

High resolution mass spectrometry was performed on an ESI-Q-TOF system (maXis, Bruker Daltonics, Germany). The instrument was operated in wide pass quadrupole mode, for MS experiments, with the TOF data being collected between m/z 100–5000 with low-collision energy of 10–15 eV.

High resolution experiments were performed by [REDACTED] (MS LOC, ETH Zürich). If not otherwise noted, the isotope of highest abundance was used for comparison.

9.2.3 NMR Spectrometry

^1H NMR, ^{13}C NMR, H,H-COSY , C,H-COSY and NOESY spectra were measured in different deuterated solvents and at temperatures as stated on Bruker DPX 250, Bruker AMX 300, Bruker DRX 500 or a Bruker DRX 700 spectrometer. The spectra were referenced as follows from the deuterated solvents: for CHDCl_2 $\delta(^1\text{H}) = 5.32$ ppm and CD_2Cl_2 $\delta(^{13}\text{C}) = 54.00$ ppm; for CDCl_3 $\delta(^1\text{H}) = 7.24$ ppm and $\delta(^{13}\text{C}) = 77.23$ ppm; for THF $\delta(^1\text{H}$ low field signal) = 3.58 ppm and THF- d_8 $\delta(^{13}\text{C}) = 67.57$ ppm; for $\text{C}_2\text{D}_2\text{Cl}_4$: for C_2DHCl_4 $\delta(^1\text{H}) = 5.91$ ppm and $\delta(^{13}\text{C}) = 74.20$ ppm; for DMSO $\delta(^1\text{H}) = 2.50$ ppm and $\delta(^{13}\text{C}) = 39.51$ ppm.

The temperature dependent experiments were performed between 298 K and 393 K and regulated by a standard ^1H methanol (low temperature) and glycol (high temperature) NMR sample.

9.2.4 Elemental Analysis

Elemental analysis of solid samples was carried out on a Foss Heraeus Vario EL as a service of the Institute for Organic Chemistry, Johannes Gutenberg-University of Mainz. All samples were dried under high vacuum overnight in

order to remove possible residuals of solvent molecules and humidity. Values for waxy pyrenocyanines show higher variance than 0.40 % from calculated values because of the difficulties to remove residual solvents and atmospheric gases like CO₂.

9.2.5 UV/vis Spectroscopy

The spectra are recorded in given concentrations and solvents on a Perkin-Elmer Lambda 900 UV/Vis/NIR spectrometer. The molar extinctions are given in the unit $\text{m}^2\text{mol}^{-1}$ which is consistent with the SI standard. Unless otherwise noted, a concentration of 10^{-5} mol/l was used for absorption between 0.1 and 1 at the wavelength region of experimental interest.

For temperature dependent measurements temperature was controlled using Perkin-Elmer PTP6 Peltier Temperature Programmer.

9.2.6 Fluorescence Spectroscopy

Fluorescence spectra were recorded using a SPEX-Fluorolog II (212) device with PMT R 508 and PMT R 928 detectors. Quartz cuvettes from Hellma with 1 cm thickness were applied.

9.2.7 IR Spectroscopy

A Nicolet 730 FT-IR spectrometer was used for recording IR spectra. Samples were deposited on the diamond crystal and pressed on it with a stamp. 64 measurements were recorded for each sample, the background was subtracted.

9.2.8 Voltammetry

Cyclic voltammetry was measured on a Princeton Applied Research Parstat 2273 instrument in anhydrous DCM under argon atmosphere in a total volume of 2 ml. Recrystallized and dried tetrabutylammonium hexafluorophosphate (Bu_4NPF_6) was used as conductive salt at 0.1 M concentration. To a 1 mM solution of the sample compound ferrocene was added as internal standard in equimolar concentration (1 mM). A platinum working electrode (0.5 mm diameter), a platinum wire as counter electrode, and a silver wire as quasi-reference electrode were applied. Scan rates between 25 mV/s and 100 mV/s gave best curves and are mentioned for each measurement. The peaks were calibrated according to the half-wave potential of ferrocene. The onset potentials were determined for the evaluation.

Differential Pulse Voltammetry was performed under same conditions mentioned above.

9.2.9 Field-Effect Transistors

Device fabrications and evaluations: For all devices, heavily doped silicon wafers with a 200 nm thick thermally grown silicon dioxide layer have been used as substrates. For the bottom gate, top contact OFETs, source and drain electrodes with channel geometries of $W/L = 20$ were defined by a shadow mask, followed by Au evaporation to a height of 100 nm. In order to avoid interface trapping the silicon dioxide was modified by the gas phase processed (120°C) hexamethyldisilazane (HMDS). For the solution processing of the semiconductor the common organic solvent toluene has been used (2 mg/ml).

The transistor characteristics were studied under exclusion of UV-light at room temperature inside a nitrogen filled glovebox with an oxygen and

humidity level below 0.1 ppm. The device characteristics have been measured with a Keithley 4200 semiconductor characterization system.

The charge carrier mobilities were calculated *via*

$$I_{SD,sat} = \frac{W}{2L} \mu_{sat} C_i (V_{SG} - V_T)^2$$

with the current in the saturation region $I_{SD,sat}$, channel width W , channel length L ($W/L = 20$), capacitance per unit area of the gate insulator $C_i = 2.6 \times 10^{-8} \text{ Fcm}^{-2}$, the saturated charge-carrier field-effect mobility μ_{sat} , and the threshold voltage V_T .

9.2.10 X-Ray Scattering

Single crystal: Data collections for the crystal-structure analysis were performed on a Nonius-KCCD diffractometer. (Dr. [REDACTED])

Film X-ray: X-ray diffraction (XRD) measurements were recorded on a Siemens D-500 powder diffractometer (Cu-K α : 1.541 Å) with scan rate of 0.1°/20 s. ([REDACTED])

9.2.11 2D Wide Angle X-Ray Scattering

2D Wide Angle X-Ray Scattering was done in collaboration with Dr. [REDACTED], [REDACTED] and [REDACTED] from the Max Planck Institute for Polymer research in Mainz. The experiments were performed by using a rotating anode (Rigaku 18 kW) X-ray beam with pinhole collimation and a two-dimensional Siemens detector. A double-graphite monochromator for the CrK α radiation ($\lambda=0.154$) was used. The samples were prepared as thin filaments of 0.7 mm diameter by filament extrusion using a

home-made miniextruder and were positioned perpendicular to the incident X-ray beam and vertical to the 2D detector for the X-ray experiments.

9.2.12 Scanning Tunneling Microscopy

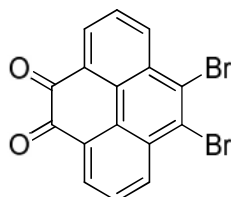
Scanning Tunneling Microscopy was done in collaboration with Dr. [REDACTED] (Katholieke Universiteit Leuven, Belgium). All experiments were performed at room temperature (20-22°C) using a PicoLE (Agilent) operating in constant-current mode with the tip immersed in the supernatant liquid. Prior to imaging, the pyrenocyanine molecules were dissolved in either 1-phenyloctane or tetradecane at concentrations between 1 and 3×10^{-5} M and a drop of this solution was applied onto a freshly cleaved surface of highly oriented pyrolytic graphite (HOPG). The experiments were repeated in several sessions using different tips to check for reproducibility and to avoid experimental artefacts, if any. The unit cell parameters were determined by examining at least 10 images and only the average values are reported. After the determination of the unit cell from the acquired STM images, a molecular model of the observed monolayer is constructed using HyperChem program. The imaging parameters are indicated in the figure caption: tunneling current (I_t), and sample bias (V_t).

9.2.13 Electron Spin Resonance Spectroscopy

ESR spectra were recorded in dilute, oxygen-free solutions at a concentration of $\sim 10^{-4}$ M, using a Bruker X-band spectrometer ESP300 E, equipped with an NMR gaussmeter (Bruker ER035), a frequency counter (Bruker ER041XK) and a variable temperature control continuous flow N₂ cryostat (Bruker B-VT 2000). The *g*-factor corrections were obtained using the DPPH (*g* = 2.0037) as a standard.

9.3 Donor/Acceptor Pyrenes

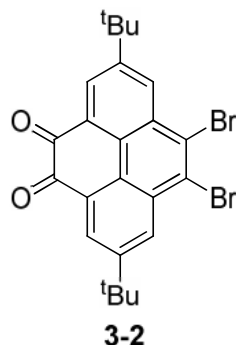
9.3.1 9,10-Dibromopyrene-4,5-dione



3-1

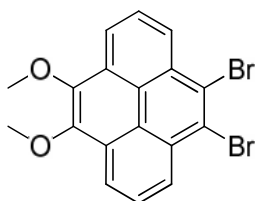
To a solution of 4,5-diketopyrene (2.0 g, 8.61 mmol) in 20 ml concentrated sulfuric acid N-bromosuccinimide (3.07 g, 17.25 mmol) was added and stirred for 4 hours at room temperature. The reaction mixture was precipitated in 2 L H₂O/ice, collected by filtration, washed with water and dried under high vacuum to give 9,10-dibromopyrene-4,5-dione in quantitative yield as bright brownish solid (mp: 360 °C (decomposition)); ¹H NMR (500 MHz, DMSO-d₆, 120°C) δ/ppm 8.72 (d, *J* = 8.3 Hz, 2H), 8.47 (d, *J* = 7.4 Hz, 2H), 7.98 (t, *J* = 7.9 Hz, 2H); ¹³C NMR (126 MHz, DMSO-d₆, 120°C) δ/ppm 178.07, 134.59, 130.24, 130.14, 129.45, 128.99, 127.55, 125.20; elemental analysis (%) found: C, 49.41; H, 1.73 - calculated for C₁₆H₆Br₂O₂: C, 49.27; H, 1.55.

9.3.2 9,10-Dibromo-2,7-di-*tert*-butylpyrene-4,5-dione



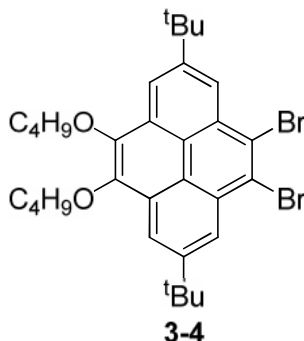
To a solution of 2,7-di-*tert*-butylpyrene-4,5-dione (3.00 g, 8.71 mmol) in 20 ml concentrated sulfuric acid N-bromosuccinimide (3.10 g, 17.42 mmol) was added and stirred for 4 hours at room temperature. The reaction mixture was precipitated in 2 L H₂O/ice, collected by filtration, washed with water and dried under high vacuum. The crude product was purified using column chromatography on silica with dichloromethane as eluent to give 9,10-dibromo-2,7-di-*tert*-butylpyrene-4,5-dione in 80 % yield as orange solid (mp: 225°C decomp.); MS (FD, 8 kV) m/z = 502.6 g/mol - calculated: 502.0 g/mol for C₂₄H₂₂Br₂O₂; ¹H NMR (250 MHz, CD₂Cl₂) δ 8.74 (d, J = 2.0 Hz, 2H), 8.59 (d, J = 2.0 Hz, 2H), 1.51 (s, 18H); ¹³C NMR (75 MHz, CD₂Cl₂) δ 180.54, 153.27, 133.53, 131.81, 130.44, 129.76, 127.24, 126.96, 36.04, 31.41; IR (neat, 1/λ in cm⁻¹) 2958, 2906, 2870, 1673, 1599, 1441, 1363, 1236, 1144, 1115, 1093, 974, 891, 800, 717, 667, 636, 580; elemental analysis (%) found: C, 58.30; H, 4.71 - calculated C₂₄H₂₂Br₂O₂: C, 57.39; H, 4.42.

9.3.3 4,5-Dibromo-9,10-dimethoxyppyrene

**3-3**

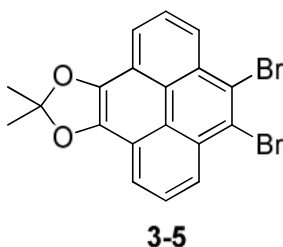
9,10-Dibromopyrene-4,5-dione (1.0 g, 2.56 mmol), Bu_4NBr (0.578 g, 1.79 mmol) and $\text{Na}_2\text{S}_2\text{O}_4$ (1.34 g, 7.7 mmol) were suspended in 16 ml THF and 9 ml water. Me_2SO_4 (1.8 g, 13.3 mmol) was added followed by 7 ml 4.5 M aqueous KOH and the reaction mixture was stirred capped with a condenser at 40°C overnight. DCM was added, the organic phase was extracted, dried over MgSO_4 and the organic solvent were removed under vacuum. Column chromatography on silica with PE:DCM 1:1, followed by crystallization from Ethanol gave 4,5-dibromo-9,10-dimethoxyppyrene (0.695 g, 1.66 mmol) as colorless crystals in 65 % yield (mp: 176 °C); MS (FD, 8 kV) m/z = 420.3 g/mol - calculated: 420.1 g/mol for $\text{C}_{18}\text{H}_{12}\text{Br}_2\text{O}_2$; ^1H NMR (300 MHz, CD_2Cl_2) δ /ppm 8.66 (dd, J = 8.0, 1.0 Hz, 2H), 8.59 (dd, J = 7.9, 0.9 Hz, 2H), 8.13 – 8.05 (m, 2H), 4.20 (s, 6H); ^{13}C NMR (75 MHz, CD_2Cl_2) δ /ppm 144.96, 130.88, 129.14, 127.71, 127.12, 126.74, 122.75, 121.73, 61.67; elemental analysis (%) found: C, 51.07; H, 2.89 - calculated for $\text{C}_{18}\text{H}_{12}\text{Br}_2\text{O}_2$: C, 51.46; H, 2.88.

9.3.4 4,5-Dibromo-9,10-dibutoxy-2,7-di-*tert*-butylpyrene



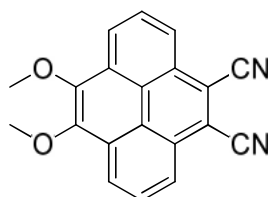
9,10-Dibromo-2,7-di-*tert*-butylpyrene-4,5-dione (2.30 g, 4.58 mmol), tetrabutylammonium bromide (1.03 g, 3.21 mmol) and sodium dithionite (2.39 g, 13.74 mmol) were suspended in a mixture of 35 ml THF and 20 ml water and stirred vigorously for five minutes at room temperature. 1-Bromobutane (1.96 ml, 18.32 mmol) and 15 ml of a 4 M aqueous potassium hydroxide solution were added subsequently the mixture was stirred at 40°C overnight. After dilution with dichloromethane the organic phase was separated and the aqueous phase was extracted with dichloromethane two times. Combined organic phases were dried over MgSO₄ and the solvent were removed under reduced pressure. The crude product was adsorbed on silica and purified by column chromatography with PE and crystallized from ethyl acetate twice to give 4,5-dibromo-9,10-dibutoxy-2,7-di-*tert*-butylpyrene (1.17 g, 3.79 mmol) as colorless solid in 41 % yield (mp: 170°C); MS (FD, 8 kV) m/z = 616.9 g/mol - calculated: 616.1 g/mol for C₃₂H₄₀Br₂O₂; ¹H NMR (250 MHz, CD₂Cl₂) δ /ppm 8.72 (d, J = 1.8 Hz, 2H), 8.67 (d, J = 1.9 Hz, 2H), 4.36 (t, J = 6.4 Hz, 4H), 2.04 – 1.90 (m, 4H), 1.78 – 1.66 (m, 4H), 1.62 (s, 18H), 1.07 (t, J = 7.3 Hz, 6H); ¹³C NMR (75 MHz, CD₂Cl₂) δ /ppm 150.75, 144.47, 130.57, 129.25, 127.25, 124.02, 120.99, 118.98, 74.02, 36.20, 33.30, 32.24, 20.26, 14.40; elemental analysis (%) found: C, 62.75; H, 6.91 - calculated C₃₂H₄₀Br₂O₂: C, 62.35; H, 6.54.

9.3.5 9,10-Dibromopyrene-4,5-diolacetone



9,10-Dibromopyrene-4,5-dione (0.5 g, 1.28 mmol) and sodium carbonate (1.09 g, 10.26 mmol) were suspended in 300 ml of a 1:1:1 mixture of acetonitrile, THF and water and degassed with argon. 2-Nitropropane (1.15 ml, 12.82 mmol) was added dropwise and the mixture was stirred at 55°C overnight. Most of the organic solvents were evaporated and the crude product was extracted with dichloromethane. The organic phase was dried over MgSO_4 , removed and the residue was purified over silica column PE: DCM 5:1 to yield 9,10-dibromopyrene-4,5-diolacetone (0.339 g, 0.785 mmol) as yellow solid in 61 % yield (mp: 242°C); MS (FD, 8 kV) $m/z = 431.0$ g/mol - calculated: 431.9 g/mol for $\text{C}_{19}\text{H}_{12}\text{Br}_2\text{O}_2$; ^1H NMR (300 MHz, CD_2Cl_2) δ/ppm 8.60 (dd, $J = 8.0, 1.1$ Hz, 2H), 8.25 (dd, $J = 7.8, 1.1$ Hz, 2H), 8.07 (t, $J = 7.9$ Hz, 2H), 1.94 (s, 6H); ^{13}C NMR (63 MHz, THF) δ/ppm 138.97, 131.74, 128.24, 127.97, 126.09, 121.87, 121.52, 121.45, 120.03, 26.33; elemental analysis (%) found: C, 52.53; H, 3.03 - calculated for $\text{C}_{19}\text{H}_{12}\text{Br}_2\text{O}_2$: C, 52.81; H, 2.80.

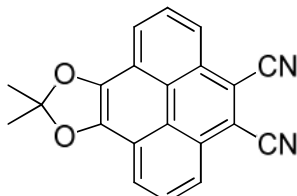
9.3.6 9,10-Dimethoxypyrene-4,5-dicarbonitrile



3-6

4,5-Dibromo-9,10-dimethoxypyrene (1.50 g, 3.57 mmol) and copper(I) cyanide (1.6 g, 17.9 mmol) in 60 ml dry *N*-methylpyrrolidone were heated under argon for three days at 190°C. After cooling the reaction mixture to 60°C, an excess of Mohr's salt ($\text{Fe}(\text{NH}_4)_2(\text{SO}_4)_2 \cdot 6\text{H}_2\text{O}$) in water was added and stirred for two hours. The crude product was extracted with dichloromethane, dried over MgSO_4 and the solvents removed under reduced pressure. Silica chromatography using DCM as eluent gave 9,10-dimethoxypyrene-4,5-dicarbonitrile (0.50 g, 1.60 mmol) as orange solid in 45 % yield (mp: 287°C); MS (FD, 8 kV) $m/z = 312.2$ g/mol - calculated: 312.1 g/mol for $\text{C}_{20}\text{H}_{12}\text{N}_2\text{O}_2$; ^1H NMR (500 MHz, CD_2Cl_2) δ /ppm 8.77 (dd, $J = 7.9, 0.9$ Hz, 2H), 8.60 (dd, $J = 7.8, 0.9$ Hz, 2H), 8.28 (t, $J = 7.9$ Hz, 2H), 4.23 (s, 6H); ^{13}C NMR (126 MHz, CD_2Cl_2) δ 145.32, 129.67, 128.55, 127.23, 124.67, 124.50, 123.30, 117.90, 115.76, 61.78; IR (neat, $1/\lambda$ in cm^{-1}) 2995, 2937, 2852, 2835, 2227 ($\text{CN}_{\text{Nitrile}}$), 1614, 1587, 1547, 1473, 1444, 1412, 1327, 1311, 1282, 1257, 1165, 1146, 1105, 1095, 1032, 1016, 945, 798, 715; elemental analysis (%) found: C, 76.83; H, 3.85; N, 8.97 – calculated for $\text{C}_{20}\text{H}_{12}\text{N}_2\text{O}_2$: C, 76.91; H, 3.87; N, 8.97.

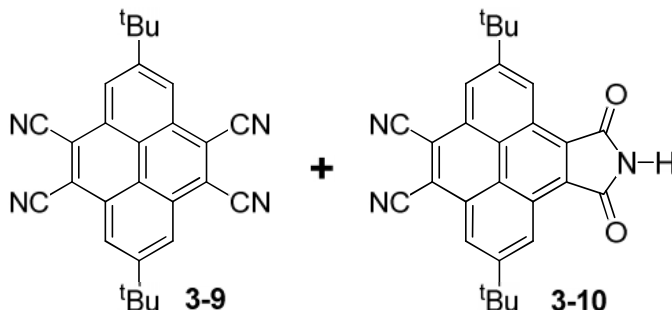
9.3.7 9,10-Dihydroxyacetoneid-pyrene-4,5-dicarbonitrile



3-7

9,10-Dibromopyrene-4,5-diolacetoneid (2.00 g, 4.63 mmol) and copper(I) cyanide (5.20 g, 58.06 mmol) in 80 ml dry *N*-methylpyrrolidone were heated under argon for three days at 190°C. After cooling the reaction mixture to 60°C, an excess of Mohr's salt ($\text{Fe}(\text{NH}_4)_2(\text{SO}_4)_2 \cdot 6\text{H}_2\text{O}$) in water was added and stirred for two hours. The crude product was extracted with dichloromethane, dried over MgSO_4 and the solvents removed under reduced pressure. Silica chromatography using PE: DCM 1:4 as eluent gave 9,10-dihydroxyacetoneid-pyrene-4,5-dicarbonitrile (0.72 g, 2.22 mmol) as red solid in 48 % yield (mp: 297 °C); MS (FD, 8 kV) $m/z = 323.9$ g/mol - calculated: 324.1 g/mol for $\text{C}_{21}\text{H}_{12}\text{N}_2\text{O}_2$; ^1H NMR (250 MHz, CD_2Cl_2) δ/ppm 8.53 (dd, $J = 7.8, 0.9$ Hz, 2H), 8.43 (dd, $J = 7.9, 1.0$ Hz, 2H), 8.25 (t, $J = 7.9$ Hz, 2H), 1.96 (s, 6H); ^{13}C NMR (75 MHz, CD_2Cl_2) δ/ppm 139.00, 128.35, 127.60, 123.23, 122.29, 121.77, 121.61, 121.40, 118.31, 115.66, 26.50; IR (neat, $1/\lambda$ in cm^{-1}) 3064, 2995, 2937, 2229 ($\text{CN}_{\text{Nitrile}}$), 1647, 1597, 1552, 1454, 1377, 1313, 1217, 1165, 1122, 1016, 964, 763, 731, 710, 648, 523; elemental analysis (%) found: C, 77.63; H, 3.65; N, 8.72 – calculated for $\text{C}_{21}\text{H}_{12}\text{N}_2\text{O}_2$: C, 77.77; H, 3.73; N, 8.64.

9.3.8 2,7-Di-*tert*-butylpyrene-4,5,9,10-tetracarbonitrile



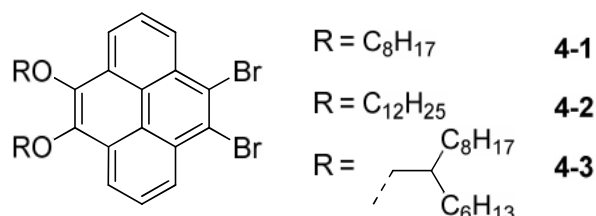
4,5,9,10-Tetrabromo-2,7-di-*tert*-butylpyrene (2.00 g, 3.17 mmol) and copper(I) cyanide (2.20 g, 25.40 mmol) in 60 ml NMP were heated under argon for three days at 190°C. After cooling the reaction mixture to 60°C, an excess of Mohr's salt ($\text{Fe}(\text{NH}_4)_2(\text{SO}_4)_2 \cdot 6\text{H}_2\text{O}$) in water was added and stirred for two hours. The crude product was extracted with dichloromethane, dried over MgSO_4 and the solvents removed under reduced pressure. Silica chromatography using DCM: PE 3:2 as eluent gave **3-9** and **3-10**.

3-9: slightly yellow solid; yield 8 % (0.10 g, 0.24 mmol); mp: decomposition >300°C; MS (FD, 8 kV) m/z = 413.6 g/mol - calculated: 414.2 g/mol for $\text{C}_{28}\text{H}_{22}\text{N}_4$; ^1H NMR (300 MHz, CD_2Cl_2) δ /ppm 8.93 (s, 4H), 1.67 (s, 18H); ^{13}C NMR (75 MHz, CD_2Cl_2) δ /ppm 154.55, 127.32, 127.24, 123.64, 118.79, 115.10, 36.63, 31.83; IR (neat, $1/\lambda$ in cm^{-1}) 2966, 2920, 2871, 2231, 1601, 1462, 1400, 1365, 1254, 1236, 1153, 1120, 958, 885, 727, 650, 559; elemental analysis (%) found: C, 80.72; H, 5.42; N, 13.08 – calculated for $\text{C}_{28}\text{H}_{22}\text{N}_4$: C, 81.13; H, 5.35; N, 13.52.

3-10: yellow solid (toluene); yield 19 % (0.26 g, 0.59 mmol); mp: decomposition >400°C °C; MS (FD, 8 kV) m/z = 432.7 g/mol - calculated: 433.2 g/mol for $\text{C}_{28}\text{H}_{23}\text{N}_3\text{O}_2$; ^1H NMR (300 MHz, CD_2Cl_2) δ /ppm 9.68 (d, J = 1.8 Hz, 2H), 8.84 (d, J = 1.8 Hz, 2H), 7.81 (s, 1H (N-H), 1.66 (s, 18H); ^{13}C NMR (75 MHz, THF) δ /ppm 170.95, 153.85, 130.60, 127.95, 126.49, 125.96, 125.90, 125.19, 118.96, 115.60, 36.79, 32.01.

9.4 4,5-Pyrenocyanines

9.4.1 4,5-Dibromo-9,10-dialkoxypyrene



9,10-Dibromopyrene-4,5-dione (1 eq.), tetrabutylammonium bromide (0.7 eq.) and sodium dithionite (3.0 eq.) were suspended in a 1.75 : 1 mixture of THF and water and stirred vigorously for five minutes at room temperature. 1-Bromoalkane (5.2 eq.) and 4 M aqueous potassium hydroxide solution (12.7 eq.) were added subsequently the mixture was stirred at 40°C overnight. After dilution with dichloromethane the organic phase was separated and the aqueous phase was extracted with dichloromethane two times. Combined organic phases were dried over $MgSO_4$ and the solvent was removed under reduced pressure. The crude product was adsorbed on silica and purified by column chromatography to give 4,5-dibromo-9,10-dialkoxypyrenes.

4,5-Dibromo-9,10-bis(octyloxy)pyrene (4-1):

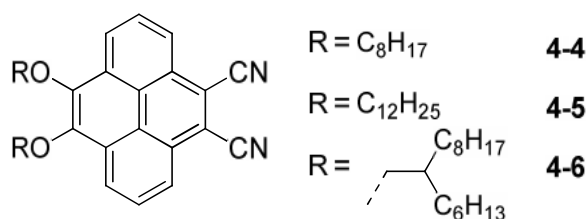
Chromatography with PE: DCM 5:1; yield: 72 % (2.28 g, 3.69 mmol) colorless solid (mp: 52°C); MS (FD, 8 kV) $m/z = 615.8$ g/mol - calculated: 616.4 g/mol for $C_{32}H_{40}Br_2O_2$; 1H NMR (250 MHz, CD_2Cl_2) δ/ppm 8.68 (dd, $J = 8.0, 1.0$ Hz, 2H), 8.62 (dd, $J = 7.9, 1.0$ Hz, 2H), 8.10 (t, $J = 8.0$ Hz, 2H), 4.33 (t, $J = 6.7$ Hz, 4H), 2.04 – 1.90 (m, 4H), 1.68 – 1.55 (m, 4H), 1.31 (s, 16H), 0.95 – 0.84 (m, 6H); ^{13}C NMR (75 MHz, CD_2Cl_2) δ/ppm 144.32, 130.92, 129.71, 127.66, 127.13, 126.62, 122.81, 121.91, 74.46, 32.46, 31.13, 30.12, 29.92, 26.88, 23.28, 14.46; elemental analysis (%) found: C, 62.25; H, 6.47 – calculated for $C_{32}H_{40}Br_2O_2$: C, 62.35; H, 6.54.

4,5-Dibromo-9,10-bis(dodecyloxy)pyrene (4-2):

Chromatography with PE: DCM 5:1; yield 90 % (2.52 g, 3.46 mmol) colorless solid (mp: 71°C); MS (FD, 8 kV) $m/z = 728.0$ g/mol - calculated: 728.3 g/mol for $C_{40}H_{56}Br_2O_2$; 1H NMR (300 MHz, CD_2Cl_2) δ/ppm 8.65 (dd, $J = 8.0, 0.9$ Hz, 2H), 8.60 (dd, $J = 7.9, 0.9$ Hz, 2H), 8.08 (t, $J = 8.0$ Hz, 2H), 4.32 (t, $J = 6.6$ Hz, 4H), 2.08 – 1.89 (m, 4H), 1.70 – 1.54 (m, 4H), 1.49 – 1.22 (m, 32H), 0.89 (t, $J = 6.7$ Hz, 6H); ^{13}C NMR (75 MHz, CD_2Cl_2) δ/ppm 144.29, 130.87, 129.67, 127.62, 127.11, 126.59, 122.77, 121.88, 74.43, 32.54, 31.13, 30.31, 30.27, 30.16, 29.97, 26.88, 23.30, 14.48; elemental analysis (%) found: C, 65.89; H, 7.79 - calculated for $C_{40}H_{56}Br_2O_2$: C, 65.93; H, 7.75.

4,5-Dibromo-9,10-bis(2-hexyldecyloxy)pyrene (4-3):

Chromatography with PE; yield 30 % (1.29 g, 1.53 mmol) colorless oil; MS (FD, 8 kV) $m/z = 839.9$ g/mol - calculated: 840.4 g/mol for $C_{48}H_{72}Br_2O_2$; 1H NMR (300 MHz, CD_2Cl_2) δ/ppm 8.66 (d, $J = 7.9$ Hz, 2H), 8.62 (d, $J = 7.9$ Hz, 2H), 8.08 (t, $J = 8.0$ Hz, 2H), 4.21 (d, $J = 6.0$ Hz, 4H), 2.08 – 1.95 (m, 2H), 1.77 – 1.21 (m, 48H), 0.97 – 0.82 (m, 12H); ^{13}C NMR (75 MHz, CD_2Cl_2) δ/ppm 144.44, 130.90, 129.66, 127.60, 127.13, 126.57, 122.80, 121.88, 77.62, 39.97, 32.54, 32.03, 32.02, 30.77, 30.44, 30.28, 30.00, 27.58, 27.55, 23.33, 23.30, 14.49; elemental analysis (%) found: C, 68.82; H, 8.24 – calculated for $C_{48}H_{72}Br_2O_2$: C, 68.56; H, 8.63.

9.4.2 4,5-Dialkoxy-9,10-dicyanopyrene

To a solution of 4,5-dibromo-9,10-dialkoxypyrene (1 eq.) in dry NMP copper(I) cyanide (4 eq.) was added and stirred under argon at 180°C for three

days. The mixture was cooled to 60°C and an aqueous solution of $(\text{NH}_4)_2\text{Fe}(\text{SO}_4)_2$ was added and stirred for two hours at 60°C. After cooling to room temperature the product was extracted with dichloromethane and the solvents were removed under reduced pressure. Silica chromatography gave 4,5-dialkoxy-9,10-dicyanopyrenes.

9,10-Bis(octyloxy)pyrene-4,5-dicarbonitrile (4-4):

Chromatography DCM:PE 1:1; yield 78 % (1.93 g, 3.80 mmol) yellow solid (mp: 52°C); MS (FD, 8 kV) $m/z = 508.7$ g/mol - calculated: 508.3 g/mol for $\text{C}_{34}\text{H}_{40}\text{N}_2\text{O}_2$; ^1H NMR (300 MHz, THF- d_8) δ/ppm 8.79 (dd, $J = 7.9, 0.9$ Hz, 2H), 8.59 (dd, $J = 7.8, 0.8$ Hz, 2H), 8.30 (t, $J = 7.9$ Hz, 2H), 4.39 (t, $J = 6.6$ Hz, 4H), 2.07 – 1.93 (m, 4H), 1.69 – 1.59 (m, 4H), 1.53 – 1.26 (m, 16H), 0.91 (t, $J = 6.8$ Hz, 6H); ^{13}C NMR (75 MHz, THF- d_8) δ/ppm 145.22, 130.59, 129.06, 127.87, 125.12, 124.82, 123.65, 118.35, 115.77, 74.88, 33.01, 31.59, 30.66, 30.47, 27.39, 23.73, 14.60; elemental analysis (%) found: C, 80.10; H, 8.04; N, 5.47 – calculated for $\text{C}_{34}\text{H}_{40}\text{N}_2\text{O}_2$: C, 80.28; H, 7.93; N, 5.51.

9,10-Bis(dodecyloxy)pyrene-4,5-dicarbonitrile (4-5):

Chromatography DCM:PE 2:1; yield 74 % (0.941 g, 1.516 mmol) yellow solid (mp: 73°C); MS (FD, 8 kV) $m/z = 620.5$ g/mol - calculated: 620.4 g/mol for $\text{C}_{42}\text{H}_{56}\text{N}_2\text{O}_2$; ^1H NMR (300 MHz, THF- d_8) δ/ppm 8.79 (dd, $J = 7.9, 0.9$ Hz, 2H), 8.60 (dd, $J = 7.9, 0.9$ Hz, 2H), 8.31 (t, $J = 7.9$ Hz, 2H), 4.39 (t, $J = 6.6$ Hz, 4H), 2.06 – 1.94 (m, 4H), 1.71 – 1.59 (m, 4H), 1.52 – 1.25 (m, 32H), 0.94 – 0.85 (m, 6H); ^{13}C NMR (75 MHz, THF- d_8) δ/ppm 145.22, 130.59, 129.07, 127.88, 125.13, 124.83, 123.66, 118.36, 115.78, 74.88, 33.06, 31.59, 30.83, 30.81, 30.71, 30.50, 27.39, 23.74, 14.60; elemental analysis (%) found: C, 81.19; H, 8.85; N, 4.85 – calculated for $\text{C}_{42}\text{H}_{56}\text{N}_2\text{O}_2$: C, 81.24; H, 9.09; N, 4.51.

9,10-Bis(2-hexyldecyloxy)pyrene-4,5-dicarbonitrile (4-6):

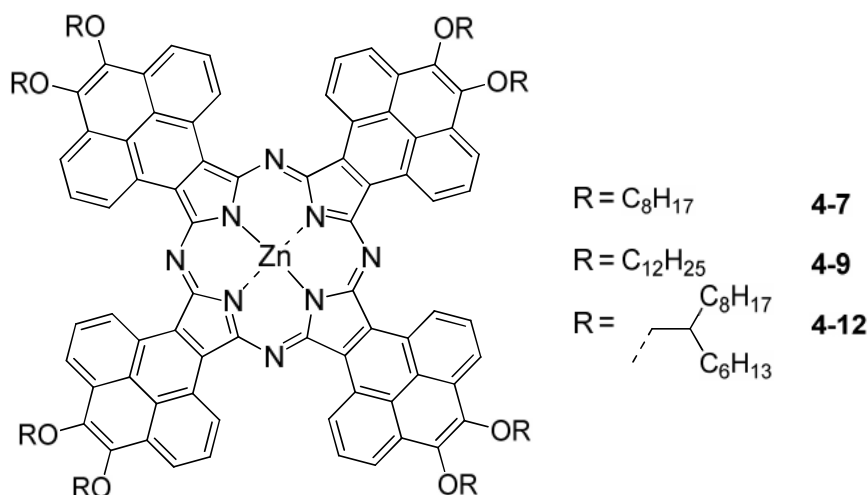
Chromatography DCM:PE 3:2; yield 79 % (0.934 g, 1.516 mmol) yellow oil; MS (FD, 8 kV) $m/z = 732.0$ g/mol - calculated: 732.6 g/mol for $\text{C}_{50}\text{H}_{72}\text{N}_2\text{O}_2$; ^1H NMR (250 MHz, CD_2Cl_2) δ/ppm 8.75 (dd, $J = 7.9, 0.8$ Hz, 2H), 8.51 (dd, $J = 7.8, 0.8$ Hz, 2H), 8.22 (t, $J = 7.9$ Hz, 2H), 4.24 (d, $J = 6.0$ Hz, 4H), 2.15 – 1.94 (m, 2H), 1.78 – 1.21 (m, 48H), 0.97 – 0.80 (m, 12H);

^{13}C NMR (63 MHz, CD_2Cl_2) δ/ppm 144.79, 130.08, 128.38, 127.11, 124.73, 124.23, 123.15, 117.70, 115.68, 77.73, 39.94, 32.54, 31.98, 30.75, 30.42, 30.28, 30.00, 27.56, 27.54, 23.33, 23.30, 14.50; elemental analysis (%) found: C, 81.66; H, 9.90; N, 3.87 - calculated for $\text{C}_{50}\text{H}_{72}\text{N}_2\text{O}_2$: C, 81.92; H, 9.90; N, 3.82.

9.4.3 4,5,15,16,26,27,37,38-

Octakis(alkoxy)tetra[4,5]pyrenocyanine Zinc(II)

(ZnPyc- C_x):



4,5-Dialkoxy-9,10-dicyanopyrenes (1 eq.) and metal chloride ZnCl_2 (0.28 eq.) were suspended in dry isopentanol and degassed with argon. DBU (1 eq.) was added and the mixture was stirred under reflux for two days. After cooling to room temperature the solution was precipitated in methanol:water 1:1 and the solid was collected by filtration. Size exclusion chromatography with dichloromethane gave zinc pyrenocyanines.

4,5,15,16,26,27,37,38-Octakis(octyloxy)tetra[4,5]pyrenocyanine Zinc(II) (4-7):

Dark blue wax; yield 26 % (0.132 g, 0.063 mmol); ^1H NMR (500 MHz, $\text{C}_2\text{D}_2\text{Cl}_4$, 393K, 10mg/ml) δ/ppm 9.64 (br s, 8H), 7.87 (br s, 8H), 7.36 (br s, 8H), 4.38 (br s, 16H), 2.16 (br s, 16H), 1.90 (br s, 16H), 1.81 – 1.49 (br m,

64H), 1.14 (br s, 24H); IR (neat, $1/\lambda$ in cm^{-1}) 2922, 2850, 1620, 1591, 1543, 1464, 1406, 1384, 1325, 1259, 1225, 1157, 1101, 1043, 951, 796, 715; HRMS (ESI): m/z calculated for $[\text{C}_{136}\text{H}_{160}\text{N}_8\text{O}_8\text{Zn}+\text{H}]^+$: 2098.1723 - found: 2098.1800; elemental analysis (%) found: C, 77.09; H, 7.45; N, 5.11 – calculated for $\text{C}_{136}\text{H}_{160}\text{N}_8\text{O}_8\text{Zn}$: C, 77.78; H, 7.68; N, 5.34.

4,5,15,16,26,27,37,38-Octakis(dodecyloxy)tetra[4,5]pyrenocyanine

Zinc(II) (4-9):

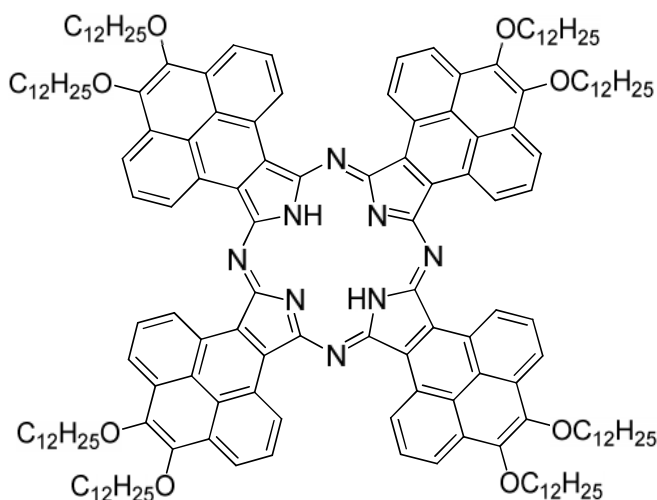
Dark blue wax; yield 34 % (0.143 g, 0.056 mmol); ^1H NMR (500 MHz, $\text{C}_2\text{D}_2\text{Cl}_4$, 393K, 10mg/ml) δ /ppm 10.07 (br s, 8H), 8.07 (br s, 8H), 7.69 (br s, 8H), 4.46 (br s, 16H), 2.22 (br s, 16H), 1.92 (br s, 16H), 1.85 – 1.31 (br m, 128H), 1.01 (br s, 24H); IR (neat, $1/\lambda$ in cm^{-1}) 2920, 2852, 1622, 1591, 1466, 1406, 1325, 1259, 1157, 1103, 1045, 958, 796, 717; HRMS (ESI): m/z calculated for $[\text{C}_{168}\text{H}_{224}\text{N}_8\text{O}_8\text{Zn}+\text{H}]^+$: 2546.6731 - found: 2546.6718; elemental analysis (%) found: C, 78.63; H, 8.81; N, 4.39 – calculated for $\text{C}_{168}\text{H}_{224}\text{N}_8\text{O}_8\text{Zn}$: C, 79.16; H, 8.86; N, 4.40.

4,5,15,16,26,27,37,38-Octakis(2-hexyldecyloxy)tetra[4,5]pyrenocyanine

Zinc(II) (4-12):

Dark blue wax; yield 32 % (0.164 g, 0.065 mmol); ^1H NMR (500 MHz, THF-d_8 , 298K, 25mg/ml) δ /ppm 11.56 (d, $J = 6.6$ Hz, 8H), 8.68 (d, $J = 6.9$ Hz, 8H), 8.61 (t, $J = 6.7$ Hz, 8H), 4.65 – 4.50 (m, 16H), 2.34 – 2.23 (m, 8H), 2.12 – 2.00 (m, 16H), 1.97 – 1.86 (m, 16H), 1.85 – 1.43 (m, 160H), 1.18 – 1.07 (m, 24H), 1.07 – 0.96 (m, 24H); ^{13}C NMR (176 MHz, THF-d_8 , 298K, 25mg/ml) δ /ppm 155.63, 144.60, 135.08, 129.71, 128.32, 127.05, 126.68, 124.78, 121.11, 77.41, 41.04, 41.03, 33.55, 33.51, 33.36, 33.34, 32.98, 32.97, 32.79, 31.83, 31.50, 31.49, 31.30, 31.27, 30.91, 30.89, 28.60, 28.56, 28.53, 24.15, 24.12, 23.98, 23.97, 14.99, 14.95, 14.87, 14.84; IR (neat, $1/\lambda$ in cm^{-1}) 2922, 2852, 1620, 1589, 1463, 1403, 1385, 1259, 1225, 1157, 1101, 1039, 957, 798, 717; HRMS (ESI): m/z calculated for $[\text{C}_{200}\text{H}_{288}\text{N}_8\text{O}_8\text{Zn}+\text{H}]^+$: 2995.1739 - found: 2995.1674; elemental analysis (%) found: C, 78.61; H, 9.72; N, 3.55 - calculated $\text{C}_{200}\text{H}_{288}\text{N}_8\text{O}_8\text{Zn}$: C, 80.13; H, 9.68; N, 3.74.

9.4.4 4,5,15,16,26,27,37,38-Octakis(dodecyloxy)-45H,47-tetra[4,5]pyrenocyanine (H₂Pyc-C₁₂)

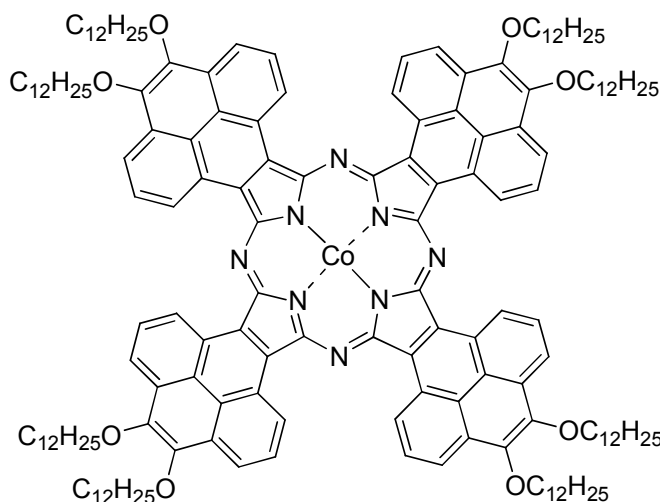


4-8

9,10-Bis(dodecyloxy)pyrene-4,5-dicarbonitrile (**4-5**) (0.250 g, 0.403 mmol) was suspended in dry isopentanol and degassed with argon. DBU (66 μ l, 0.443 mmol) was added and the mixture was stirred under reflux for two days. After cooling to room temperature the solution was precipitated in methanol:water 1:1 and the solid was collected by filtration. Size exclusion chromatography with dichloromethane gave metal free pyrenocyanine **4-8** as dark blue wax in yield 6 % (0.015 g, 0.006 mmol); ¹H NMR (700 MHz, CD₂Cl₂, 298K, 11mg/ml) δ /ppm 9.31 (br s, 8H), 7.72 (br s, 8H), 7.29 (br s, 8H), 4.46 (br s, 16H), 2.21 (br s, 16H), 2.09 – 1.35 (br m, 144H), 1.09 (br s, 24H), -6.70 (br s, 1H), -9.53 (br s, 1H); IR (neat, 1/ λ in cm⁻¹) 3298 (N-H), 2920, 2850, 1622, 1593, 1466, 1406, 1383, 1327, 1255, 1217, 1101, 1039, 795, 760, 715, 683; HRMS (ESI): m/z calculated for [C₁₆₈H₂₂₆N₈O₈+H]⁺: 2484.7596 - found: 2484.7642.

9.4.5 4,5,15,16,26,27,37,38-

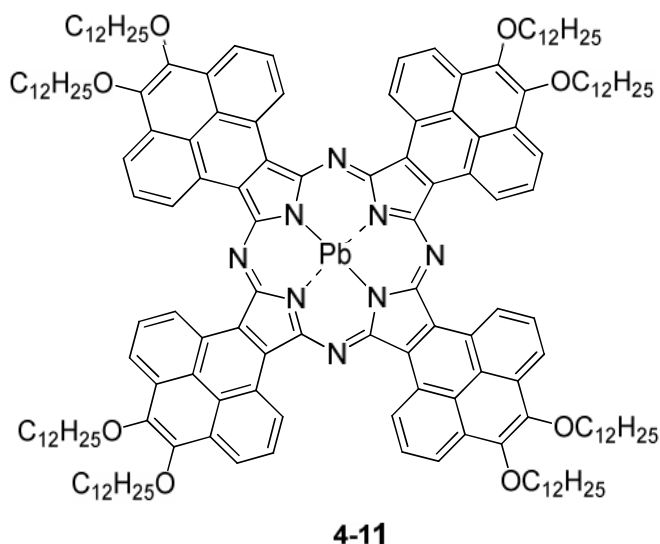
Octakis(dodecyloxy)tetra[4,5]pyrenocyanine cobalt(II) (CoPyc-C₁₂):



4-10

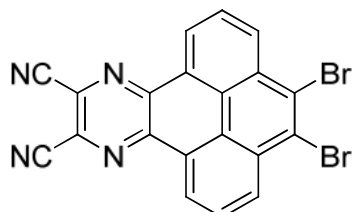
9,10-Bis(dodecyloxy)pyrene-4,5-dicarbonitrile (**4-5**) (0.100 g, 0.161 mmol) and Co(OAc)₂ (0.008 g, 0.045 mmol) were suspended in dry isopentanol and degassed with argon. DBU (25 μ l, 0.161 mmol) was added and the mixture was stirred under reflux for two days. After cooling to room temperature the solution was precipitated in methanol:water 1:1 and the solid was collected by filtration. Size exclusion chromatography with dichloromethane gave pyrenocyanine **4-10** as blue wax in yield 18 % (0.018 g, 0.007 mmol); IR (neat, $1/\lambda$ in cm^{-1}) 2920, 2852, 1623, 1597, 1466, 1408, 1385, 1324, 1294, 1259, 1157, 1103, 1045, 958, 796, 715; HRMS (ESI): m/z calculated for $[\text{C}_{168}\text{H}_{224}\text{N}_8\text{O}_8\text{Co}+\text{H}]^+$: 2541.6772 - found: 2541.6730;

9.4.6 4,5,15,16,26,27,37,38-Octakis(dodecyloxy)tetra[4,5]pyrenocyanine lead(II) (PbPyc-C₁₂)



9,10-Bis(dodecyloxy)pyrene-4,5-dicarbonitrile (**4-5**) (0.250 g, 0.403 mmol) and lead chloride PbCl₂ (0.063 g, 0.226 mmol) were suspended in dry isopentanol and degassed with argon. DBU (60 µl, 0.403 mmol) was added and the mixture was stirred under reflux for two days. After cooling to room temperature the solution was precipitated in methanol:water 1:1 and the solid was collected by filtration. The precipitate was washed with THF and DCM and the lead pyrenocyanine **4-11** was obtained as dark purple wax in yield 32 % (0.087 g, 0.032 mmol); ¹H NMR (500 MHz, Tol-d₈, 393K) δ/ppm 10.53 (br s, 8H), 8.59 (br s, 8H), 7.98 (br s, 8H), 4.87 – 4.63 (m, 16H), 2.55 – 2.28 (m, 16H), 2.07 – 2.01 (m, 16H), 1.88 – 1.78 (m, 16H), 1.78 – 1.70 (m, 16H), 1.70 – 1.62 (m, 16H), 1.62 – 1.56 (m, 16H), 1.56 – 1.47 (m, 32H), 1.47 – 1.38 (m, 32H), 1.00 (s, 24H); IR (neat, 1/λ in cm⁻¹) 2918, 2850, 1622, 1591, 1466, 1383, 1323, 1271, 1254, 1219, 1101, 795, 769, 715; HRMS (ESI): m/z calculated for [C₁₆₈H₂₂₄N₈O₈Pb+H]⁺ (A+5): 2691.7252 - found: 2691.7254; elemental analysis (%) found: C, 76.06; H, 8.66; N, 4.15 – calculated for C₁₆₈H₂₂₄N₈O₈Pb: C, 74.99; H, 8.39; N, 4.16.

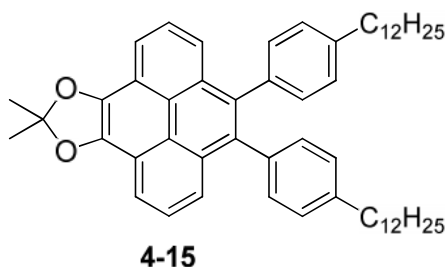
9.4.7 4,5-Dibromophenanthro[4,5-fgh]quinoxaline-10,11-dicarbonitrile



4-13

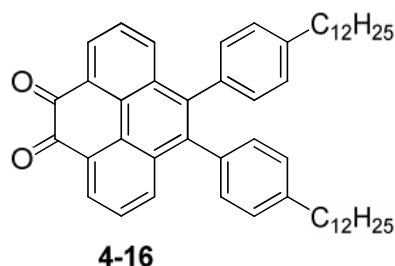
9,10-Dibromopyrene-4,5-dione (1.500 g, 0.756 mmol) and diaminomaleonitrile (0.624 mg, 5.769 mmol) were dissolved in 50 ml *o*-dichlorobenzene. 50 ml glacial acetic acid were added and the mixture was heated under reflux for 3.5 hours. The reaction mixture was poured into 1 L of methanol and the solid was collected by filtration. After refluxing the crude product in 30% HNO₃ for 2 h the mixture was cooled to room temperature and filtrated to obtain 4,5-dibromophenanthro[4,5-fgh]quinoxaline-10,11-dicarbonitrile (1.331 g, 2.88 mmol) as light brown solid in 75 % yield; MS (FD, 8 kV) $m/z = 461.7$ g/mol - calculated: 461.9 g/mol for C₂₀H₆Br₂N₄; ¹H NMR (500 MHz, DMSO-d₆, 373 K) δ 9.50 (d, $J = 7.6$ Hz, 2H), 9.02 (d, $J = 7.9$ Hz, 2H), 8.42 (t, $J = 7.9$ Hz, 2H).

9.4.8 9,10-Bis(4-dodecylphenyl)pyrene-4,5-diolacetonide



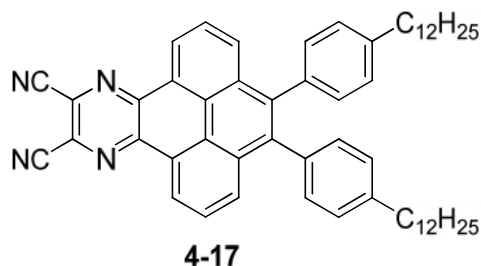
To 9,10-dibromopyrene-4,5-diolacetonide (0.050 g, 0.116 mmol), 4-dodecylphenylboronic acid (0.134 g, 0.463 mmol) and potassium phosphate (0.160 g, 0.694 mmol) in a dried Schlenk flask, 5 ml THF and 5 μ l water were added and degassed with argon for 10 minutes. After addition of palladium acetate (0.006 g, 0.012 mmol) and SPhos (0.013 g, 0.012 mmol) the reaction mixture was degassed again and stirred at room temperature for 16 hours. The crude product was extracted with dichloromethane and the organic phase was washed with water, dried over MgSO_4 and the solvents were removed under reduced pressure. Chromatography over silica with PE: DCM 9:1 yielded 9,10-bis(4-dodecylphenyl)pyrene-4,5-diolacetonide (0.065 g, 0.085 mmol) as yellow solid in 73 % yield (mp: 143°C); MS (FD, 8 kV) $m/z = 763.3$ g/mol - calculated: 762.5 g/mol for $\text{C}_{55}\text{H}_{70}\text{O}_2$; ^1H NMR (300 MHz, CD_2Cl_2) δ /ppm 8.17 (dd, $J = 7.7, 0.9$ Hz, 2H), 7.92 (t, $J = 7.8$ Hz, 2H), 7.74 (dd, $J = 7.9, 0.8$ Hz, 2H), 7.20 - 7.06 (m, 8H), 2.67 - 2.55 (m, 4H), 1.95 (s, 6H), 1.68 - 1.55 (m, $J = 13.0, 6.1$ Hz, 4H), 1.39 - 1.21 (m, 36H), 0.88 (t, $J = 6.5$ Hz, 6H); ^{13}C NMR (75 MHz, CD_2Cl_2) δ /ppm 141.85, 138.84, 138.33, 137.31, 132.62, 131.61, 128.19, 126.42, 123.73, 121.18, 121.14, 120.16, 117.44, 36.18, 32.54, 32.00, 30.32, 30.27, 30.14, 29.98, 29.83, 26.47, 23.29, 14.46; elemental analysis (%) found: C, 85.92; H, 9.57 - calculated for $\text{C}_{55}\text{H}_{70}\text{O}_2$: C, 86.56; H, 9.25.

9.4.9 9,10-Bis(4-dodecylphenyl)pyrene-4,5-dione



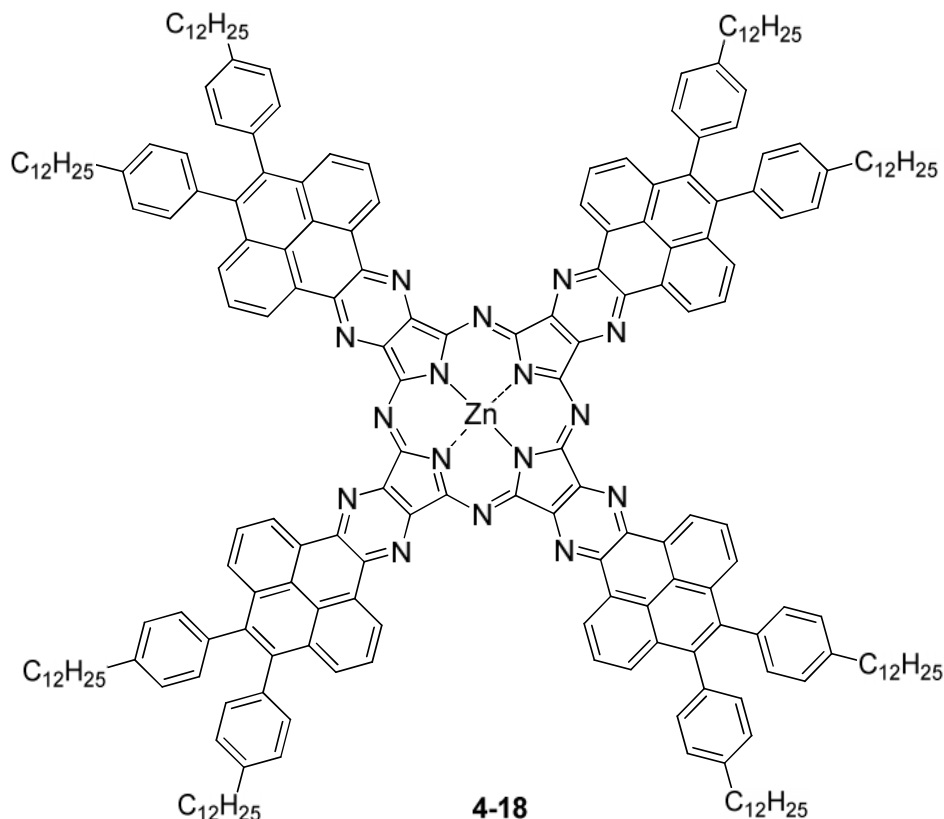
9,10-Bis(4-dodecylphenyl)pyrene-4,5-diolacetone (2.285 g, 2.994 mmol) was dissolved in 400 ml of a 1:1 mixture of chloroform and trifluoroacetic acid and stirred at 50°C for four hours while air was bubbled through the solution. The solvents were removed under reduced pressure and the residue was purified over a silica column with pure DCM to yield 9,10-bis(4-dodecylphenyl)pyrene-4,5-dione (1.458 g, 2.022 mmol) as red solid in 68 % yield (mp: 229°C); MS (FD, 8 kV) $m/z = 721.1$ g/mol - calculated: 720.5 g/mol for $C_{52}H_{64}O_2$; 1H NMR (300 MHz, CD_2Cl_2) δ/ppm 8.42 (dd, $J = 7.4, 1.3$ Hz, 2H), 7.89 (dd, $J = 8.3, 1.3$ Hz, 2H), 7.62 (dd, $J = 8.2, 7.4$ Hz, 2H), 7.15 – 7.03 (m, 8H), 2.65 – 2.54 (m, 4H), 1.67 – 1.52 (m, $J = 14.0, 7.1$ Hz, 4H), 1.28 (s, 36H), 0.88 (t, $J = 6.7$ Hz, 6H); ^{13}C NMR (75 MHz, CD_2Cl_2) δ/ppm 181.17, 142.40, 138.64, 136.00, 135.86, 133.18, 131.29, 130.52, 130.16, 128.60, 128.40, 128.34, 36.14, 32.53, 31.94, 30.31, 30.27, 30.26, 30.11, 29.97, 29.79, 23.29, 14.46; IR (neat, $1/\lambda$ in cm^{-1}) 2918, 2850, 1674, 1599, 1523, 1281, 1184, 1082, 1022, 804, 714, 525; elemental analysis (%) found: C, 86.13; H, 9.01 - calculated for $C_{52}H_{64}O_2$: C, 86.62; H, 8.95.

9.4.10 4,5-Bis(4-dodecylphenyl)phenanthro[4,5-*fgh*]quinoxaline-10,11-dicarbonitrile



9,10-Bis(4-dodecylphenyl)pyrene-4,5-dione (0.600 g, 0.756 mmol) and diaminomaleonitrile (0.126 mg, 1.166 mmol) were dissolved in 10 ml *o*-dichlorobenzene. 20 ml glacial acetic acid were added and the mixture was heated under reflux for 6 hours. The crude product was extracted with dichloromethane and the solvents were removed under reduced pressure. The crude product was adsorbed on silica and purified by column chromatography with PE: DCM 1:1 as eluent to give 4,5-bis(4-dodecylphenyl)phenanthro[4,5-*fgh*]quinoxaline-10,11-dicarbonitrile (0.376 g, 0.474 mmol) as orange solid in 55 % yield (mp: 243°C decomp.); MS (FD, 8 kV) m/z = 793.4 g/mol - calculated: 792.5 g/mol for $C_{56}H_{64}N_4$; 1H NMR (300 MHz, CD_2Cl_2) δ /ppm 9.04 (dd, J = 7.6, 1.2 Hz, 2H), 7.99 (dd, J = 8.1, 1.1 Hz, 2H), 7.89 (t, J = 7.9 Hz, 2H), 7.16 (s, 8H), 2.68 – 2.59 (m, 4H), 1.70 – 1.59 (m, 4H), 1.30 (s, 36H), 0.89 (t, J = 6.6 Hz, 6H); ^{13}C NMR (75 MHz, CD_2Cl_2) δ /ppm 143.63, 142.45, 138.72, 136.13, 132.35, 131.64, 131.39, 130.71, 128.51, 127.80, 126.21, 126.19, 125.02, 114.42, 36.21, 32.55, 32.00, 30.35, 30.30, 30.16, 29.99, 29.86, 23.30, 14.48; IR (neat, $1/\lambda$ in cm^{-1}) 2956, 2920, 2850, 1603, 1595, 1512, 1468, 1396, 1363, 1213, 1111, 1024, 860, 810, 721, 638, 575, 523; elemental analysis (%) found: C, 84.40; H, 8.33; N 7.10 - calculated for $C_{56}H_{64}N_4$: C, 84.80; H, 8.13; N, 7.06.

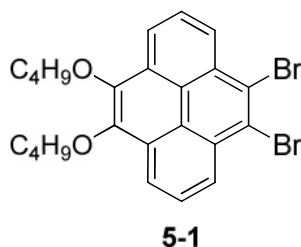
9.4.11 Pyrenopyrazinocyanine



4,5-Bis(4-dodecylphenyl)phenanthro[4,5-*fgh*]quinoxaline-10,11-dicarbonitrile (0.100 g, 0.126 mmol) and zinc chloride (0.005 g, 0.035 mmol) were suspended in dry isopentanol and degassed with argon. DBU (19 μ l, 0.126 mmol) was added and the mixture was stirred under reflux overnight. After cooling to room temperature the solution was precipitated in methanol:water 1:1 and the solid was collected by filtration. Size exclusion chromatography with dichloromethane gave pyranzine-extended zinc pyrenocyanine (0.014 g, 0.004 mmol) as black solid in 13 % yield; IR (neat, $1/\lambda$ in cm^{-1}) 2922, 2850, 1729, 1606, 1556, 1500, 1464, 1402, 1354, 1311, 1245, 1161, 1122, 1022, 939, 806, 723; HRMS (MALDI, 3-HPA): m/z calculated for $[\text{C}_{224}\text{H}_{256}\text{N}_{16}\text{Zn}+\text{H}]^+$ (A+3): 3237.9950 - found: 3237.9956.

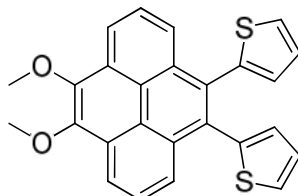
9.5 Dithienobenzo[e]pyrenes

9.5.1 4,5-Dibromo-9,10-dibutoxypyrene



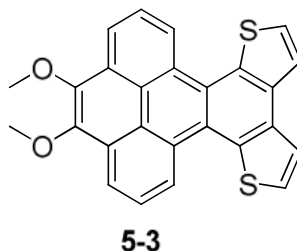
9,10-Dibromopyrene-4,5-dione (3.00 g, 7.69 mmol), tetrabutylammonium bromide (1.74 g, 5.38 mmol) and sodium dithionite (4.02 g, 23.08 mmol) were suspended in a mixture of 52 ml THF and 30 ml water and stirred vigorously for five minutes at room temperature. 1-Bromobutane (3.3 ml, 30.8 mmol) and 22 ml of a 4 M aqueous potassium hydroxide solution were added subsequently the mixture was stirred at 40°C overnight. After dilution with dichloromethane the organic phase was separated and the aqueous phase was extracted with dichloromethane two times. Combined organic phases were dried over MgSO_4 and the solvent were removed under reduced pressure. The crude product was adsorbed on silica and purified by column chromatography with PE and crystallized from ethanol to give 4,5-dibromo-9,10-dibutoxypyrene (1.92 g, 3.79 mmol) as colorless solid in 50 % yield (mp: 84°C); MS (FD, 8 kV) m/z = 504.4 g/mol - calculated: 504.0 g/mol for $\text{C}_{24}\text{H}_{24}\text{Br}_2\text{O}_2$; ^1H NMR (250 MHz, CD_2Cl_2) δ /ppm 8.66 (dd, J = 8.0, 1.0 Hz, 2H), 8.61 (dd, J = 7.9, 1.0 Hz, 2H), 8.09 (t, J = 8.0 Hz, 2H), 4.34 (t, J = 6.6 Hz, 4H), 2.06 – 1.88 (m, 4H), 1.76 – 1.57 (m, 4H), 1.05 (t, J = 7.3 Hz, 6H); ^{13}C NMR (63 MHz, CD_2Cl_2) δ 144.27, 130.86, 129.66, 127.64, 127.10, 126.59, 122.76, 121.86, 74.12, 33.19, 20.09, 14.38; elemental analysis (%) found: C, 58.09; H, 5.12 – calculated for $\text{C}_{24}\text{H}_{24}\text{Br}_2\text{O}_2$: C, 57.16; H, 4.80.

9.5.2 4,5-Dimethoxy-9,10-bis(thien-2-yl)pyrene

**5-2**

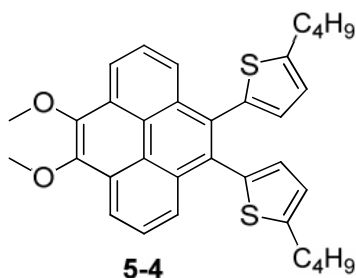
A solution of 4,5-dibromo-9,10-dimethoxypyrene (0.3 g, 0.714 mmol) in 10 ml dry toluene was degassed with argon for 15 minutes. $\text{Pd}(\text{PPh}_3)_4$ (0.025 g, 0.021 mmol) and 2-(tributylstannyl)thiophene (0.8 g, 2.14 mmol) were added, degassed for additional 5 minutes and refluxed under argon overnight. The organic solvent was removed under reduced pressure and the residue was purified over a silica column PE: DCM 2:1 and crystallized from ethanol to give 4,5-dimethoxy-9,10-bis(thien-2-yl)pyrene (0.210 g, 0.492 mmol) as slightly yellow solid in 69 % yield (mp: 182 °C); MS (FD, 8 kV) $m/z = 426.5$ g/mol - calculated: 426.1 g/mol for $\text{C}_{26}\text{H}_{18}\text{O}_2\text{S}_2$; ^1H NMR (300 MHz, CD_2Cl_2) δ/ppm 8.55 (dd, $J = 6.8, 2.1$ Hz, 2H), 8.04 – 7.96 (m, 4H), 7.43 (dd, $J = 4.9, 1.5$ Hz, 2H), 7.11 – 7.06 (m, 4H), 4.23 (s, 6H); ^{13}C NMR (75 MHz, CD_2Cl_2) δ/ppm 145.13, 140.17, 133.39, 132.16, 130.15, 128.78, 127.01, 126.82, 126.79, 124.87, 123.10, 120.61, 61.65; elemental analysis (%) found: C, 73.07; H, 4.16; S, 14.81 - calculated for $\text{C}_{26}\text{H}_{18}\text{O}_2\text{S}_2$: C, 73.21; H, 4.25; S, 15.03.

9.5.3 10,11-Dimethoxy-benzo[8,9]triphenyleno[1,2-*b*:4,3-*b'*]dithiophene



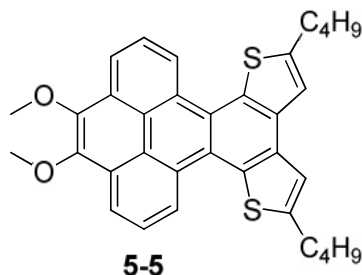
A solution of 4,5-dimethoxy-9,10-di-(thien-2-yl)pyrene (0.255 g, 0.598 mmol) and iodine (0.303 g, 1.196 mmol) in 255 ml toluene was degassed with argon for 15 minutes and irradiated in a quartz tube at 300 nm overnight. The reaction mixture was washed with aqueous Na_2SO_3 solution, dried over MgSO_4 and the organic solvents were removed. Crystallization from ethanol gave 10,11-dimethoxy-benzo[8,9]triphenyleno[1,2-*b*:4,3-*b'*]dithiophene (0.120 g, 0.283 mmol) as slightly yellow crystals in 47 % yield (mp: 198 °C); MS (FD, 8 kV) $m/z = 424.2$ g/mol - calculated: 424.1 g/mol for $\text{C}_{26}\text{H}_{16}\text{O}_2\text{S}_2$; ^1H NMR (300 MHz, CD_2Cl_2) δ/ppm 9.59 (dd, $J = 8.1, 0.8$ Hz, 2H), 8.63 (dd, $J = 7.9, 0.8$ Hz, 2H), 8.21 (t, $J = 8.0$ Hz, 2H), 8.01 (d, $J = 5.6$ Hz, 2H), 7.85 (d, $J = 5.5$ Hz, 2H), 4.25 (s, 6H); ^{13}C NMR (75 MHz, CD_2Cl_2) δ/ppm 144.85, 136.14, 134.30, 129.57, 129.10, 128.07, 126.83, 125.90, 123.97, 122.91, 122.80, 120.87, 61.68; elemental analysis (%) found: C, 73.01; H, 3.87; S, 15.04 - calculated for $\text{C}_{26}\text{H}_{16}\text{O}_2\text{S}_2$: C, 73.56; H, 3.80; S, 15.11.

9.5.4 4,5-Bis(5-butylthien-2-yl)-9,10-dimethoxypyrene



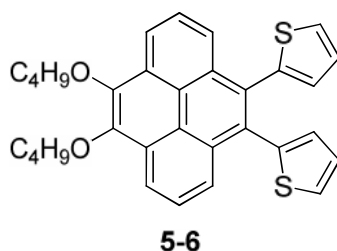
A solution of 4,5-dibromo-9,10-dimethoxypyrene (1.500 g, 3.571 mmol) in 150 ml dry toluene was degassed with argon for 15 minutes. $\text{Pd(PPh}_3)_4$ (0.413 g, 0.357 mmol) and tributyl(5-butylthiophen-2-yl)stannane (7.4 g, 17.2 mmol) were added, degassed for additional 5 minutes und refluxed under argon overnight. The organic solvent was removed under reduced pressure and the residue was purified over silica column PE: DCM 4:1 to give 4,5-bis(5-butylthien-2-yl)-9,10-dimethoxypyrene (1.546 g, 2.870 mmol) as yellow solid in 80 % yield (mp: 77°C); MS (FD, 8 kV) $m/z = 538.5$ g/mol - calculated: 538.2 g/mol for $\text{C}_{34}\text{H}_{34}\text{O}_2\text{S}_2$; ^1H NMR (250 MHz, CD_2Cl_2) δ/ppm 8.53 (dd, $J = 7.8, 1.1$ Hz, 2H), 8.15 (dd, $J = 7.9, 1.1$ Hz, 2H), 7.99 (t, $J = 7.9$ Hz, 2H), 6.84 (d, $J = 3.4$ Hz, 2H), 6.76 (d, $J = 3.4$ Hz, 2H), 4.23 (s, 6H), 2.84 (t, $J = 7.4$ Hz, 4H), 1.77 – 1.60 (m, 4H), 1.50 – 1.31 (m, 4H), 0.96 (t, $J = 7.3$ Hz, 6H); ^{13}C NMR (63 MHz, CD_2Cl_2) δ/ppm 147.44, 145.09, 137.58, 133.68, 132.23, 129.70, 128.70, 126.68, 124.93, 123.88, 123.04, 120.35, 61.62, 34.48, 30.24, 22.63, 14.21; elemental analysis (%) found: C, 75.72; H, 6.36; S, 11.70 - calculated for $\text{C}_{34}\text{H}_{34}\text{O}_2\text{S}_2$: C, 75.80; H, 6.36; S, 11.90.

9.5.5 2,5-Dibutyl-10,11-dimethoxy-benzo[8,9]triphenyleno[1,2-*b*:4,3-*b'*]dithiophene



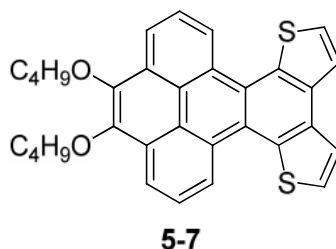
A solution of 4,5-bis(5-butylthien-2-yl)-9,10-dimethoxypyrene (0.700 g, 1.299 mmol) and iodine (0.660 g, 2.599 mmol) in 700 ml toluene was degassed with argon for 15 minutes and irradiated in a quartz tube at 300 nm overnight. The reaction mixture was washed with aqueous Na_2SO_3 solution, dried over MgSO_4 and the organic solvents were removed. The crude product was purified over silica column PE: DCM 2:1 to give 2,5-dibutyl-10,11-dimethoxy-benzo[8,9]triphenyleno[1,2-*b*:4,3-*b'*]dithiophene (0.424 g, 0.790 mmol) as yellow solid in 61 % yield (mp: 164°C); MS (FD, 8 kV) $m/z = 536.5$ g/mol - calculated: 536.2 g/mol for $\text{C}_{34}\text{H}_{32}\text{O}_2\text{S}_2$; ^1H NMR (300 MHz, CD_2Cl_2) δ/ppm 9.53 (d, $J = 8.0$ Hz, 2H), 8.60 (d, $J = 7.9$ Hz, 2H), 8.19 (t, $J = 8.0$ Hz, 2H), 7.60 (s, 2H), 4.24 (s, 6H), 3.12 (t, $J = 7.6$ Hz, 4H), 1.99 – 1.84 (m, 4H), 1.62 – 1.46 (m, 4H), 1.03 (t, $J = 7.4$ Hz, 6H); ^{13}C NMR (75 MHz, CD_2Cl_2) δ/ppm 148.32, 144.81, 136.29, 133.03, 129.81, 129.00, 126.66, 125.06, 123.89, 122.74, 120.45, 119.62, 61.66, 34.04, 30.67, 22.94, 14.23; elemental analysis (%) found: C, 75.20 ; H, 6.21; S, 11.58 - calculated for $\text{C}_{34}\text{H}_{32}\text{O}_2\text{S}_2$: C, 76.08; H, 6.01; S, 11.95.

9.5.6 4,5-Dibutoxy-9,10-bis(thien-2-yl)-pyrene



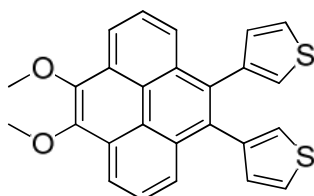
A solution of 4,5-dibromo-9,10-dibutoxypyrene (0.600 g, 1.190 mmol) in 20 ml dry toluene was degassed with argon for 15 minutes. $\text{Pd(PPh}_3)_4$ (0.041 g, 0.036 mmol) and 2-(tributylstannyl)thiophene (1.332 g, 3.570 mmol) were added, degassed for additional 5 minutes and refluxed under argon overnight. The organic solvent was removed under reduced pressure and the residue was purified over silica column PE: DCM 2:1 and crystallized from ethanol to give 4,5-dibutoxy-9,10-bis(thien-2-yl)-pyrene (0.384 g, 0.752 mmol) as colorless solid in 63 % yield (mp: 108°C); MS (FD, 8 kV) $m/z = 510.3$ g/mol - calculated: 510.2 g/mol for $\text{C}_{32}\text{H}_{30}\text{O}_2\text{S}_2$; ^1H NMR (250 MHz, CD_2Cl_2) δ 8.56 (dd, $J = 6.4, 2.6$ Hz, 2H), 8.04 – 7.93 (m, 4H), 7.42 (dd, $J = 4.9, 1.4$ Hz, 2H), 7.13 – 7.03 (m, 4H), 4.38 (t, $J = 6.6$ Hz, 4H), 2.06 – 1.90 (m, 4H), 1.76 – 1.59 (m, 4H), 1.06 (t, $J = 7.4$ Hz, 6H); ^{13}C NMR (63 MHz, CD_2Cl_2) δ 144.39, 140.22, 133.34, 132.11, 130.12, 129.31, 127.00, 126.79, 126.72, 124.69, 123.07, 120.73, 74.05, 33.24, 20.12, 14.40; elemental analysis (%) found: C, 73.73; H, 6.01; S, 12.06 - calculated for $\text{C}_{32}\text{H}_{30}\text{O}_2\text{S}_2$: C, 75.26; H, 5.92; S, 12.56.

9.5.7 10,11-Dibutoxy-benzo[8,9]triphenyleno[1,2-*b*:4,3-*b'*]dithiophene



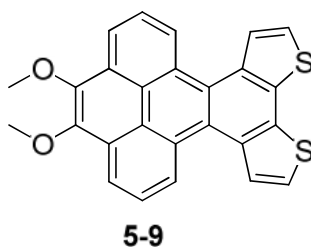
A solution of 4,5-dibutoxy-9,10-bis(thien-2-yl)-pyrene (0.378 g, 0.743 mmol) and iodine (0.377 g, 1.486 mmol) in 350 ml toluene was degassed with argon for 15 minutes and irradiated in a quartz tube at 300 nm overnight. The reaction mixture was washed with aqueous Na_2SO_3 solution, dried over MgSO_4 and the organic solvents were removed. Crystallization from ethanol gave 10,11-dibutoxy-benzo[8,9]triphenyleno[1,2-*b*:4,3-*b'*]dithiophene (0.272 g, 0.535 mmol) as yellow crystals in 72 % yield (mp: 128°C); MS (FD, 8 kV) m/z = 507.9 g/mol - calculated: 508.2 g/mol for $\text{C}_{32}\text{H}_{28}\text{O}_2\text{S}_2$; ^1H NMR (300 MHz, CD_2Cl_2) δ /ppm 9.56 (dd, J = 8.1, 0.9 Hz, 2H), 8.63 (dd, J = 7.9, 0.9 Hz, 2H), 8.19 (t, J = 8.0 Hz, 2H), 7.98 (d, J = 5.6 Hz, 2H), 7.82 (d, J = 5.5 Hz, 2H), 4.38 (t, J = 6.6 Hz, 4H), 2.07 – 1.93 (m, 4H), 1.78 – 1.61 (m, 4H), 1.08 (t, J = 7.4 Hz, 6H); ^{13}C NMR (75 MHz, CD_2Cl_2) δ /ppm 144.13, 136.08, 134.28, 129.59, 129.50, 127.99, 126.72, 125.88, 123.80, 122.87, 122.77, 120.99, 74.11, 33.28, 20.16, 14.43; elemental analysis (%) found: C, 75.41; H, 5.47; S, 12.37 - calculated for $\text{C}_{32}\text{H}_{28}\text{O}_2\text{S}_2$: C, 75.55; H, 5.55; S, 12.61.

9.5.8 4,5-Dimethoxy-9,10-bis(thien-3-yl)pyrene

**5-8**

A suspension of 4,5-dibromo-9,10-dimethoxypyrene (1.5 g, 3.57 mmol), 3-thienylboronic acid (1.827 g, 14.283 mmol) and Na_2CO_3 (1.083 g, 10.212 mmol) in a mixture of 31.5 ml toluene, 31.5 ml ethanol and 10.5 ml water was degassed with argon for 15 minutes. $\text{Pd}(\text{PPh}_3)_4$ (0.414 g, 0.357 mmol) was added, degassed for additional 5 minutes und refluxed under argon overnight. The organic solvent was removed under reduced pressure and the residue was purified over silica column PE: DCM 3:2 and crystallized from ethanol to give 4,5-dimethoxy-9,10-bis(thien-3-yl)pyrene (1.220 g, 2.86 mmol) as colorless crystals in 80 % yield (mp: 229 °C); MS (FD, 8 kV) m/z = 426.3 g/mol - calculated: 426.6 g/mol for $\text{C}_{26}\text{H}_{18}\text{O}_2\text{S}_2$. ^1H NMR (300 MHz, CD_2Cl_2) δ /ppm 8.52 (dd, J = 6.5, 2.4 Hz, 2H), 8.01 – 7.91 (m, 4H), 7.35 (dd, J = 4.9, 3.0 Hz, 2H), 7.15 (s, 2H), 7.05 (s, 2H), 4.23 (s, 6H); ^{13}C NMR (75 MHz, CD_2Cl_2) δ /ppm 145.17, 139.99, 134.28, 131.89, 131.07, 128.82, 126.64, 125.29, 125.05, 124.56, 122.94, 120.06, 61.65; elemental analysis (%) found: C, 73.18; H, 4.29; S, 15.10 – calculated for $\text{C}_{26}\text{H}_{18}\text{O}_2\text{S}_2$: C, 73.21; H, 4.25; S, 15.03.

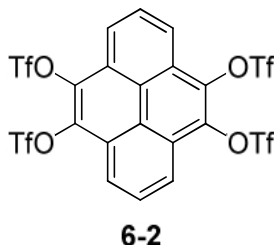
9.5.9 10,11-Dimethoxy-benzo[8,9]triphenyleno[2,1-*b*:3,4-*b'*]dithiophene



To a solution of 4,5-dimethoxy-9,10-di(thien-3-yl)pyrene (0.400 g, 0.938 mmol) in 100 ml dry dichloromethane, FeCl_3 (0.319 g, 1.969 mmol) in 6 ml nitromethane was added dropwise under vigorous stirring at room temperature while argon was bubbled through the solution. The reaction mixture was stirred for 15 minutes, quenched by the addition of zinc powder and the crude mixture was filtered over a silica plug. The organic solvent was evaporated under reduced pressure and the residue was purified over silica column PE: DCM 3:1 to give 10,11-dimethoxy-benzo[8,9]triphenyleno[2,1-*b*:3,4-*b'*]dithiophene (0.202 g, 0.48 mmol) as yellow solid in 51 % yield (mp: 201 °C); MS (FD, 8 kV) $m/z = 425.1$ g/mol - calculated: 424.5 g/mol for $\text{C}_{26}\text{H}_{16}\text{O}_2\text{S}_2$; ^1H NMR (300 MHz, CD_2Cl_2) δ/ppm 8.88 (d, $J = 7.9$ Hz, 2H), 8.47 (dd, $J = 7.8, 0.9$ Hz, 2H), 8.32 (d, $J = 5.7$ Hz, 2H), 7.97 (t, $J = 7.9$ Hz, 2H), 7.51 (d, $J = 6.7$ Hz, 2H), 4.24 (s, 6H); ^{13}C NMR (75 MHz, CD_2Cl_2) δ/ppm 144.85, 134.71, 134.04, 129.83, 128.81, 127.59, 126.38, 126.01, 124.75, 124.69, 122.52, 119.93, 61.59; elemental analysis (%) found: C, 73.30; H, 3.76; S, 14.95 - calculated for $\text{C}_{26}\text{H}_{16}\text{O}_2\text{S}_2$: C, 73.56; H, 3.80; S, 15.11.

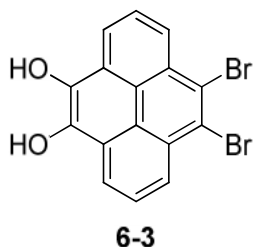
9.6 Hexaaryl[*a,c,fg,j,l,op*]tetracenes

9.6.1 4,5,9,10-Tetratriflatopyrene



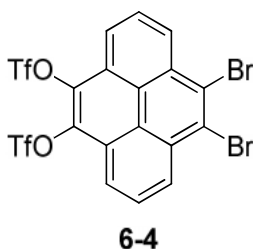
In a dried flask pyrene-4,5,9,10-tetraone (1.68 g, 6.41 mmol) and palladium on carbon (0.4 g) were stirred vigorously in dry 40 ml THF under hydrogen atmosphere for four hours. Dry pyridine (10.3 ml, 128.1 mmol) and trifluoromethane sulfonic acid anhydride (8.6 ml, 51.25 mmol) were added successively at -78°C and let warm to room temperature overnight. The reaction mixture was poured over water and was extracted with DCM. The organic phase was dried over MgSO_4 and the solvent was removed under reduced pressure. The crude product was dissolved in DCM and precipitated in methanol. Crystallization from chloroform gave 4,5,9,10-tetratriflatopyrene (0.267 g, 0.34 mmol) as colorless crystals in 5 % yield (mp: 216°C (decomposition)); MS (FD, 8 kV) $m/z = 793.6$ g/mol - calculated: 793.9 g/mol for $\text{C}_{20}\text{H}_6\text{F}_{12}\text{O}_{12}\text{S}_4$; ^1H NMR (500 MHz, $\text{C}_2\text{Cl}_4\text{D}_2$, 120°C) δ/ppm 8.68 (d, $J = 8.0$ Hz, 4H), 8.38 (t, $J = 8.0$ Hz, 2H); ^{13}C NMR (126 MHz, $\text{C}_2\text{Cl}_4\text{D}_2$, 120°C) δ/ppm 136.84, 128.84, 125.27, 124.13, 123.92, 119.04 (q, $^1J(\text{CF}) = 321.7$ Hz); elemental analysis (%) found: C, 30.20; H, 0.59; S, 16.10 - calculated $\text{C}_{20}\text{H}_6\text{F}_{12}\text{O}_{12}\text{S}_4$: C, 30.23; H, 0.76; S, 16.14.

9.6.2 4,5-Dibromo-9,10-dihydroxypyrene



9,10-Dibromopyrene-4,5-dione (2.88 g, 7.39 mmol) and sodium dithionite (5.17 g, 29.7 mmol) were suspended in a mixture of 200 ml water and 300 ml THF and stirred for four hours. 250 ml dichloromethane were added and the organic layer was separated, dried over MgSO_4 and the solvent was evaporated under reduced pressure. After drying under high vacuum 4,5-dibromo-9,10-dihydroxypyrene (2.37 g, 6.04 mmol) was obtained as brownish solid in 82 % yield. ^1H NMR (250 MHz, DMSO-d_6) δ /ppm 9.54 (s, 2H), 8.61 (d, $J = 7.9$ Hz, 2H), 8.53 (d, $J = 7.9$ Hz, 2H), 8.17 (t, $J = 8.0$ Hz, 2H). Singulett at 9.54 ppm disappeared after addition of one drop D_2O .

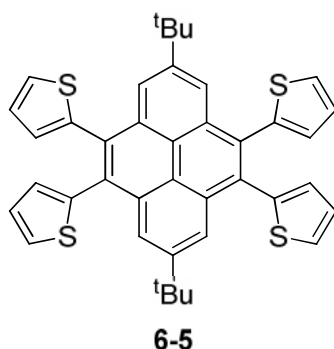
9.6.3 4,5-Dibromo-9,10-ditriflatopyrene



In a dried flask with a septum 4,5-dibromo-9,10-dihydroxypyrene (5.77 g, 14.72 mmol) were dissolved in 400 ml of dry THF under argon and dry pyridine (7.0 g, 88.5 mmol) were added. After cooling to -78°C trifluoromethane sulfonic acid anhydride (12.5 g, 44.3 mmol) was added dropwise und stirring and the reaction mixture was warmed to room

temperature overnight. The organic solvents were removed under reduced pressure and the residue was purified over silica column PE: DCM 7:1 to obtain 4,5-dibromo-9,10-ditriflatopyrene (2.23 g, 3.40 mmol) as colorless solid in 23 % yield (mp: 195 °C (decomposition)); MS (FD, 8 kV) m/z = 655.9 g/mol - calculated: 655.8 g/mol for $C_{18}H_6Br_2F_6O_6S_2$; 1H NMR (300 MHz, CD_2Cl_2 , 40°C) δ /ppm 8.96 (dd, J = 8.1, 0.9 Hz, 2H), 8.62 (dd, J = 8.0, 0.7 Hz, 2H), 8.30 (t, J = 8.1 Hz, 2H); ^{13}C NMR (126 MHz, CD_2Cl_2) δ /ppm 136.76, 131.19, 130.67, 129.19, 127.92, 125.16, 124.31, 123.05, 119.37 (q, $^1J(CF)$ = 320.9 Hz); elemental analysis (%) found: C, 32.27; H, 0.90; S, 9.72 - calculated $C_{18}H_6Br_2F_6O_6S_2$: C, 32.95; H, 0.92; S, 9.77.

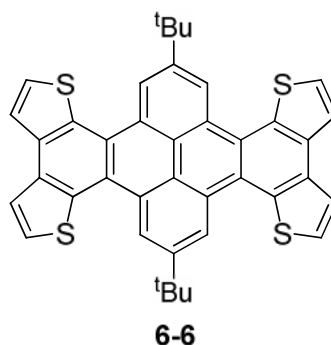
9.6.4 2,7-Di-*tert*-butyl-4,5,9,10-tetra-(thien-2-yl)pyrene



A solution of 2,7-di-*tert*-butyl-4,5,9,10-tetrabromopyrene (0.5 g, 0.794 mmol) in 15 ml dry toluene was degassed with argon for 15 minutes. $Pd(PPh_3)_4$ (0.055 g, 0.048 mmol) and 2-tributylstannylthiophene (1.77 g, 4.76 mmol) were added, degassed for additional 5 minutes and refluxed under argon overnight. The organic solvent was removed under reduced pressure and the residue was purified over silica column PE: DCM 5:1 to give 2,7-di-*tert*-butyl-4,5,9,10-tetra-(thien-2-yl)pyrene (0.245 g, 0.381 mmol) as slightly yellow solid in 48 % yield (mp > 400 °C); 1H NMR (500 MHz, $THF-d_8$) δ /ppm = 8.21 (s, 4H), 7.48 (dd, J = 4.3, 2.1 Hz, 4H), 7.08 – 7.05 (m, 8H), 1.31 (s, 18H); ^{13}C NMR (126 MHz, $THF-d_8$) δ /ppm 150.43, 137.12, 135.05, 129.47, 128.83,

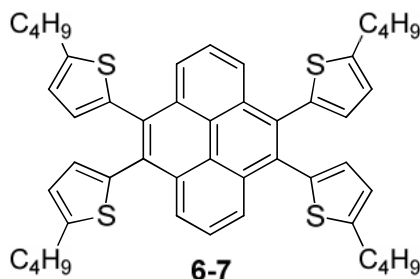
125.89, 123.77, 123.72, 123.41, 36.98, 32.56; HRMS (ESI): m/z calculated for $[C_{40}H_{34}S_4+H]^+$: 643.1616 - found: 643.1601.

9.6.5 8,17-Di-*tert*-butyl-dibenzo[*fg,op*]tetrathieno[*a,c,j,l*]-tetracene



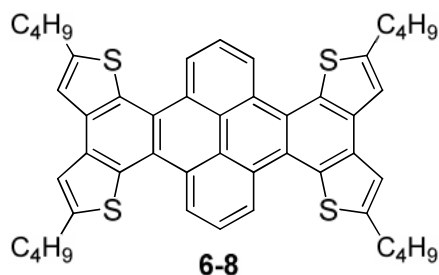
A solution of 2,7-di-*tert*-butyl-4,5,9,10-tetra(2-thiopheno) pyrene (0.125 g, 0.194 mmol) and iodine (0.189 g, 0.747 mmol) in 120 ml toluene was degassed with argon for 15 minutes and irradiated in a quartz tube at 300 nm overnight. The reaction mixture was washed with aqueous Na_2SO_3 solution, dried over $MgSO_4$ and the organic solvents were removed. Purification over silica flash gel with PE: DCM 4:1 gave 8,17-di-*tert*-butyl-dibenzo[*fg,op*]-tetrathieno[*a,c,j,l*]tetracene (0.074 g, 0.116 mmol) as slightly yellow solid in 60 % yield (mp > 400 °C); 1H NMR (300 MHz, THF- d_8) δ /ppm 9.69 (s, 4H), 8.16 (d, J = 5.6 Hz, 4H), 8.00 (d, J = 5.6 Hz, 4H), 1.82 (s, 18H); ^{13}C NMR (126 MHz, THF- d_8) δ /ppm 150.43, 137.12, 135.05, 129.47, 128.83, 125.89, 123.77, 123.72, 123.41, 36.98, 32.56; HRMS (ESI): m/z calculated for $[C_{40}H_{30}S_4+H]^+$: 639.1303 - found: 639.1296.

9.6.6 4,5,9,10-Tetrakis-(5-*n*-butylthien-2-yl)pyrene



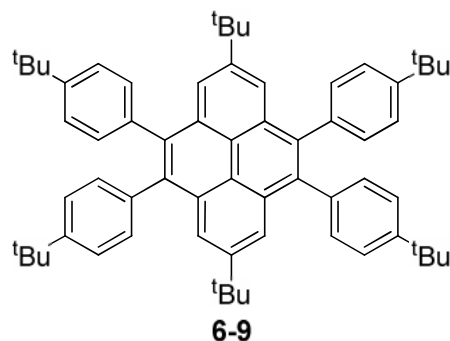
In a dried flask with a condenser 4,5-dibromo-9,10-ditriflatopyrene (0.5 g, 0.76 mmol) and 2-tributylstannyl-5-*n*-butylthiophene (3.1 g, 7.2 mmol) in 50 ml dry toluene were degassed with argon. Tetrakis(triphenylphosphine)-palladium(0) (0.096 g, 0.08 mmol) was added and the mixture was refluxed while the reaction was monitored by TLC. Two further portions of 2-tributylstannyl-5-*n*-butylthiophene (3.1 g, 7.2 mmol) were added after 7 hours and 16 hours of reflux. After cooling to room temperature the organic solvents were removed under reduced pressure and the residue was purified over silica column PE: DCM 5:1 and crystallization from ethanol to obtain 4,5,9,10-tetrakis-(5-*n*-butylthien-2-yl)pyrene (0.239 g, 0.32 mmol) as slightly yellow crystals in 42 % yield (mp: 159 °C); ^1H NMR (300 MHz, CD_2Cl_2) δ /ppm 8.21 (d, $J = 7.9$ Hz, 4H), 7.91 (t, $J = 7.9$ 2H), 6.86 (d, $J = 3.4$ Hz, 4H), 6.76 (d, $J = 3.4$ Hz, 4H), 2.84 (t, $J = 7.5$ Hz, 8H), 1.68 (m, 9H), 1.40 (m, 9H), 0.96 (t, $J = 7.3$ Hz, 13H); ^{13}C NMR (75 MHz, CD_2Cl_2) δ /ppm 147.50, 137.69, 133.71, 132.11, 129.74, 126.64, 126.06, 124.66, 123.93, 34.50, 30.27, 22.64, 14.21; HRMS (ESI): m/z calculated for $[\text{C}_{48}\text{H}_{50}\text{S}_4+\text{H}]^+$: 755.2868 - found: 755.2857.

9.6.7 2,5,11,14-Tetra-*n*-butyl-dibenzo[*fg,op*]-tetrathieno[*a,c,j,l*]tetracene



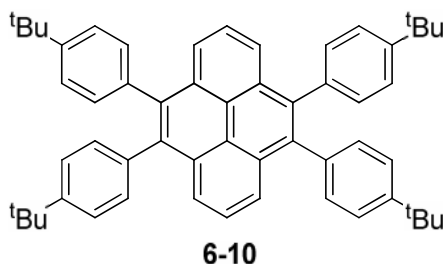
To a solution of 4,5,9,10-tetrakis(5-butylthiophen-2-yl)pyrene (0.33 g, 0.44 mmol) in 80 ml dry dichloromethane, FeCl_3 (0.32 g, 1.97 mmol) in 5.5 ml nitromethane was added dropwise under vigorous stirring at room temperature while argon was bubbled through the solution. The reaction mixture was stirred for 30 minutes, quenched by the addition of zinc powder and the crude mixture was filtered over a silica plug. The organic solvent was evaporated under reduced pressure and the residue was purified by flash silica column PE: EtOAc 9.5:0.5 followed by recycling GPC to give 2,5,11,14-tetra-*n*-butyl-dibenzo[*fg,op*]-tetrathieno[*a,c,j,l*]tetracene (0.056 g, 0.075 mmol) as yellow solid in 17 % yield (mp: 192 °C); ^1H NMR (300 MHz, CD_2Cl_2) δ /ppm 9.25 (d, $J = 8.0$ Hz, 4H), 8.07 (t, $J = 8.0$ Hz, 2H), 7.46 (s, 4H), 3.06 (t, $J = 7.6$ Hz, 8H), 1.88 (m, 8H), 1.52 (m, 8H), 1.02 (t, $J = 7.3$ Hz, 12H); ^{13}C NMR (75 MHz, CD_2Cl_2) δ /ppm 148.24, 136.18, 133.09, 129.09, 126.39, 124.77, 124.62, 124.08, 119.61, 34.02, 30.74, 22.97, 14.25; HRMS (ESI): m/z calculated for $[\text{C}_{48}\text{H}_{46}\text{S}_4+\text{H}]^+$: 751.2555 - found: 751.2547.

9.6.8 2,7-Di-*tert*-butyl-4,5,9,10-tetrakis(4-*tert*-butylphenyl)pyrene



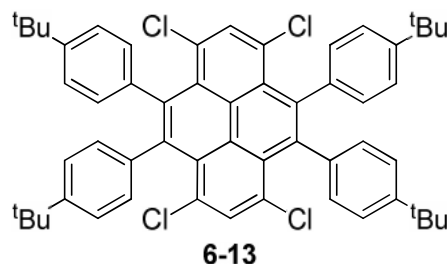
In a dried flask with a condenser 4,5,9,10-tetrabromo-2,7-di-*tert*-butylpyrene (1.5 g, 2.4 mmol), 4-*tert*-butylphenylboronic acid (2.5 g, 14.2 mmol), sodium carbonate (21.2 g, 200 mmol), 100 ml water and 200 ml toluene were degassed with argon. Tetrakis(triphenylphosphine)palladium(0) (0.28 g, 0.24 mmol) was added and the mixture was refluxed under vigorous stirring for 4 days. 1 g of the boronic acid was added each day. The hot mixture was transferred into a separating funnel, the water phase was released and the organic was cooled to room temperature. Precipitate was collected by filtration and dried under vacuum to give 2,7-di-*tert*-butyl-4,5,9,10-tetrakis(4-*tert*-butylphenyl)pyrene (1.3 g, 1.5 mmol) as colorless solid in 64 % yield (mp > 400°C); MS (FD, 8 kV) $m/z = 843.2$ g/mol - calculated: 842.6 g/mol for $C_{64}H_{74}$; 1H NMR (500 MHz, $C_2D_2Cl_4$, 120°C) δ /ppm 7.94 (s, 4H), 7.25 (d, $J = 8.8$ Hz, 8H), 7.16 (d, $J = 8.1$ Hz, 8H), 1.31 (s, 36H), 1.24 (s, 18H); ^{13}C NMR (126 MHz, $C_2D_2Cl_4$, 120°C) δ /ppm 149.38, 148.36, 147.06, 138.26, 137.34, 131.32, 124.22, 122.34, 122.19, 35.40, 34.54, 31.76, 31.55.

9.6.9 4,5,9,10-Tetrakis(4-*tert*-butylphenyl)pyrene



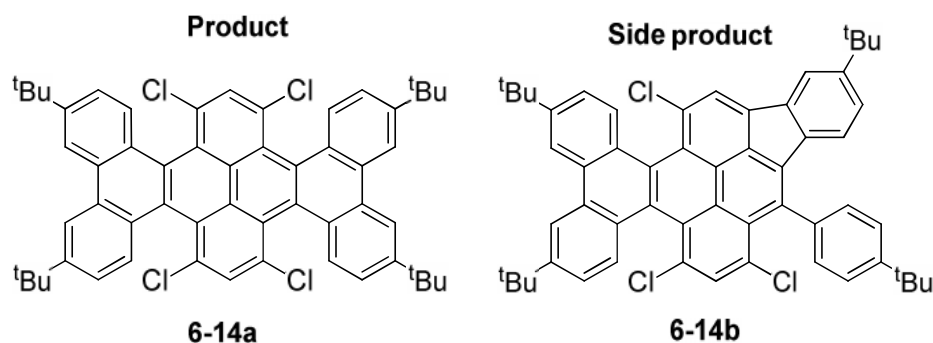
In a dried flask with a condenser 4,5-dibromo-9,10-ditriflatopyrene (1.00 g, 1.51 mmol), 4-*tert*-butylphenylbromic acid (1.63 g, 9.14 mmol), sodium carbonate (14.84 g, 140 mmol), 70 ml water and 140 ml toluene were degassed with argon. Tetrakis(triphenylphosphine)palladium(0) (0.18 g, 0.15 mmol) was added and the mixture was refluxed under vigorous stirring overnight. The hot mixture was transferred into a separating funnel, the water phase was released and the organic was cooled to room temperature. The precipitate was collected by filtration and the filtrate was removed under reduced pressure. The solids were combined and crystallized from chloroform to give 4,5,9,10-tetrakis(4-*tert*-butylphenyl)pyrene (0.79 g, 1.08) as colorless crystals in 72 % yield (mp > 400°C); ^1H NMR (500 MHz, $\text{C}_2\text{D}_2\text{Cl}_4$, 120°C) δ /ppm 7.98 (d, $J = 7.8$ Hz, 4H), 7.78 (t, $J = 7.9$ Hz, 2H), 7.24 (d, $J = 7.7$ Hz, 8H), 7.15 (d, $J = 7.9$ Hz, 8H), 1.30 (s, 36H); ^{13}C NMR (126 MHz, CDCl_3 , 50°C) δ /ppm 149.46, 138.43, 137.13, 131.66, 131.23, 125.93, 125.10, 124.52, 124.14, 34.70, 31.60; HRMS (ESI): m/z calculated for $[\text{C}_{56}\text{H}_{58}+\text{H}]^+$: 731.4611 - found: 731.4608.

9.6.10 4,5,9,10-Tetrakis(4-*tert*-butylphenyl)-1,3,6,8-tetrachloropyrene



To a solution of 4,5,9,10-tetrakis(4-*tert*-butylphenyl)pyrene (0.50 g, 0.68 mmol) in 150 ml chloroform sulfuryl chloride (2.8 ml, 34.5 mmol) in 6 ml acetic acid was added dropwise and stirred for 30 minutes. The addition of sulfuryl chloride in acetic acid was repeated and monitored by FD-Mass until fourfold chlorination was completed. The reaction mixture was poured on crushed ice and was neutralized using aqueous sodium carbonate solution. After extraction with DCM the organic phase was dried over MgSO_4 and the solvents removed under reduced pressure. Crystallization from ethanol gave 4,5,9,10-tetrakis(4-*tert*-butylphenyl)-1,3,6,8-tetrachloropyrene (0.384 g, 0.442 mmol) as yellow solid in 65 % yield (mp: 395°C); MS (FD, 8 kV) m/z = 869.2 g/mol - calculated: 868.3 g/mol for $\text{C}_{56}\text{H}_{54}\text{Cl}_4$; ^1H NMR (300 MHz, CDCl_3) δ /ppm 7.88 (s, 2H), 7.07 (d, J = 8.6 Hz, 8H), 6.98 (d, J = 8.5 Hz, 8H), 1.23 (s, 36H); ^{13}C NMR (75 MHz, CDCl_3) δ /ppm 149.50, 138.94, 137.45, 134.72, 131.64, 131.06, 128.58, 126.80, 123.43, 34.58, 31.56; HRMS (ESI): m/z calculated for $[\text{C}_{56}\text{H}_{54}\text{Cl}_4+\text{H}]^+$: 867.3052 - found: 867.3052; elemental analysis (%) found: C, 76.41; H, 6.26 – calculated for $\text{C}_{56}\text{H}_{54}\text{Cl}_4$: C, 77.41; H, 6.26.

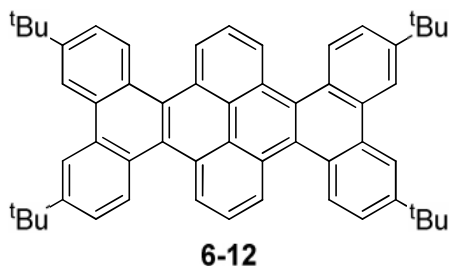
9.6.11 3,6,14,17-Tetra-*tert*-butyl-9,11,20,22-tetrachlorohexabenzo[*a,c,fg,j,l,op*]tetracene



(75 MHz, CD₂Cl₂) δ /ppm 150.99, 134.20, 132.39, 131.64, 131.28, 131.13, 125.08, 124.41, 124.30, 124.15, 118.86, 35.74, 31.74; HRMS (ESI): m/z calculated for [C₅₆H₅₀Cl₄+NH₄]⁺: 880.3005 - found: 880.3001.

Side product **6-14b**: red solid in 46 % yield; MS (FD, 8 kV) m/z = 829.2 g/mol - calculated: 828.3 g/mol for C₅₆H₅₁Cl₃; ¹H NMR (700 MHz, CDCl₃) δ /ppm 8.58 (d, J = 1.8 Hz, 1H), 8.57 (d, J = 1.8 Hz, 1H), 8.43 (s, 1H), 8.02 (s, 1H), 8.02 (d, J = 8.3 Hz, 1H), 7.94 (d, J = 1.7 Hz, 1H), 7.86 (d, J = 8.5 Hz, 1H), 7.67 (dd, J = 8.4, 1.8 Hz, 1H), 7.62 – 7.58 (m, 3H), 7.50 (dd, J = 8.3, 1.7 Hz, 1H), 7.46 (d, J = 7.8 Hz, 1H), 7.08 (dd, J = 8.1, 1.8 Hz, 1H), 6.35 (d, J = 8.2 Hz, 1H), 1.53 (s, 9H), 1.52 (s, 9H), 1.50 (s, 9H), 1.38 (s, 9H); ¹³C NMR (176 MHz, CDCl₃) δ /ppm 152.33, 151.58, 150.23, 149.76, 140.65, 137.40, 137.14, 136.13, 135.89, 135.08, 133.50, 133.09, 131.72, 131.24, 130.96, 130.43, 130.37, 130.30, 130.06, 129.67, 129.58, 129.50, 128.43, 127.73, 127.55, 126.93, 125.51, 125.50, 125.48, 125.28, 125.12, 125.03, 124.54, 123.90, 123.54, 122.38, 119.18, 119.01, 118.70, 35.43, 35.34, 35.28, 35.07, 31.91, 31.83, 31.78, 31.68. (one C_{arom} signal is not resolved).

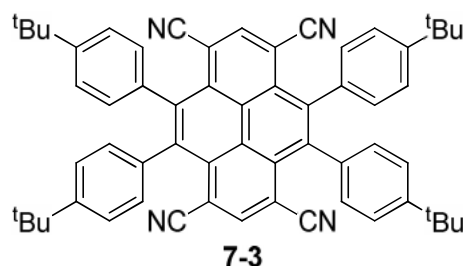
9.6.12 3,6,14,17-Tetra-*tert*-butylhexabenzo[*a,c,fg,j,l,op*]-tetracene



To a solution of 9,11,20,22-tetrachloro-3,6,14,17-(tetra-*tert*-butyl)hexabenzo[*a,c,fg,j,l,op*]tetracene (0.0018 g, 2 nmol) in 0.5 ml dry toluene tributyltin hydride (0.3 ml) and AIBN (0.005 g, 0.03 mmol) were added. The reaction mixture was heated to 110°C and stirred overnight. After cooling to room temperature toluene was removed and the crude product was purified by flash silica column chromatography using PE:DCM (7:1) as eluent to obtain traces of 3,6,14,17-tetra-*tert*-butylhexabenzo[*a,c,fg,j,l,op*]tetracene as yellow solid; ^1H NMR (300 MHz, CD_2Cl_2) δ /ppm 8.96 (d, $J = 8.0$ Hz, 4H), 8.80 (d, $J = 8.7$ Hz, 4H), 8.75 (d, $J = 1.9$ Hz, 4H), 8.06 (t, $J = 8.0$ Hz, 2H), 7.72 (dd, $J = 8.7$, 1.9 Hz, 4H), 1.53 (s, 36H); HRMS (ESI): m/z calculated for $[\text{C}_{56}\text{H}_{54}+\text{H}]^+$: 727.4298 - found: 727.4287.

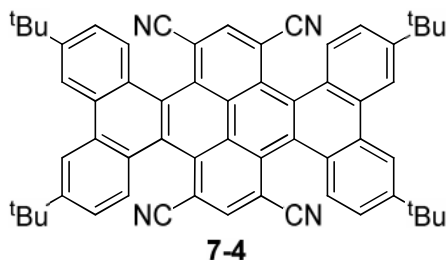
9.7 *Peri*-Pentacene

9.7.1 4,5,9,10-Tetrakis(4-*tert*-butylphenyl)pyrene-1,3,6,8-tetracarbonitrile



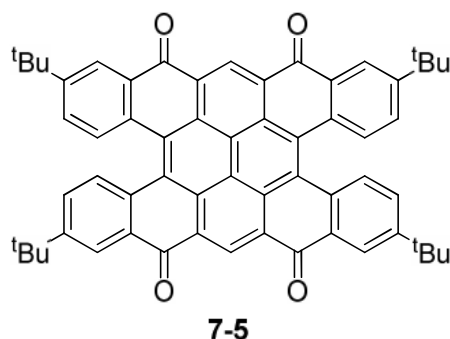
4,5,9,10-Tetrakis(4-*tert*-butylphenyl)-1,3,6,8-tetrachloropyrene (2.328 g, 2.679 mmol) and copper(I) cyanide (5.471 g, 61.091 mmol) were suspended in 80 ml dry *N*-methylpyrrolidone under argon and stirred at 180°C for three days. After cooling the reaction mixture to 60°C an excess of Mohr's salt ($\text{Fe}(\text{NH}_4)_2(\text{SO}_4)_2 \cdot 6\text{H}_2\text{O}$) in water was added and stirred for two hours. The crude product was extracted with dichloromethane, dried over MgSO_4 and the solvents removed under reduced pressure. Silica chromatography using DCM as eluent gave 4,5,9,10-tetrakis(4-*tert*-butylphenyl)pyrene-1,3,6,8-tetracarbonitrile (1.218 g, 1.466 mmol) as yellow solid in 55 % yield (mp > 400°C); MS (FD, 8 kV) m/z = 830.2 g/mol - calculated: 830.4 g/mol for $\text{C}_{60}\text{H}_{54}\text{N}_4$; ^1H NMR (300 MHz, CD_2Cl_2) δ /ppm 8.66 (s, 2H), 7.30 (d, J = 8.3 Hz, 8H), 7.14 (d, J = 8.2 Hz, 8H), 1.31 (s, 36H); ^{13}C NMR (75 MHz, CD_2Cl_2) δ /ppm 153.21, 143.56, 142.96, 134.65, 134.30, 132.04, 125.20, 124.40, 116.22, 111.27, 35.13, 31.57; IR (neat, $1/\lambda$ in cm^{-1}) 3080, 3029, 2956, 2902, 2868, 2218 ($\text{CN}_{\text{Nitrile}}$), 1614, 1531, 1475, 1458, 1400, 1363, 1302, 1269, 1203, 1113, 1016, 935, 889, 860, 837, 796, 734, 669, 569; elemental analysis (%) found: C, 85.68; H, 6.96; N, 6.47 – calculated for $\text{C}_{60}\text{H}_{54}\text{N}_4$: C, 86.71; H, 6.55; N, 6.74.

9.7.2 3,6,14,17-Tetra-*tert*-butylhexabenzo[*a,c,fg,j,l,op*]-tetracene-9,11,20,22-tetracarbonitrile



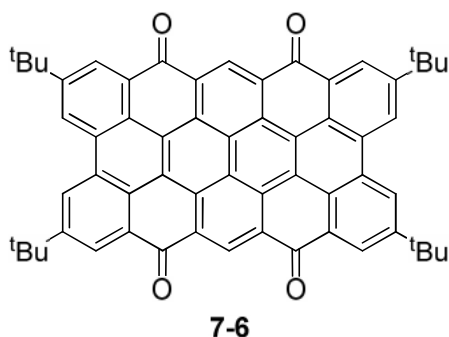
To a solution of 4,5,9,10-tetrakis(4-*tert*-butylphenyl)pyrene-1,3,6,8-tetracarbonitrile (0.005 g, 0.006 mmol) in dry dichloromethane and a 1:1 mixture of PIFA/ $\text{BF}_3 \cdot \text{Et}_2\text{O}$ (3eq., 0.065 M) in dichloromethane was added dropwise at -40°C under argon. The reaction mixture was stirred for 3.5 hours and warmed to room temperature overnight. After addition of water the organic phase was separated, dried over MgSO_4 , filtered and the solvent was removed under reduced pressure. Column chromatography with pure dichloromethane gave 3,6,14,17-tetra-*tert*-butylhexabenzo[*a,c,fg,j,l,op*]tetracene-9,11,20,22-tetracarbonitrile (0.0006 g, 0.0007 mmol) as orange solid in 12 % yield; ratio of conformers distinguishable by ^1H -NMR 3.8:1 : ^1H NMR (700 MHz, CD_2Cl_2) δ/ppm 8.89 (s, 2H), 8.82 (d, $J = 1.6$ Hz, 4H), 8.23 (d, $J = 8.5$ Hz, 4H), 7.88 (dd, $J = 8.5, 1.6$ Hz, 4H), 1.60 (s, 36H); ^1H NMR (700 MHz, CD_2Cl_2) δ/ppm 8.81 (d, $J = 1.5$ Hz, 4H), 8.69 (s, 2H), 8.31 (d, $J = 8.4$ Hz, 4H), 7.91 (dd, $J = 8.5, 1.6$ Hz, 4H), 1.60 (s, 36H); due to low concentrated solution only one signal of the major conformer could be detected in carbon NMR, ^{13}C NMR (176 MHz, CD_2Cl_2) δ/ppm 153.81, 140.17, 132.48, 132.36, 132.15, 131.42, 130.55, 126.64, 125.83, 120.84, 118.14, 109.66, 108.60, 36.01, 31.68. HRMS (ESI): m/z calculated for $[\text{C}_{60}\text{H}_{50}\text{N}_4 + \text{NH}_4]^+$: 844.4374 - found: 844.4378.

9.7.3 2,7,13,18-Tetra-*tert*-butyldinaphtho[1,2,3-*gh*:1',2',3'-*tu*]pyranthrene-9,11,20,22-tetraone



4,5,9,10-Tetrakis(4-*tert*-butylphenyl)pyrene-1,3,6,8-tetracarboxylic diimide (0.100 g, 0.120 mmol) was heated in 60 ml of a 2:1 mixture of concentrated sulfuric acid and water at 160°C overnight. The reaction mixture was poured on crushed ice and neutralized with sodium carbonate. The crude product was extracted with dichloromethane, the organic phase was dried over MgSO₄ and the solvent was removed under reduced pressure. Column chromatography on silica with DCM followed by 9:1 DCM: EtOAc yielded 2,7,13,18-tetra-*tert*-butyldinaphtho[1,2,3-*gh*:1',2',3'-*tu*]pyranthrene-9,11,20,22-tetraone (0.065 g, 0.078 mmol) as dark purple solid in 65 % yield (mp > 400°C); ratio of conformers distinguishable by ¹H-NMR 2:1 : ¹H NMR (250 MHz, CD₂Cl₂) δ/ppm 9.09 (s, 2H), 8.24 (d, *J* = 2.2 Hz, 4H), 7.86 (d, *J* = 8.5 Hz, 4H), 7.41 (dd, *J* = 8.5, 2.2 Hz, 4H), 1.47 (s, 36H); ¹H NMR (250 MHz, CD₂Cl₂) δ/ppm 8.67 (s, 2H), 8.10 (d, *J* = 2.0 Hz, 4H), 7.59 (d, *J* = 8.5 Hz, 4H), 7.29 (dd, *J* = 8.5, 2.2 Hz, 4H), 1.46 (s, 36H); ¹³C NMR (176 MHz, CD₂Cl₂) δ/ppm 183.32, 154.59, 134.26, 132.66, 132.26, 131.96, 131.62, 129.82, 127.40, 126.93, 124.42, 120.67, 35.71, 31.38; ¹³C NMR (176 MHz, CD₂Cl₂) δ/ppm 182.98, 154.43, 133.95, 132.55, 132.23, 130.87, 130.60, 129.51, 127.20, 126.11, 124.11, 120.03, 35.65, 31.40; IR (neat, 1/λ in cm⁻¹) 2956, 2904, 2868, 1653 (C=O), 1601, 1547, 1446, 1394, 1361, 1304, 1238, 1180, 1147, 980, 949, 885, 841, 806, 779, 712, 607; HRMS (ESI): *m/z* calculated for [C₆₀H₅₀O₄+H]⁺: 835.3782 - found: 835.3798.

9.7.4 2,5,11,14-Tetra-*tert*-butyltetrabenzo[*bc,ef,mn,pq*]-ovalene-7,9,16,18-tetraone



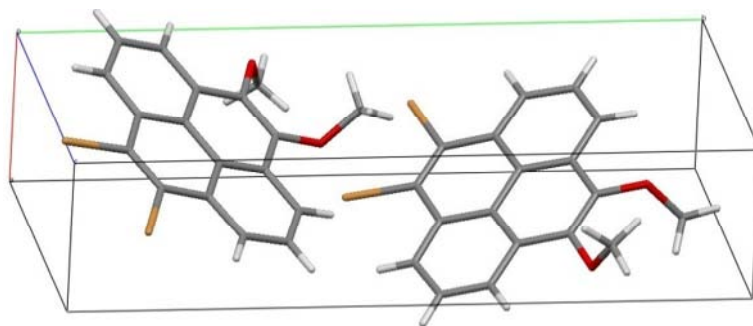
Traces of 3,6,14,17-tetra-*tert*-butylhexabenzo[*a,c,fg,j,l,op*]tetracene-9,11,20,22-tetracarbonitrile were heated in 30 ml of a 2:1 mixture of concentrated sulfuric acid and water at 160°C for two hours. The reaction mixture was poured on crushed iced and filtered over teflon filter paper. The product was dissolved in concentrated acid to yield a purple solution.

IR (on teflon filter, $1/\lambda$ in cm^{-1}) 2960, 2925, 2873, 1658 (C=O), 1592, 1481, 1363; MS (MALDI, DTCB matrix) $m/z = 831.03$ g/mol - calculated: 831.35 g/mol for $[\text{C}_{60}\text{H}_{46}\text{O}_4+\text{H}]^+$.

9.8 Crystal Data

The single crystal analysis was performed on a Nonius-KCCD diffractometer with a Mo-K α ($\lambda = 0.71923$ Å, graphite monochromatized) at a temperature of 150 K to 120 K. The structures were solved by direct methods (Shelxs) and refined on F with anisotropic temperature factors for all non-hydrogen atoms. The H atoms were refined with fixed isotropic temperature factors in the riding mode.

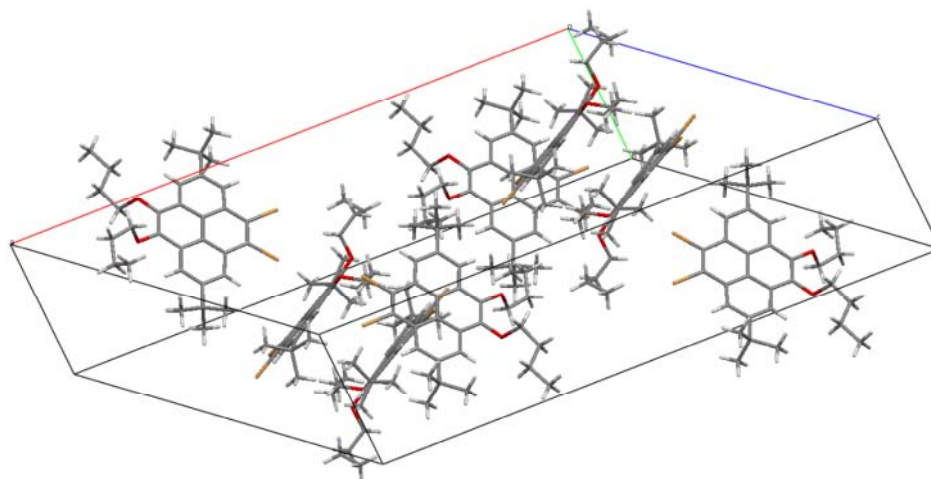
9.8.1 4,5-Dibromo-9,10-dimethoxypyrene (3-3)



$C_{18}H_{12}Br_2O_2$, $M_r = 420.10$ g/mol, monoclinic, space group $P2_1$, $a = 4.1977(2)$ Å, $b = 18.0487(9)$ Å, $c = 9.8546(5)$ Å, $\beta = 93.489(3)^\circ$, $V = 745.23(6)$ Å³, $Z = 2$, $D_x = 1.87$, 8472 reflections measured, 3959 unique reflections, $R_{int} = 0.0006$, 3383 reflections observed ($I > 2\sigma(I)$), $R = 0.059$, $R_w = 0.065$.

Cambridge Crystallographic Data Centre identifier: CCDC-819580

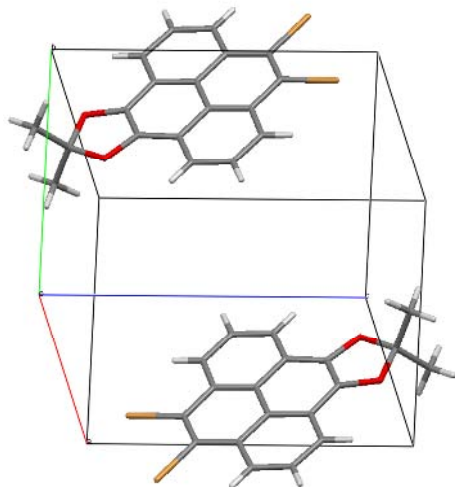
9.8.2 4,5-Dibromo-9,10-dibutoxy-2,7-di-*tert*-butylpyrene (3-4)



$\text{C}_{32}\text{H}_{40}\text{Br}_2\text{O}_2$, $M_r = 616.48$ g/mol, monoclinic, space group $C2/c$, $a = 32.7176(9)$ Å, $b = 9.3992(6)$ Å, $c = 25.0158(9)$ Å, $\beta = 130.050(2)^\circ$, $V = 5888.7(5)$ Å³, $Z = 8$, $D_x = 1.39$, 9237 reflections measured, 5703 unique reflections, $R_{\text{int}} = 0.0007$, 3802 reflections observed ($I > 2.5\sigma(I)$), $R = 0.060$, $R_w = 0.071$.

Cambridge Crystallographic Data Centre identifier: CCDC-874824

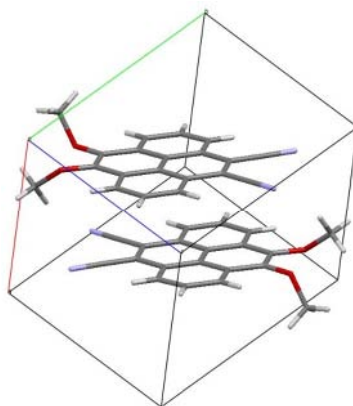
9.8.3 9,10-Dibromopyrene-4,5-diolactonide (3-5)



$\text{C}_{19}\text{H}_{12}\text{Br}_2\text{O}_2$, $M_r = 432.11$ g/mol, triclinic, space group P-1, $a = 7.0896(4)$ Å, $b = 9.7320(9)$ Å, $c = 11.0373(9)$ Å, $\alpha = 99.588(4)^\circ$, $\beta = 91.694(4)^\circ$, $\gamma = 96.224(4)^\circ$, $V = 745.58(10)$ Å³, $Z = 2$, $D_x = 1.92$, 8885 reflections measured, 4121 unique reflections, $R_{\text{int}} = 0.0009$, 3201 reflections observed ($I > 3\sigma(I)$), $R = 0.052$, $R_w = 0.048$.

Cambridge Crystallographic Data Centre identifier: CCDC-874828

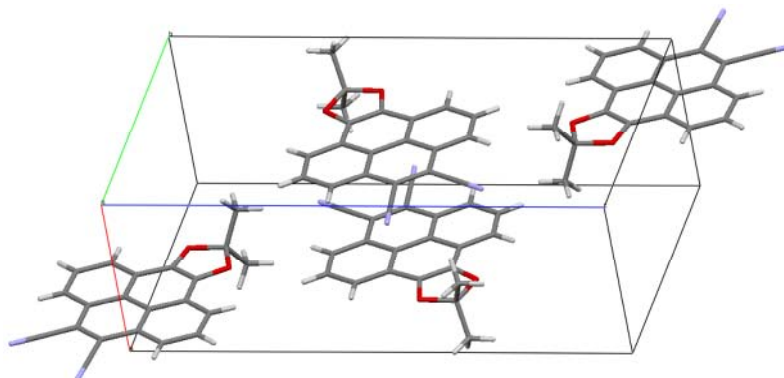
9.8.4 9,10-Dimethoxypyrene-4,5-dicarbonitrile (3-6)



$\text{C}_{20}\text{H}_{12}\text{N}_2\text{O}_2$, $M_r = 312.33$ g/mol, triclinic, space group P-1, $a = 7.0844(2)$ Å, $b = 10.1531(4)$ Å, $c = 10.6861(4)$ Å, $\alpha = 105.7881(17)^\circ$, $\beta = 98.355(2)^\circ$, $\gamma = 96.968(2)^\circ$, $V = 721.27(5)$ Å³, $Z = 2$, $D_x = 1.44$, 9567 reflections measured, 4343 unique reflections, $R_{\text{int}} = 0.0007$, 3298 reflections observed ($I > 3\sigma(I)$), $R = 0.047$, $R_w = 0.057$.

Cambridge Crystallographic Data Centre identifier: CCDC-874821

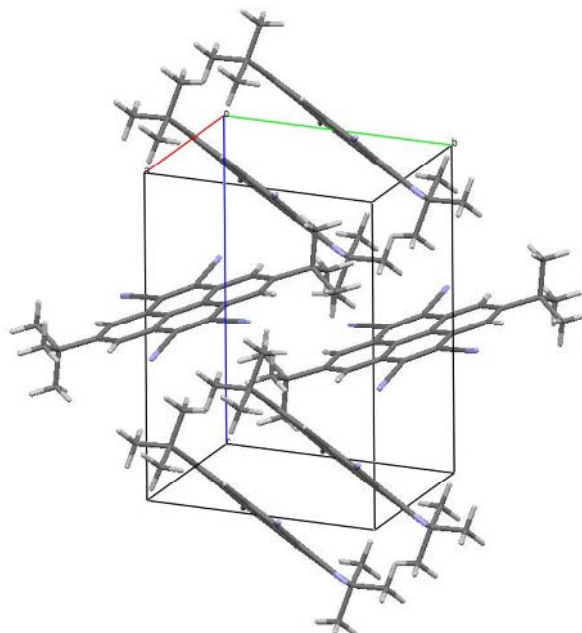
9.8.5 9,10-Dihydroxyacetone-4,5-dicyanopyrene (3-7)



$C_{21}H_{12}N_2O_2$, $M_r = 324.34$ g/mol, orthorhombic, space group $Pmcn$, $a = 6.8305(2)$ Å, $b = 11.0589(5)$ Å, $c = 19.8828(9)$ Å, $\alpha = \beta = \gamma = 90^\circ$, $V = 1501.90(11)$ Å³, $Z = 4$, $D_x = 1.43$, 12552 reflections measured, 2085 unique reflections, $R_{int} = 0.0007$, 1709 reflections observed ($I > 2\sigma(I)$), $R = 0.042$, $R_w = 0.050$.

Cambridge Crystallographic Data Centre identifier: CCDC-874825

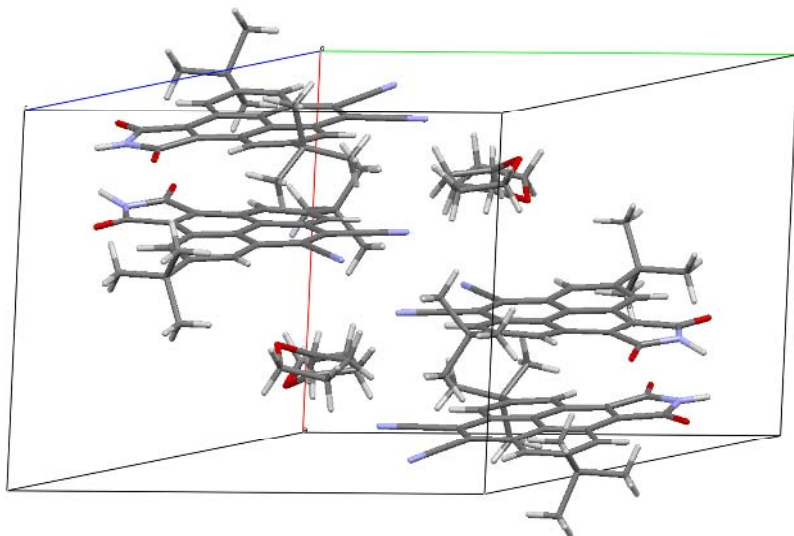
9.8.6 2,7-Di-*tert*-butylpyrene-4,5,9,10-tetracarbonitrile (3-9)



$\text{C}_{28}\text{H}_{22}\text{N}_4$, $M_r = 414.50$ g/mol, monoclinic, space group $P2_1/n$, $a = 9.0368(3)$ Å, $b = 9.2187(5)$ Å, $c = 13.5180(6)$ Å, $\beta = 97.088(2)^\circ$, $V = 1117.54(9)$ Å³, $Z = 2$, $D_x = 1.23$, 10908 reflections measured, 3549 unique reflections, $R_{\text{int}} = 0.0005$, 2034 reflections observed ($I > 3\sigma(I)$), $R = 0.078$, $R_w = 0.099$.

Cambridge Crystallographic Data Centre identifier: CCDC-874822

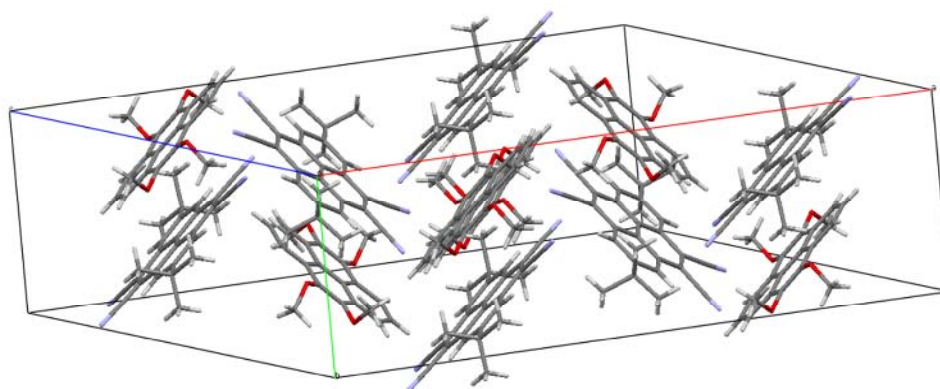
9.8.7 2,7-Di-*tert*-butylpyrene-4,5-imido-9,10-dicarbonitrile (3-10)



$\text{C}_{64}\text{H}_{62}\text{N}_6\text{O}_6$ (THF solvate), $M_r = 1011.23$ g/mol, triclinic, space group P-1, $a = 13.2330(6)$ Å, $b = 15.3610(7)$ Å, $c = 15.4910(6)$ Å, $\alpha = 118.777(2)^\circ$, $\beta = 100.222(3)^\circ$, $\gamma = 95.473(3)^\circ$, $V = 2655.9(2)$ Å³, $Z = 2$, $D_x = 1.26$, 31239 reflections measured, 14837 unique reflections, $R_{\text{int}} = 0.0005$, 9331 reflections observed ($I > 3\sigma(I)$), $R = 0.097$, $R_w = 0.015$.

Cambridge Crystallographic Data Centre identifier: CCDC-874823

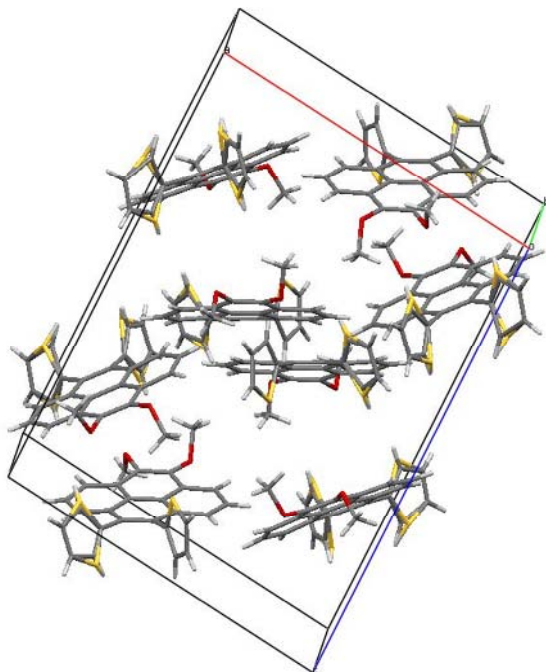
9.8.8 4,5,9,10-Tetramethoxypyrene - 2,7-Di-*tert*-butylpyrene-4,5,9,10-tetracarbonitrile (CT3-8/3-9)



$C_{24}H_{20}N_2O_2$, $M_r = 368.44$ g/mol, monoclinic, space group $C2/c$, $a = 27.8417(8)$ Å, $b = 9.5837(2)$ Å, $c = 18.0087(5)$ Å, $\beta = 129.6059(8)^\circ$, $V = 3702.15(17)$ Å³, $Z = 8$, $D_x = 1.32$, 17548 reflections measured, 5370 unique reflections, $R_{int} = 0.0005$, 4007 reflections observed ($I > 3\sigma(I)$), $R = 0.044$, $R_w = 0.054$.

Cambridge Crystallographic Data Centre identifier: CCDC-874820

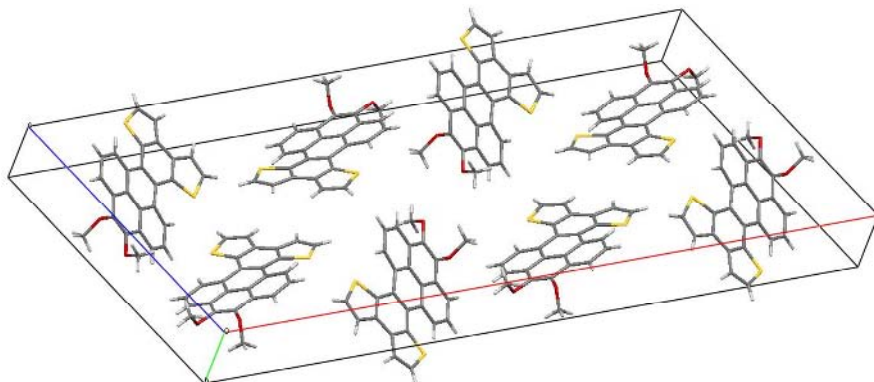
9.8.9 4,5-Dimethoxy-9,10-bis(thien-2-yl)pyrene (5-2)



$\text{C}_{26}\text{H}_{18}\text{O}_2\text{S}_2$, $M_r = 426.56$ g/mol, monoclinic, space group $P2_1/c$, $a = 15.6328(4)$ Å, $b = 12.5156(3)$ Å, $c = 20.7675(6)$ Å, $\beta = 95.9799(15)^\circ$, $V = 4041.13(18)$ Å³, $Z = 8$, $D_x = 1.40$, 29758 reflections measured, 10750 unique reflections, $R_{\text{int}} = 0.0005$, 7211 reflections observed ($I > 3\sigma(I)$), $R = 0.058$, $R_w = 0.069$.

Cambridge Crystallographic Data Centre identifier: CCDC-819581

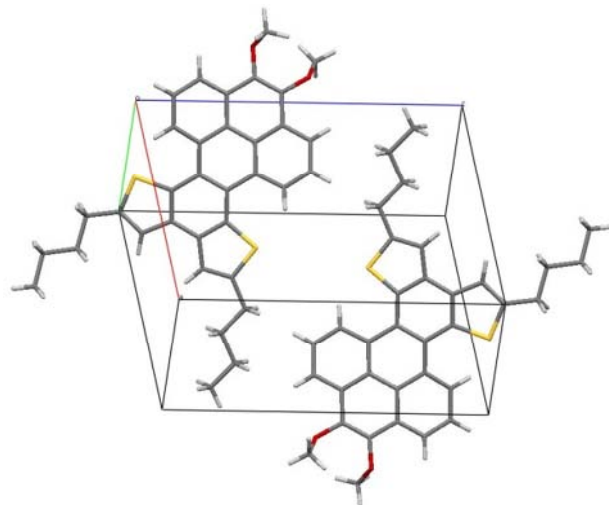
9.8.10 10,11-Dimethoxy-benzo[8,9]triphenyleno[1,2-*b*:4,3-*b'*]dithiophene (5-3)



$C_{26}H_{16}O_2S_2$, $M_r = 424.54$ g/mol, monoclinic, space group $C2/c$, $a = 46.7200(10)$ Å, $b = 4.29240(10)$ Å, $c = 18.9060(7)$ Å, $\beta = 101.0025(15)^\circ$, $V = 3721.74(18)$ Å³, $Z = 8$, $D_x = 1.52$, 16633 reflections measured, 5130 unique reflections, $R_{int} = 0.0006$, 3476 reflections observed ($I > 3\sigma(I)$), $R = 0.039$, $R_w = 0.046$.

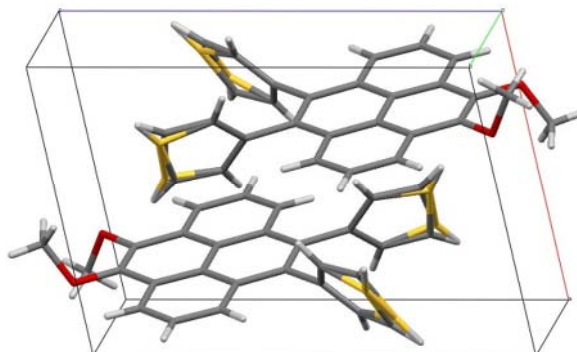
Cambridge Crystallographic Data Centre identifier: CCDC-819579

**9.8.11 2,5-Dibutyl-10,11-dimethoxy-benzo[8,9]
triphenyleno[1,2-*b*:4,3-*b'*]dithiophene (5-5)**



$C_{34}H_{32}O_2S_2$, $M_r = 536.76$ g/mol, triclinic, space group P-1, $a = 9.3175(2)$ Å, $b = 9.7533(2)$ Å, $c = 15.2643(3)$ Å, $\alpha = 77.9756(10)^\circ$, $\beta = 82.2680(12)^\circ$, $\gamma = 74.8558(13)^\circ$, $V = 1304.89(5)$ Å³, $Z = 2$, $D_x = 1.37$, 19787 reflections measured, 8294 unique reflections, $R_{int} = 0.0008$, 6495 reflections observed ($I > 3\sigma(I)$), $R = 0.047$, $R_w = 0.056$.

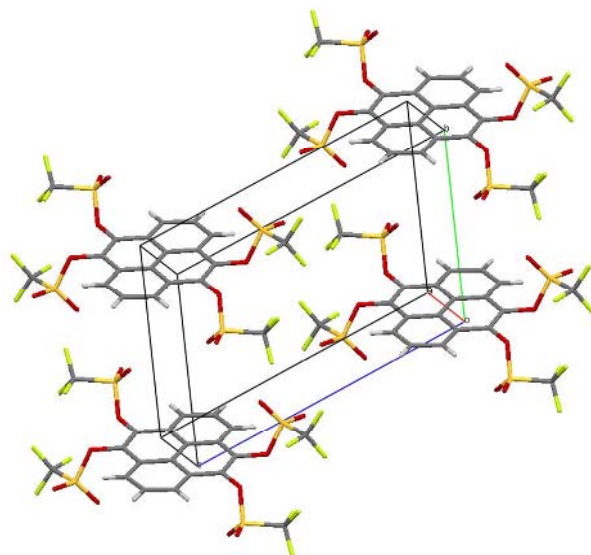
Cambridge Crystallographic Data Centre identifier: CCDC-874826

9.8.12 4,5-Dimethoxy-9,10-bis(thien-3-yl)pyrene (5-8)

$\text{C}_{26}\text{H}_{18}\text{O}_2\text{S}_2$, $M_r = 426.56$ g/mol, triclinic, space group P-1, $a = 9.0830(3)$ Å, $b = 9.1170(2)$ Å, $c = 13.4430(4)$ Å, $\alpha = 105.7370(16)^\circ$, $\beta = 92.5870(13)^\circ$, $\gamma = 104.8740(16)^\circ$, $V = 1027.67(5)$ Å³, $Z = 4$, $D_x = 1.38$, 13860 reflections measured, 5966 unique reflections, $R_{\text{int}} = 0.0006$, 4697 reflections observed ($I > 3\sigma(I)$), $R = 0.082$, $R_w = 0.091$.

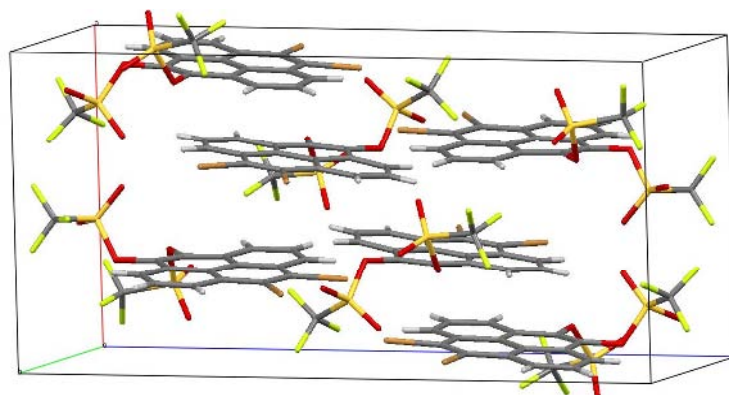
Cambridge Crystallographic Data Centre identifier: CCDC-874827

9.8.13 4,5,9,10-Tetratriflatopyrene (6-2)



$\text{C}_{10}\text{H}_3\text{F}_6\text{O}_6\text{S}_2$, $M_r = 397.25$ g/mol, triclinic, space group P-1, $a = 5.0041(2)$ Å, $b = 9.4388(5)$ Å, $c = 14.0451(8)$ Å, $\alpha = 101.515(3)^\circ$, $\beta = 96.482(3)^\circ$, $\gamma = 97.466(3)^\circ$, $V = 637.91(6)$ Å³, $Z = 2$, $D_x = 2.07$, 9295 reflections measured, 3668 unique reflections, $R_{\text{int}} = 0.0006$, 2767 reflections observed ($I > 3\sigma(I)$), $R = 0.037$, $R_w = 0.044$.

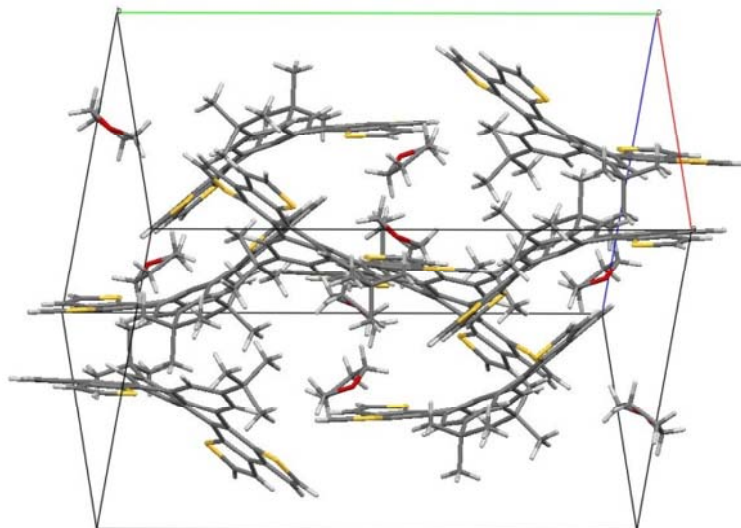
Cambridge Crystallographic Data Centre identifier: CCDC-830174

9.8.14 4,5-Dibromo-9,10-ditriflatopyrene (6-4)

$C_{54}H_{18}Br_6F_{18}O_{18}S_6$, $M_r = 1968.51$ g/mol, triclinic, space group $P-1$, $a = 10.9121(2)$ Å, $b = 13.4556(3)$ Å, $c = 21.4689(5)$ Å, $\alpha = 101.7495(9)^\circ$, $\beta = 92.3718(12)^\circ$, $\gamma = 92.6724(11)^\circ$, $V = 3078.67(11)$ Å³, $Z = 2$, $D_x = 2.12$, 41342 reflections measured, 19342 unique reflections, $R_{int} = 0.0010$, 13576 reflections observed ($I > 3\sigma(I)$), $R = 0.050$, $R_w = 0.058$.

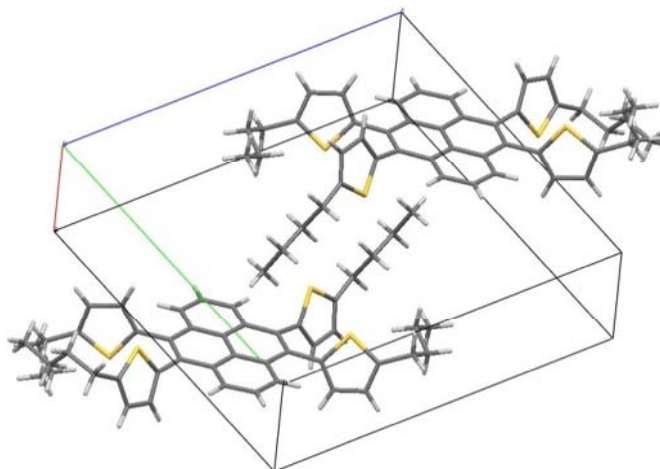
Cambridge Crystallographic Data Centre identifier: CCDC-830175

**9.8.15 8,17-Di-*tert*-butyl-dibenzo[*fg,op*]-
tetrathieno[*a,c,j,l*]tetracene (6-6)**



$C_{44}H_{38}O_1S_4$ - THF solvate, $M_r = 711.05$ g/mol, monoclinic, space group $C 2/c$, $a = 14.1748(3)$ Å, $b = 23.6414(6)$ Å, $c = 20.9266(3)$ Å, $\beta = 100.2563(12)^\circ$, $V = 6900.7(3)$ Å³, $Z = 8$, $D_x = 1.37$, 35577 reflections measured, 9591 unique reflections, $R_{int} = 0.0005$, 7683 reflections observed ($I > 3\sigma(I)$), $R = 0.045$, $R_w = 0.054$.

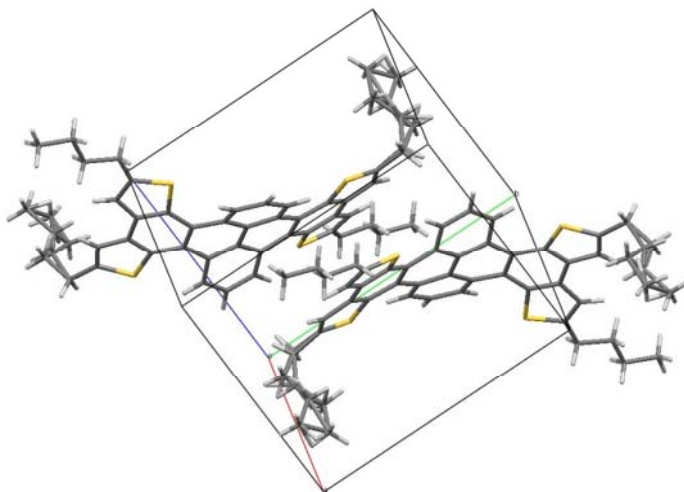
Cambridge Crystallographic Data Centre identifier: CCDC-830176

9.8.16 4,5,9,10-Tetrakis-(5-*n*-butylthien-2-yl)pyrene (6-7)

$C_{48}H_{50}S_4$, $M_r = 755.19$ g/mol, triclinic, space group P-1, $a = 9.5284(6)$ Å, $b = 14.0861(7)$ Å, $c = 16.0076(9)$ Å, $\alpha = 71.062(4)^\circ$, $\beta = 88.429(3)^\circ$, $\gamma = 80.284(4)^\circ$, $V = 2002.2(2)$ Å³, $Z = 2$, $D_x = 1.25$, 17173 reflections measured, 8785 unique reflections, $R_{int} = 0.0009$, 2767 reflections observed ($I > 3\sigma(I)$), $R = 0.058$, $R_w = 0.056$.

Cambridge Crystallographic Data Centre identifier: CCDC-830177

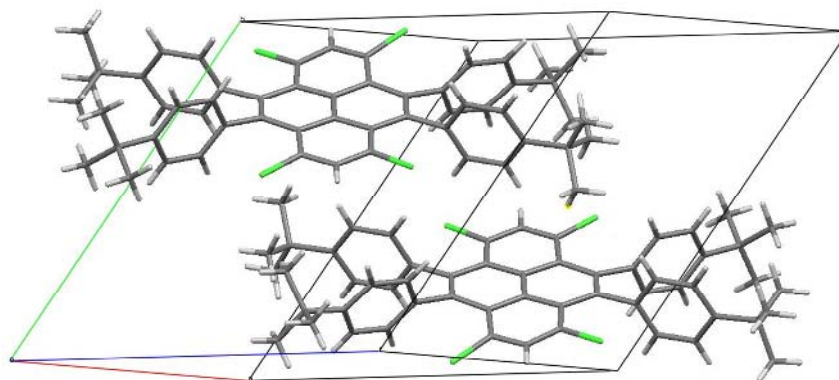
**9.8.17 2,5,11,14-Tetra-*n*-butyl-dibenzo[*fg,op*]-
tetrathieno[*a,c,j,l*]tetracene (6-8)**



$C_{48}H_{46}S_4$, $M_r = 751.16$ g/mol, triclinic, space group P-1, $a = 7.5858(3)$ Å, $b = 13.6821(7)$ Å, $c = 18.7826(9)$ Å, $\alpha = 74.530(2)^\circ$, $\beta = 88.182(3)^\circ$, $\gamma = 87.442(3)^\circ$, $V = 1876.54(15)$ Å³, $Z = 2$, $D_x = 1.33$, 18603 reflections measured, 9872 unique reflections, $R_{\text{int}} = 0.0006$, 7683 reflections observed ($I > 3\sigma(I)$), $R = 0.072$, $R_w = 0.024$.

Cambridge Crystallographic Data Centre identifier: CCDC-830178

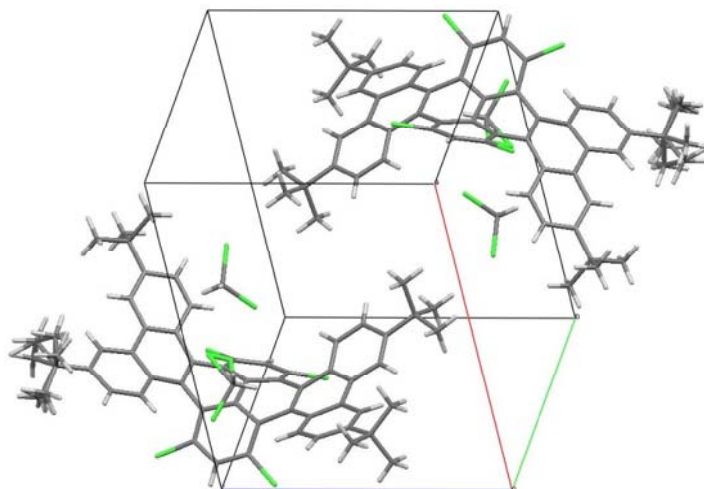
9.8.18 4,5,9,10-Tetrakis(4-*tert*-butylphenyl)-1,3,6,8-tetrachloropyrene (6-13)



$\text{C}_{56}\text{H}_{54}\text{Cl}_4$, $M_r = 868.86$ g/mol, triclinic, space group P-1, $a = 12.2920(3)$ Å, $b = 14.2477(5)$ Å, $c = 15.5606(5)$ Å, $\alpha = 64.5718(11)^\circ$, $\beta = 82.6821(16)^\circ$, $\gamma = 66.9643(15)^\circ$, $V = 2262.21(13)$ Å³, $Z = 2$, $D_x = 1.28$, 27213 reflections measured, 12489 unique reflections, $R_{\text{int}} = 0.0006$, 9312 reflections observed ($I > 3\sigma(I)$), $R = 0.083$, $R_w = 0.030$.

Cambridge Crystallographic Data Centre identifier: CCDC-843999

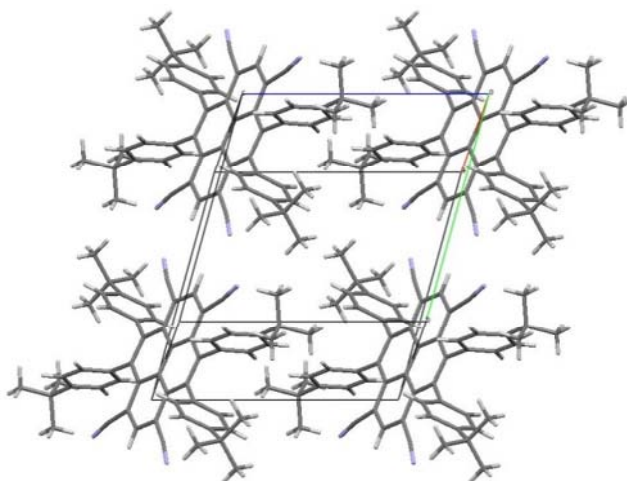
9.8.19 3,6,14,17-Tetra-*tert*-butyl-9,11,20,22-tetrachloro-hexabenzo[*a,c,fg,j,l,op*]tetracene (6-14a)



$C_{58}H_{54}Cl_8 - 2 CD_2Cl_2$ solvate, $M_r = 1034.69$ g/mol, triclinic, space group P-1, $a = 13.4013(3)$ Å, $b = 14.4519(2)$ Å, $c = 14.7883(3)$ Å, $\alpha = 71.3208(11)^\circ$, $\beta = 80.4669(10)^\circ$, $\gamma = 67.4754(11)^\circ$, $V = 2503.25(9)$ Å³, $Z = 2$, $D_x = 1.37$, 37065 reflections measured, 14585 unique reflections, $R_{int} = 0.0005$, 11034 reflections observed ($I > 3\sigma(I)$), $R = 0.046$, $R_w = 0.057$.

Cambridge Crystallographic Data Centre identifier: CCDC-844001

9.8.20 4,5,9,10-Tetrakis(4-tert-butylphenyl)pyrene-1,3,6,8-tetracarbonitrile (7-3)



$\text{C}_{30}\text{H}_{27}\text{N}_2$, $M_r = 415.56$ g/mol, triclinic, space group P-1, $a = 8.7013(2)$ Å, $b = 11.8886(4)$ Å, $c = 11.9312(5)$ Å, $\alpha = 73.0482(16)^\circ$, $\beta = 88.035(2)^\circ$, $\gamma = 79.886(2)^\circ$, $V = 1162.08(7)$ Å³, $Z = 2$, $D_x = 1.19$, 15614 reflections measured, 6747 unique reflections, $R_{\text{int}} = 0.0006$, 4235 reflections observed ($I > 3\sigma(I)$), $R = 0.050$, $R_w = 0.062$.

Cambridge Crystallographic Data Centre identifier: CCDC-844000

10 List of Publications

1. F. E Alemdaroglu, W. Zhuang, L. Zöphel, W. Wang, R. Berger, J. P. Rabe, A. Herrmann: Generation of Multiblock Copolymers by PCR: Synthesis, Visualization and Nanomechanical Properties. *Nano Letters* **2009**, 9, 3658-3662.
2. L. Zöphel, K. Eisele, R. Gropeanu, A. Rouhanipour, K. Koynov, I. Lieberwirth, K. Müllen, T. Weil: Preparation of Defined Albumin-Polymer Hybrids for Efficient Cell Transfection. *Macromolecular Chemistry and Physics* **2010**, 211, 146-153.
Frontispiece. *Macromolecular Chemistry and Physics* 2/2010, DOI: 10.1002/macp.201090002.
3. L. Zöphel, D. Beckmann, V. Enkelmann, D. Chercka, R. Rieger, K. Müllen: Asymmetric pyrene derivatives for organic field-effect transistors. *Chemical Communications* **2011**, 47, 6960-6962.
4. L. Zöphel, V. Enkelmann, R. Rieger, K. Müllen: Saddle Shaped Hexaaryl[*a,c,fg,j,l,op*]tetracenes from 4,5,9,10-Tetrafunctionalized Pyrenes. *Organic Letters* **2011**, 13, 4506-4509.

5. L. Zöphel, K. Mali, P. S. Reddy, M. Wagner, S. De Feyter, W. Pisula, K. Müllen: 4,5-Pyrenocyanine – Just Another Phthalocyanine? *Chemistry – A European Journal* **2012**, 18, 3264-3276.
6. L. Zöphel, P. Gao, V. Enkelmann, M. Baumgarten, M. Wagner, K. Müllen: Towards the *peri*-Pentacene Framework, *in preparation*.
7. K. Mali, L. Zöphel, O. Ivasenko, K. Müllen, S. De Feyter: Lead Pyrenocyanine Exhibits Non-planar Adsorption Geometries at the Liquid-Solid Interface, *in preparation*.

11 Acknowledgements

[Redacted text block]

[Redacted text block]

[Redacted text block]

[illegible]

12 Curriculum Vitae

PERSONAL DETAILS

Name Lukas Julian Zöphel

Academic title Diplom Chemiker

| | |
|----------------|-------------------|
| Place of birth | Kirchheimbolanden |
|----------------|-------------------|

Nationality German

UNIVERSITY EDUCATION

SCHOOL EDUCATION

██████████

SCIENTIFIC PROGRAMS and CONFERENCES
